The Design and Synthesis of Duocarmycin-based Conjugates for Targeted Delivery to Tumours

Oliver Cartwright

A thesis submitted for the degree of Doctor of Philosophy

School of Pharmacy

University of East Anglia

Declaration

This thesis has been submitted to the University of East Anglia for the Degree of Doctor of Philosophy and is, to the best of my knowledge, original except where stated, referenced and acknowledged.

Oliver Cartwright

Abstract

The CC-1065 and duocarmycin family of compounds are ultrapotent antitumour antibiotics which demonstrate activity in the picomolar range. These agents exert their biological effect through a sequence selective alkylation at the N3 position of adenine resulting in apoptosis. Despite the potential of this family to exert themselves as successful chemotherapeutic agents, a lack of clinical success has been observed for these compounds. This has been attributed to a lack of selectivity resulting in off-target side effects and toxicity. For this reason, research now focuses on ways in which these alkylating agents could realise their potential using tumour specific, targeted delivery strategies.

Herein, we investigate the use of a duocarmycin SA analogue, functionalised for solid phase synthesis, in the design of conjugates for targeted delivery to cancerous tissue via the Thomsen-Friedenreich antigen (T-antigen). This antigen is overexpressed in 90% of primary human carcinomas, yet is cryptic in healthy cells, therefore presenting itself as an ideal moiety for the delivery of duocarmycin agents to cancerous tissue.

The research presented in this thesis will begin with detailing the synthesis of the Fmoc-duocarmycin SA analogue along with attempted modifications to the synthetic route to try and achieve greater efficiency. Additionally, this chapter will detail investigations into alternative protecting group removal strategies to improve the effectiveness of this analogues use in solid phase synthesis. The chapters subsequent to this will detail the design, synthesis and biological evaluation of a series of duocarmycin-based conjugates for targeted delivery to the T-antigen. These conjugates involve the use of T-antigen specific lectins and peptides. Furthermore, the development of a gold nanoparticle delivery system involving duocarmycin and a T-antigen specific lectin will be detailed. The investigations presented herein provide scope for future investigations into the design of clinically successful duocarmycin-based conjugates.

Acknowledgements

First of all I would like to thank my supervisors, Prof. Mark Searcey and Prof. David Russell for all their continued support and advice throughout my PhD and also for the opportunity in providing work for such an interesting subject area. The ever present 'anything exciting happened?' question from Mark has always kept me alert and striving for success even if my face would say otherwise!

I would also like to thank my fellow lab members for their advice over the past 4 years. A special thanks must go to Dr Andrew Beekman, Dr Ryan Tinson, Dr Marco Commineti, Dr Maria Marin and Lučka Bibič who have been a continuous support network during my studies. The advice and comments (often hilarious and gif-based *cough Lucka cough*) have been invaluable for completing this thesis. Additionally, my PhD would not have been so fun without a good group of friends who have played a role in keeping me sane over the years. I am sure these guys know who they are! Without you (and the drinks), this journey would certainly not have been so smooth and fun!

Of course, the people outside of the lab have played as big a role as those within the lab. For this, I would like to thank my family and friends who have always supported my studies throughout my life and I am sure will continue to do so into the future.

Finally, a special thanks must go to my partner, Nat. You have been with me throughout the many highs and lows and always provided a place to allow me to 'switch off' from science when that was what I needed the most. Your constant belief and positivity have been invaluable, especially when I lacked belief in myself. I must also thank you for the many hours spent listening to my presentations about 'gold nanoparticles' and 'Fmoc/Boc deprotections'. Your helpful 'What are you chattin' about?' comments have been a constant source of feedback throughout. Should you not take anything else away from my work, at least you have a solid knowledge of these two areas.

Contents

List of Figures:

List of Schemes:

List of Tables:

Abbreviations:

2-Cltrt	2-Chlorotrityl
αCHCA	α-cyano-4-hydroxycinnamic acid
ABL	*Agaricus bisporus* lectin
ACN	acetonitrile
ADC	antibody drug conjugate
AIBN	azobisisobutyronitrile
AuNP	gold nanoparticle
BnBr	benzyl bromide
Boc	tert-butyloxycarbonyl
Boc_2O	di-tert-butyl dicarbonate
BSA	bovine serum albumin
CBI	cyclopropabenzo[e]indolone
CDR	complementary determining regions
CML	chronic myelogenous leukemia
COSY	correlation spectroscopy
CPI	cyclopropylpyrrolo[e]indolone
CYP	cytochrome P450 enzyme
DAR	drug-antibody ratio
DBCO	dibenzocyclooctyl
DCC	N,N'-dicyclohexylcarbodiimide
DCM	dichloromethane
DCU	dicyclohexylurea
DHB	2,5 dihydroxybenzoic acid
DHFR	dihydrofolate reductase
DIPEA	N,N-diisopropylethylamine
DMAP	4-dimethylaminopyridine
DMF	N,N-dimethylformamide
DMSO	dimethylsulfoxide
DSA	duocarmycin SA

ECL	*erythrina cristagalli* lectin
EDCI	1-ethyl-3-(3-dimethylaminopropyl)carbodiimide
EDT	1,2-ethanedithiol
EPR	enhanced permeability and retention effect
FITC	fluorescein isothiocyanate
Fmoc	fluorenylmethyloxycarbonyl
FR	framework regions
Fv	variable fragment
GOS	galactose oxidase-Schiff
HATU	1-[Bis(dimethylamino)methylene]-1H-1,2,3-triazolo[4,5-b]pyridinium 3- oxid hexafluorophosphate
HBTU	O-(Benzotriazol-1-yl)-N,N,N′,N′-tetramethyluronium hexafluorophosphate HCl hydrochloric acid
HEPES	4-(2-hydroxyethyl)-1-piperazineethanesulfonic acid
HER2	human epidermal growth factor 2
HOBt	1-hydroxybenzotriazole
HPA	helix pomatia agglutinin
HPLC	high performance liquid chromatography
HSQC	heteronuclear single quantum correlation
IC_{50}	half maximal inhibitory concentration
Jac	jacalin
K_d	dissociation constant
LC-MS	liquid chromatography–mass spectrometry
LeY	Lewis Y antigen
LSPR	localised surface plasmon resonance
MAb	monoclonal antibody
MALDI	matrix assisted laser desorption ionisation
MeOH	methanol
MES	4-Morpholineethanesulfonic acid
ML-1	mistletoe lectin 1
MMAE	monomethyl auristatin

MTS 3-(4,5-dimethylthiazol-2-yl)-5-(3-carboxymethoxyphenyl)-2-(4- sulfophenyl)-2H-tetrazolium

MTX methotrexate

MWCO molecular weight cut-off

NaH sodium hydride

NHS N-hydoxysuccinimide

NIS N-iodosuccinimide

PABA *para*-aminobenzoic acid

PBS phosphate buffered saline

PI3Kβ phosphoinositide 3-kinase β

PCB *para*-chlorobenzyl

PDC peptide-drug conjugate

PEG polyethylene glycol

PES phenazine ethosulfate

PMB *para*-methoxybenzyl

PNA peanut agglutinin

PSA polysialic acid

PyBop (Benzotriazol-1-yloxy)tripyrrolidinophosphonium hexafluorophosphate

SAMB N'-succinimidyl 4-N-(2'-acetylthiopropionyl)-N-methyl-4-aminobutyrate

sLeA sialyl Lewis A antigen

sLeX sialyl Lewis X

SMCC (succinimidyl 4-(N-maleimidomethyl)cyclohexane-1-carboxylate)

SPOS solid phase organic synthesis

SPPS solid phase peptide synthesis

T-antigen Thomsen Friedenreich antigen

TBAF tetrabutylammonium fluoride solution

TEM transmission electron microscope

TFA trifluoroacetic acid

THF tetrahydrofuran

TIPS	triisopropylsilane
TK	tyrosine kinase
TNF	tumour necrosis factor
TTMSS	tris(trimethylsilyl)silane

Chapter 1 - Introduction

1.1 The War on Cancer

Despite the 'war on cancer' having lasted almost 50 years, the development of new anticancer therapeutics remains a major challenge.[1] Oncology has one of the poorest records for investigational drugs in clinical development, with success rates that are more than three times lower than for cardiovascular disease (Figure 1.1).[2] This difficulty stems from the way in which this malignant disease manifests itself within the organism it affects. Cancer occurs when a single cell in a tissue is genetically damaged or modified to produce cells with the ability to proliferate uncontrollably; leading to the formation of tumours. Due to the metastatic nature of cancer, this disease can spread to areas distant from the initial site of occurrence, leading to loss of function of affected organs or tissues.[3] The characteristic that makes cancer so difficult to treat is the inherent similarities, in terms of biochemistry, that exist between cancer cells and healthy cells. This makes it very difficult to achieve selective delivery of drugs to cancer cells rather than healthy cells.

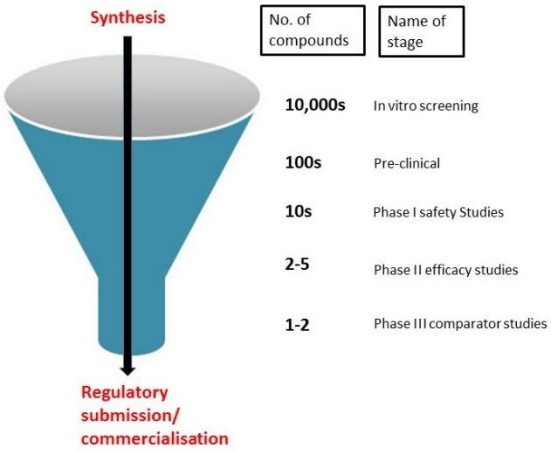

Figure 1.1: demonstration of the difficult journey from the synthesis of lead compounds through to commercialisation. This pathway is of particular issue in the development of cancer related treatments.

The current choice of therapy for cancer depends on the extent to which the disease has manifested itself within the body and also the extent to which it has metastasised. For example, surgery is a localised treatment – it only treats the part of the body operated on and so it may cure cancer that is completely contained in one area and has not spread. Usually, the earlier a

cancer is found the easier it is to remove. If the cancer has metastasised to other areas of the body however, a systemic therapy involving the administration of cytotoxic small molecules into the body is usually utilised. This way, the drug does not just localise in one place.[4]

Cytotoxic drugs known to man are in abundance. However, the number of these drugs that have shown success within clinical trials and animal models are comparatively small. This has been put down to a lack of identification of unique biochemical aspects of malignancies that could be exploited to target tumour cells over healthy living cells.[5] More recently, advances within this area have been made with Gleevec and Trastuzumab providing just two examples of now clinically approved agents which make use of the different biochemical properties of the two cell types.[6]

Despite this struggle to find ideal clinical candidates from known cytotoxic agents, the success in terms of survival rates when it comes to cancer can be attributed to the many years of chemotherapy based research. This research has laid the foundations for current cancer therapies which have enhanced our ability to combat the disease.

1.1.1 Chemotherapy – A History

Chemotherapy has been one of the foremost approaches for the treatment of cancer for more than half a century and consists of the administration of drugs which cause cell death through interference of fundamental steps in the cell lifecycle.

The first cytotoxic compounds to be administered in human patients in the late 1940s were the nitrogen mustards, chlorambucil and cyclophosphamide (Figure 1.2), which are able to alkylate DNA irreversibly leading to eventual cell death.[7] Around the same time came the observation that folic acid stimulated cancer growth, which prompted the development of folate analogues that could prevent DNA synthesis by inhibiting dihydrofolate reductase (DHFR).[1]

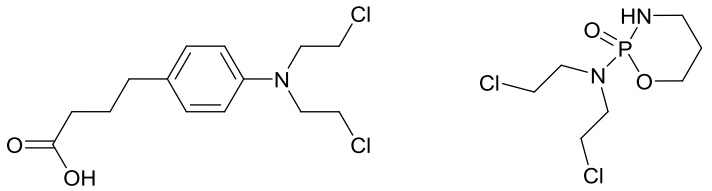

a. Chlorambucil b. Cyclophosphamide

Figure 1.2: structures of Chlorambucil and Cyclophosphamide.

Following on from this early stage rational drug design, the elucidation of the structure of DNA brought about the development of nucleoside analogues such as thioguanine, 5-fluoruracil and gemcitabine (Figure 1.3) which induce apoptosis by blocking the elongation of DNA strands.[8] With DNA being vital to the normal functioning of a cell as well as being important in allowing cell proliferation, DNA represented an attractive target for anticancer agents. Soon after, the serendipitously-discovered cytotoxic effects of cisplatin (Figure 1.3) gave rise to the biological evaluation of different platinum(II) complexes, which are able to crosslink DNA strands by binding to guanine and adenine residues.[9] The realisation of DNA being a major target for chemotherapy was further enforced through the discovery of a class of natural products called anthracyclines. Drugs in this family include daunorubicin and doxorubicin (Figure 1.3) which are known to cause cell death by additional means such as intercalation into DNA, generation of free radicals, DNA cross linking and interference with helicase activity.[10] Besides the use of DNA-interacting agents, significant anticancer effects were provided by the administration of inhibitors of repair proteins topoisomerase I and II. These proteins are involved in fundamental arrangements of the DNA structure, being able to break the single-(topoisomerase I) or double-strand (topoisomerase II) and then rejoin the DNA ends. Drugs such as etoposide, teniposide and camptothecins are able to stabilise DNA-topoisomerase complexes, thus blocking the progression of the replication fork.[11]

In addition to DNA and DNA-interacting proteins, microtubules represent a validated target in chemotherapy. Vinca alkaloids, e.g. vincristine and vinblastine and their derivatives, were initially found to bind tubulin, inhibiting the microtubule formation and inducing cell apoptosis.[12] The

isolation of paclitaxel (Figure 1.3) from the Pacific yew, *Taxus brevifolius* in 1971, gave rise to the successful use of taxanes for cancer treatment.[13] While vinca alkaloids affect the rates of tubulin polymerization, taxanes inhibit microtubule depolymerisation and also presented an exciting new class of antitumour agents.[14]

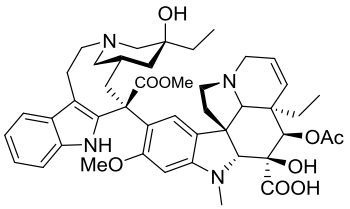

a) Vinblastine (vinca alkaloid)
av IC_{50} (M): $6.4X10^{-10}$ (99 cell lines)

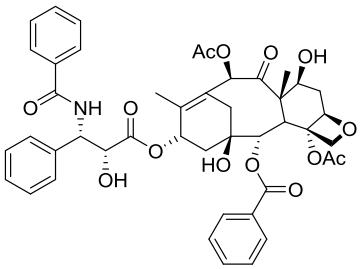

b) Paclitaxel (taxanes)
av. IC_{50} (M): 9.6×10^{-9} (94 cell lines)

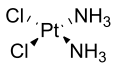

c) **Cisplatin** (Platinum complex)
av IC_{50} (M): 4.3×10^{-6} (13 cell lines)

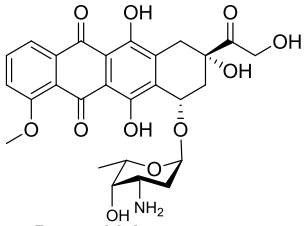

d) **Doxorubicin** (anthracyclines)
av. IC_{50} (M): 8.4×10^{-8} (85 cell lines)

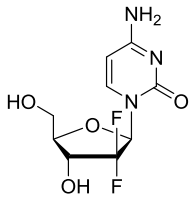

e) **Gemcitabine** (nucleoside analogue)
av. IC_{50} (M): 6.0×10^{-7} (13 cell lines)

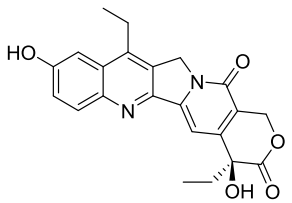

f) **SN-38** (camptothecins)
av IC_{50} (M): 4×10^{-10} (11 cell lines)

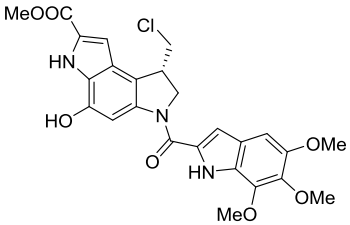

g) **Duocarmycin SA** (Duocarmycins)
av. IC_{50} (M): 6.2×10^{-10} (15 cell lines)

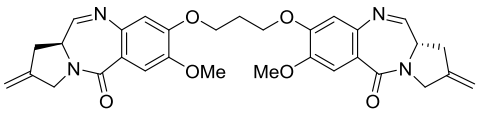

h) **SJG-136** (Pyrrolobenzodiazepines)
av. IC_{50} (M): 4.7×10^{-9} (8 cell lines)

Figure 1.3: molecular structures, and growth inhibition data of some of the most potent cytotoxic agents. Average (av.) of IC_{50} values reported for a variable number of human cancer cell lines (in brackets).[15, 16, 17, 18]

Due to the presence of preferential targets for cancer treatment in both healthy and diseased cells, the antitumour efficacy of these conventional chemotherapeutics is limited by their nonspecific action against normal cells, especially to rapidly growing cells such as bone marrow, cells of hair follicles and mucous membrane cells. As a result, these anticancer agents are characterised by a narrow therapeutic window, that is, the quantitative relationship between efficacy and safety. Moreover, the ability of low-molecular weight cytotoxic compounds to reach cancer cells is often impaired by different physiological barriers such as, tumour interstitial pressure and diffusion through the tumour endothelium or extracellular matrix. Degradation processes that convert the anticancer drugs into inactive metabolites as well as drug resistance mechanisms present more obstacles to the success of these agents.[19]

In principle, the treatment efficiency of these compounds can be improved by increasing the doses, but this approach commonly results in severe side-effects. The administration of combinations of anticancer drugs with different mechanisms of action and non-overlapping toxicity profiles was one of the first strategies to improve the efficacy of conventional chemotherapeutics; multidrug therapy became a standard modality for the treatment of most cancers. As an additional strategy, anticancer drugs derived from natural sources became the object of intense research aimed at the discovery of new cytotoxic agents with improved anticancer activity. These significant efforts led to the development of a variety of both tubulin-targeted and DNA-interacting agents with higher antiproliferative activity than conventional chemotherapeutics. However, the mere enhancement of the cell-killing power of cytotoxic drugs did not result in increased therapeutic indices. Indeed, the clinical evaluations of these new cytotoxic agents were often discontinued, due to the occurrence of severe side-toxicities at low administration doses.

1.1.2 Targeted Chemotherapy

The fundamental drawbacks of cytotoxic agents discussed above prompted the development of targeted therapies. This approach may selectively kill the diseased tissue while sparing healthy cells, hence dramatically improving the

therapeutic index of existing therapies.[20] In 1913, Paul Ehrlich described the concept of a 'magic bullet' i.e. a medicine that can selectively target specific microorganisms, and this concept is now the corner stone of the majority of research into this area. Based on the understanding of molecular principles of genetic and pathological processes that contribute to tumour growth, a large variety of new tumour targeting strategies could be developed.[21] For example, it was found that the altered activity or the overexpression of key tyrosine kinase (TK) proteins in tumours result in the abnormal phosphorylation of target effectors that activate signalling pathways and drive cancer cell growth. Therefore, the use of selective kinase inhibitors as targeted anticancer agents gained popularity amongst the pharmaceutical industries.[22] Approved by the FDA in 2001, imatinib was the first compound of this class to enter the market. This drug is indicated for the treatment of chronic myelogenous leukemia patients expressing the BCRABL fusion protein, which is the result of an abnormal gene translocation.[23] While imatinib was the 5th best-selling anticancer drug in 2014, at least 20 other receptor TK inhibitors (e.g. sunitinib, erlotinib, crizotinib, axitinib and gefitinib) have broken into the market as inhibitors of aberrant phosphorylations in various cancers, such as renal cell carcinoma, and non-small cell lung cancer.[24]

Besides the active research on inhibitors of receptor tyrosine kinases, a large variety of "targeted" pharmacological approaches still rely on the administration of traditional cytotoxic agents, which are chemically modified or incorporated within suitable macromolecular structures to improve their therapeutic window. For example, anticancer agents have been incorporated into nanoparticles (e.g. liposomes, polymers and micelles) to exploit the leaky vasculature of several tumour masses.[25] Unlike in normal tissues, solid tumour vasculature allows the extravasation of these large nanomedicines, resulting in a more selective drug accumulation at the tumour site. This is termed the enhanced permeability and retention (EPR) effect.[26]

Among the known hallmarks of cancer, the EPR effect is arguably the most exploited strategy to improve the delivery of cytotoxic agents to tumours and, relying on the pathological features of the targeted tissue, is generally

classified as a “passive drug targeting” approach. Examples of passively-targeted nanomedicines that have been approved for clinical use are both PEGylated (Doxil®/Caelyx®) and non-PEGylated (Myocet®/, Daunoxome®) liposomal anthracyclines, and albumin-based pacitaxel (Abraxane®).[27]

As an alternative to passive drug targeting approaches, the evidence that tumours often express different receptors, enzymes and other proteins in higher amounts than normal tissues, gave rise to active drug targeting strategies. Here, recognition of tumour cells is made possible by the covalent conjugation of cytotoxic agents to targeting vehicles that bind specific tumour antigens. Such vehicles have included but are not limited to monoclonal antibodies, vitamins, peptides and substrate analogues. These drug delivery systems are designed to release the cytotoxic payload only after the ligand binding to the target.[28]

These active targeting strategies have shown promise for the improvement of existing, known chemotherapeutic agents. Of particular success and interest has been the development of antibody-drug conjugates.

1.2 Antibody Drug Conjugates

Antibody-drug conjugates (ADCs) are composed of a recombinant monoclonal antibody (mAb) connected via a synthetic linker to a highly cytotoxic drug molecule.[29] These agents became of interest for the treatment of cancer due to the combination of antitumour potency of cytotoxic small-molecule drugs with the selective targeting properties and advantageous pharmacokinetic profile of antibodies. The way in which these agents work relies on the delivery of a cytotoxic warhead to a specific location by the antibody. The ADC is then taken up by the cell, usually by receptor mediated endocytosis, where, upon lysosomal degradation, the active warhead is released (Figure 1.4).[30]

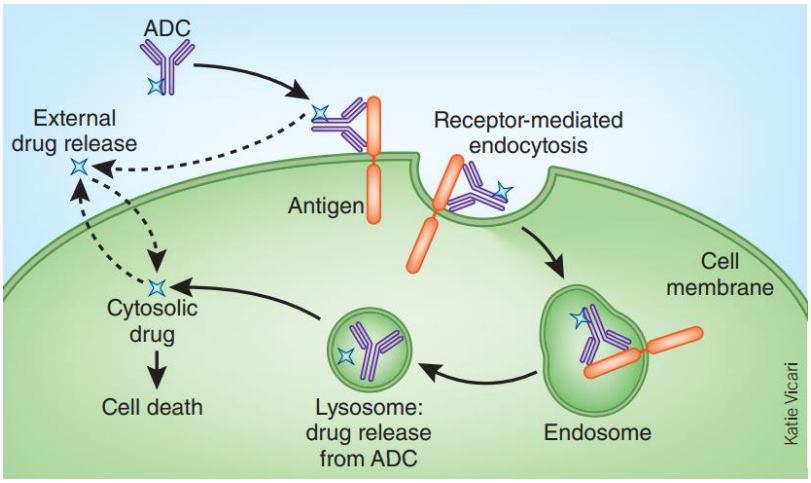

Figure 1.4: schematic representation of the mechanism of drug delivery mediated by ADCs.[31]

The development of ADCs is not a recent idea with the first use within animal models coming in the 1960s.[32] Since this date, the interest levels surrounding ADCs has risen dramatically due to the potential of these agents to change the way we look at chemotherapy. Since the first approval of Mylotarg® in 2000 and its subsequent withdrawal in the year 2010, the ADC market has evolved considerably. In the last eight years, the market has witnessed an increasing interest from drug developers and healthcare investors alike. Post the commercialisation of brentuximab vedotin (Adcetris®) in 2011 and trastuzumab emtanzine (Kadcyla®) in 2013, there was a temporary, but evident, decline in the popularity of ADCs.[33] This was attributed to the fact that no new ADC candidates were approved after 2013 and the focus had shifted to other novel therapies. However, the recent approval of Besponsa® and re-approval of Mylotarg® has renewed the interest in the domain. This is evident when you look at current clinical trials with over 60 ADCs undertaking the process.[34]

1.2.1 First Generation Antibody-Drug Conjugates

The development of ADCs was driven by the need to improve the tumour selectivity of clinically used anticancer drugs. The limited efficacy of many of these drugs can be attributed to their insufficient therapeutic window so finding novel ways to overcome this limitation was prerequisite. Despite little understanding of which roles antibodies play within cancer, it became clear that many mAbs displayed preferential binding to tumour cells. These

studies paved a way towards an idea of mAbs being used as delivery vehicles for current antitumour agents. Initially the agents of interest included doxorubicin, vinblastine and melphalan. In spite of initial focus lying on the antibody and cytotoxic drug, it became evident that the linker which connects these two components is also of vital importance. With encouraging preclinical results, a number of these first generation ADCs moved into phase I clinical trials with a doxorubicin based ADC eventually reaching phase II clinical trials (Figure 1.5).[34] However, all of these initial ADCs failed to progress beyond this stage due to a lack of clinically meaningful therapeutic activity and poor selectivity profiles.

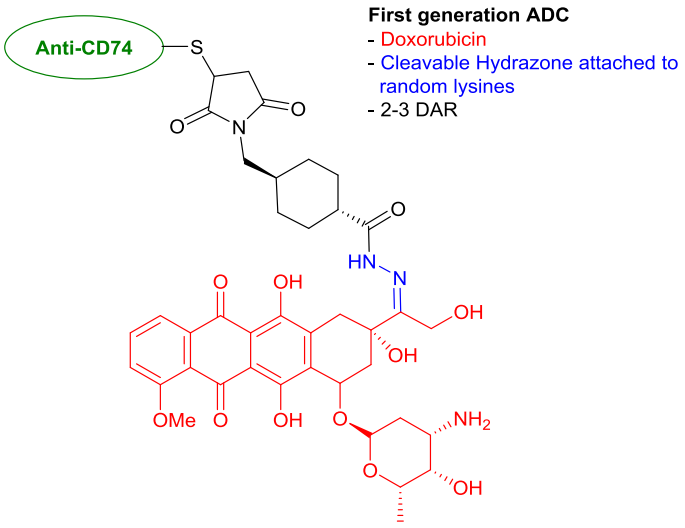

Figure 1.5: example of a first generation antibody-drug conjugate.

1.2.2 Improved ADC Development

With this lack of success in clinical trials, it was clear that a more careful consideration of each individual component of the ADC was required. It was hoped that through this, a more successful outcome within trials could be achieved.

The cytotoxic agent

With an understanding of the processes involved in cellular uptake of ADCs came the realisation that warheads with sub nanomolar activity were needed to achieve the potencies required for success within patients. This realisation

was achieved through research that suggested the delivery of cytotoxic molecules to tumours via an antibody was limited by two factors:

1. The number of antigen molecules present on the cell surface

2. Internalisation of cell-surface bound antigen-antibody complex or intracellular processing to release the active drug moiety.[34]

For this reason, current ADC research focuses on the discovery and exploitation of more potent cytotoxic agents. Moreover, with many cytotoxic agents being hydrophobic and likely to result in antibody aggregation upon conjugation, synthetic strategies to overcome this have been at the forefront of much research. Antimitotic agents and DNA interacting agents are two broad cytotoxic drug classes which have received an increase in attention for research surrounding ADC development. For example, the maytansinoid and auristatin families are two drug classifications which are often seen to dominate the ADC clinical landscape. This is due to their potent biological activity and also their success in previously approved ADCs.[35] The antimitotic agent maytansine (Figure 1.6), for example, has been adapted for inclusion onto an antibody to produce the clinically approved Kadcyla®.[36] In terms of DNA interacting agents, the calicheamicin (Figure 1.6) family is employed in the formation of Besponsa® which is the most recently approved ADC available.[37] These DNA interacting agents have been some of the most potent antitumour agents discovered to date and work through inducing DNA cleavage via the formation of diradical based species and subsequent hydrogen abstraction from both strands of the duplex DNA. This process ultimately leads to cellular death.[38]

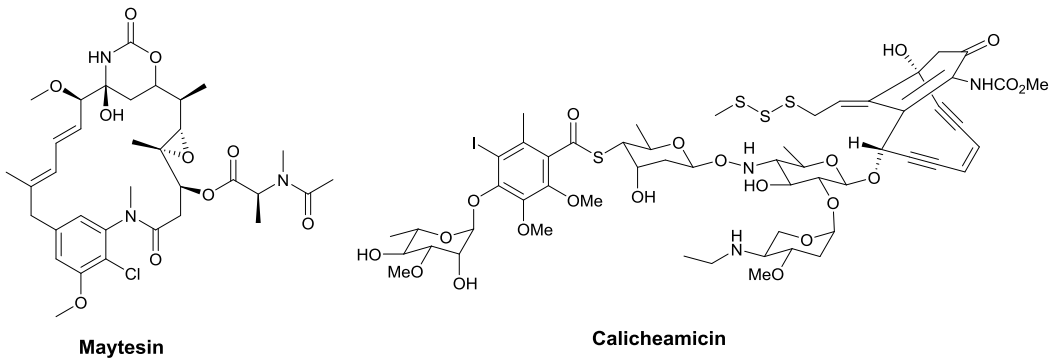

Figure 1.6: structures of Maytesin and Calcheamicin – commonly employed warheads in antibody-drug conjugates.

Other DNA damaging agents currently under study for the development of ADC like systems include the duocarmycins and pyrrolebenzodiazapines which both show activity to the desired picomolar range.[39]

The Linker

The key function of the linker is to provide a stable connection between the cytotoxic agent and the antibody, thus allowing for preferential systemic circulation and an avoidance of systemic toxicity. Despite the need for this stability during circulation, the linker should permit ADC cleavage upon internalisation to allow for the targeted cellular release of the potent cytotoxic drug. It is therefore of importance that a balance between these two factors is achieved and this is seen as one of the main challenges when it comes to ADC development.[34]

Linkers which are currently employed within approved second and third generation ADCs are broadly classified into cleavable and non-cleavable varieties (Table 1.1).[40] Cleavable linkers can not only be sensitive to lysosomal proteases, but also to the acidic pH within the cell and to cellular reducing agents such as glutathione. Examples of such linkers include the acid sensitive hydrazone linker, the now widely used cathepsin B sensitive valine-citrulline bond and also a glutathione cleavable disulphide bridge.[41] Non-cleavable linkers are designed to enhance the systemic circulation properties and unlike cleavable linkers, rely on the proteolytic degradation of the ADC to release the linker-drug moiety attached to the antibody. Examples of non-cleavable linkers include the thioether linker succinimidyl-4-(*N*-maleimidomethyl) cyclohexane-1-carboxylate (SMCC) or a maleimidocaproic acid linker.[42]

Table 1.1: commonly employed linker strategies used in antibody-drug conjugates broadly classified as cleavable and non-cleavable. The cleavage sites are shown in red.

Cleavable Linkers	Non-cleavable Linkers
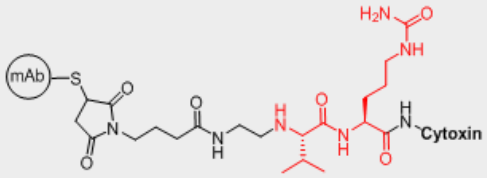 Peptide Cleavable Sequence (Protease)	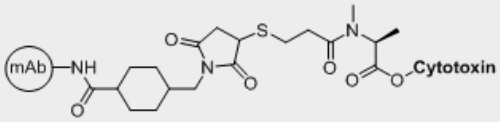 N-maleimidomethylcyclohexane-1-carboxylate
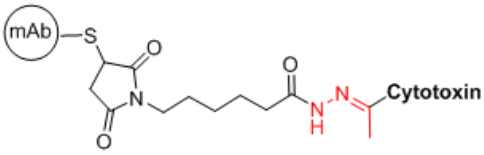 Hydrazone (Acid Labile)	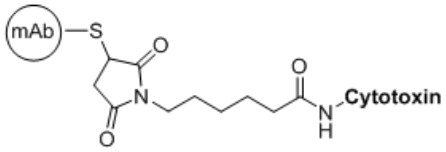 Maleimidocaproyl
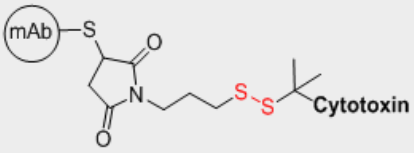 Disulphide (glutathione)	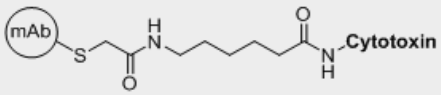 mercaptoacetamidocaproyl

A more recently discovered consideration when discussing the linker employed for ADCs is the potential for what is known as the by-stander effect. Solid tumours often express the target antigen in a heterogeneous manner. As a result, ADCs that selectively kill only antigen-positive cells and spare neighbouring antigen-negative cancer cells may be ineffective in eradicating such tumours. Therefore, ADCs may be designed to kill not only antigen-positive cells but also other cells in the vicinity, irrespective of the expression of the target antigen.[43] This can be achieved by consideration of the linker degradation processes.[44] For example a combination of a disulphide bridge along with a Monomethyl auristatin E (MMAE) payload has seen desirable bystander effects since the disulphide bridge can be cleaved outside of the cell releasing the neutral MMAE, which is able to cross

biomembranes and hence exert its effect on those tumour cells that may not display the targeted antigen.[45-47]

The Antibody

Structurally, all antibodies consist of two heavy and two light chains forming two Fab arms containing identical domains at either end. This is then attached by a flexible hinge region to the stem of the antibody, the Fc domain (Figure 1.7).[48] The Fab domains consist of two variable and two constant domains, with the two variable domains making up the variable fragment (Fv), which provides the antigen specificity of the antibody. Each variable domain contains three hypervariable loops, known as complementarity determining regions (CDRs), evenly distributed between four less variable framework (FR) regions. It is the CDRs that provide a specific antigen recognition site on the surface of the antibody and the hypervariability of these regions enables antibodies to recognise an almost unlimited number of antigens.[49]

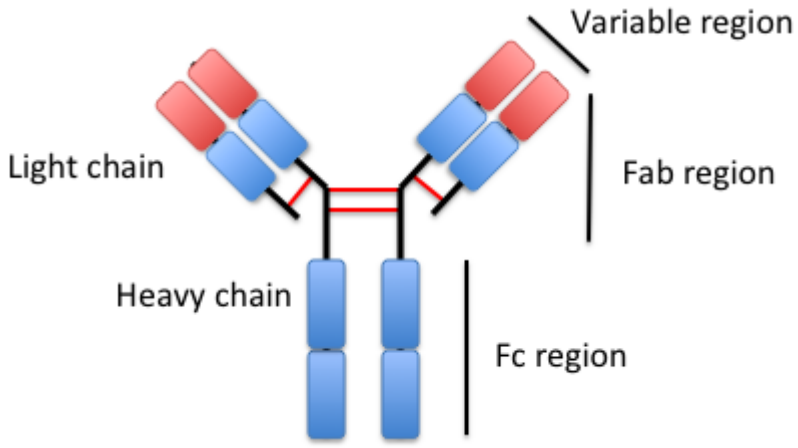

Figure 1.7: schematic representation of the structure of an antibody. The red section depicts the variable region whilst blue depicts the constant region.[62]

The key function of the antibody in an ADC is to preferentially bind to antigens on the target cell and hence concentrate the cytotoxic agent at the desired location. It is therefore important that the target antigen should have high expression levels in tumours and little or no expression in normal tissues. This ensures that the release of the cytotoxic agent at undesired locations is avoided and hence toxicities are reduced. Of similar importance is the requirement of the antigen to be accessible to the circulating mAb and

also the requirement of the antibody to be efficiently internalised upon binding to the antigen. This internalisation usually occurs through receptor-mediated endocytosis which the efficiency of is often dependent upon the nature of the receptor.[50]

The discovery of antigens and its antibodies that fit the above criteria is not a trivial task. Therefore much research still focuses on this area. The human epidermal growth factor receptor 2 (HER2) is currently one of the most understood and targeted receptors with the ADC Kadcyla® exerting its activity through an interaction with this antigen.[36] More recent developments when it comes to the antibody employed in ADC systems is the use of a biparatopic antibody. A biparatopic antibody is one in which the first antigen-binding moiety and the second antigen-binding moiety bind to different epitopes on the same antigen. A biparatopic antibody may also bind to two epitopes on the same antigen molecule, or it may bind to epitopes on two different antigen molecules.[51] The use of such a system has shown success over current ADC systems employed in the clinic. For example, Coats and co-workers showed how a biparatopic based HER2 targeting ADC can enhance toxin delivery and induce a greater breadth of tumour killing in comparison to trastuzumab emtansine.[52]

1.2.3 Current Antibody-Drug Conjugates

Through careful consideration of the above key parameters, the success of ADCs within clinical development has improved dramatically. As previously discussed, four ADCs are now approved for clinical use by the FDA and many more are in clinical development. Despite second generation antibody drug conjugates overcoming many of the hurdles preventing the success of the first generation, these agents are still not without remaining challenges. These enduring concerns have expedited the introduction of a third generation of ADCs which seek to reduce the heterogeneous nature of these agents through the introduction of site specific conjugations. This allows for defined drug antibody ratios (DARs) (Figure 1.8).[53] This is seen as of paramount importance for the continuing success of these systems into the future. Additionally, to further increase the therapeutic index of ADCs, improvements must be made either in the potency of the cytotoxic agent to

lower the minimum effective dose or in tumour selectivity to increase the maximum tolerated dose.[34] Therefore, within ADC research, there remains a need to discover and optimise highly efficient and active payloads for use in such systems.

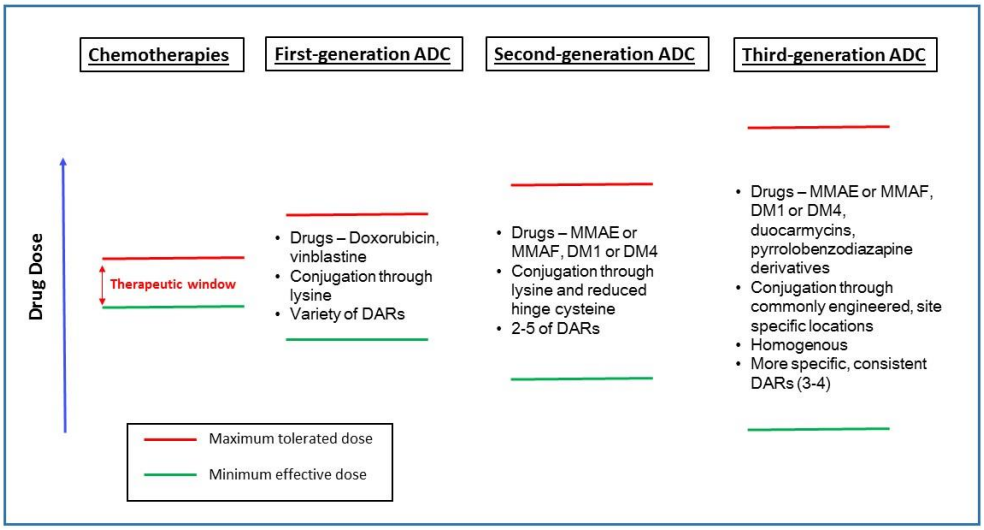

Figure 1.8: schematic demonstrating the progression of antibody drug conjugates from first generation through to third and also the effect this has had on the therapeutic window of ADCs.

Table 1.2: examples of ADCs currently approved or progressing within clinical trials.[34]

Agent	Developer	Status	Antigen/ Target	Cytotoxin	Linker
Brentuximab vedotin (Adcetris)	Seattle Genetics/Takeda	Entered market 2011	CD30	MMAE	Val-Cit
Glembatumumab vedotin	Celldex	Pivotal phase II	CPNMB	MMAE	Val-Cit
Depatuxizumab mafodotin	Seattle Genetics	Phase II	CD19	MMAF	Maleimido-caproic acid
AGS-16C3F	Agensys/Astellas	Phase II	ENPP3	MMAF	Maleimido-caproic acid
PSMA ADC	Progenics/Seattle genetics	Phase II	PSMA	MMAE	Val-Cit
Polatuzumab vedotin	Genentech/Roche	Phase II	CD79b	MMAE	Val-Cit
CDX-014	Celldex	Phase I/II	TIM1	MMAE	Val-Cit
Enfortumb vedotin	Agensys/Astellas	Phase I	Nectin 4	MMAE	Val-Cit
Telisotuzumab	AbbVie/Pierre Fabre	Phase I	HGFR	MMAE	Val-Cit
Trastuzumab emtansine (Kadcyla)	ImmunoGen	Entered market 2013	HER2	DM1	SMCC
Mirvetuximab soravtansine	ImmunoGen	Phase III	FOLR1	DM4	Sulfo-SPDB
Coltuximab ravtansine	ImmunoGen	Phase II	CD19	DM4	SPDB
Naratuximab emtansine	ImmunoGen	Phase II	CD37	DM1	SMCC
Indatuximab ravtansine	Biotest	Phase II	CD138	DM4	SPDB
Anetumab ravtansine	Bayer HealthCare	Phase II	Mesothelin	DM4	SPDB
SAR408701	Sanofi	Phase II	CEACAM5	DM4	SPDB
Gemtuzumab ozogamicin	Pfizer		CD33	CM1	Hydrazone
Inotuzumab ozogamicin (Besponsa)	Pfizer	Entered market 2017	CD22	CM1	Hydrazone
PF-06647263	Pfizer/AbbVie	Phase I	Ephrin A4	CM1	Hydrazone
Vadastuximab talrine	Seattle Genetics	Phase III	CD33	SGD1882	Val-Ala
SGN-CD70A	Seattle Genetics	Phase I	CD70	SGD1882	Val-Ala
Rovalpituzumab tesirine	AbbVie	Phase III	DLL3	SG3199	PEG8-Val-Ala
Trastuzumab duocarmazine	Synthon	Phase I	HER2	*Seco*-DUBA	Val-Cit
Sacituzumab govitecan	Immunomedics	Phase III	TROP2	SN38	CL2A
Labetuzumab govitecan	Immunomedics	Phase II	CEACAM5	SN38	CL2A
IMGN779	ImmunoGen	Phase I	CD33	DGN462	Sulfo-SPDB

1.3 CC-1065 and the Duocarmycin Family

CC-1065 and the duocarmycins (Figure 1.9) are a family of ultrapotent, antitumour antibiotic natural products isolated from broth cultures of Streptomyces species.[54, 55] In 1978 the parent member of this family, CC-1065, was reported by Upjohn company and since then this class of compounds have captivated scientists and researchers worldwide.[56] This interest can be attributed to the impressive potency of these agents which at the time of discovery were some of the most potent to be discovered matched only by calicheamicin and other enediyne based agents. Following on from the isolation of CC-1065 came the discovery of a related set of compounds called the duocarmycins.[57] With similar potencies and related structures, these agents further ignited interest into the class of ultrapotent cytotoxic agents. More recently, the discovery and elucidation of the yatakemycin structure and its impressive biological activity has kept interest in these agents alive.[54]

As with many of the cytotoxic, natural product based compounds, the CC-1065 and duocarmycins have shown little success within clinical trials and this has been attributed to a combination of extreme potency and lack of selectivity. Despite this, research into these agents has adapted by studying ways in which these compounds can be successfully utilised or modified in order to improve their therapeutic window.

The following section will summarise the isolation, biological activity and mechanistic details of this exciting class of compounds. Details of recent research and strategies to get these compounds to succeed within a clinical setting will then be addressed.

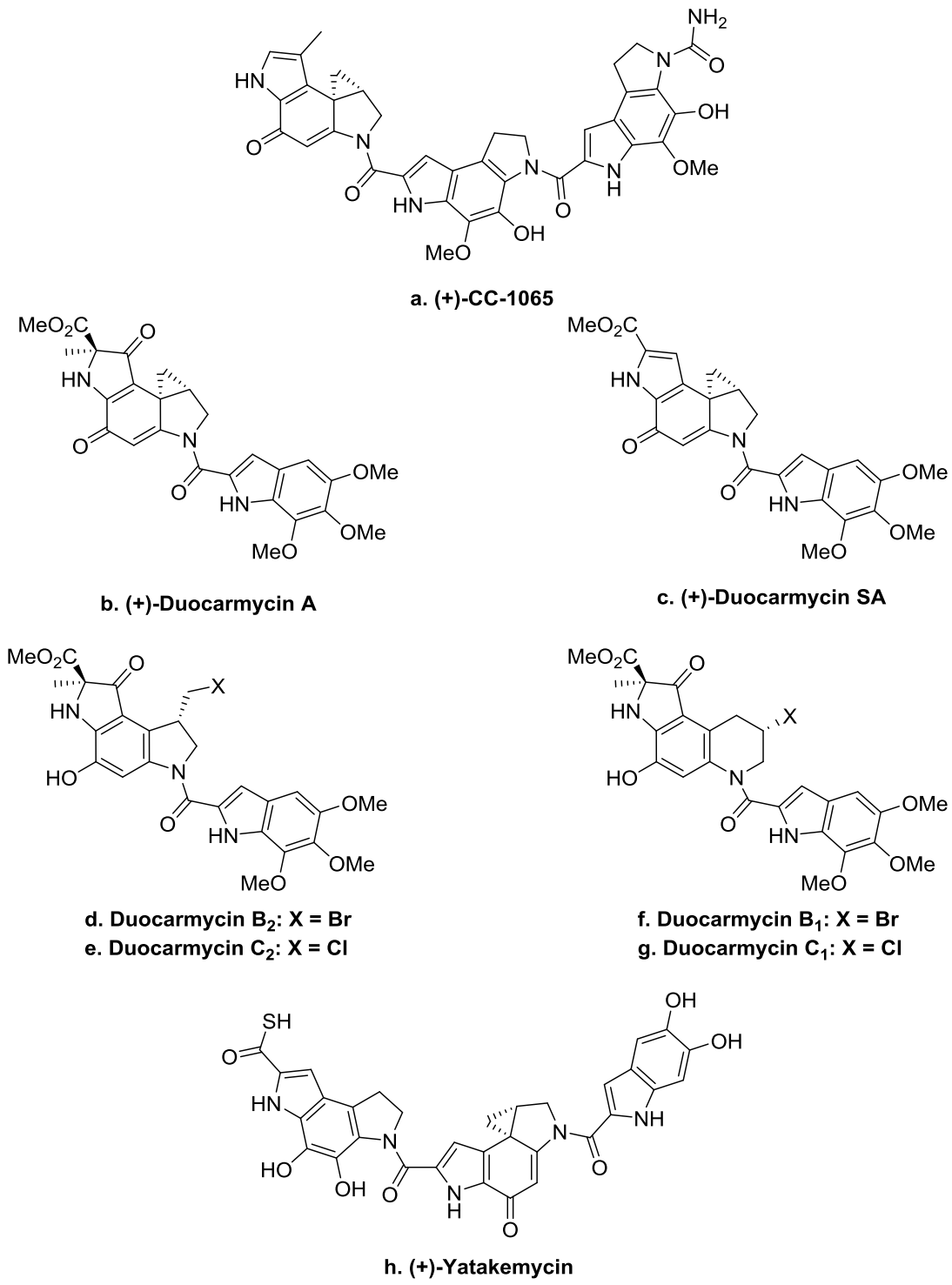

Figure 1.9: structures of CC-1065, duocarmycin A, SA, B_1, C_1, B_2, C_2 and Yatakeymcin

1.3.1 Isolation

During screening for soil cultures that produced agents with cytotoxic activity against L1210 cells in culture and *in vivo* activity against P388 leukaemia in mice, the potent antitumour antibiotic, CC-1065 was isolated from

Streptomyces zelensis.[58] The production, *in vitro* biological activity and microbiological assays for this agent were all completed and as mentioned, resulted in much interest into this compound. Studies into the structure of CC-1065 allowed for the derivation of a remarkably curved shape, which had charge density allowing for binding into the grooves of the DNA double helix. These findings along with the presence of an alkylating moiety led to the assumption that CC-1065 exerts its biological activity through a selective alkylation of DNA.[59]

Further screening studies resulted in the discovery of a class of antibiotics which were found to be very similar to CC-1065. The duocarmycins were isolated during screening for new antitumour antibiotics from actinomycetes. Initially this class of compounds consisted of duocarmycin A, B_1, B_2, C_1 and C_2; all produced by *Streptomyces*.[57] Later this was added to by duocarmycin SA which displayed IC_{50} values of 10^{-12} M - 10^{-9} M on HeLa S3 cells. Upon the derivation of the structure of these compounds and the discovered similarities which existed between them and CC-1065, it was assumed that both share a similar mechanism of biological activity.[60]

1.3.2 Biological Activity

CC-1065 and the duocarmycins share many common structural features of known DNA minor groove binders including netropsin and distamycin and hence it came as no surprise that these agents also bound to the minor groove. This is demonstrated in Figure 1.10, which also shows how the opposite enantiomer to the natural product binds in the opposite direction.[55]

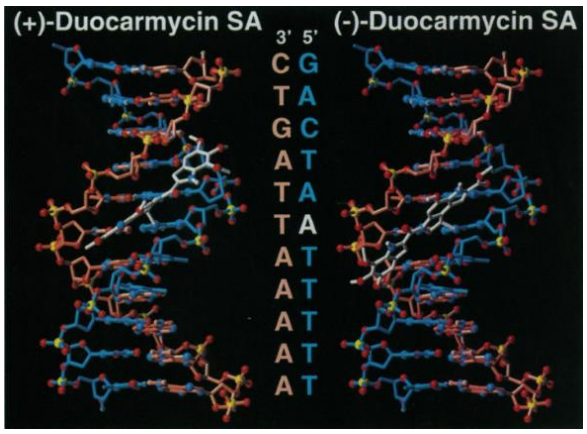

Figure 1.10: comparison stick models demonstrating the binding and alkylation of the natural (left) and unnatural (right) enantiomers of duocarmycin SA. The natural enantiomer binds in the 3' to 5' direction while the unnatural enantiomer binds 5' to 3'.[55]

The structures of this family of compounds were derived using NMR and other spectroscopic techniques. The CC-1065 and duocarmycins were all found to contain two distinct moieties with varying roles (Figure 1.11).[61, 62]

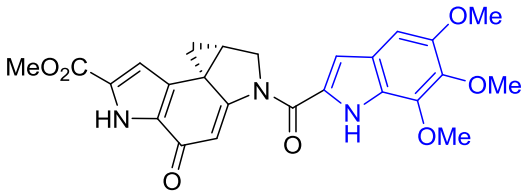

Alkylating Subunit Binding Subunit

Figure 1.11: structure of duocarmycin SA demonstrating the key subunits vital for the binding to and alkylation of DNA. The black region depicts the alkylating subunit whilst the blue section depicts the binding subunit.

The biological effect of the family occurs due to a sequence-selective alkylation of DNA. The reversible, stereoelectronically controlled adenine-N3 addition to the least substituted cyclopropane carbon has been found to occur within selected AT rich sites in the minor groove.[63] GC rich sequences tend to be wider and have more steric hindrance and are hence less favoured. This alkylation is thought to instigate a cascade of cellular events leading to apoptosis.[64] Despite over 40 years of research, the particular events which lead to apoptosis are still not universally reported. Extensive efforts have been devoted to determine the origin of the DNA alkylation selectivity, to establish the link between DNA alkylation and the resultant biological properties and to define the fundamental principles underlying the relationships between structure, chemical reactivity, and biological activity.

As well as their incredible potency, a further intriguing property discovered for this class of compounds was their stability. The solvolysis half-life at pH 7.6 for duocarmycin SA is estimated to be 820 years and when compared to the half-life for DNA alkylation (1.2 h) a rate enhancement of 7 x 10^6 is found.[65] Further studies found that the solvolysis reactivity of the CC-1065 and duocarmycin family is increased at acidic pH and this led to the assumption and possibility of an acid catalysed reaction occurring.[66, 67] However, this interaction and the mechanism behind it was further complicated when it was found that the more solvolytically stable an agent

was, the more potent its biological activity exerted. This idea of DNA-catalysed reactions was not unheard of with other cases being reported for platinum adduct formation amongst others. What was unusual however was the magnitude of the rate enhancement and a number of mechanisms to explain this were proposed.

The first of these mechanisms to be suggested was the local acid catalysis and bonding driven binding model (Figure 1.12). This model suggests that the selectivity of this family of compounds for its alkylation of DNA lay only within the alkylating subunit and that the binding subunit was necessary only for greater affinity binding. This mechanism however did not explain why, upon binding to DNA, the CC-1065 and duocarmycins alkylating subunit became much more reactive.[68] The model was therefore added to by the suggestion that local differences in pH on the DNA was resulting in this activity. These differences could be due to a protonated phosphodiester on the DNA backbone which could interact with the carbonyl of the minor groove binder.[69]

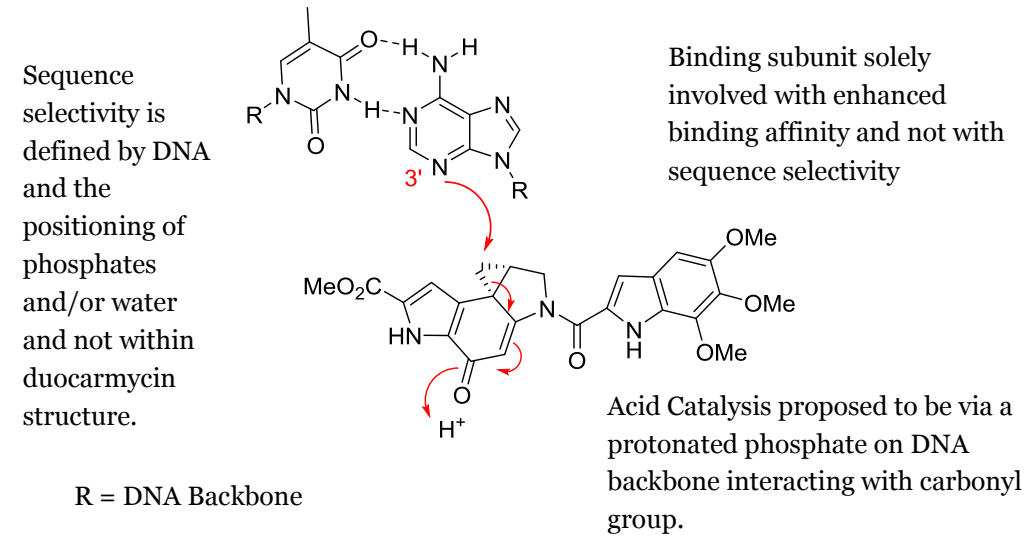

Figure 1.12: scheme showing a possible mechanism the DNA alkylation by the duocarmycin family of compounds - The local acid catalysis and bonding driven binding model.

Upon the completion of studies which utilised the comparison between synthetic analogues and the natural compounds, it became evident that the bonding-driven binding model was unable to explain the true mechanism of the duocarmycin family. A mechanism in which an alkylation event occurs based upon a non-covalent binding seemed to be more appropriate. These

studies involving the natural product analogues showed that the acid catalysis proposal concerning the protonated phosphate backbone interaction could not occur since when the carbonyl is alkylated or removed, a similar alkylation specificity is achieved. This showed that the carbonyl is not involved with sequence selectivity. Furthermore, a subunit which contains a carbonyl group which is completely inaccessible to the DNA backbone maintains full biological activity of the natural product..[69, 70]

These studies described above along with many others led to the proposal of the binding-driven bonding model (Figure 1.13) by Boger *et al.*[71] This model suggests that upon interaction with the DNA backbone, the duocarmycin undergoes a conformational change i.e. a twist in the structure between the alkylation and binding subunits. Bound to DNA, the molecule adopts a helical conformation where the two subunits are twisted approximately 45° with respect to one another. Although the bound agent sustains full amide character, the N12 is no longer co-planar with the cyclohexadienone system and so the vinylogous amide character is significantly disrupted. This in turn activates the cyclopropane ring to attack by the N3 position of adenine. This proposal of a disruption as a result of a conformation change has been reinforced by NMR studies involving the duocarmycins bound to the DNA.

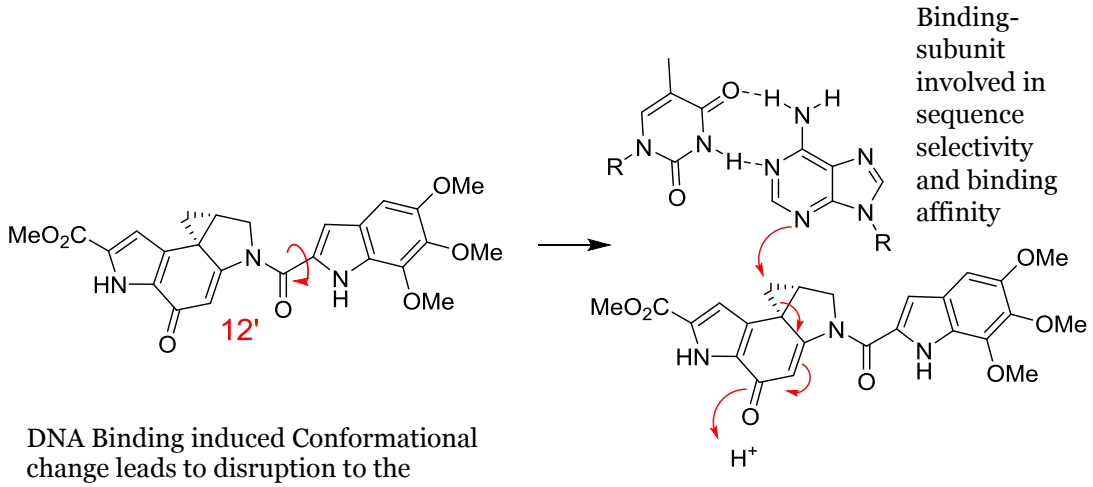

Figure 1.13: scheme showing the binding-driven bonding model of DNA alkylation by duocarmycin SA. This mechanism is now favoured over previously proposed mechanism.

1.3.3 Clinical Results of the Duocarmycins

The potency and broad spectrum of antitumour activity of the CC-1065 and duocarmycin family of compounds has demonstrated the potential of these agents as clinical candidates. Unfortunately, these agents showed unacceptably high toxicities for systemic use, and poor specificity meant they never fulfilled their potential as possible chemotherapeutic agents. CC-1065 showed a delayed death profile due to catastrophic hepatotoxicity in experimental animals.[72] Similarly, despite showing good stability-activity profiles, with no hepatotoxicity, duocarmycin SA was also found to be too toxic. This delayed toxicity has been attributed to the degree of reversibility of the DNA alkylation and hence to the level of non-covalent binding stabilisation of the reversible DNA adduct.[73] Regardless of these findings, duocarmycin SA remains the most promising starting point for the development of this family due to its reduced toxicity and notable potency.

In order for this class of compounds to fulfil their potential and gain an improved therapeutic index it was necessary to fully understand their reactivity and structural properties. This would allow for the development of compounds that may present improved biological profiles.

1.3.4 Alkylating Unit Structures

Despite the clinical failures of these compounds, much interest still existed. For instance, some research groups set out to investigate the synthesis and biological activity of alkylating pharmacophores and analogues. It was hoped that these investigations would allow for a clear relationship between structure, reactivity and biological activity. This in turn could enable these compounds to be adapted for clinical purposes.

Within these studies a group of alkylating pharmacophores were produced which include the subunits CI, CBI, CBQ and CPzI all of which differ slightly from the naturally occurring alkylating subunits found in DSA and CC-1065 (Figure 1.14). These various analogues of the alkylating subunit are now commonly employed in the ongoing research primarily due to their synthetic accessibility.

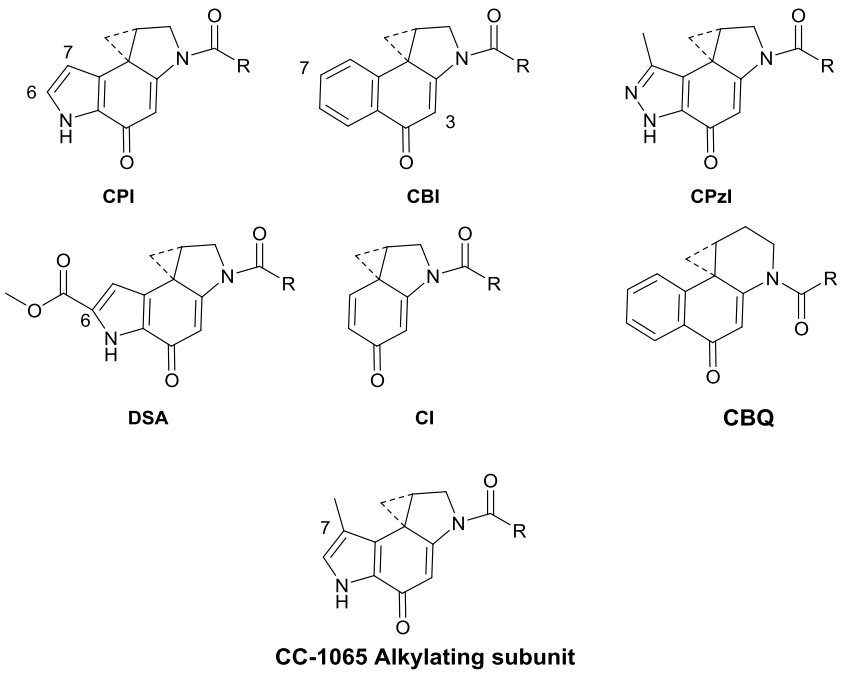

Figure 1.14: structure of the commonly studied alkylation subunit analogues.

What became clear from these structure-activity relationship studies was the novel parabolic correlation between the stability of these compounds and their potency. The overly reactive species will be nonselective with their reactivity to biological nucleophiles, whereas the species which are too unreactive will not have the ability to alkylate the DNA. A balance between these two properties is of paramount importance and investigations to find the peak of this correlation were carried out. It was found that duocarmycin SA alkylation subunit (DSA) lies at the peak whereas the CC-1065 subunit for example was too reactive and hence did not lie at the optimal position.[74, 75] This again shows that duocarmycin SA presents itself as an ideal starting point for further investigations. The CBI subunit (Figure 1.14) has been used extensively in SAR and prodrug strategy studies and this can be attributed to its chemical stability and ease of synthesis. This particular alkylating subunit is now commonly employed in duocarmycin ADCs which are in clinical development.

The extensive nature of the SAR studies, into the CC-1065 and duocarmycin family of compounds along with Boger's mechanistic studies allowed for a thorough understanding of the way in which these agents act and behave depending on their structures. This laid the seed for the design of strategies

such as prodrug formation, which may act to improve the therapeutic index of these agents.

1.3.5 General Prodrug Strategies

Despite their failure within a clinical setting, the CC-1065 and duocarmycin family of compounds still present an opportunity to develop an efficacious therapeutic agent. The recognition of a lack of selectivity in this family expedited strategies to overcome this flaw. One of the explored strategies has been the formation of prodrug analogues. A prodrug is a compound that, upon administration into an *in vivo* setting undergoes chemical conversion, often by metabolic processes, into an active pharmacological agent. The foundation of this strategy for agents such as the duocarmycins, is that these metabolic processes that form the active agent only occur within the vicinity of cancerous cells or tissue, thereby leaving healthy cells unharmed.

The majority of duocarmycin based prodrug strategies have relied on the masking of the required cyclopropane ring within the alkylating subunit of the active agent. The masking of this part of the molecule has been achieved through the formation of what is known as the *seco* form of the drug (Scheme 1.1). This involves the formation of a ring-opened derivative of the spirocyclopropyl-cyclohexadienone unit in which, a leaving group, commonly a halide, is employed. This leaving group can leave upon subsequent formation of the cyclohexadienone. In order to prevent this spontaneous cyclisation occurring before arrival at a specific *in vivo* target, a prodrug based strategy has been the addition of a group on the phenolic OH. Significant research has demonstrated a range of functionalities suitable for inclusion at this position to allow for successful chemical conversion to the active duocarmycin at the desired site.

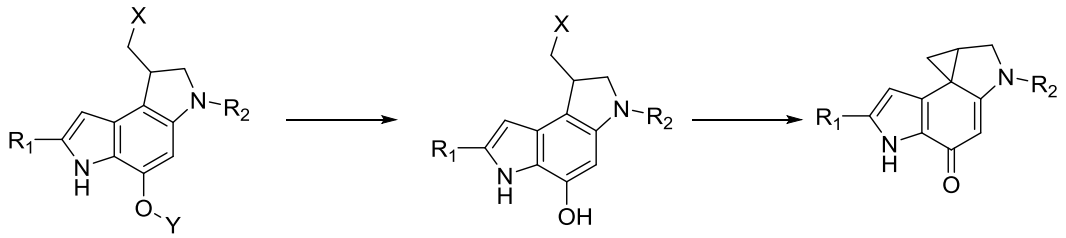

Prodrug Derivative ***seco* form** **Active Cyclohexadienone**

Where X = Leaving group (halide/sulfate)
Y = Cleavable protecting group (preventing spirocyclisation)

Scheme 1.1: activation of a protected *seco* based prodrug to give the pharmacologically active cyclohexadienone.

What follows is a non-exhaustive list of clinical candidates and chemical entities which have employed CC-1065/duocarmycin based prodrug strategies. The chosen compounds are those which have seen most success or generated most interest.

Carzelesin (Scheme 1.2) carries a phenyl carbamate unit attached to the phenol along with an additional diethylamine unit to increase the solubility of the drug. Activation of carzelesin requires two steps, (*a*) hydrolysis of the phenylurethane substituent to form U-76073, followed by (*b*) ring closure to form the cyclopropyl-containing DNA-reactive U-76074 (Scheme 1.2).[76] Although carzelesin was less potent in terms of *in vitro* cytotoxicity and *in vivo* optimal dosage, it was therapeutically more efficacious against mouse L1210 leukemia than was U-76074. Despite this impressive activity and demonstration of the utilisation of a carbamate prodrug strategy, Carzelesin failed to progress further than phase II trials due to the found haematologic toxicity of the drug.[77]

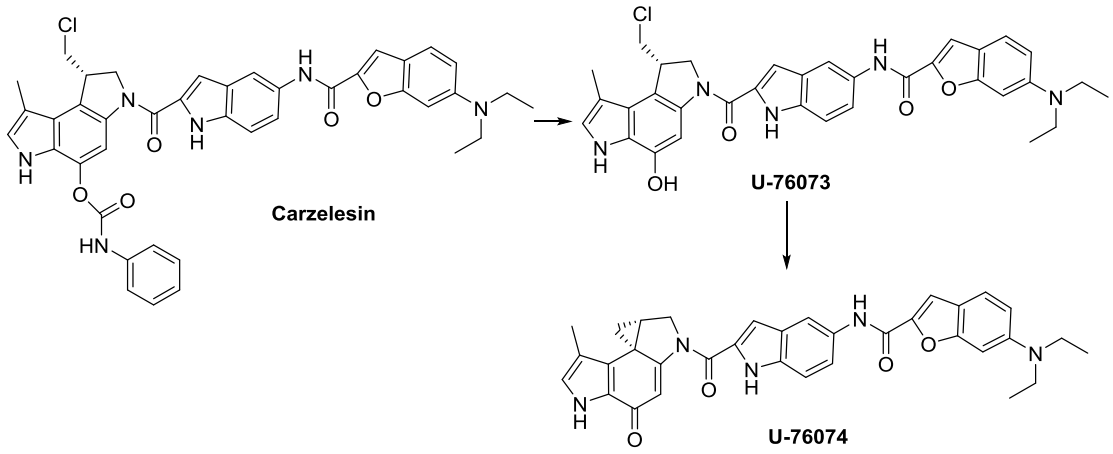

Scheme 1.2: activation of Carzelesin to give pharmacologically active U-76074.

Similarly, KW-2189 was a prodrug developed based upon an analogue of duocarmycin A, DU-86 (Scheme 1.3).[78] This agent was developed to be activated through enzyme hydrolysis to release DU-86. Despite the presence of the deactivating carbamate, KW-2189 was shown to be able to alkylate DNA prior to the removal of this moiety.[79] This is thought to be due to an alternative mechanism. KW-2189 was found to show insufficient antitumour activity in patients with malignant melanoma or advanced renal cell carcinoma, and hence further studies were not continued. However, KW-2189 has more recently been shown to be active in patients with hepatocellular carcinoma in a phase II clinical trial.[80]

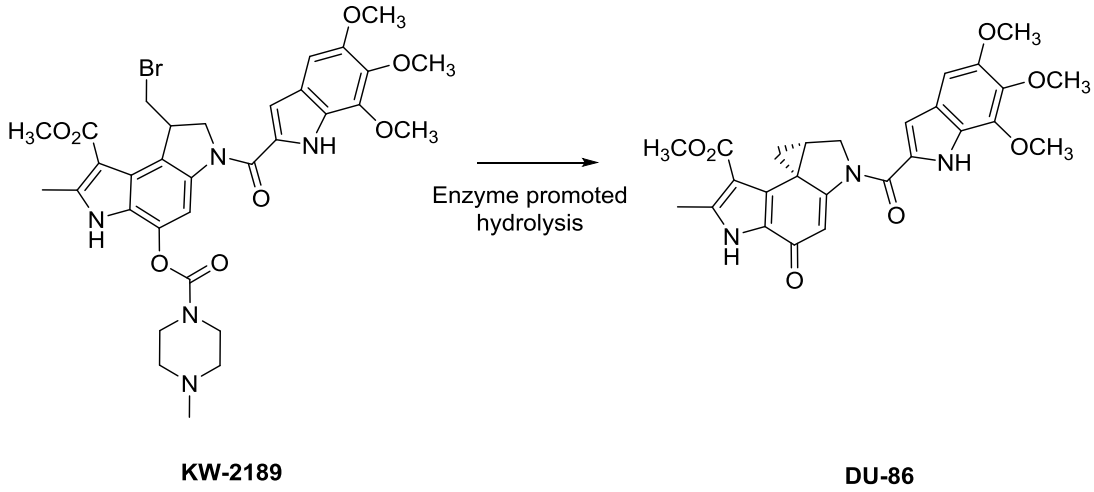

Scheme 1.3: structure and activation of KW-2189.

Further carbamate based prodrug strategies have included the introduction of an enzyme cleavable peptide sequence onto the phenolic OH (Figure 1.15). The cathepsin B cleavable Cbz-Val-Cit-PAMA was introduced by Venkatesan and co-workers, which, upon enzyme cleavage undergoes a self-immolative breakdown to deliver the pharmacologically active compound.[81] Since the cathepsin B enzyme is over expressed within cancerous cells in comparison to normal cells, this prodrug strategy presents an ability to introduce specificity into these agents. These peptide sequences have shown great success within numerous clinical candidates for achieving targeted activation at a specific location. Despite this, these sequences are not synthetically accessible and hence new routes towards making these amino acid-duocarmycin based agents would be desirable.

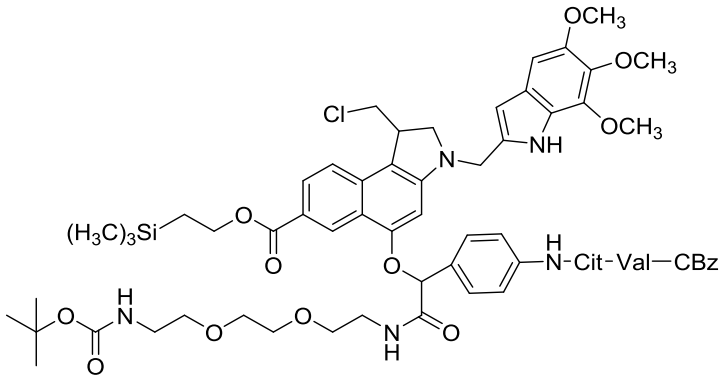

Figure 1.15: carbamate based prodrug utilising a cleavable peptide sequence.

Further strategies utilising the addition of moieties to the phenol of the *seco* form of the alkylating subunits make use of sugar conjugation (Figure 1.16). A galactoside protected methyl-*seco*-CBI analogue has been shown to hold a 770-fold increase in activity in the presence of galactosidase – an enzyme over expressed within cancerous cells (Figure 1.16).[82] Analogues of this agent with increased water solubility also greatly increased prodrug effectiveness demonstrating IC_{50s} which matched the free drug.[83] Studies which also took this analogue and removed the methyl substituent and introduced a water soluble DNA binding unit, further improved activity resulting in a significant IC_{50} value of 16 pM in the presence of galactosidase.[84]

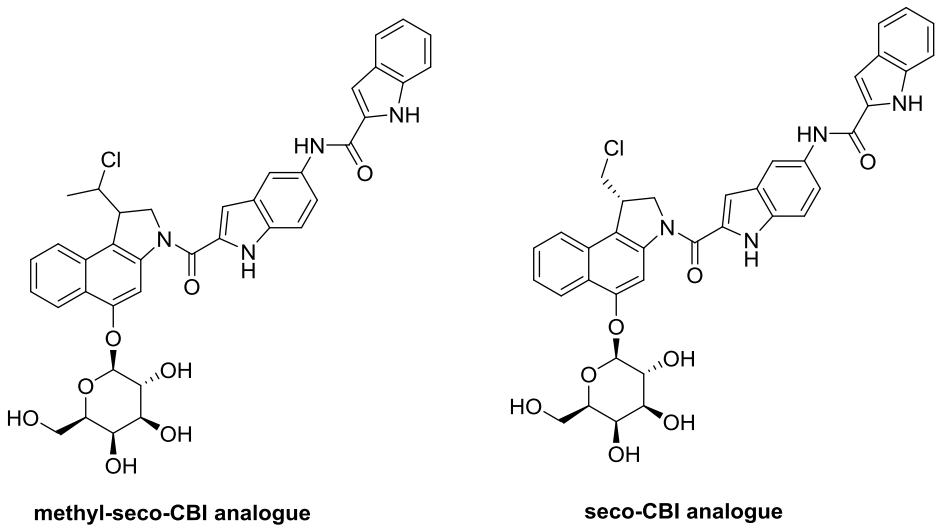

Figure 1.16: example structures of galactoside based prodrugs.

More recent strategies have employed the development of prodrugs which are photoactivatable. This strategy involves the introduction of a moiety, again attached to the phenol of the *seco* form of the active drug, which can be removed upon photoirradiation. Tietze and co-workers demonstrated the potential of this area (Scheme 1.4). The determination of the *in vitro* cytotoxicity by using an HTCFA-test revealed a QIC_{50} value of 8200 and the prodrug was shown to be more than two million times less cytotoxic than the corresponding *seco*-drug. With the *seco*-drug displaying an IC_{50} value of about 110 fM this agent warrants more research to further realise its potential.[85]

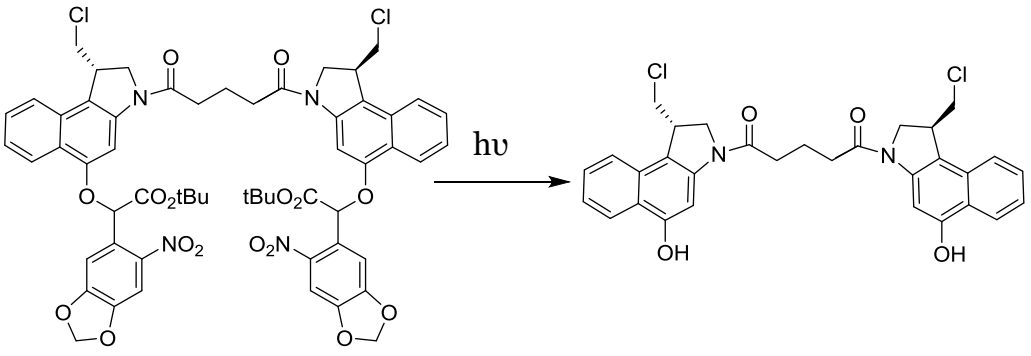

Scheme 1.4: example of a photoactivatable duocarmycin based prodrug and its activation.

Although incorporating protecting group strategies onto the phenolic oxygen has yielded some success in these agents, it can be easily imagined how this strategy could also have some drawbacks. Of particular importance could be

the lability of the protecting group during systemic circulation. With these compounds having the ability to spirocyclise to form the pharmacologically active compound, it can be proposed that this process, through deprotection of the phenol, could happen prior to arrival at a desired site. This in turn would account for the high toxicities that are retained for some of these agents despite the protecting strategy being in place.

Despite prodrug strategies further cementing the potential of the duocarmycin family of compounds for possible use as a cancer therapeutic, these strategies have yet to lead to the formation of a clinically successful candidate. Although this maybe the case, these studies were not without fruition. The formation of these compounds demonstrated the success of strategies including cleavable peptide sequences, locking compounds into the *seco* form and allowing for *in vitro/ in vivo* spirocyclisation.

With this lack of clinical success, trends within duocarmycin based research moved onto the use of these agents within antibody-drug conjugate like systems. It is thought that these systems could harness the potential of this family of compounds, with their ultra-potent activity, to create a clinically successful agent.

1.3.6 Duocarmycin in ADCs

With little success in the utilisation of other strategies to improve the therapeutic window of the duocarmycin family of compounds, focus turned onto the application of these agents within antibody-drug conjugate systems. With their impressive potency, reaching IC_{50}'s in the picomolar range, these compounds make an ideal candidate for introduction into such systems.

As it stands, the duocarmycins have been introduced into a number of conjugates with the marked distinction between these entities coming in the way or position at which the duocarmycin is conjugated to the antibody.

One such way in which this has been achieved is through a linker from the antibody to the binding subunit of the duocarmycin. As touched upon in Section 1.3.5., it could be that this strategy holds an advantage in that without conjugation via the phenolic oxygen, concerns about premature release of the

warhead due to the lability of this bond could be reduced. This therefore, could yield more desirable biological activities. This was demonstrated by ImmunoGen in work in which a CBI analogue was conjugated to an anti-CD19 or anti-CD56 antibody (Figure 1.17).[86] This work shows the use of the *seco* form of the drug molecule, as opposed to the spirocyclised active compound, in ADC systems – something which is now common practice. In this conjugate an unprotected form of the *seco* CBI unit was utilised along with two indole units, included to act as binding subunits in order to maximise biological activity. Prior to conjugation of the CBI analogue, the antibody was functionalised with SAMB (N'-succinimidyl 4-N-(2'-acetylthiopropionyl)-N-methyl-4-aminobutyrate) in order to provide a site of addition for the payload. This artificially introduced site was then deprotected using hydroxylamine before addition of the CBI based unit. The system described, demonstrated potent *in vitro* activity, in the range of 0.1 nM, and was shown to be selective for cell lines that expressed the specific antigen. The conjugates were also tested in a mouse xenograft model of leukaemia and had activity that compared well to commercial chemotherapeutics. Despite these positive results, these conjugates were not taken forward for further development due to their instability and poor aqueous solubility.[87]

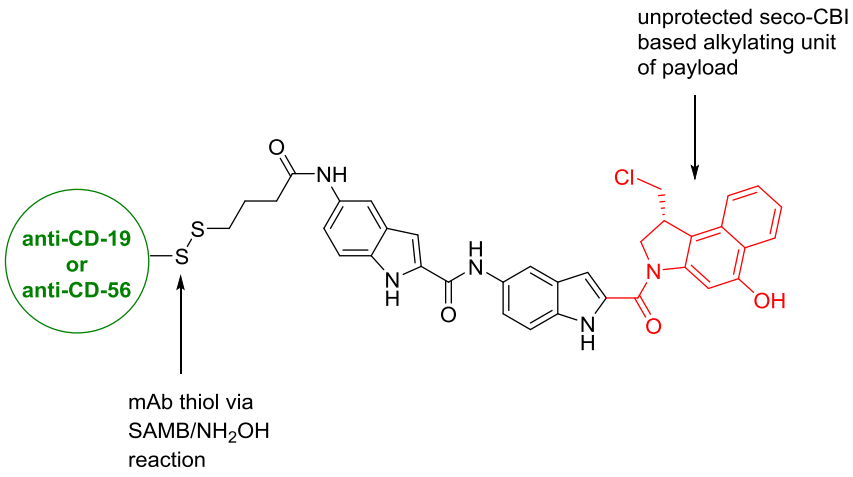

Figure 1.17: structure of a duocarmycin ADC in which the antibody is linked to the warhead through the binding subunit.

As a follow on from this initial work came the rationale that prodrug strategies such as those described earlier on in this chapter could be utilised

alongside the benefit of the targeting capabilities of an antibody. Through protection of the phenolic oxygen of the alkylating subunit of duocarmycin agents with a labile group, premature spirocyclisation within circulation could be prevented thereby further improving the therapeutic window of these ADC systems. One example of this is a strategy that utilises a carbamate based prodrug of a *seco*-CBI based payload. MDX-1203, is an ADC that was developed by Bristol-Meyers Squibb and reached Phase I clinical trial.[88] In this example, the payload is constituted by a duocarmycin MA (CBI + binding unit) protected as a carbamate (Figure 1.18). This example also demonstrates the use of a cleavable peptide sequence, which aims to aid the release of the payload from the antibody post arrival at the desired site of activity. The use of these cleavable peptide sequences, as discussed in the previous chapter has demonstrated a large amount of success in a variety of duocarmycin and non-duocarmycin based systems. A human monoclonal anti-CD70 antibody was chosen to target the CD70 receptor overexpressed in lymphomas but also in a number of solid tumours. The bioconjugation was obtained via maleimide-thiol reaction. The clinical trial highlighted delayed toxicity at the highest concentration tested, as observed for other non ADC duocarmycin derivatives. This could be as a direct result of early payload release. At the same concentration, sensitisation was also observed. Although efficacy is not the focus of Phase I clinical trials, it was noted that, depending on the dose administered, the best cases were either disease progression at lower doses, or stable disease at higher doses.[89] The development of this ADC has been terminated.

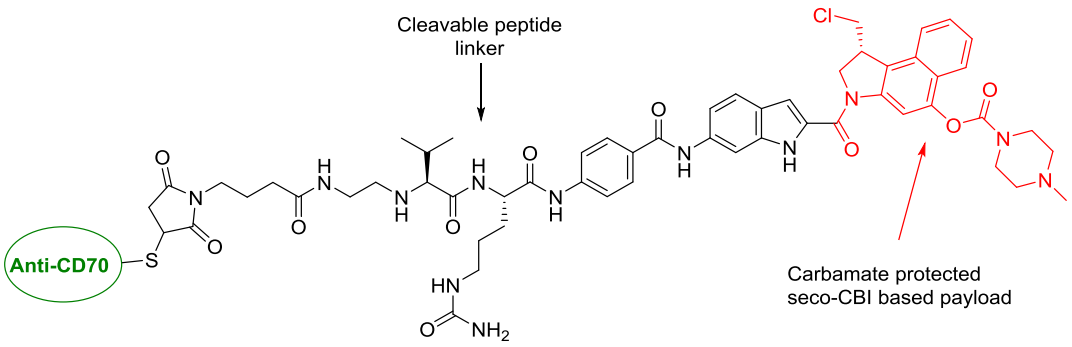

Figure 1.18: example of a duocarmycin ADC which utilises a carbamate based prodrug strategy.

With the solubility of duocarmycin based ADCs being a recurring issue in terms of clinical progression, ImmunoGen have reported conjugates (DC4 and DC44) which employ the use of a CC-1065 analogue with a phosphate group introduced onto the phenolic oxygen (Figure 1.19).[87] Not only does this act with similarities to the carbamate group in terms of hydrolytic release but it also aids aqueous solubility and stability. It was also hoped that the use of this group could reduce interpatient variability and be more efficient in comparison to other analogues. The bifunctional SMCC or SPDB linkers were exploited in the preparation of these conjugates. In the case of DC4 and DC44 anti-CanAg conjugates, the linker did not affect the biological activity or selectivity against CanAg positive COLO 205 cells versus A375, CanAg negative. Impressively, in these cell lines it was shown that the ADC is more potent than the free drug. This could be attributed to a more efficient delivery of the payload to the desired location. In comparison to the CanAg conjugates, the efficacy of the anti-CD19 conjugates was reliant on the nature of the linker with non-cleavable crosslinks leading to a considerably reduced potency. This was consistent for the DC44 conjugate with an SPDB linker, whose disulphide is more hindered and hence less labile to reduction pathways. It also appeared that Ramos cells, used as CD19 positive models in this study, produce slow rates of dephosphorylation which, coupled with a slow release of the payload, greatly affected the cytotoxicity of the conjugates in this model.

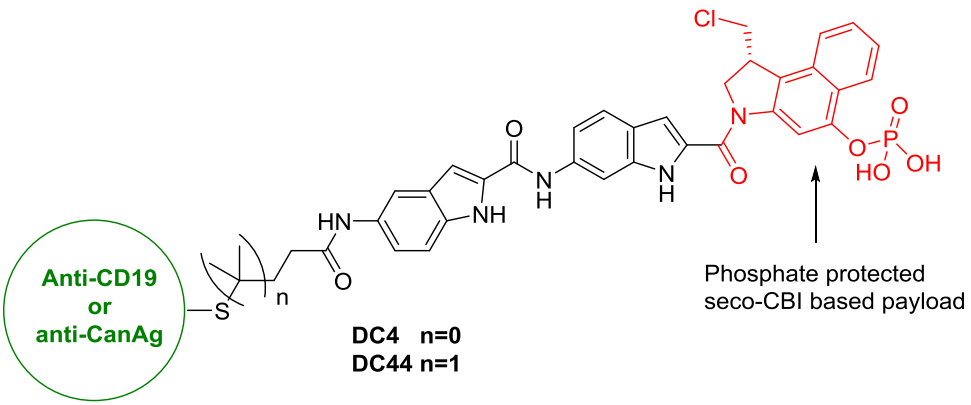

Figure 1.19: example of a duocarmycin ADC which utilises a phosphate base prodrug strategy. The phosphate group on the phenolic oxygen via hydrolysis to allow for spircyclisation to form the active duocarmycin warhead.

More recently within the field of duocarmycin-based ADCs has been a shift to a strategy which employs a conjugation route from duocarmycin to antibody via the phenolic oxygen of the duocarmycin. This strategy again combines the directing ability of the antibody with a prodrug approach in which the cleavage of the payload from the antibody will only result in the liberation of the pharmacologically active component. As of today this strategy has provided the most clinical success, most notably with Synthons's ADC, SYD985 (Scheme 1.5).[90, 91] The preparation of this conjugate involves the use of the HER2 targeting antibody, trastuzumab, which has been approved for breast cancer treatment in its own right. The conjugate also employs a cathepsin B cleavable peptide linker, PABC-Cit-Val, and a self immolative unit to release the free duocarmycin payload composed of *seco*-DUBA and an azaindole based binding subunit.

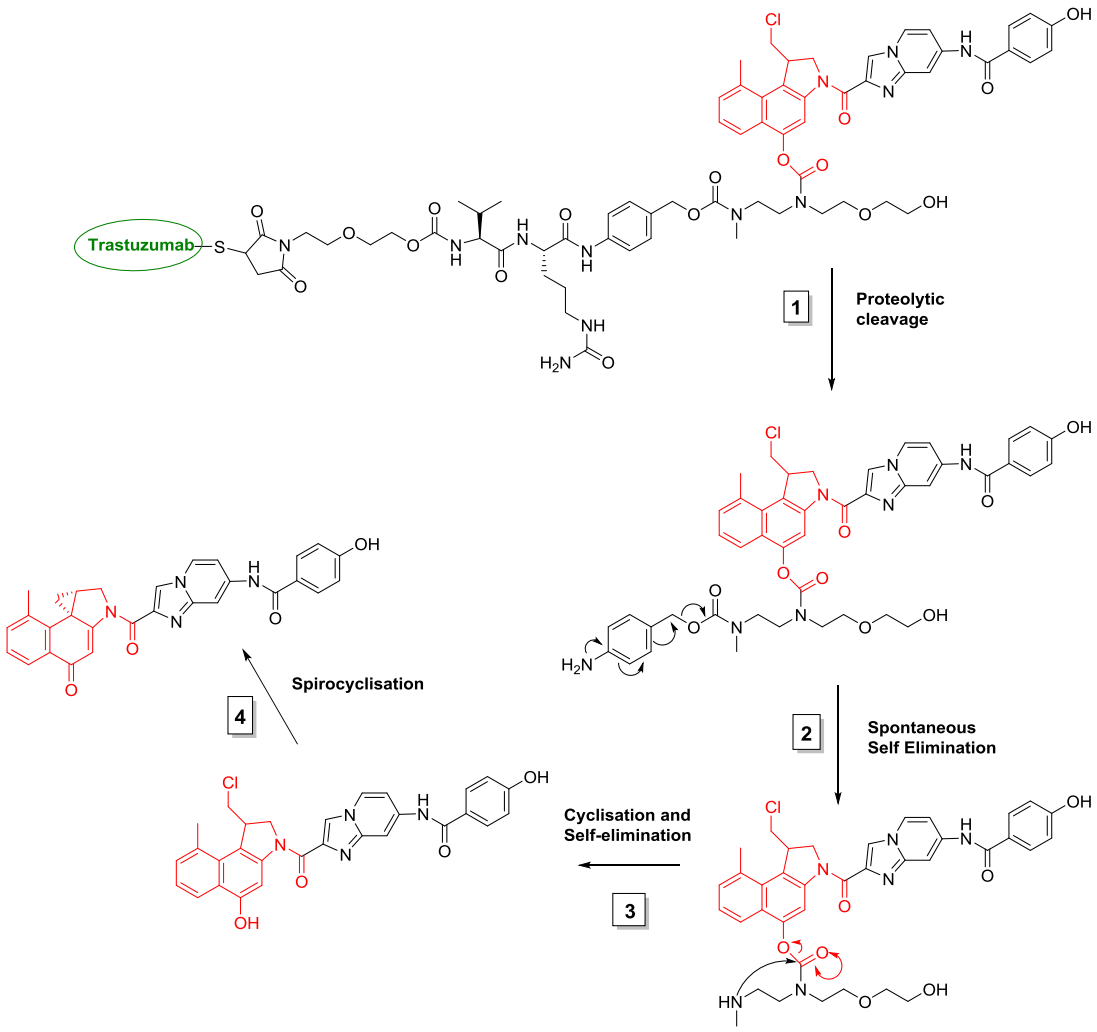

Scheme 1.5: scheme showing the activation of an antibody-drug conjugate, SYD983, which undergoes a four step mechanism to release the active duocarmycin.

Promising results were obtained for this conjugate in initial stages of Phase I clinical trials. Most noticeably, very high response rates and durable responses were observed in patients whose cancers were refractory to HER2-targeted agents, including trastuzumab and trastuzumab emtansine following treatment with SYD985 at doses from 1.2 mg/kg onwards.[92] As a result of these notable results, SYD985 has been granted fast track designation by the FDA. This designation is for the treatment of patients diagnosed with HER2-positive metastatic breast cancer who have progressed after different HER2-targeting treatment regimens, or have progressed during or after treatment with trastuzumab emtansine.

With these results, it is clear that employing an ADC or targeted delivery based system for the duocarmycin family of compounds has the promise to

yield real, clinical success for the first time for this class. Despite this, the generation and discovery of new antibodies is not trivial. In addition, the formation of new ADCs for various forms of cancer would require a number of these systems being generated which incorporate different antibodies. This again is certainly not a trivial task and hence whilst this area certainly provides promise, it could be that other targeting moieties and other unexplored targets could present advantages over antibody based delivery systems.

1.4 Aberrant Glycosylation Patterns in Cancer

The discovery that carbohydrate binding proteins (lectins) selectively agglutinate cancer cells gave an initial indication of the presence of certain variances between surface expressed carbohydrates in healthy and cancerous cells.[93, 94] Many carbohydrate patterns have been associated with the cancerous phenotype. Some include the over or underexpression of naturally occurring glycans, whilst more useful for targeted therapy purposes are those that show the novel expression of glycans only found in foetuses.[95] These provide an ideal target for delivery systems to explore. There are three main types of cell surface glycoproteins: asparagine attached N-linked glycans, O-linked glycans that are attached to serine or threonine residues, and glycosaminoglycans that are linked to serine residues. O-linked glycans were originally discovered in mucin, a protein found in mucus, and were therefore termed mucin-type glycans - many cancer-associated carbohydrates are known to be of this type.[96]

DNA mutations can lead to the overexpression, underexpression, or deletion of many genes resulting in a direct effect on the subsequent products, which can therefore be overexpressed, underexpressed or missing, respectively.[97] Altered levels of enzymes responsible for post-transcriptional glycosylation can be attributed to many of the glycan variations associated with cancer. A frequent change in surface carbohydrates of cancer cells is an increase in the amount of branching of N-glycans, which can be a direct consequence of the increased activity of the enzyme N-acetylglucosaminyltransferase V (GlcNAc-TV).[98] This enzyme causes branching of β1-6GlcNAc, which are further positions for the attachment of terminal sialic acid residues. Increased

activity of sialyltransferases causes an overall increase in sialylation of N-linked glycans, a common development in core carbohydrate structures at the surface of cancer cells. Early studies have established the relationship between excessive sialylation and increased metastasis. The overexpression of glycosyltransferases has also been connected to malignancy, as the downstream effect of the activity of these enzymes leads to the overexpression of many cancer-associated terminal glycan epitopes.[99] These include the Thomsen-Friedenreich (T) antigen, the Tn antigen, sialyl-Tn, polysialic acid (PSA), Sialyl Lewis A (sLea), Lewis Y (LeY) and Sialyl Lewis X (sLeX) (Table 1.3).

Table 1.3: cancer associated glycan epitopes and their respective structures expressed in symbol nomenclature.

Name	Structure
Tn antigen	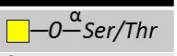
Sialyl-Tn antigen	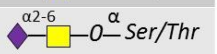
T antigen	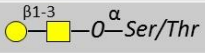
Sialyl-T antigen	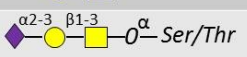
Lewis Y	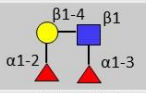
Sialyl Lewis A	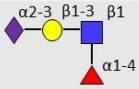
Sialyl Lewis X	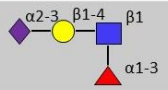
Polysialic Acid	

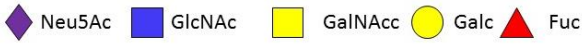

With a number of these glycans showing desirable levels of overexpression in cancer cells, it is clear that these antigens present themselves as ideal targets in addition to those commonly employed in current ADCs. Furthermore, with glycan binding often being correlated to improved cellular uptake, these relatively unexplored targets warrant greater levels of interest in the field of targeted chemotherapy. Of course, in order for this potential to be realised, moieties which specifically recognise and bind to these glycans with high affinity are required.

1.4.1 Targeting Cancer Associated Glycans

Numerous reports have confirmed the potential of lectins as tumour targeting agents, therapeutic agents and adjuvants for current cancer treatments. What follows is a non-exhaustive summary of lectins found to have cancer targeting and therapeutic properties. Discussed below some examples of lectins shown to demonstrate these properties whilst Table 1.4 provides a more exhaustive list of tumour targeting lectins.

Mistletoe (*Viscum album*) extracts have seen widespread use in pre-clinical and clinical studies for the treatment of a number of different cancers. The active component of mistletoe extracts is a lectin named mistletoe lectin-1 (ML-1).[100] Mistletoe extracts under clinical investigations include Iscador, Eurixor, Helixor, Lektinol, Isorel, Abnoba-viscum and recombinant ML-1. Phase I and II clinical trials have explored the efficacy of mistletoe extracts in the treatment of many different cancers including colorectal carcinoma, ovarian cancer, renal cell carcinoma, lung cancer and stomach cancer.[101, 102] These trials have demonstrated an increased quality of life, prolonged survival and reduction in the number of side effects in comparison with current treatments. The lectin consists of two chains; a cytotoxic enzymatic A chain and a sialic acid-binding B chain. The ML-1 displays specificity for gangliosides and glycoproteins expressing terminal Neu5Acα2- 6Gal1-4GlcNAc-, the overexpression of which has been associated with carcinomas. The therapeutic effect of ML-1 is a synergistic effect of both its direct cytotoxic effects and indirect immunomodulatory effects. The A chain is responsible for inducing apoptosis at low femtomolar-picomolar concentrations and the lectin can also activate immune cells, such as natural-killer cells, and heighten their cytotoxicity.[103, 104]

Peanut agglutinin (PNA), a further lectin, has been shown to selectively bind to the T-antigen but not the sialylated form of the antigen.[105] PNA only agglutinates human erythrocytes upon neuraminidase treatment, and has been shown to bind to MCF-7 and MDA-MB231 breast cancer cells with varying affinities.[106-108] PNA also binds to the sub-normal, non-tumorigenic breast cell line MCF-10A, although it's affinity is 10-fold lower towards the non-immortalised variant cell line MCF-10M. Despite the fact that the lectin has also been found to selectively target a variety of colon cancer cell lines,

PNA also demonstrates some undesirable activity for therapeutic purposes in that it is able to stimulate proliferation of some cells lines such as HT-29.[109]

The lectin extracted from *Artocarpus integrifolia* (jackfruit), jacalin, is also a T-antigen specific lectin.[110] This lectin has previously been shown to aid in both the targeted delivery and uptake of anticancer based therapeutics.[111] With its impressive specificity and selectivity for the cancer associated T-antigen, jacalin has the potential to impose itself as a validated targeted delivery moiety. More details on this lectin along with previous examples of targeted delivery using jacalin will be discussed in Chapter 3.

Table 1.4: examples of cancer targeting lectins alongside their associated antigen and cancer cell reactivity. [102, 109, 110, 112]

Lectin	Species	Carbohydrate Specificity	Tumour Antigen	Cancer Cell Reactivity
Mistletoe lectin 1	*Viscum album*	Neu5Acα2-6Gal1-4GlcNAc-	-	-
***Agaricus bisporus* lectin**	*Agaricus bisporus*	-Galβ-1,3GalNAc-α-*O*-ser/thr	T-antigen Sialyl-T antigen	Caco-2, HT-29, MCF-7 breast cancer cells
Peanut agglutinin	*Arachis hypogaea*	Galβ-1,3GalNAc-α*O*-ser/thr	T antigen	MCF-7, MDA-MB-231, HT-29, HCT-15
Jacalin	*Artocrapus integrifolia*	Galβ-1,3GalNAc-α-*O*-ser/thr	T antigen	Caco-2, HT-29
***Erythrina cristagalli* lectin**	*Erythrina cristagalli*	Galβ-1,4GlcNAc	Type II antigen	Caco-2

Owing to their remarkable specificity for a variety of cancer-associated carbohydrate based antigens, the lectins described above are proposed to be powerful prospective cancer targeting ligands. The specificity of lectins towards cancer cells, in addition to the remarkable biological effects that lectins can exert, such as apoptosis induction, inhibition of proliferation and immunomodulation, make lectins attractive multifunctional candidates for the targeted therapy of cancer.

As well as lectins, a number of peptides and small molecules have also been discovered which have demonstrated specific and selective binding to cancer associated glycans. It could be therefore that these moieties, like lectins,

could provide the desired properties to try and achieve the targeted delivery of current cytotoxic agents to cancerous tissue thereby improving their therapeutic index. Specifically, it is possible that these agents could present a new, unexplored area to achieve the targeted delivery of the duocarmycin family of compounds to cancer cells. This, along with what has been learnt through prodrug and ADC system development, could help to further realise the potential of these compounds as future cancer based therapeutics.

1.5 Thesis Outline

The work presented in this thesis focuses on the use of a duocarmycin analogue for the design and synthesis of conjugates to target the Thomsen-Friedenreich antigen expressed on cancer cells. **Chapter 2** of this thesis will detail the synthesis of a benzyl protected duocarmycin SA analogue that is suitably functionalised for Fmoc solid phase synthesis. This chapter will also look at attempted modifications made to the synthetic route and structure of this unit to try and achieve more efficient use on the solid phase. Finally, additional benzyl deprotection strategies to yield active duocarmycin conjugates will be addressed.

Chapter 3 will detail the design and synthesis of a variety of duocarmycin-lectin conjugates. This chapter will make use of the T-antigen targeting lectin, jacalin. A variety of conjugation chemistries will be investigated to synthesis these conjugates including EDC/NHS chemistry, Thiol maleimide chemistry and azide-alkyne click chemistry.

Chapter 4 will address the synthesis of a duocarmycin-peptide drug conjugate. The peptide utilised in this chapter has been shown to selectively bind the T-antigen with affinities comparable to many lectins. The incorporation of cleavable sequences into these conjugates will be looked at in this chapter as well as the biological evaluation of the peptide-drug conjugates synthesised.

Finally, **Chapter 5** will detail the design, synthesis and biological evaluation of a gold nanoparticle based system for the targeted delivery of duocarmycin conjugates to the T-antigen. These nanoparticles will utilise an active

targeting strategy through employing the jacalin lectin introduced in Chapter 2.

Chapter 2 - Optimisation of the Synthesis of Fmoc-DSA-OH and Investigations into Alternative Approaches to Benzyl Deprotection

2.1 Introduction

2.1.1 Synthetic Routes to Duocarmycin SA and other Members of the Family

Since the isolation and determination of the biological activity of the CC-1065 and duocarmycin family of compounds, the derivation of synthetic routes to these agents has been extensive.[113] Of particular interest from a synthetic organic chemistry perspective was the alkylating unit of these agents, with this subunit containing the majority of the key functionalisation. As discussed in Chapter 1, structure-activity relationship studies into these agents identified the minimum required pharmacophore along with a number of other alkylating subunit analogues. These analogues allow for accessibility to the potent biological activity of these agents whilst simplifying the synthetic routes. Of particular importance in terms of this was the discovery of the CBI unit which is now commonly utilised due to its ease of synthesis.

In spite of these new accessible analogues, due to its impressive potency and desirable biological activity, duocarmycin SA continued to present an ideal pharmacophore for analogue synthesis and studies into this compound specifically are also extensive.

The first total synthesis of duocarmycin SA was reported by Boger *et al.* (Scheme 2.1) in 1992 and was based on a previously reported strategy involving sequential regiospecific nucleophilic substitution reactions of substituted p-quinone diimines.[114] Critically, the synthetic route disclosed also allowed for the isolation of both enantiomers of the alkylating unit. This would come to aid the understanding of the importance of this particular characteristic in the natural products.

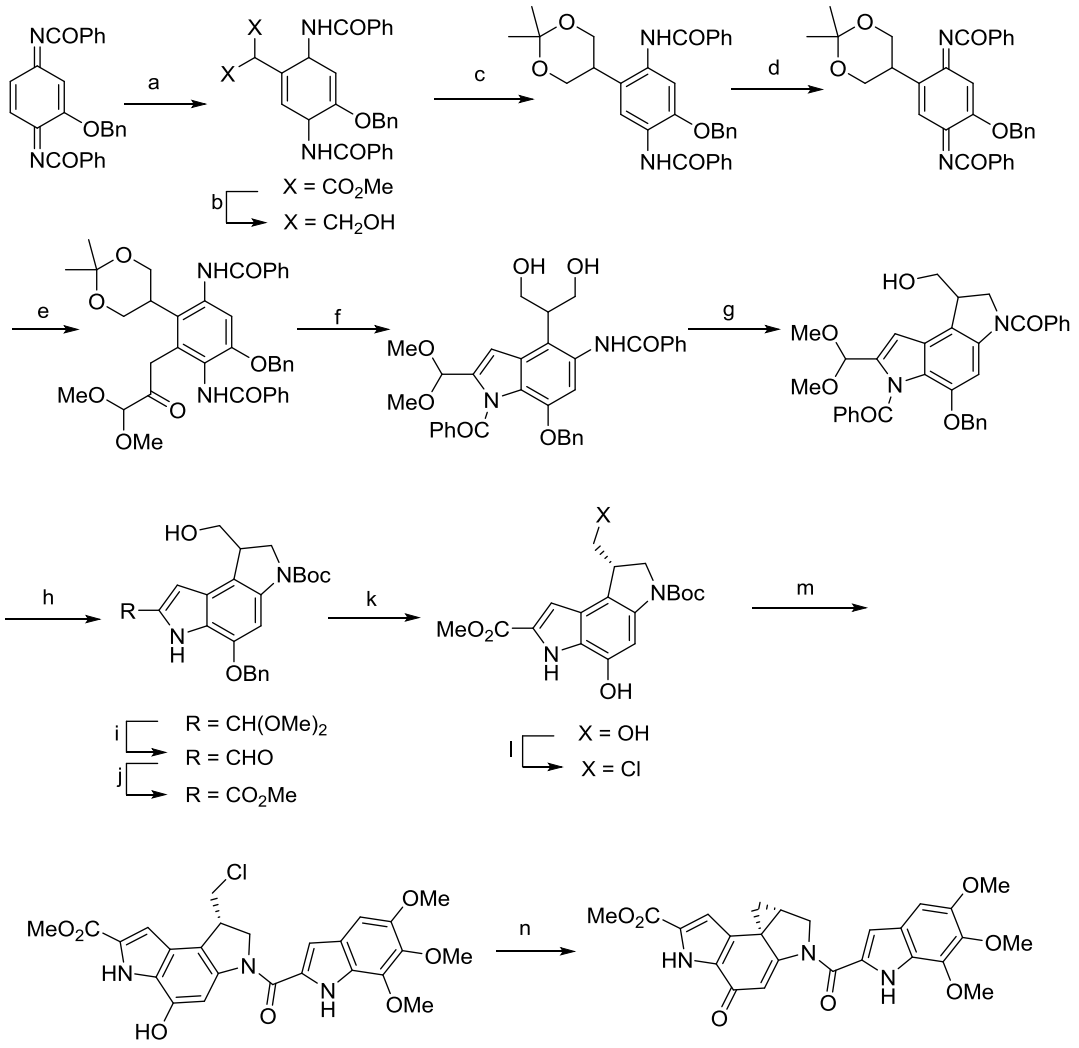

Scheme 2.1: a: $CH(CO_2Me)_2$, $NaOCH_3$, THF, 64% b: $NaBH_4$, EtOH, 71%, c: $Me_2C(OMe)_2$, TsOH, DMF, 99% d: $Pb(OAc)_4$, $CHCl_3$, 100%, e: pyruvaldehyde dimethyl acetal, THF, pH 4 phosphate buffer, 61% f: HCl, MeOH, 91%, g: DEAD-Ph_3P, THF, 100% h: NH_2NH_2-EtOH, reflux, then Boc_2O, THF 67% i: DMSO-pH 4 buffer-dioxane, reflux, 91% j: MnO_2, NaCN, HOAc, MeOH, 89%, K: 10% Pd/C 25% Aq. HCO_2NH_4, THF, 77% l: PPh_3, CCl_4, DCM, 81% m: HCl then 5,6,7-trimethoxyindole-2-carboxylic acid, EDCI, $NaHCO_3$,DMF, 61% n: NaH, THF, DMF, 87%.

Following on from Boger's initial total synthesis, Natsume and co-workers reported a 12-step total synthesis of duocarmycin SA starting from a pyrrole unit and proceeding via a tetrahydroquinolinol derivative (Scheme 2.2).[115] This work was later progressed and built upon through an adaptation of this synthesis to provide the first enantioselective route to both the natural and unnatural enantiomers of duocarmycin SA.[116]

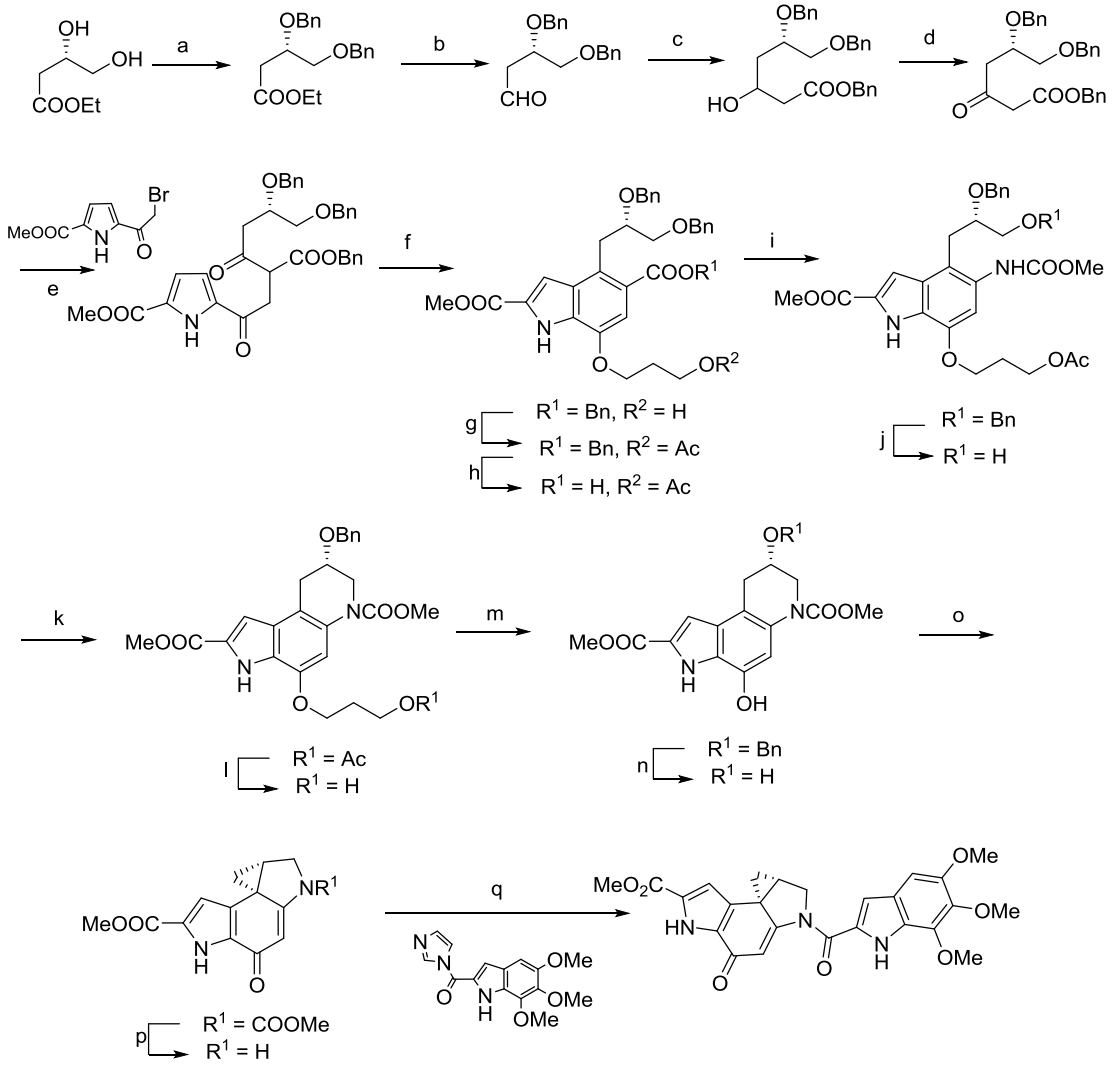

Scheme 2.2: a: $Cl_3CC(=NH)OBn$, CF_3SO_3H, cyclohexane-DCM, 52%. b: DIBAL, PhMe, 87%. c: LDA, CH_3COOBn, THF, 78%. d: Dess-Martin periodinane, DCM, 86% e: ^tBuOK, THF, 86% f: 2-ethyl-2-methyl-1,3-dioxane, BF_3.OEt, DCM, 54% g: Ac_2O, pyridine, DCM, 97%. h: H_2, 10 %Pd/C, EtOAc, 75%. i: DPPA, iso-Pr_2NEt, benzene, MeOH, reflux, 69%. j: BBr_3, DCM, 61%. k: DEAD, PPh_3, THF, 90%. l: K_2CO_3, MeOH, 98%. m: Dess-Martin periodinane, DCM, then Et_3N, DCM, reflux 86%. n: H_2, $Pd(OH)_2$, MeOH, 96% o: N-piperidyl-CO-N=N-CO-N-piperidyl, nBu_3P, THF, 88%, p: K_2CO_3, MeOH, 96% q, NaH, DMF, THF, 74%.

Subsequent to this initial work, further efforts focused on ways in which these syntheses could be streamlined to provide an easier and more accessible route to the natural products. Of particular importance within this area was the development of a route to the formation of the fused three ring system via a 5-*exo*-trig free radical reaction (Scheme 2.3). This strategy was first described by Boger and co-workers in 1995 and utilised a TEMPO-trap version to synthesise a *seco*-CBI based analogue of the natural product.[117]

This route was developed further 2 years later by Patel *et al.* and involved the incorporation of a 3-chloropropene group as the reactive alkene that generates the indoline ring system. This ideally set up the *seco* form ready for base catalysed ring closure with the chloromethyl group being in the required position.[118, 119] With this strategy now being a commonly utilised reaction within the synthesis of these natural products and subsequent analogues, further modifications have been made which allow for this reaction to be completed without the use of the undesirable tributyltin hydride.[120]

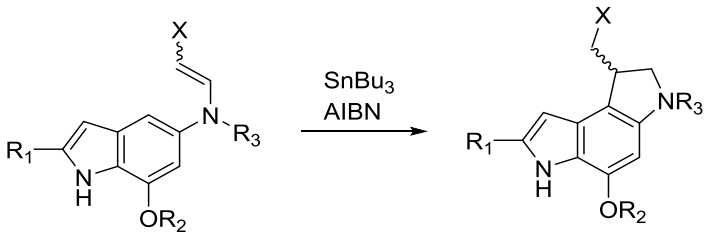

Scheme 2.3: Example reaction and conditions used for the 5-exo-trig free radical reaction to form the indoline ring.

In 2003, an efficient and concise synthesis of duocarmycin SA was presented by Tietze and co-workers which made use of this fundamental, commonly employed, 5-*exo*-trig reaction (Scheme 2.4).[121] This synthetic strategy also utilised many other now commonly employed steps in the synthesis of these agents, and was also a first example of using a Fischer indole synthesis for duocarmycin SA. This provided an ideal route to the highly functionalised central indole unit from commercially available starting materials.

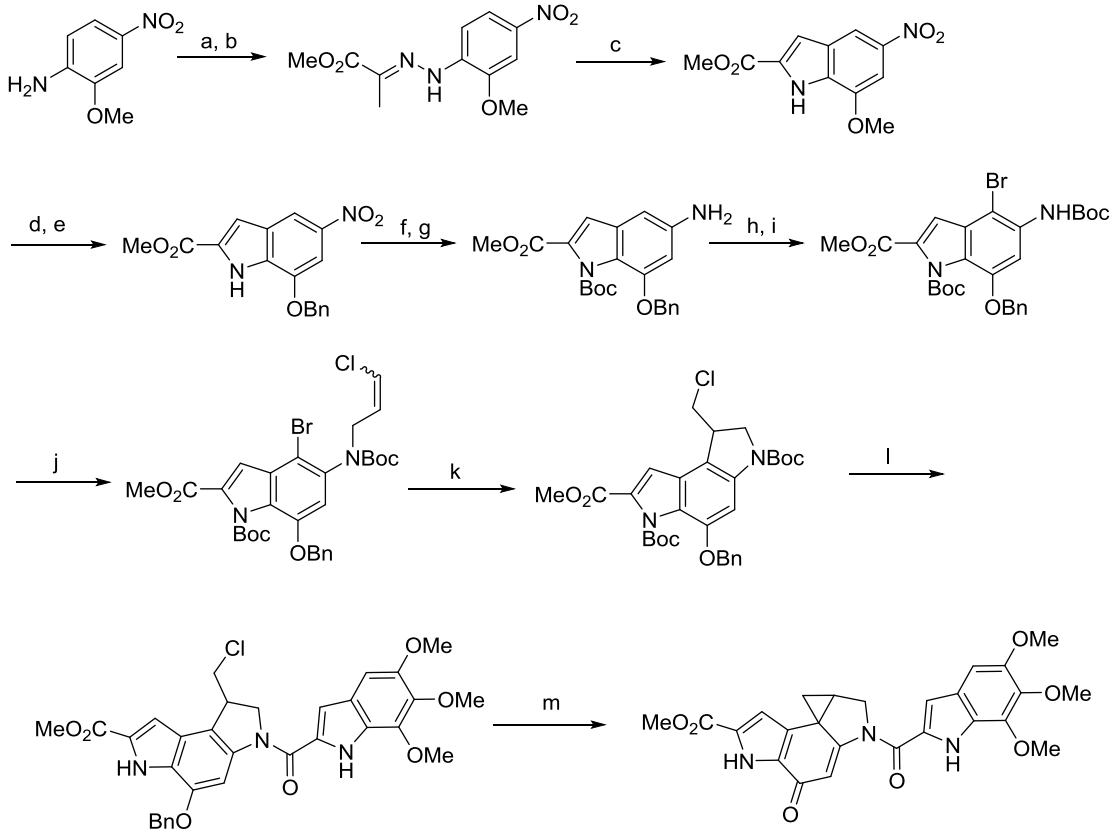

Scheme 2.4: a: $NaNO_2$, HCl, 5 min, $SnCl_2$, -20 °C 1h, 70%. b: NaOAc, methyl pyruvate, MeOH, rt, 16 h, 99% c: PPA, xylene, 120 °C, 18h, 64%. d: $AlCl_3$, DCM, rt, 72h, 70% e: BnBr, K_2CO_3, acetone, 40 °C, 8h, 88%. f: Boc_2O, DMAP, THF, rt, 1h, 98%. G: Lindlar catalyst, quinolone, EtOAc, H_2, rt, 18 h, 91%. h: Boc_2O, THF, rt, 18 h, 89%. i: NBS, THF, -78 °C, 4 h, 88%. j: NaH, DMF, rt, 30 mins, (E/Z)-1,3-dichloropropene, rt, 12 h, 92% k: TTMSS, AIBN, benzene, 80 °C, 3 h, 79% l: 4M HCl/EtOAc, 2 h, rt; TMI-CO_2H, EDC, DMF, rt, 18 h, 51% m: NH_4HCO_2, Pd/C, THF, 40 °C, 2 h, 91%.

Other commonly utilised synthetic approaches to the central indole unit now involve a sequential coupling and cyclisation reaction between aryl halides and methyl propiolate. This strategy was utilised by Sakamoto and co-workers for the synthesis of duocarmycin SA and made use of a Negishi coupling (Scheme 2.5).[122]

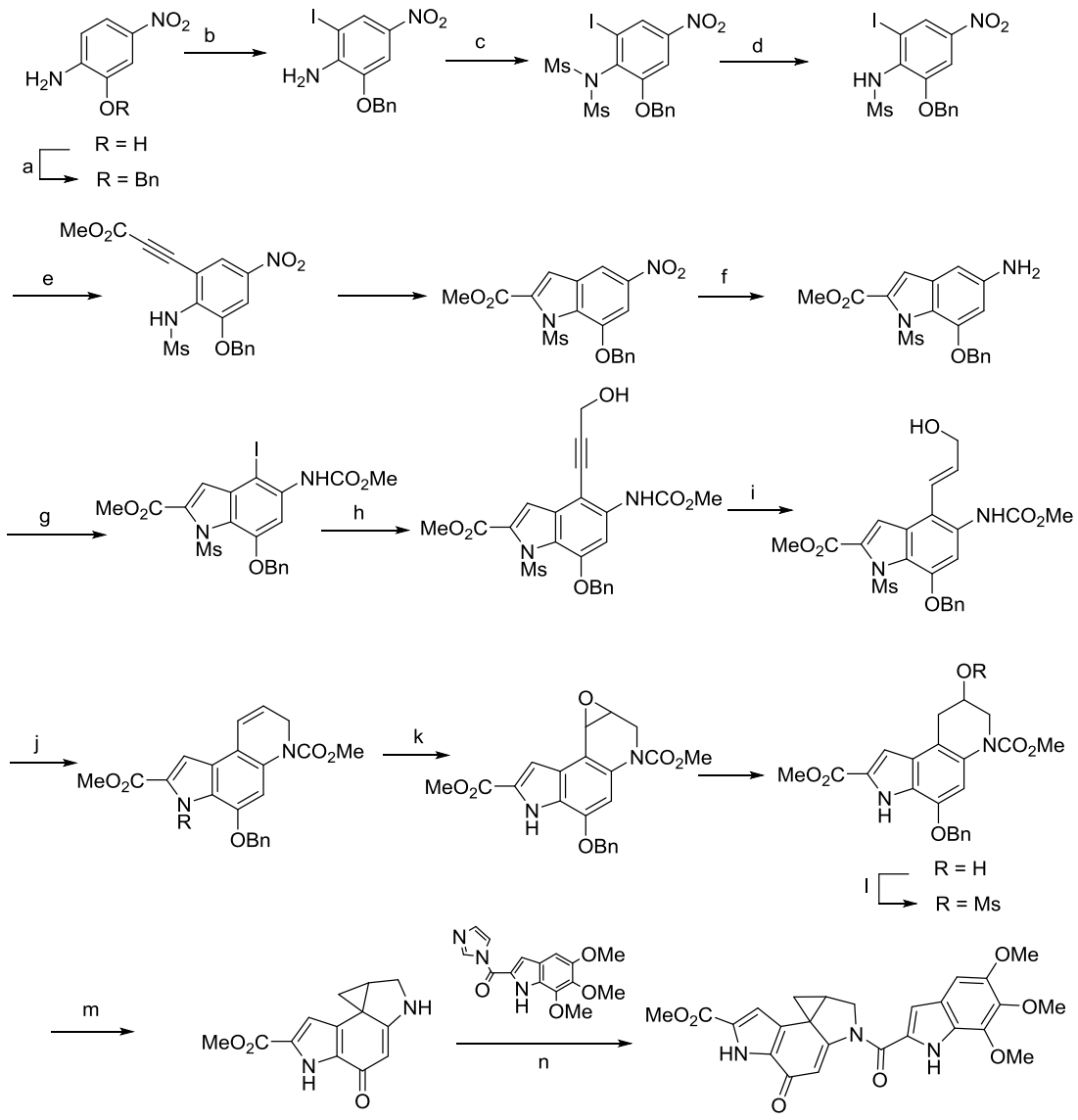

Scheme 2.5: a: BnBr, K_2CO_3, acetone, reflux, 93%, b: ICl, THF, reflux, 91%, c: NaH, MsCl, THF, rt, d: TBAF, THF, rt, 75%, e: methyl propiolate, $Pd(PPh_3)_4$, $ZnBr_2$, DIPEA, THF, reflux, 56%, f: H_2, PtO_2, AcOEt, rt, g: NIS, THF, 0 °C, 5 min, $ClCO_2Me$, DMAP, pyridine, 0 °C, 74% h: propargyl alcohol, CuI, $PdCl_2(PPh_3)_2$, THF, Et_3N, 50 °C, 83%, i: H_2, Pd-C, quinolone, THF-MeOH, rt, j: DEAD, PPh_3, THF, rt then K_2CO_3, MeOH, rt, 99%, k: MCPBA, DCM, 0 °C, 5 min, then Et_3SiH, $BF_3.OEt_2$, 0 °C, 42%, l: MsCl, Et_3N, DCM, rt, 75%, m: H_2, $Pd(OH)_2$, MeOH, rt, then K_2CO_3, MeOH, rt, 83% n: K_2CO_3, DMF, rt, 53%.

Despite the success and common utilisation of the 5-*exo*-trig radical cyclisation reaction, the drawback is that the alkylating subunit formed is racemic and hence the enantiomers need separating post synthesis. More recently, an alternative approach which led to the asymmetric synthesis of duocarmycin SA was presented by Boger and co-workers. (Scheme 2.6).[120] In this route a ring closing procedure was adopted that involved the use of a

Grignard/transmetallation reaction on a stereo-defined glycerol derivative. This enabled the generation of a fused six membered pyranose ring which upon coupling with a binding subunit, could be closed using ADDP and Bu_3P in a Mitsunobu activation and subsequent displacement of the secondary alcohol to generate the natural stereochemistry in the final product.

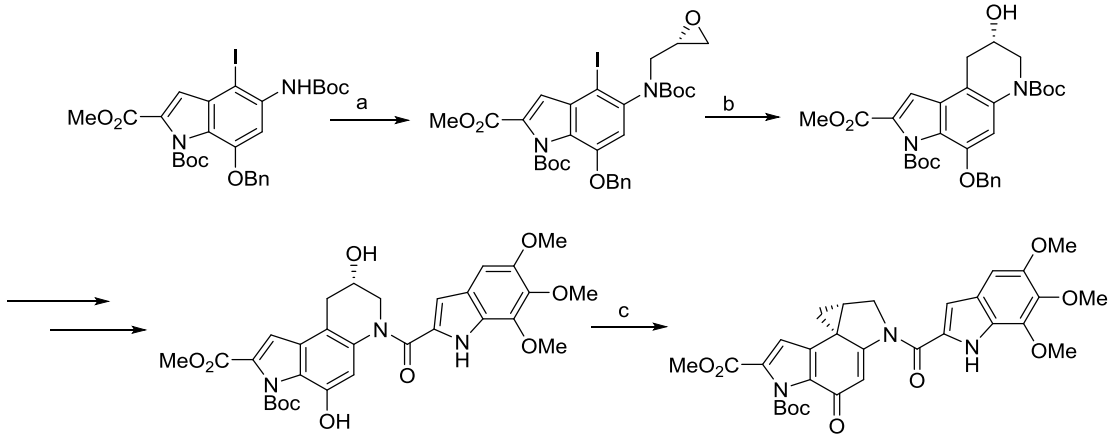

Scheme 2.6: a: (S)-glycidyl-3-nosylate, NaH, 92% b: iPrMgCl, CuI-PBu3, 69%, c: ADDP, PBu_3, 62%,

In spite of the impressive and imaginative chemical routes employed above to achieve the total synthesis of duocarmycin SA, the majority of these approaches involve a large number of steps and are not trivial. This makes the formation of analogues of this agent using these routes particularly difficult. Because of this, further synthetic strategies were required that would allow for quick and easy synthesis of analogues of these agents for various purposes. This would allow for more efficient investigations into the targeted delivery of these agents to cancer cells.

As can be seen in most of these total syntheses of duocarmycin SA and other members of the family, the final step often involves the coupling of the DNA binding unit to the more difficult to synthesise alkylating subunit. This has been commonly achieved through the use of peptide coupling reagents such as EDC. It was this realisation that prompted Searcey and co-workers to visualise the structures of these natural compounds as being made by amino acid like building blocks. Through this visualisation it could be ascertained that these structures could be synthesised through an advantageous solid

phase chemistry protocol. This would allow the generation of a large number of analogues of varying degrees of complexity with relative ease. In order to achieve this, the group set about the synthesis of a duocarmycin SA based alkylating subunit, suitably substituted for Fmoc based solid phase synthesis (Figure 2.1).[123] The route to this unit employed many elements of the fundamental chemistry presented in earlier total syntheses of duocarmycin SA. As in Tietze's total synthesis, this alkylating subunit was locked into the *seco* form using benzyl protection of the phenolic oxygen which upon removal provided the active agents.

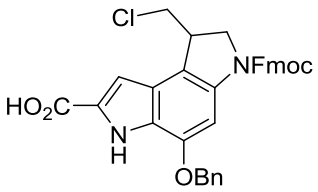

2.10

Benzyl protected Fmoc-DSA-OH

Figure 2.1: Structure of duocarmycin SA alkylating unit suitably substituted for use in Fmoc based solid phase peptide chemistry.

What can also be imagined is the potential use of this analogue of the alkylating subunit for the synthesis of potential warheads for conjugation to various targeting agents. These could include antibodies, small molecules or even nanoparticle based drug delivery moieties. Of particular interest would be the ease of incorporation of various functionalities or peptide based cleavable sequences into these systems thanks to the solid phase capabilities of the alkylating unit.

2.2 Aims of the Research Reported in this Chapter

The work in this chapter encompasses efforts towards the total synthesis of a duocarmycin SA alkylating subunit suitably substituted for use in Fmoc based solid phase chemistry. This was achieved through a 13 step synthesis which will be discussed in detail along with various attempted modifications to improve the efficiency of the synthesis. To further add to the analogues usefulness on the solid phase, the synthesis of a binding subunit, also substituted for Fmoc based solid phase synthesis, will be discussed.

The chapter will also cover general strategies utilised throughout this body of work for the introduction of the duocarmycin SA alkylating unit on to the solid phase. This includes the use of specific resins, coupling conditions and cleavage conditions.

As a progression from this, the chapter will also look into attempts made to further advance this analogue through the incorporation of different orthogonal phenolic protecting groups to replace the benzyl group. This is in an attempt to help further realise the potential of this unit for use in solid phase peptide chemistry.

2.3 Results and Discussion

2.3.1 Synthesis of Benzyl Protected seco-DSA Substituted for Solid Phase Peptide Synthesis

The synthesis of the benzyl protected Fmoc substituted DSA alkylating subunit (Fmoc-DSA-OH) was achieved following the route reported by Searcey and co-workers which is summarised in Scheme 2.7.[123]

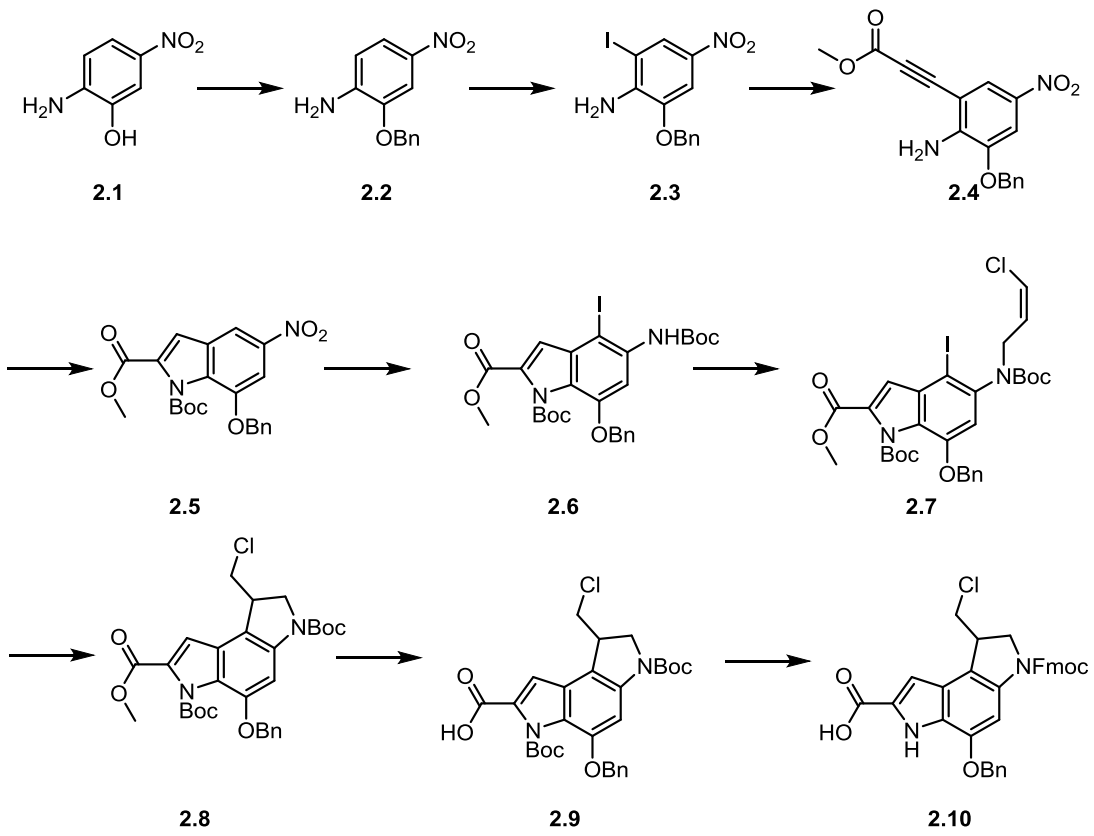

Scheme 2.7: Synthetic route of Fmoc-DSA-OH as presented by Searcey and co-workers

This large scale route was adapted slightly to allow for efficient completion within a research laboratory. A 25 g scale was deemed reasonable as a starting point for the synthesis to allow for sufficient product to be formed but also an ability to complete the route without difficulty using equipment available. The reported synthesis provides the monomer for solid phase synthesis in a racemic mixture from which the resulting enantiomers can be isolated. This was considered acceptable since it allows for formation of a protected *seco* form of the agent in large quantities. Not only does this prevent large scale formation of ultra-potent cytotoxic agents in the lab, but also fewer steps are required since spirocyclisation post benzyl deprotection can be achieved *in vivo*.

The synthesis began when the phenolic oxygen of 25 g of 2-amino-5-nitro-phenol (**2.1**) was benzyl protected using benzyl bromide and potassium carbonate (Scheme 2.8). The benzyl group provides an ideal protecting strategy due to its stability which allows it to remain in place throughout the total synthesis of **2.10**. Purification of the product could be achieved without

column chromatography through precipitation on the addition of water. This was ideal when working on such large scales. After filtration and product drying, the benzyl protected compound, **2.2**, was obtained as a pure compound in high yield (99%) as a yellow solid.

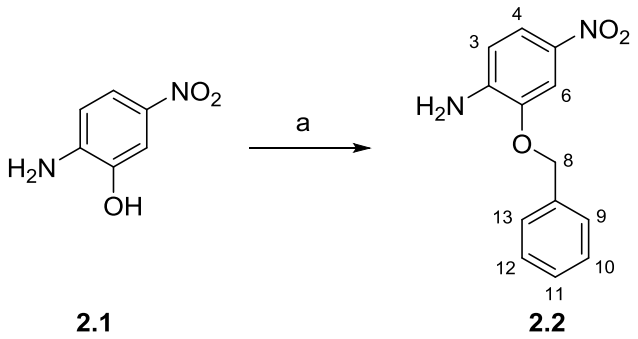

2.1 **2.2**

Scheme 2.8: a BnBr, K_2CO_3, DMF, 3 h, rt, 99%

The structure of **2.2** was confirmed through ^{1}H NMR which demonstrated the presence of 5 aromatic protons at 7.37-7.48 ppm as a multiplet. The presence of the benzylic protons at carbon 8 (see Scheme 2.8 for compound numbering) were also evident as a singlet at 5.22 ppm. Evidence of the desired benzylic protection of the phenol rather than the amine was presented through the appearance of two protons as a broad singlet representing the exchangeable hydrogens of the amine. This side reaction, although possible, can be seen as less likely due to the amine being para to an electron-withdrawing and hence deactivating nitro group. Mass spectrometry also confirmed the desired mass of 245.0924 gmol^{-1}.

The next step in the synthesis was regioselective iodination at the 3 position (Scheme 2.9), to allow for the subsequent cross coupling to occur in the desired location. This was attained through the use of N-iodosuccinimide and catalytic amounts of sulphuric acid. This gave over 50 g of **2.3** with a yield of 93%. Again, product purification could be realised through precipitation on the addition of water.

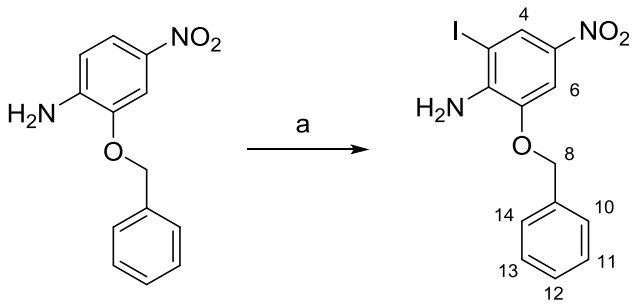

2.2 **2.3**

Scheme 2.9: a: b: NIS, H_2SO_4, DMF, 3 h, rt, 93%.

The compound was characterised through ^{1}H NMR which showed product formation through the absence of a doublet peak with integration 1 corresponding to the C3 position in **2.2**. The preservation of protons at positions C4 and C6 and hence the desired reaction regioselectivity was demonstrated through the presence of two doublets each with coupling values of 2.1 Hz representing long range coupling. The doublet of doublet character of the proton at C4 was lost. A shift of the C4 proton downfield respective to that seen in **2.2** was also evident which was expected with the addition of a deactivating iodine substituent to the aromatic ring. The proton at C6 is less affected by this iodine addition due to mesomeric effects. The addition of the iodine at the desired C3 position can be explained due to the deactivating character of the nitro group to electrophilic aromatic substitution at *ortho* and *para* positions and activation of the single *ortho*-position next to the electron-donating amino group.

The next step involved a Negishi-Sonogashira style coupling with methyl propiolate to give **2.4** (Scheme 2.10), followed by subsequent cyclisation to form the central indole unit. Previous work into this step demonstrated that the Negishi style coupling using $Pd(PPh_3)_2Cl_2$, DIPEA, $ZnBr_2$ in DMF at 66 ^{0}C provided the desired coupled product in a relatively good yield (76%). This synthesis was conducted in 5 batches and resulted in the formation of over 30 g of the coupled product in a 70% yield. A proposed mechanism for this step is shown in Scheme 2.11 with common palladium catalysed mechanistic steps allowing the coupling reaction to proceed.

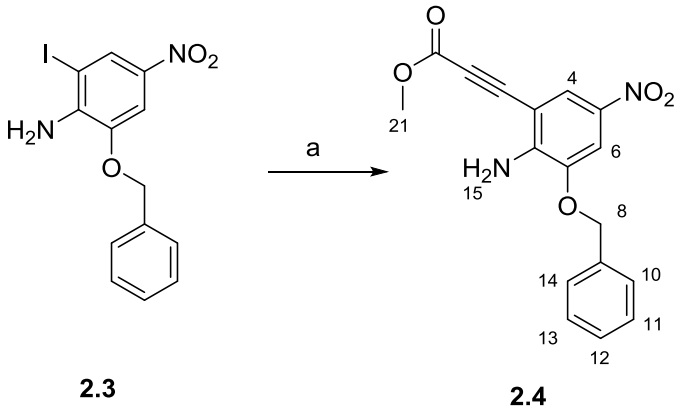

2.3 **2.4**

Scheme 2.10: a: methyl propiolate, $Pd(PPh_3)_2Cl_2$, DIPEA, $ZnBr_2$, DMF, 16 h, 66 °C, 70%.

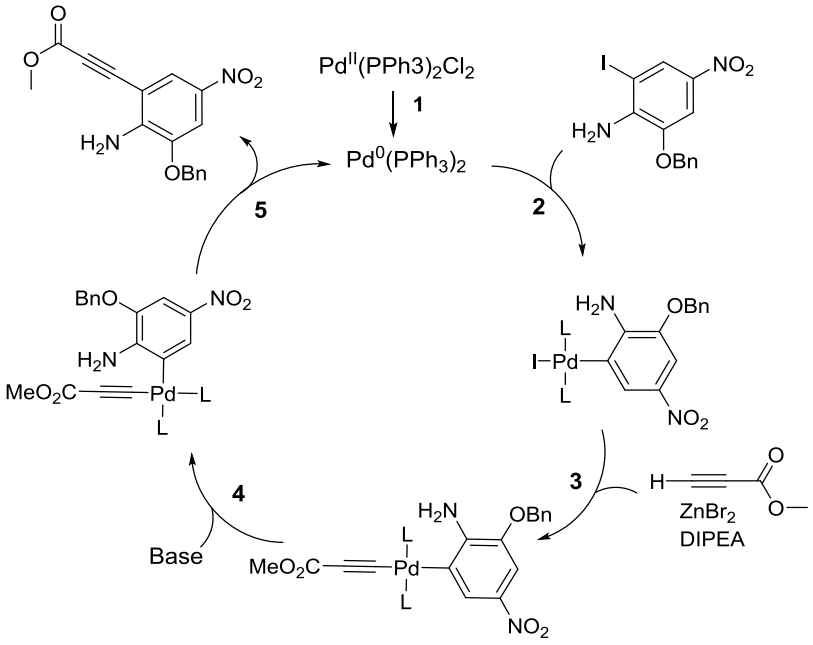

Scheme 2.11: Proposed mechanism for the Sonogashira style methyl propiolate coupling. 1: Ligand displacement to give active Pd(0), 2, Oxidative addition of iodoaryl starting material, 3, transmetallation with zinc bromide, 4, cis/trans isomerisation around central palladium complex, 5, reductive elimination to give product and reform Pd(0) active catalyst.

Upon column chromatography purification, the resulting orange solid was characterised using ^{1}H NMR which showed the presence of a peak corresponding to the methyl ester at 3.89 ppm. In addition, removal of the iodine was indicated through the upfield shift of the proton at C4. ^{13}C NMR also showed the presence of 4 new carbons further indicative of a successful coupling. Furthermore, IR presented solid evidence of reaction success through formation of a carbonyl peak at 1692 cm^{-1}.

Following on from this palladium cross coupling, it was next required to cyclise this intermediate to form the central indole unit (Scheme 2.12). This was previously achieved through the use of tetrabutylammonium fluoride in THF under reflux. In this study, the reaction was conducted on 3 batches and the crude was immediately Boc protected at the indole nitrogen using Boc_2O and DMAP.

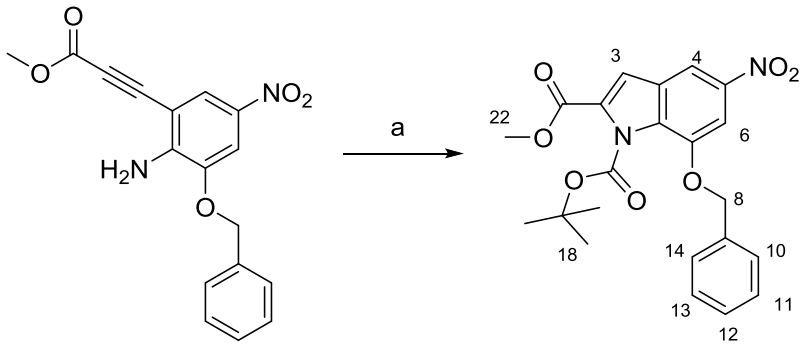

2.4 **2.5**

Scheme 2.12: a: 1 M TBAF in THF, THF, 1 h, reflux, then Boc_2O, DMAP, DCM, 3 h, rt 16-45% over 2 steps.

The product was confirmed through the appearance of a doublet at 7.35 ppm representing the proton at the C3 position of the indole (see Scheme 2.12 for numbering). With a coupling constant of 2.1 Hz being observed for protons at the C3, C4 and C6 position, it is clear that there is long range coupling occurring through the π system. In addition, the aniline protons from **2.4** were removed suggesting ring closure via the amine to form the indole. Also present was a singlet which integrated for nine protons at 1.42 ppm representing the *tert*-butyl of the Boc group.

The mechanism for this TBAF promoted ring closure is not trivial and a universally accepted mechanism is currently not available. Sakamoto and co-workers have studied the details of this reaction and showed two significant findings; 1, both a fluoride anion and a tetrabutylammonium cation are required for the ring closure and 2, ^1H NMR demonstrates the formation of NBu_3 during the reaction.[124] With this in mind a mechanism as depicted in Scheme 2.13 was proposed in which initial alkyne activation via

tetrabutylammonium coordination leads to polarisation of the bond allowing attack via the aniline lone pair.

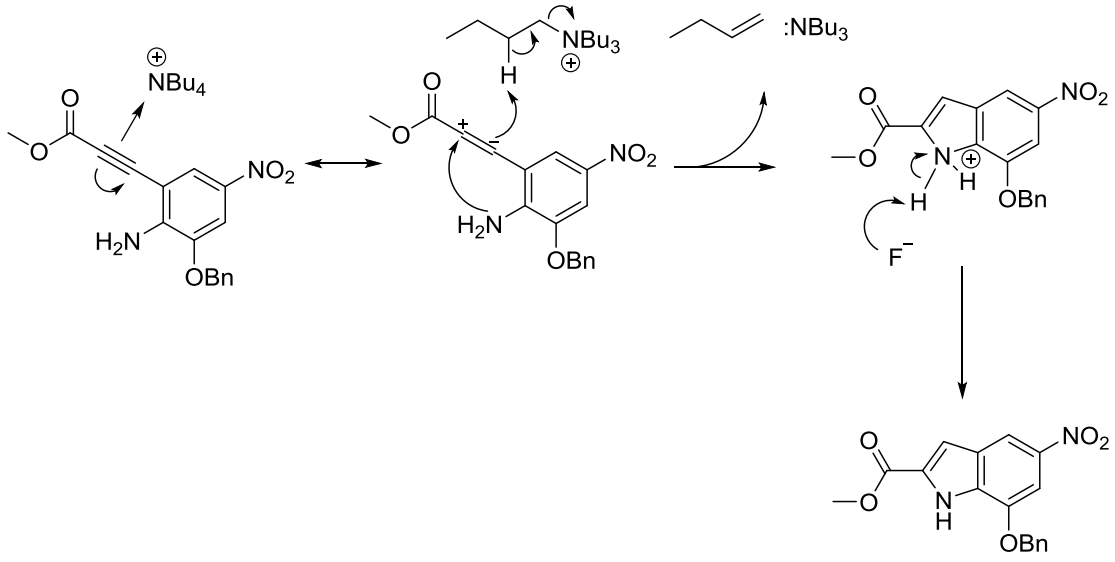

Scheme 2.13: Sakamoto *et al.* proposed mechanism for the TBAF mediated ring closure to form the indole.

Despite successful synthesis of the desired indole, the yields for this step were erratic, ranging from only 16% up to 50%. It was for this reason that further studies were completed in an attempt to achieve improved, more consistent yields and also to potentially combine the cross coupling and cyclisation steps in one. This would thereby remove a column chromatography based purification step. Previous examples of this combined step were demonstrated by Sakamoto and co-workers who, upon utilisation of a mesylate based protection of the amino group could achieve the cross coupling and cyclisation.[122] However, with the synthesis conducted here being on a much larger scale, the mesylate protecting strategy presents an increase in the number of required steps and manipulations to the final product – something which we were trying to avoid. With a similar strategy without the mesylate protecting groups not allowing for combined cross coupling and cyclisation, our attention turned to other possible routes to the indole.

One of the routes explored was the Larock indole synthesis which was proposed by Larock in 1991 (Scheme 2.14).[125] This heteroannulation reaction

proceeds under similar conditions to those employed above with a reaction between an iodo aniline agent, an alkyne and a palladium catalyst. In addition to these reactants, a potassium carbonate base, PPh_3 and LiCl are also required. Under these conditions, it has been seen that a cross coupling and subsequent cyclisation reaction can occur following a mechanism presented in Scheme 2.15.

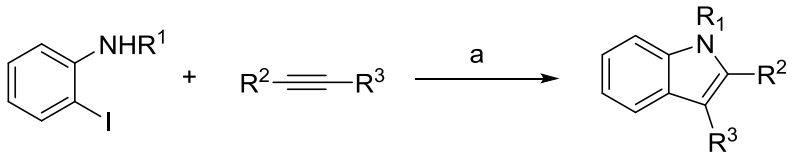

Scheme 2.14: example conditions utilised in a Larock indole synthesis, a: $Pd(OAc)_2$, K_2CO_3, PPh_3, LiCl, DMF, 100 °C.

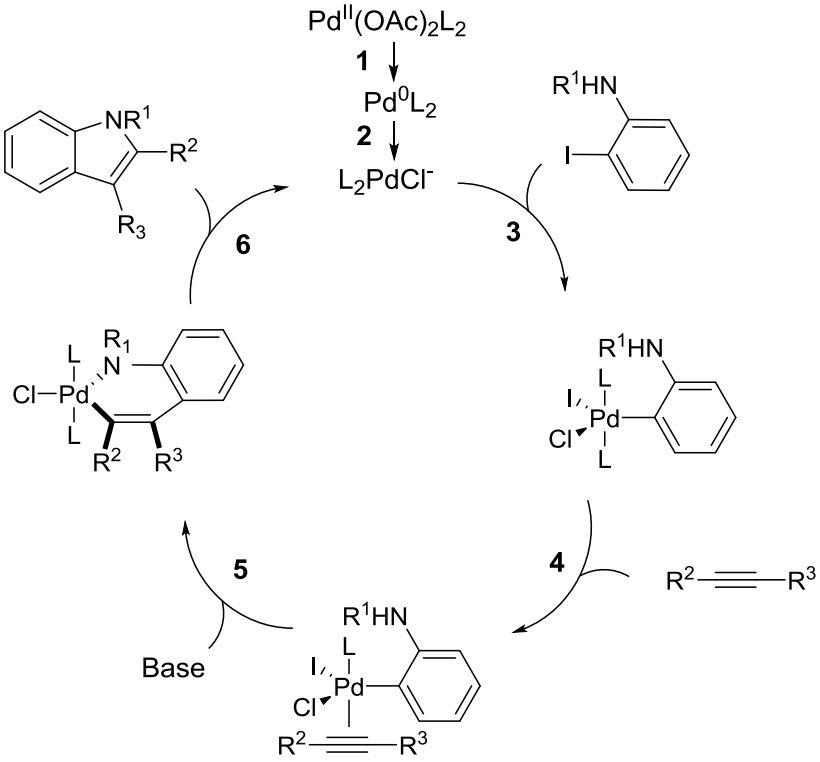

Scheme 2.15: proposed mechanism for Larock indole synthesis. 1: reduction of the Pd(II) to Pd(0), 2: coordination of the chloride to form a chloride-ligated zerovalent palladium species, 3: oxidative addition of the aryl iodide to Pd(0), 4: coordination of the alkyne to palladium of the resulting arylpalladium intermediate and subsequent syn-insertion into the arylpalladium bond, 5: nitrogen displacement of the halide to form a six-membered, heteroatom-containing palladacycle, 6: reductive elimination to form the desired indole.

A variety of conditions utilising this basic approach were explored for the synthesis of our required indole unit. These are summarised in Table 2.1.

Table 2.1: conditions employed in the attempted Larock indole synthesis to compound **2.5**.

Pd Catalyst (mol %)[a]	Base (mol equiv.)[a]	chloride[a,b]	Time (h)	Yield (%)[c]
$Pd(OAc)_2$ (5)	K_2CO_3 (4)	LiCl	12	0
$Pd(OAc)_2$ (10)	K_2CO_3 (4)	LiCl	12	5
$Pd(OAc)_2$ (10)	K_2CO_3 (4)	LiCl	24	8
$Pd(OAc)_2$ (10)	Na_2CO_3 (4)	LiCl	24	0
$Pd(OAc)_2$ (10)	K_2CO_3 (4)	N-Bu_4NCl	24	4
$Pd(OAc)_2$ (10)	K_2CO_3 (8)	LiCl	24	7
Pd(OAc)2 (10)	K_2CO_3	LiCl (2 equivalents)	24	8

[a] All molar equivalents are with respect to compound **2.4**. [b] All reactions were completed with 1 mol equivalent of chloride unless stated. [c] Isolated yields after column chromatography purification. PPh_3 was employed at 5 mol% in all conditions.

What was observed from these results was that with 10 mol% of the palladium catalyst, K_2CO_3 employed as a base and LiCl employed as a source of chloride, a successful reaction was observed. However with a yield of only 8%, this was not a viable reaction for the large scale synthesis required. In order to improve upon this value additional equivalents of K_2CO_3 and LiCl were employed but this resulted in little improvement.

With little success in terms of a combined coupling and cyclisation reaction, our attention turned to possible improvements to the cyclisation reaction with TBAF. With the yields of this step being the bottle-neck of the synthesis, alternative literature procedures were sought out. Marinelli and co-workers had previously demonstrated the potential of $NaAuCl_4 \cdot 2H_2O$ as a catalyst to achieve annulation of 2-alkynylanilines in EtOH or EtOH–water mixtures at room temperature.[126] Particularly promising was the demonstration that these conditions have achieved success on substrates with a nitro group para to the amine. This is similar to the system employed here in the DSA

synthesis and is seen as a potential barrier to these cyclisation reactions occurring. For the DSA synthesis, conditions employed involved the reaction of compound **2.4** with 0.04 mol equivalents of the gold catalyst (Scheme 2.16). Reactions were first attempted in ethanol however due to solubility issues, THF and DMF were also tested. Despite the promise of this reaction, disappointingly, no reaction was seen to arise with only retention of starting material occurring.

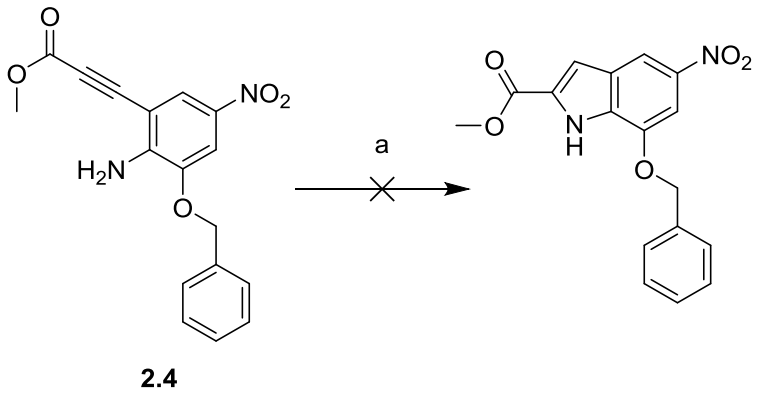

2.4

Scheme 2.16: attempted indole formation through a gold catalyst based reaction. Conditions a: $NaAuCl_4.2H_2O$, EtOH, N_2, 12 h, rt.

Further attempts to improve this cyclisation steps were made utilising a variety of different reagents summarised in Table 2.2. The rationale behind the reagents selected was to mimic the properties of tetrabutylammonium fluoride and to maybe get an enhancement of these properties to obtain a better yield.

Table 2.2: Conditions utilised for the attempted cyclisation of compound **2.4** to give the central indole unit.

Reagent	Conditions	Result
Tetrabutyl ammonium chloride	1 M solution, TFA, 1 h, reflux	indole formation but no improvement in yield (8% yield)
Tetrabutyl ammonium bromide	1 M solution, TFA, 1 h, reflux	Signs of cyclisation but reduced yield (6% yield)
Tetrabutyl ammonium iodide	1 M solution, TFA, 1 h, reflux	No reaction

With no reagents providing a clear advantage over the TBAF, and with the required indole unit already in hand it was decided that the synthesis would be continued with the existing strategy in order to progress to the final product. The majority of the routes explored here require the polarisation of the alkyne bond to give a positive charge on the carbon next to the carbonyl of the methyl ester. With this carbonyl group already holding a partial positive charge on the carbon, it is easy to imagine how this is a particularly unfavourable intermediate and hence why it could be hindering this reaction.

The next step in the synthesis involved the nitro group reduction to the amine, subsequent Boc protection of this and then selective iodination in the 4 position to give **2.6** (Scheme 2.17). Ideally, the synthesis presented by Searcey and co-workers allows these steps to be achieved in one pot without the need for purification along the way. This is achieved through reduction and Boc protection using Zinc powder, NH_4Cl, Boc_2O and DMAP and then subsequent iodination using N-iodosuccinimide and catalytic amounts of sulphuric acid. Column chromatography was utilised to isolate **2.6** in a 57% yield.

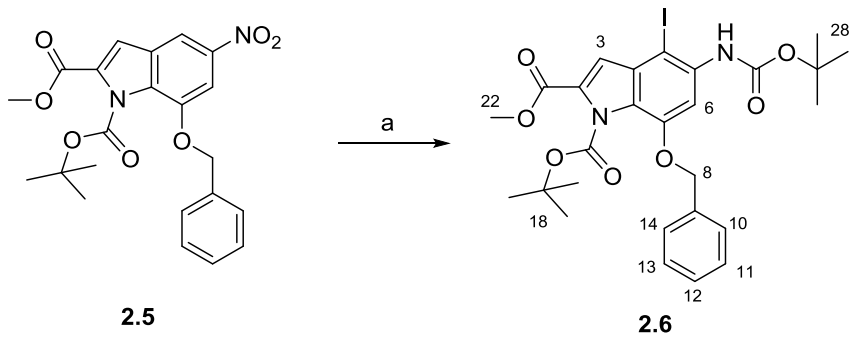

2.5 **2.6**

Scheme 2.17: a: zinc powder, NH_4Cl, Boc_2O, DMAP, water, THF, 12 h, rt, then NIS, H_2SO_4, 3 h, rt, 57% over 2 steps.

The product was confirmed with ^1H NMR, which showed a second singlet peak integrating for 9 protons at 1.54 ppm demonstrating the presence of the further *tert*-butyl group of the second Boc. Due to the removal of the withdrawing nitro group, a large upfield shift is also observed for the proton at the C6 position. In addition to this, the aromatic proton at the C4 position represented by a doublet in **2.5** was absent suggesting addition of the iodine

to the ring in the desired position. Furthermore, the addition of the iodine and its deactivating effects are seen in a downfield shift in the proton at C3 to 7.8 ppm.

What might be seen as unusual in this system is the lack of iodination at the C3 position since this is usually the most nucleophilic site on an indole. However, in **2.5**, this position is deactivated due to the Boc protection of the indole and the vicinal ester in the C2 position.

The synthesis continued with the alkylation of the Boc protected amine with 1,3-dichloropropene as a mixture of cis trans isomers to give **2.7** (Scheme 2.18). The alkylation would form the foundations of the required indoline ring. This was achieved using potassium *tert*-butoxide as a base. However, results using this base were often erratic in terms of yield and also a competing transesterification reaction occurring. Sodium hydride however, was found to be a more reliable base for the alkylation and also providing the product in a good yield of 73%. Column chromatography was utilised to isolate the resulting mixture of *cis*-and *trans* isomers which was characterised.

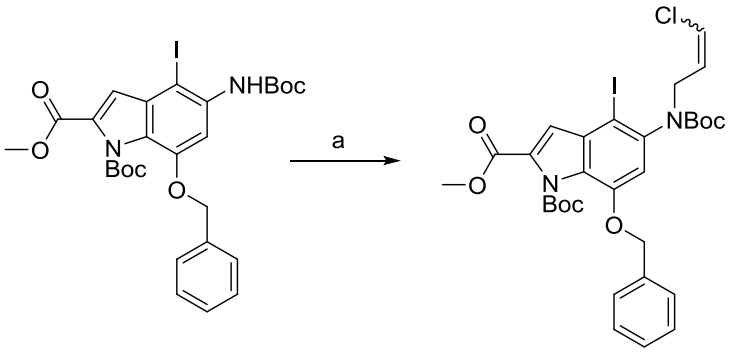

2.6 **2.7**

Scheme 2.18: a: (*E/Z*) 1,3-dichloropropene, NaH, DMF, 3 h, rt, 73%,

Whilst the *E/Z* isomer mixture of the 1,3 dicholoropropene used in the reaction has no overall effect on the subsequent reactions it does make the characterisation of **2.7** more difficult. This is due to the presence of two products within the ^{1}H NMR. Mass analysis however, was able to identify a successful reaction. ^{1}H NMR also demonstrated the success of the alkylation

with the presence of peaks within the alkene region. Presence of new peaks in the corresponding region of the ^{13}C NMR spectra provided further evidence of a successful alkylation.

The next step involved the extensively studied 5-*exo*-trig radical cyclisation step presented earlier on in this chapter in section 2.1.1. (Scheme 2.19). This was achieved here using AIBN and tristrimethylsilyl silane in toluene at reflux. After purification, the three ring fused product (**2.8**) was obtained as a colourless solid in 71% yield.

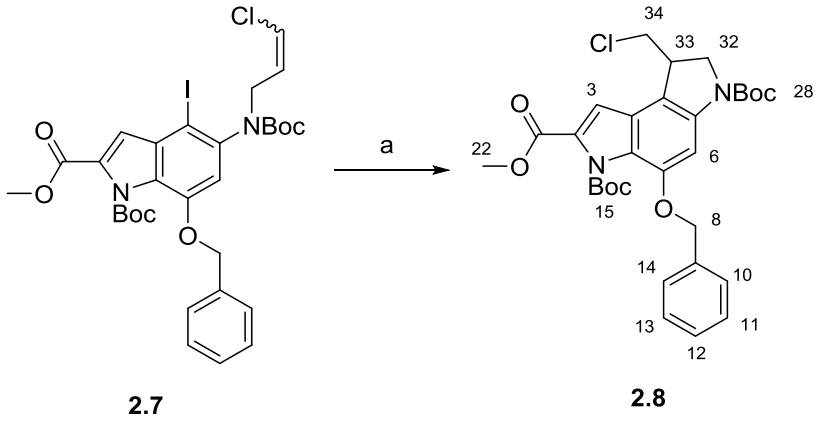

2.7 **2.8**

Scheme 2.19: a: AIBN, TTMSS, toluene, 1 h, reflux, 71%.

Evidence of the success of the reaction was demonstrated through ^{1}H NMR and ^{13}C NMR which suggested ring closure with a simplification of the spectra now that the presence of two geometrical isomers had been removed. Also, the occurrence of peaks between 3.89 and 4.13 ppm integrating for 5 protons suggested the formation of the desired 5-membered indoline ring with the presence of the protons at C32-C34 (see Scheme 2.19 for compound numbering). The splitting of the protons from this region are complex due to diastereotopic effects as a result of the introduction of a chiral centre at C33.

In order to introduce the required carboxylic acid functionality for the solid phase peptide synthesis, the methyl ester was then hydrolysed under basic conditions using a saturated aqueous solution of LiOH in methanol and THF (Scheme 2.20). Subsequent acidification and filtration of the mixture gave **2.9** in quantitative yield.

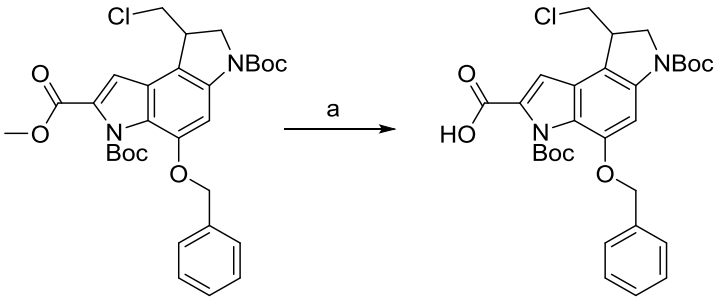

2.8 **2.9**

Scheme 2.20: a: LiOH, H_2O, MeOH, 3 h, rt, quantitative yield.

^{1}H NMR in deuterated DMSO confirmed the presence of **2.9** through a broad singlet at 13.46 ppm - the removal of the methyl ester peak at 3.86 ppm was also observed. IR confirmed the presence of the carboxylic acid through a broad peak at around 3000 cm^{-1} and a peak representing the carbonyl at 1694 cm^{-1}.

The final step of the synthesis required Boc deprotection from the indole and indoline nitrogen and subsequent, regioselective Fmoc protection of the indoline nitrogen (Scheme 2.21). The Boc deprotection was achieved through stirring the starting material in 4 M HCl in dioxane overnight. The desired Fmoc protection was then attained through reaction with Fmoc-Cl and $NaHCO_3$ in THF. Column chromatography based purification resulted in isolation of the desired final product in 84% yield.

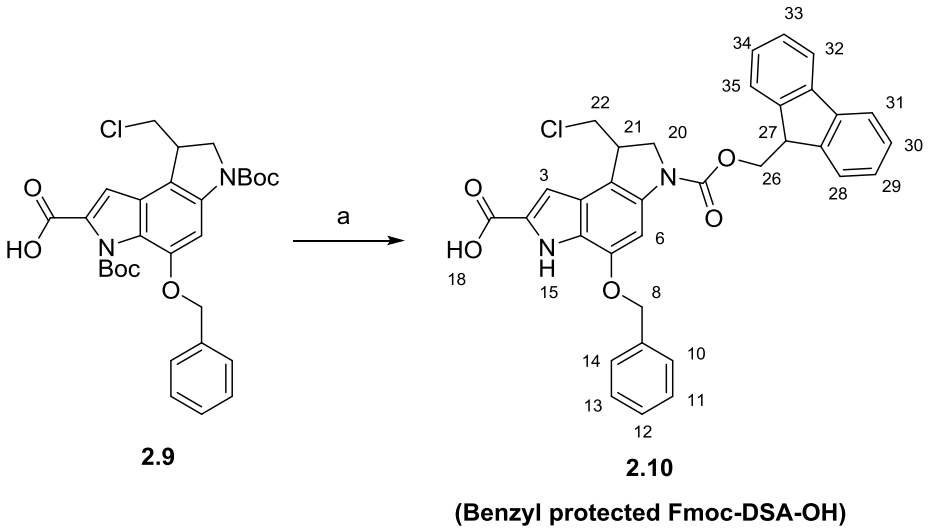

Scheme 2.21: a: 4 M HCl in dioxane, 16 h, then, Fmoc-Cl, $NaHCO_3$, THF, 10 min, rt, 84% over 2 steps.

The structure of **2.10** was confirmed through various characterisation techniques. The ^{1}H NMR demonstrated the removal of both of the Boc groups indicating the success of this part of the reaction. The rest of the ^{1}H NMR spectrum however is more complex and this has been previously demonstrated by Searcey and co-workers to be due to the presence of rotamers. This has been proposed to occur due to steric clash between the Fmoc group and the benzyl group. Accurate mass analysis showed more clearly the presence of **2.10** through an observed mass of 578.1245 along with the characteristic isotope splitting expected from the chlorine.

The 13 step synthesis, discussed above was achieved with a final overall yield of 3% giving 2.1 g of the final product. This Fmoc substituted, benzyl protected *seco*-DSA alkylating subunit could then be introduced onto the solid phase ready for further investigations in to achieving a targeted delivery of the cytotoxic agent to cancer cells.

2.3.2 Synthesis of Binding subunit analogue substituted for the solid phase

In order for **2.10** to fully realise its potential for use on the solid phase it was proposed that a compound that could represent the binding unit of the natural products would also be ideal. This unit should also be substituted for

use in Fmoc-based solid phase synthesis in order for peptide sequences to be extended from both the C-terminus and the N-terminus. Previous work on the solid phase by Searcey and co-workers utilised a 5-methoxyindole unit which capped the N-terminus and hence didn't provided the ability to grow from this end.[123] An analogue of this indole containing a primary Fmoc protected amine and a carboxylic acid was projected to be a possible alternative. The envisioned indole based binding subunit is shown in Figure 2.2.

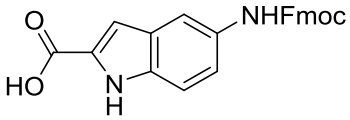

2.14

Figure 2.2: Structure of binding subunit indole, suitably substituted for use on the solid phase.

The synthesis of this subunit was to start with the commercially available ethyl 5-nitroindole-2-carboxylate (**2.11**) and a proposed route to **2.14** is shown in Scheme 2.22.

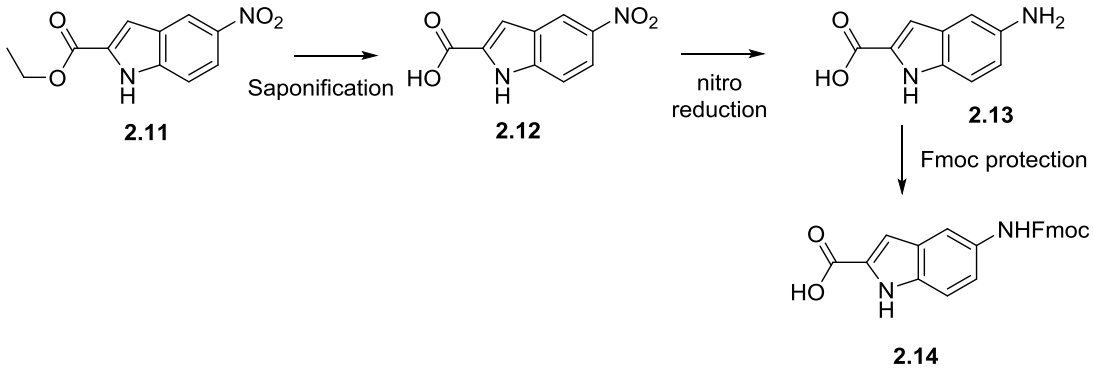

2.11 **2.12** **2.13** **2.14**

Scheme 2.22: Proposed synthetic route to **2.14**.

The hydrolysis of the ethyl ester of **2.11** was achieved under basic conditions with lithium hydroxide. The product was isolated after acidification in aqueous solution giving a quantitative yield. The hydrolysis was observed to occur with ^{1}H NMR demonstrating the presence of a peak at 12.5 ppm

representing the carboxylic acid. Absence of a triplet at 1.33 ppm and a quartet at 4.32 ppm also provided evidence of ethyl group removal.

The reduction of the nitro group was first attempted using 10% palladium on carbon along with 25% ammonium formate as a source of hydrogen. After hydrogenation, the resulting mixture was filtered directly into a solution of Fmoc-Cl in DCM. Despite this process having success with other units within our laboratory, attempted purification of the resulting mixture and subsequent characterisation showed no presence of the desired Fmoc protected subunit. An alternative reduction method was attempted using zinc powder, NH_4Cl and H_2O in THF. With this reduction method showing success for the synthesis of **2.10** it was hoped a similar result would be obtained here. However, after completing this reaction none of the desired product was obtained. The reason for the failure of these reactions was proposed to be due to the presence of the carboxylic acid. The formation of the desired carboxylic acid and amine makes isolation of the product difficult. For this reason, a new synthetic route was proposed which involved nitro reduction and protection prior to the ester hydrolysis (Scheme 2.23). A Boc protection strategy would be utilised prior to Fmoc protection due to the lability of the Fmoc group to basic conditions used for ester hydrolysis. This is similar to the strategy used in the synthesis of **2.10**.

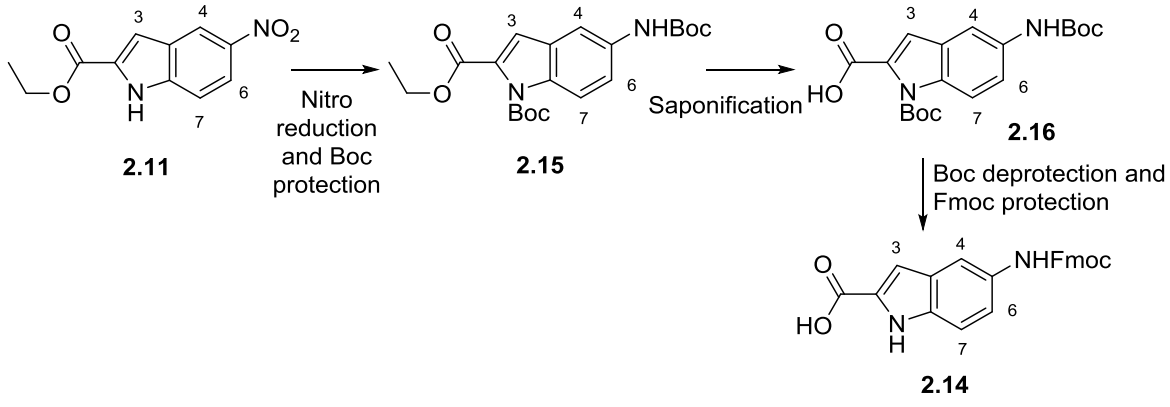

Scheme 2.23: Modified proposed route to compound 2.14 involving nitro reduction prior to ethyl ester hydrolysis.

The nitro reduction and subsequent Boc protection of 5-nitroindole-2-carboxylate (**2.11**) was achieved in one pot using zinc powder, NH_4Cl, water, Boc_2O and DMAP. Interestingly, despite one equivalent of DMAP being used, ^1H NMR demonstrated that Boc protection of the indolic nitrogen did not occur. Despite this, the product after column chromatography was taken forward onto the ethyl ester hydrolysis. The reduction of the nitro group also resulted in an observed upfield shift of the proton at C4 and C6. This can be attributed to the reduction of the electron withdrawing character at position C5.

As in the synthesis of **2.10**, the ester hydrolysis of **2.15** was achieved using lithium hydroxide. Subsequently, the isolated **2.16** was Boc deprotected using 4 M HCl in dioxane before Fmoc protection with Fmoc-Cl and $NaHCO_3$. The presence of the desired compound was confirmed through ^1H NMR, which showed the peaks of the central indole unit and also the characteristic peaks of the Fmoc unit in the aromatic region and ay 4.47 ppm and 4.31 ppm.

With an alkylating subunit (**2.10**) and a binding subunit (**2.14**) both suitably substituted for solid phase synthesis in hand, attempted synthesis of specific peptide sequences incorporating these units could be conducted. The sequences of interest would be those which aid the formation of conjugates between duocarmycin and a targeting moiety. This might include specific functionalities or the introduction of cleavable sequences.

2.3.3 Utilisation of Fmoc-DSA-OH in Solid Phase Peptide Synthesis.

2.3.3.1 Solid Phase Chemistry

The unique feature of the alkylating unit analogue which makes it such a desirable moiety is its ability to be introduced and used within solid phase organic synthesis (SPOS). In comparison to its solution phase synthesis counterpart, SPOS presents many advantageous features. Most notably of these is the removal of tedious purification steps after each chemical manipulation. With the desired molecule anchored to a solid support,

reagents utilised for reaction can simply be washed from the resin using an applicable solvent. Isolation of the final product can then be achieved via cleavage from the solid support.[127]

SPOS is of particular use in the synthesis of long chain peptides termed solid phase peptide synthesis (SPPS) which was brought about by Merrifield in the late 1960s.[128] Through anchoring a specific amino acid onto a solid support, subsequent amino acid couplings could be made without the need for long purification steps after each addition. Using orthogonal protecting groups, successive coupling and deprotection reactions could be used to build up the peptide sequences. It was this work which was fundamental in the awarding of the 1983 Nobel Prize for chemistry to Merrifield.[129] After originally being seen as a flight of fancy, the simplicity and ingenuity of this concept is depicted in the popular use of this technique and also in its ability to be automated in modern day systems. Particularly popular is the use of Fmoc based SPPS (Scheme 2.24).[127] This strategy utilises amino acids whose primary amine groups are protected with an Fmoc group. This base labile group can be removed after each coupling without any effect on the anchoring of the peptide to the resin. The linker between resin and peptide is often acid labile and so cleavage of the final peptide, along with side chain protecting group removal, is commonly achieved through the use of reagents such as trifluoroacetic acid (TFA).

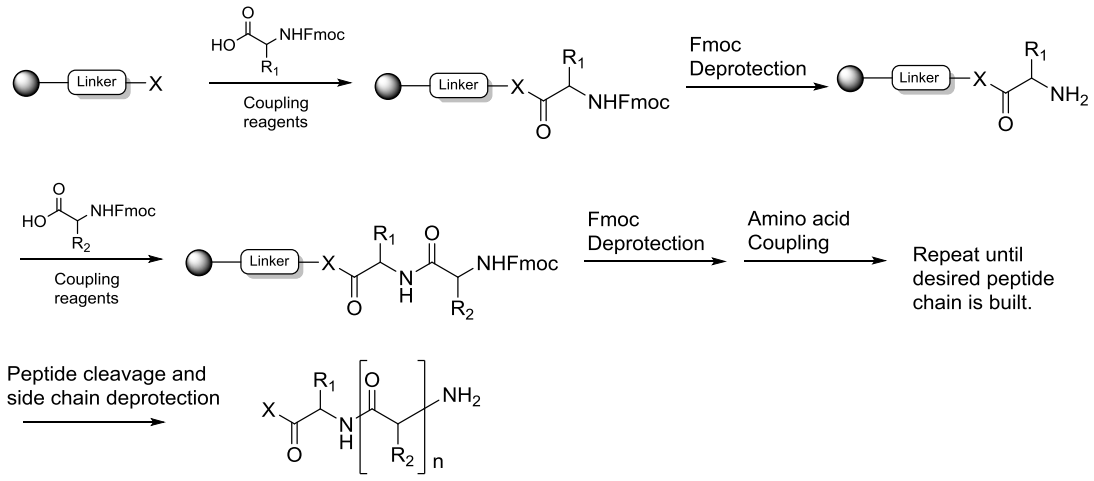

Scheme 2.24: General scheme demonstrating the route, using Fmoc SPPS, to a desired peptide using subsequent coupling and deprotection steps.

2.3.3.2 Strategies Employed for the use of Fmoc-DSA-OH in SPPS.

With the use of the above units (**2.10 and 2.14**) on the solid phase being present throughout this thesis, what follows is a summary of conditions most commonly utilised for the synthesis of specific peptides. Following on from this section, where specific peptides are introduced in the subsequent chapters, a discussion of the synthesis of these peptides will be brief unless anomalous conditions to those introduced here were used.

Previous work by Searcey and co-workers demonstrated the use of the alkylating unit synthesised above, on the solid phase.[123] This work, found the ideal conditions required to obtain the most efficient use of the subunit. Post cleavage HPLC analysis was used to study the purity of the peptide synthesised in relation to undesired side products. The conditions studied included different types of resin, coupling reagents, and cleavage conditions. The results of this study are summarised in Table 2.3.

Table 2.3: Summary of conditions found to give most efficient usage of Fmoc-DSA-OH on the solid phase.

SPPS requirement/step	Ideal Reagents and conditions
Resin [a]	2-chlorotrityl (2-Cltrt) resin or rink amide based resin. Resin swelling was achieved in dichloromethane (30 mins) and dimethylformamide (30 mins)
Coupling Reagents	(1-[Bis(dimethylamino)methylene]-1H-1,2,3-triazolo[4,5-b]pyridinium 3-oxid hexafluorophosphate) (HATU) and N,N-diisopropylethylamine (DIPEA) based couplings.
Fmoc Deprotection	40% piperidine in DMF 10mins, 20% piperidine in DMF, 5 min x2
Cleavage conditions [b]	2- Cltrt resin – 1% TFA, 10% TIPS, DCM, 3 h Rink Amide – 95% TFA, 2.5% TIPS, 2.5% H_2O, 3 h

[a] Depending on desired functionality at the C-terminus, [b] Depending on chosen resin and amino acids present within sequence.

2-Cltrt resin was found to be an ideal resin choice for utilising the benzyl protected Fmoc-DSA-OH on the solid phase. The 2-Cltrt resin can be cleaved only at the desired position and the resulting cation formed is more sterically hindered due to the larger linker structure. This means it is less likely to interact further with the synthesised structures. Additionally, the 2-Cltrt resin can be cleaved in only 1% TFA which reduces any possible acid induced degradation of the peptide which may occur in higher TFA concentrations. Although this resin demonstrated the most potential, rink amide was also shown to be an acceptable substitute should an amide based C-terminus be desired.

In terms of coupling agents, HATU and DIPEA were found to be the most ideal. This was in comparison to HBTU, PyBOP, EDC and DIC. In some instances in the work disclosed herein, HBTU and HOBt were utilised for couplings as an alternative to HATU.

With these conditions being found to provide the optimal usage of the DSA unit on the solid phase, they were mimicked for the majority of the peptides synthesised within this body of work. For peptides which were synthesised following conditions other than those found in this table, specific conditions will be disclosed where applicable.

2.3.4 Benzyl Deprotection of DSA Containing Peptides

Upon synthesis and cleavage from the resin, benzyl group deprotection is required to provide the active agents. Once the benzyl group has been removed from the phenolic oxygen, the *seco*-form of the duocarmycin analogues are no longer in a 'locked' conformation and hence are free to spirocyclise *in-vitro*. This is demonstrated in Scheme 2.25.

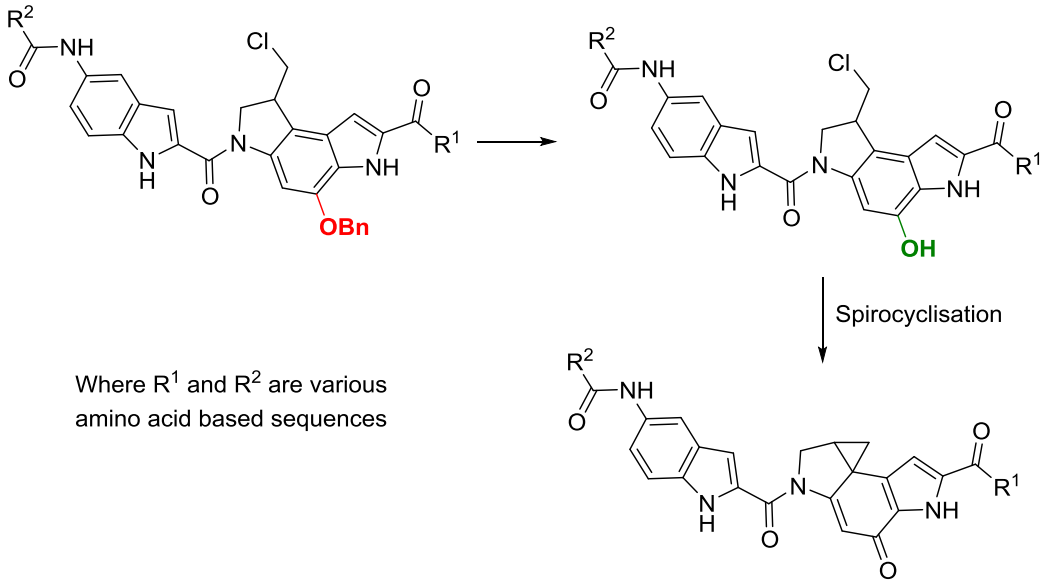

Scheme 2.25: deprotection of the benzyl group from a DSA based peptide sequence, results in an 'unlocking' of the *seco* form and hence an ability to spirocyclise to form the pharmacologically active agent.

The benzyl deprotection can be achieved through a transfer hydrogenation reaction of the starting material with 10% palladium/carbon, with 25% ammonium formate as a source of hydrogen.[21-23] These conditions were utilised for many of the peptides presented in this thesis with a general example being demonstrated in Scheme 2.26. The success of the reaction was observed via reverse-phase HPLC, which identified a shift in the main product peak subsequent to subjection to the reaction conditions. The shift to an earlier retention time indicted the formation of a more polar species which is consistent with this specific reaction. ^{1}H NMR and various mass spectrometry techniques were also used to confirm debenzylation depending on the specific species.

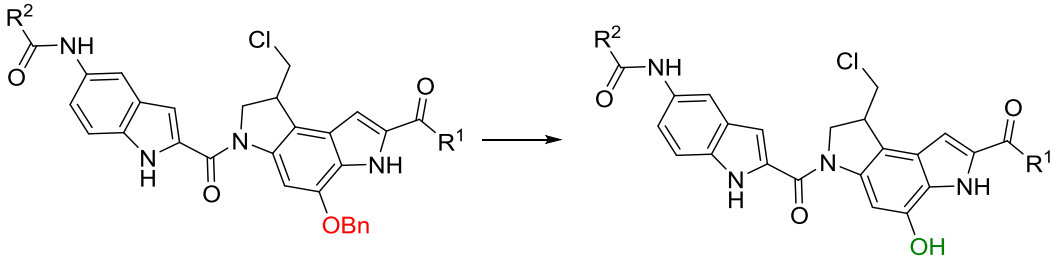

Scheme 2.26: a: 10% Pd/C, 25% Aq. HCO_2NH_4, THF/MeOH, rt, 1 h

Despite these conditions presenting a viable option for the debenzylation of a number of synthesised peptides in this thesis, it was noted that sometimes this reaction does not provide the desired outcome, resulting in either no debenzylation or mixtures of products. This has been observed for analogues of certain lengths (15+ amino acids) and also on the introduction of certain amino acids such as cysteine. The specifics of these findings will be discussed in chapters 3 and 4 where applicable. It was for this reason that an alternative set of conditions for the debenzylation reactions were sought after.

The debenzylation of various organic compounds using boron tribromide has been disclosed on numerous occasions within the literature.[130-132] It was proposed that these conditions may be useful in the debenzylation of DSA based peptide sequences due to the chemoselectivity of the described reaction. As an initial attempt, **2.10** was reacted with boron tribromide in DCM as a 1 M solution at -78 °C (Scheme 2.27).

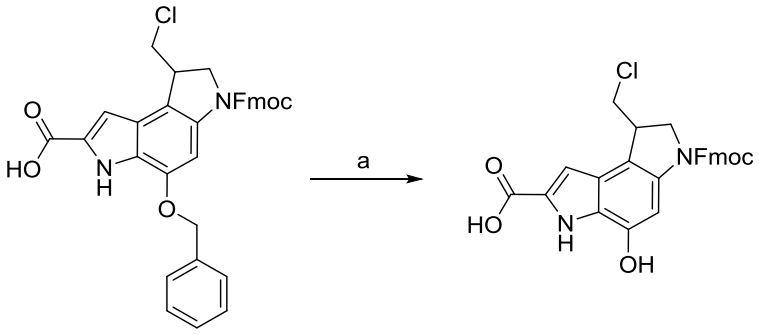

2.10 **2.17**

Scheme 2.27: a: 1 M BBr_3, DCM, -78 °C, 1 h, 64%

Monitoring of the reaction via reverse-phase HPLC demonstrated complete consumption of the starting material and formation of a new major peak. Column chromatography was utilised to isolate this peak which upon characterisation was found to be the desired debenzylated product. Specifically, ^{1}H NMR demonstrated the removal of a multiplet representing the benzyl group aromatic protons at 7.47 ppm and mass spectrometry analysis showed the desired mass of 488.13. A proposed mechanism for this transformation is shown in (Scheme 2.28) and proceeds with an initial

formation of an ether adduct followed by the loss of bromide which attacks the benzylic methylene of the zwitterionic intermediate. This results in cleavage of the C–O bond. Hydrolysis of the penultimate intermediate during aqueous workup gives the desired debenzylated compound.[133]

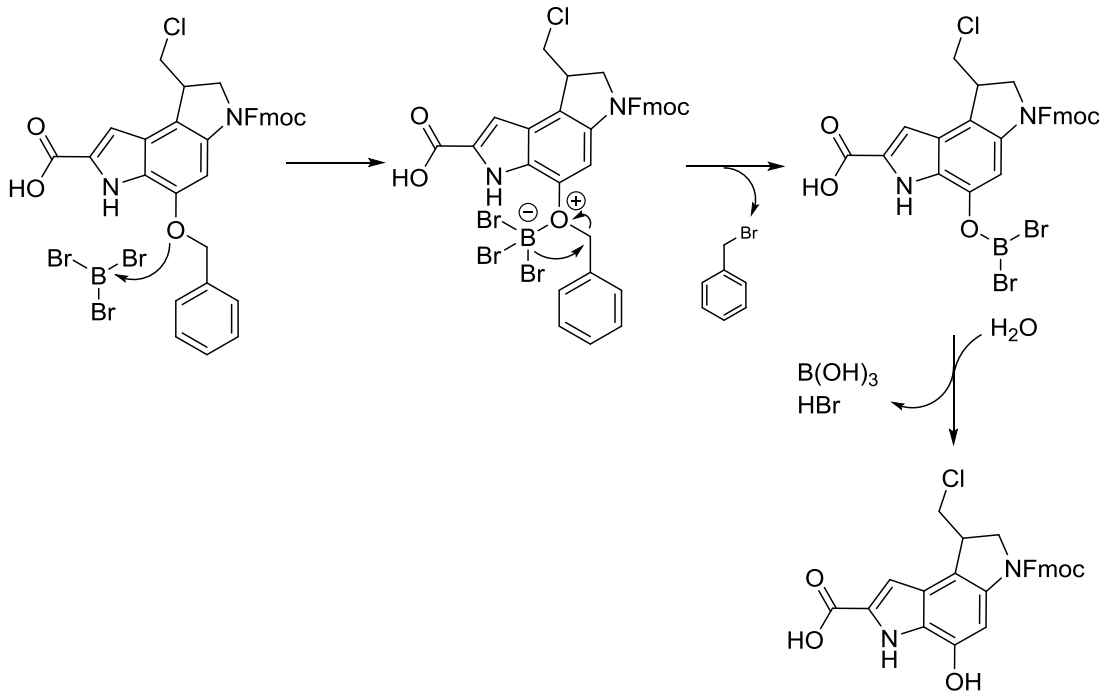

Scheme 2.28: proposed mechanism for benzyl deprotection using boron tribromide

Upon attempted mimicking of these conditions with various analogues, the boron tribromide debenzylation reaction was found to be applicable. Pleasing was the observation that these conditions or those similar, could achieve the debenzylation of larger peptide analogues where the Pd/C, HCO_2NH_4 reaction was found to be inapplicable. This will be discussed further in chapter 3. The discovery of the use of boron tribromide for the debenzylation reaction in these systems, helps to further realise the potential of this Fmoc substituted alkylating unit in solid phase synthesis. This opens up new doors for the use of this particular subunit in the further study of duocarmycin based agents.

2.3.5 The use of p-methoxybenzyl as an Alternative Protecting Group Strategy for Fmoc-DSA-OH

The benzyl group utilised in the synthesis of Fmoc-DSA-OH holds many advantages, mainly due to its lack of lability to the reaction conditions employed in the synthesis. However, as mentioned above, the removal of this group from the systems formed on the solid phase is not trivial and problems have been encountered with this on numerous occasions. In addition to this, the benzyl group removal presents an additional step post cleavage from the resin which is undesirable and often leads to reduced yields. As a consequence, it was proposed that a new protecting group strategy could be utilised to get around this. Specifically, in an ideal situation, the protecting group used would remain inert to reaction conditions employed in the solution and solid phase synthesis but be labile to possible resin cleavage conditions. This would mean that pharmacologically active systems could be isolated directly from the resin thus eliminating a post cleavage deprotection. In turn this could enhance yields and reduce handling of these extremely cytotoxic agents.

One of the protecting groups which caught our attention was the *para*-methoxybenzyl group (PMB). The foremost reason for this was its reactivity profile, which provided the ideal balance of lability and stability for use in our syntheses. The PMB group, like the benzyl group, is relatively stable and is able to remain on a phenol group under a wide variety of different conditions. Also similar is the way in which the PMB can be removed by hydrogenation.[134] In addition to this, deprotection of a PMB group has been demonstrated using oxidative conditions such as the use of DDQ.[135] However, the particular property which drew us towards this group was the multiple demonstrations of lability towards specific acidic conditions. Examples of these conditions include, but are not limited to; $MgBr_2.Et_2O$– Me_2S,[136] $SnCl_2{\cdot}2H_2O$-EtSH,[137] TMSI-TPP,[138] $AlCl_3$–$Me_2NC_6H_5$,[139] $SnCl_4$-benzenethiol[140], $CeCl_3{\cdot}7H_2O$–NaI,[141] $Ce(OTf)_3$,[142] $ZrCl_4$,[143] TfOH-N-methyl-p-toluenesulfonamide or sulfonamide-functionalized (“safety-catch”) resins,[144] and TfOH-1,3-dimethoxybenzene.[145] These conditions have been employed in a variety of systems including natural product synthesis. The desirability of this particular property lies in the fact that upon cleavage of the resin under acidic conditions, the PMB group is likely to also be removed. This would

yield pharmacologically active duocarmycin based peptides and remove the often troublesome post cleavage deprotection step (Scheme 2.29).

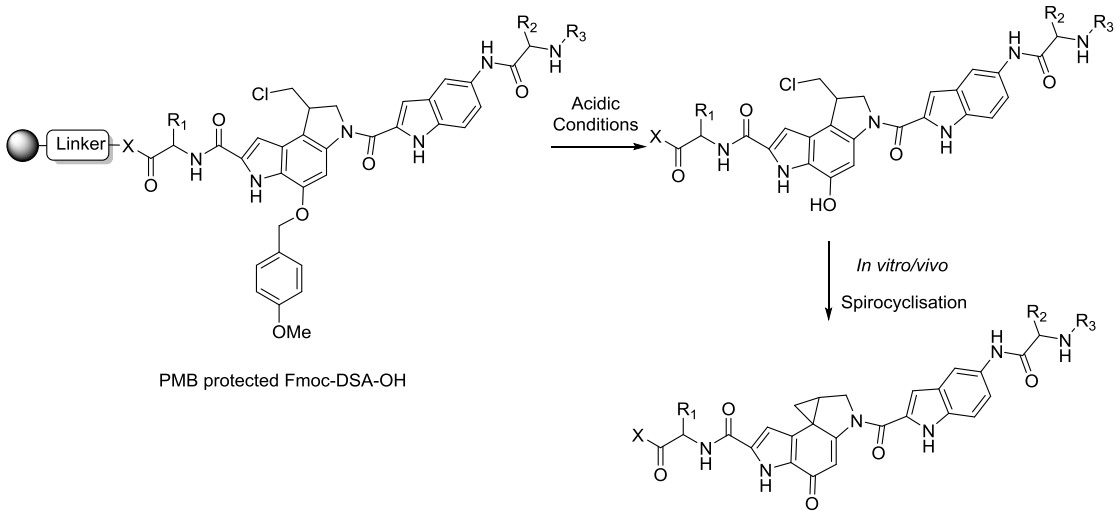

Scheme 2.29: Schematic representation of PMB group utilisation on the solid phase. It was proposed that treatment of the on resin peptide with acidic conditions could lead to combined, resin cleavage and PMB deprotection to yield active analogues.

Despite the promising nature of this strategy, it was envisioned that the final, Boc deprotection and Fmoc protection step in the Fmoc-DSA-OH synthesis could be troublesome for the PMB protected unit. This is due to the acidic conditions utilised to remove the Boc group. It was for this reason that initial attempts to obtain the desired PMB protected Fmoc-DSA-OH unit (**2.18**) was to begin with the previously synthesised benzyl protected Fmoc-DSA-OH. It was hoped that benzyl removal and subsequent PMB protection would quickly yield the desired compound (Scheme 2.30).

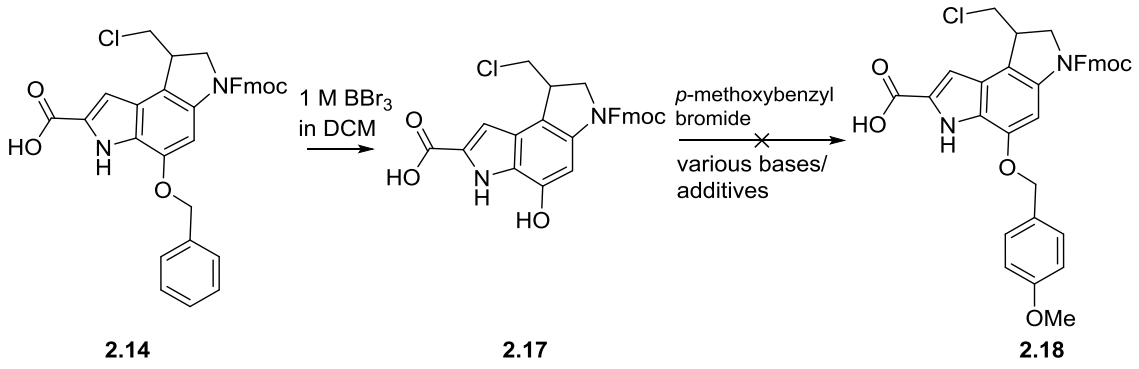

2.14 **2.17** **2.18**

Scheme 2.30: preferred route to PMB protected Fmoc-DSA-OH. PMB protection post benzyl deprotection was unsuccessful.

The deprotection of the benzyl protected Fmoc-DSA-OH unit to give **2.17** was achieved using the boron tribromide based reaction disclosed in section 2.3.4. After purification and confirmation of the desired product, the compound was then subjected to PMB protection using *p*-methoxybenzyl bromide and a variety of basic conditions. These include K_2CO_3, NaOH and NaH. The bases chosen were done so taking into consideration the presence of the base labile Fmoc group on the molecule. By attempting a variety of base strengths it was hoped that optimum conditions where the Fmoc stayed intact whilst the phenol functionality became nucleophilic enough to undergo the S_N2 reaction would be obtained. To try and promote the protection of the phenol, potassium iodide was also utilised in catalytic quantities. What was observed from these conditions was that the desired product was not formed. This was proposed to be due to the high functionality of this Fmoc-DSA-OH unit, particularly the inherent lability of the Fmoc group to basic conditions. It was unlikely that phenol protection would occur without base due to its poor nucleophilicity.

Although this was disappointing to see, the use of the PMB protecting group was pursued through starting the synthesis of the PMB protected Fmoc-DSA-OH unit starting from 2-amino-5-nitro-phenol (see Scheme 2.7 for the analogous synthesis using the benzyl protecting group strategy). In spite of the possibility of the troublesome penultimate Boc deprotection step, it was hoped that some inherent, chemical differences between the Boc and PMB group could be utilised to achieve the selective Boc deprotection. As

described above, one of the attractive properties of the PMB group was its similarities in stability to the benzyl group. It was proposed therefore that the majority of the conditions used towards **2.14** could be retained without significant modifications. Indeed, this was found to be the case. Characterisation of the products from each individual step using conditions described in Section 2.3.1. demonstrated the presence of the desired compounds. ^{1}H NMR showed the formation of the PMB group in each step with an additional singlet for the methoxy CH_3 evident at around 4 ppm. In addition to this, due to the symmetry of the PMB group aromatic protons, two peaks evident as identical multiplets were present in the aromatic regions. We were particularly pleased that the iodination reactions within the synthetic route (see Scheme 2.9 and Scheme 2.17 for the analogous reactions with the benzyl group) were found to occur with the desired regioselectivity. It could be imagined how the more reactive PMB group could have interfered with these reactions.

The synthesis proceeded smoothly up until the penultimate step of Boc deprotection of **2.19** (Scheme 2.31). Initial attempts using 4 M HCl in dioxane as used previously, resulted in what looked like completed degradation of the compound as demonstrated by a messy ^{1}H NMR with no obvious presence of characteristic peaks of these compounds. This was slightly unexpected as it was thought a combined PMB and Boc deprotection would be the only side reaction that may occur. With these conditions proving inapplicable to this system, investigations into other conditions which might be utilised successfully were made. These conditions and the results are summarised in Table 2.4.

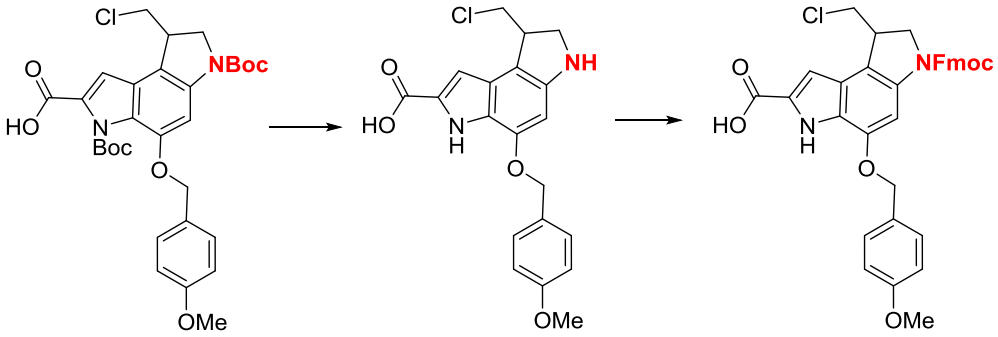

Scheme 2.31: final Boc deprotection and Fmoc protection step to give the PMB protected Fmoc-DSA-OH unit.

Table 2.4: summary of various conditions and their respective results attempted to try and achieve Boc deprotection without removal of PMB group of 2.18.

Conditions [a]	Result
4 M HCl in dioxane	Complete degradation
2 M HCl in dioxane	Partial Boc/PMB deprotection
1 M HCl in dioxane	No reaction
10% TFA in DCM	Partial Boc/PMB deprotection
5% TFA in DCM	No reaction
$SnCl_4$ in EtOAc	Complete degradation
TBAF in THF (reflux)	No reaction
Water (reflux)	No reaction

[a] All conditions were tested under various time points.

The conditions utilised and shown in Table 2.4 were rationally chosen due to their previously shown ability to Boc deprotect. It was hoped that in these mild or non-acidic conditions they could be useful for achieving the desired outcome in our compound.

With the tested conditions resulting in what looked like degradation/some other unknown side reactions or no reaction at all, the literature was further consulted to see if there may be a way around this to achieve the synthesis of **2.18**. The literature search returned a potential route by employing a *para*-chlorobenzyl (PCB) protecting group. This group has been reported as a more stable alternative to the PMB group.[146, 147] Jensen and co-workers then

disclosed the conversion of the PCB group to the PMB group through utilisation of a palladium-RockPhos ligand complex.[148] This route seemed ideal for our system as it meant the increased stability to acidic conditions of the PCB group could be utilised to synthesise the PCB protected Fmoc-DSA-OH (**2.21**). This, according to the literature could then be converted to the desired PMB protected Fmoc-DSA-OH (**2.18**) (Scheme 2.32).

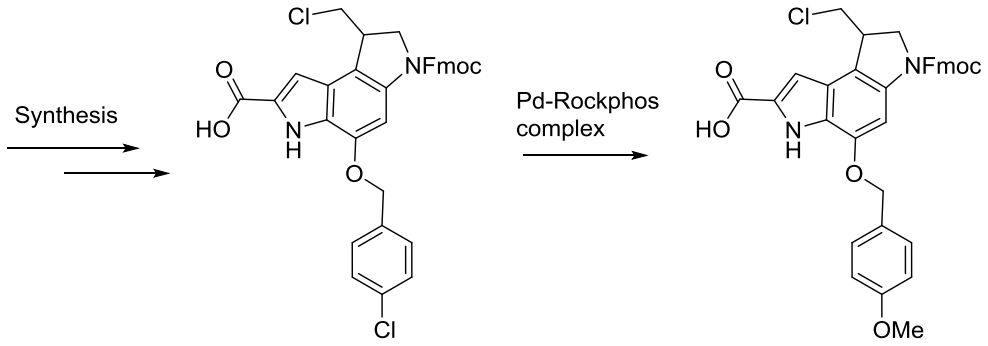

2.21
(PCB protected Fmoc-DSA-OH)

2.18

Scheme 2.32: proposed route utilising the PCB protecting group. Synthesis of PCB protected Fmoc-DSA-OH followed by conversion to the PMB protected unit using a palladium-RockPhos complex.

In order for this strategy to be investigated, the synthesis of **2.21** was carried out. Again, due to the advantageous stable nature of this protecting group, the conditions utilised for the benzyl protected Fmoc-DSA-OH could be mimicked. ^{1}H NMR provided solid evidence of reaction success with the presence of the aromatic protons of this group showing at 7.47 ppm as a multiplet. In addition, mass spectrometry demonstrated the desired masses along with the presence of the characteristic chlorine isotope pattern.

The increased stability of the PCB group to acidic conditions in comparison to the PMB group was demonstrated through a successful Boc deprotection and subsequent Fmoc protection to give the desired compound. This Boc deprotection was achieved using 4 M HCl in dioxane or with trifluoroacetic acid in DCM. Now that the PCB protected Fmoc-DSA-OH was in hand, attempts could be made to convert this to **2.18**. An initial attempt was made following the conditions describe by Jensen and co-workers.[148] These are described in Scheme 2.33.

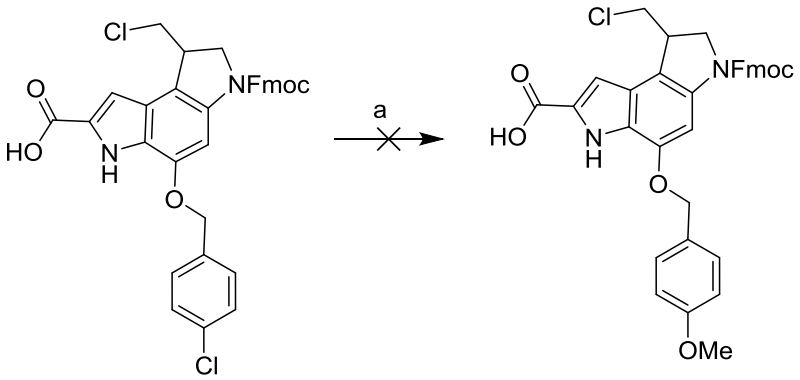

2.21 **2.18**

Scheme 2.33: a: RockPhos Pd G3 (5 mol%), RockPhos ligand (5 mol%), Cs_2CO_3, MeOH, N_2, 20 h, 60 °C.

After the 20 h reaction time course, thin layer chromatography (TLC) suggested no reaction occurring and this was confirmed by ^1H NMR which showed only the presence of starting material. As a progression from this initial attempt, alternative bases were investigated including sodium *tert*-butoxide, which Jensen and co-workers suggested can provide an ideal substitute. However, under these reaction conditions, again no conversion of the starting material was observed. Further attempts to push the reaction to completion through elevating reaction temperatures and ensuring complete exclusion of oxygen to protect the palladium catalyst all proved futile. With little success and the observation of starting material retention, it was proposed that in this system, oxidative addition of the aryl chloride was unfavourable and hence this step was hindering the progress of the PCB to PMB conversion.

2.3.6 On Resin Benzyl Deprotection Using Boron Tribromide

Despite the disappointing results obtained from the PMB based studies, achieving the benzyl deprotection on resin or alongside cleavage was still an area worth exploring. This is due to the possibility of improved yields and a more robust synthetic route to active duocarmycin based peptides. It was for this reason that the boron tribromide reaction discussed in Section 2.3.4. was further investigated. The idea was that treatment of a DSA based peptide, still on the resin, with BBr_3 could result in benzyl deprotection prior to cleavage.

Cleavage from the resin would therefore yield active analogues without the need for post cleavage manipulations (Scheme 2.34).

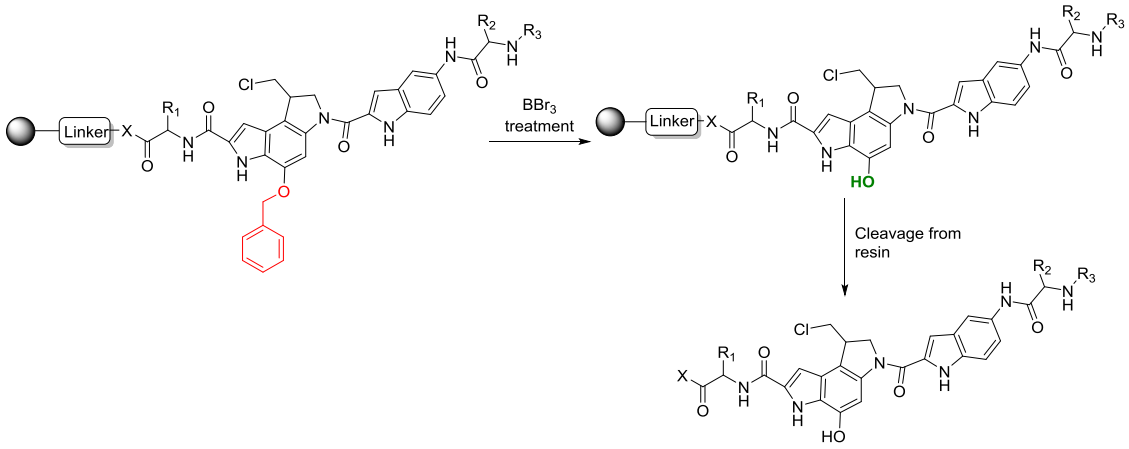

Scheme 2.34: Treatment of on resin peptide with boron tribromide could result in on resin benzyl deprotection therefore removing the need for post cleavage modifications.

With these conditions resulting in the formation of hydrogen bromide (HBr) as a side product, it was possible that resin cleavage may also be achieved in addition to benzyl deprotection. This is due to the acidic nature of HBr.

Specific examples of the peptides on which this method was utilised will be described in Chapters 3 and 4. However, what we were delighted to see from these studies was that resin treatment with the BBr_3 in DCM for 2 h did result in benzyl deprotection. HPLC analysis and post cleavage mass spectrometry studies demonstrated the success of these conditions. Especially pleasing, was the apparent result of complete benzyl deprotection occurring on the resin. This was evident since post cleavage HPLC and mass spectrometry showed no signs of the benzyl protected analogue. Although resin cleavage was not observed during BBr_3 treatment, the work in this thesis using this method was completed on a rink amide resin. The increased acid stability of this resin is likely to have had a role to play within these results. However, it is proposed that the use of the more acid labile 2-Cltrt resin with BBr_3 may yield results of combined benzyl deprotection and resin cleavage.

These results further cement the potential of the benzyl protected Fmoc-DSA-OH unit for use in solid phase peptide synthesis. The benzyl bromide

conditions reported here, greatly increase the efficiency of duocarmycin based analogue synthesis on the solid phase using this unit.

2.4 Conclusions

The aim of the work presented in this chapter was to synthesise a benzyl protected duocarmycin SA based analogue which is suitably substituted for use in solid phase peptide chemistry. As an extension to this, attempts were made to help further realise the potential of this subunit for use in solid phase chemistry.

The synthesis of the duocarmycin SA subunit, substituted for Fmoc based solid phase peptide chemistry was completed on a large scale. Efforts were made to improve some of the bottle neck steps of the synthesis that had shown reduced or erratic yields. Despite various alternative conditions being attempted, including a Larock indole synthesis, a lack of improved yields or meaningful results led us to continue the synthesis on the original path. The final benzyl protected Fmoc-DSA-OH unit was synthesised in 13 steps in an overall yield of 3%.

As an initial attempt to further enhance the utility of this unit on the solid phase, the synthesis of a binding subunit like moiety that can also be employed on a resin support was investigated. The aim of this subunit was to allow attachment to the DSA unit and also peptide chain growth at either the C or the N terminus. The synthesis of this unit proceeded from a commercially available indole and the final Fmoc, carboxylic acid substituted indole was synthesised in 3 steps with an overall yield of 45%. The utility of this unit in solid phase peptide synthesis has been established and specific examples of peptides incorporating this unit will be presented in the coming chapters.

This chapter also aims to provide details of the ideal conditions established for use of the above units on the solid phase. A 2-Cltrt resin has previously been described as an ideal resin to incorporate the Fmoc-DSA-OH unit with HATU and DIPEA based couplings also showing an ideal level of success. A

rink amide resin has been found to be useful for incorporating the DSA unit into peptide sequences where an amide functionalised C-terminus is desired.

Previously, the benzyl group deprotection from the DSA unit has been achieved with a transfer hydrogenation reaction using palladium and ammonium formate. The body of work presented in this thesis established certain examples where these conditions are inapplicable. For this reason investigations to find alternative conditions for the benzyl deprotection were conducted. The use of boron tribromide to achieve this manipulation was found to be desirable in its capacity to be applicable for a wide variety of DSA containing peptides. For peptides where the transfer hydrogenation was shown to be unsuccessful, the boron tribromide conditions yielded the desired benzyl deprotected, active peptides in reasonable yields. Following on from these initial investigations, we were pleased to find that these boron tribromide based conditions can be applied to peptides still on the resin. This means that benzyl deprotection can be achieved before peptide cleavage. This work therefore enhances the use of this analogue on the solid phase since it removes the need for post cleavage modifications which have been found to greatly reduce the yield of the final peptides. Furthermore, removal of the benzyl group before cleavage reduces the need to handle these cytotoxic agents in the laboratory.

Finally, to further improve the efficiency of the Fmoc-DSA-OH compound in solid phase peptide chemistry investigations into alternative protecting groups for the subunit as opposed to the benzyl group were conducted. This was carried out since the benzyl group deprotection has been shown to be tricky in specific examples and also requires an additional step to be removed. It was proposed that an alternative protecting group could be utilised which can be removed during peptide cleavage from the resin under acidic conditions. A PMB protecting group was suggested to be a reasonable alternative for these studies. The synthesis of the final PMB protected Fmoc-DSA-OH unit was found to be intractable due to the need to remove Boc groups with acidic conditions during the synthesis. This was shown to result in either premature PMB deprotection or compound degradation. A PCB protecting group was reported in the literature that shows increased acidic

stability and can be transformed into the PMB under a single step using a palladium catalyst. The synthesis of a PCB protected Fmoc-DSA-OH unit was therefore completed. However, conversion of this into the PMB protected Fmoc-DSA-OH unit was found to be unsuccessful under a variety of conditions. Despite the lack of success with the two protecting groups studied here, further protecting groups could be investigated which may allow for combined deprotection and resin cleavage. If success could be found within this area, a dramatic improvement to the efficiency of using this duocarmycin SA analogue on the solid phase would be made.

2.5 Experimental

2.5.1 General Procedures

Reagents and Solvents

All chemicals were reagent grade and were purchased from Sigma Aldrich, Fisher Scientific, Fluorochem and Tokyo Chemical Industry. Anhydrous solvents were bought from Sigma Aldrich and assumed to conform to specification.

Physical Characterisation and Spectroscopic Techniques

^{1}H- and ^{13}C-NMR spectra were recorded on a Bruker spectrometer operating at 400 MHz (^{1}H) or 100 MHz (^{13}C) using the specified deuterated solvent. The chemical shifts for both ^{1}H- and ^{13}C were recorded in ppm and were referenced to the residual solvent peak of $CHCl_3$ at 7.26 ppm (^{1}H) and 77.0 ppm (^{13}C) or DMSO-d_6 at 2.50 ppm (^{1}H) and 39.5 ppm (^{13}C). Multiplicities in the NMR spectra are described as s = singlet, d = doublet, t = triplet, q = quartet, m = multiplet, br = broad, and combinations thereof; coupling constants are reported in Hz. Assignments, where conspicuous, have been confirmed by appropriate 2D NMR experiments. MALDI was performed on Kratos Analytical Axima MALDI-TOF. Low resolution mass spectra were recorded using a Shimadzu LCMS 2010EV operated under electrospray ionisation mode. Accurate mass spectra were recorded at the EPSRC National Mass Spectroscopy Service Centre, Swansea or The John Innes Centre, Norwich Research Park. Melting points were recorded using open

capillary tubes on a Mel-Temp electrothermal melting point apparatus, melting points are uncorrected. Infrared spectra were recorded as neat samples using a PerkinElmer Spectrum BX with ATR attachment.

Chromatographic Techniques

Thin-layer chromatography was performed on aluminum plates coated with 0.2 mm silica gel-60 F_{254}. After elution, the TLC plates were visualized under UV light. Flash chromatographic separations were performed on silica gel for column chromatography (particle size 60 μm). Analytical RP-HPLC was performed on an Agilent 1200 using an Agilent eclipse XDB-C18 column, 4.6 x 150 mm, 5 μM and a flow rate of 1 mL/min. Solvent A = Water + 0.05% TFA and Solvent B = MeOH + 0.05% TFA. Gradient 5% B up to 95% B over 20 minutes. Detection wavelength 214 nm and 254 nm. Semi-preparative RP-HPLC was performed on an Agilent 1200 using an Agilent eclipse XDB-C18 column, 9.4 x 250 mm, 5 μM and a flow rate of 4 mL/min. Solvent A = Water + 0.05% TFA and Solvent B = MeOH + 0.05% TFA. Gradient 5% B up to 95% B over 20 minutes. Detection wavelength 214 nm and 254 nm. Preparative RP-HPLC was performed on an Agilent 1200 using an Agilent eclipse XDB-C18 column, 21.2 x 150 mm, 5 μM and a flow rate of 20 mL/min. Solvent A = 95% H_2O + 5% MeOH + 0.05% TFA and Solvent B = 95% MeOH + 5% H_2O + 0.05% TFA. Gradient 5% B up to 95% B over 20 minutes.

2.5.2 Synthesis of Fmoc-DSA-OH (2.10)

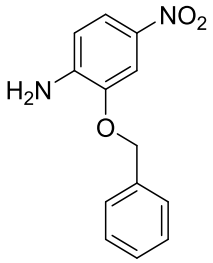

2.2

BnBr (21.0 mL, 178 mmol) was added dropwise to a stirring suspension of 2-amino-5-nitrophenol (25.0 g, 162 mmol) and K_2CO_3 (49.3 g, 257 mmol) in DMF (250 mL) at room temperature. After 3 h, the reaction mixture was poured over crushed ice and allowed to rest for 30 minutes. The precipitate was collected by filtration and triturated with cold water before drying under

vacuum. This yielded 38.98 g of **2.2** as a yellow/brown solid (99 %). Rf 0.17 (20% ethyl acetate in hexane); mp. 145-146 °C (lit.[122] 144–145 °C). ^{1}H NMR ($CDCl_3$, 400 MHz) δ 7.83 (1H, dd, J = 2.3, 8.7), 7.77 (1H, d, J = 2.3), 7.37–7.46 (5H, m), 6.65 (1H, d, J = 8.8), 5.15 (2H, s), 4.60 (2H, brs). ^{13}C NMR ($CDCl_3$, 100 MHz) δ 144.7, 143.1, 138.9, 135.7, 128.9, 128.6, 127.9, 119.3, 112.3, 107.3, 70.9. IR (neat) νmax 3480, 3359, 1622, 1579, 1517, 1479, 1385, 1292, 1222, 1092, 1007, 869, 817, 755, 744, 697 cm^{-1}.

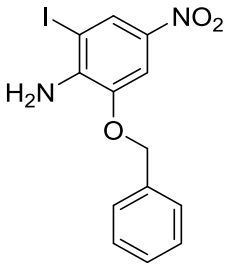

2.3

H_2SO_4 (844 μL, 162 mmol) was added to a stirring solution of **2.2** (39.98 g, 159 mmol) in DMF (590 mL), followed by portionwise addition of NIS (53.9 g, 239 mmol) at room temperature. After 2 h the reaction mixture was poured over crushed ice and left to rest for 30 minutes. The precipitate was collected by filtration and triturated with cold water, followed by cold hexane before drying under vacuum. This yielded 54.85 g of **2.3** as a bright yellow solid (93%). Rf 0.31 (20% ethyl acetate in hexane); mp 101-102 °C (lit.[122] 105–106 °C). ^{1}H NMR ($CDCl_3$, 400 MHz) δ 8.31 (1H, d, J = 2.3), 7.76 (1H, d, J = 2.3), 7.41–7.47 (5H, m) 5.18 (2H, s), 5.04 (2H brs). ^{13}C NMR ($CDCl_3$, 100 MHz) δ 144.0, 143.2, 138.7, 135.2, 128.9, 128.8, 128.2, 128.0, 106.6, 78.4, 71.4. IR (neat) νmax 3476, 3379, 3358, 2357, 2333, 1606, 1587, 1497, 1451, 1311, 1282, 1238, 1099, 1037, 1024, 819, 740, 726, 693 cm^{-1}.

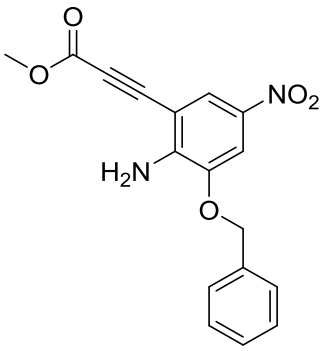

2.4

2.3 (10.0 g, 27 mmol) was dissolved in anhydrous DMF (300 mL). The resulting solution was degassed with a stream of N_2 for 50 minutes prior to addition of methyl propiolate (9.0 mL, 108 mmol), $Pd(PPh_3)_2Cl_2$ (0.95 g, 1.35 mmol), $ZnBr_2$ (24.29 g, 108 mmol) and DIPEA (19.1 mL, 108 mmol). The reaction mixture was then heated to 66 °C and stirred overnight under N_2. After cooling to room temperature the reaction was poured over crushed ice, and the resulting chocolate colour precipitate collected by filtration. The reaction was repeated four times and the precipitates combined prior to absorption on to silica. Elution through a silica plug with 50% ethyl acetate and hexane afforded 37 g of **2.4** as an orange solid (76%). Rf 0.14 (20% ethyl acetate in hexane); mp 130-132 °C (lit.[123] 136–139 °C). ^{1}H NMR ($CDCl_3$, 400 MHz) δ 8.05 (1H, d, J = 2.4), 7.76 (1H, d, J = 2.4), 7.40–7.47 (5H, m), 5.35 (2H, brs), 5.18 (2H, s), 3.87 (3H, s). ^{13}C NMR ($CDCl_3$, 100 MHz) δ 154.0, 146.6, 144.4, 137.6, 135.1, 128.9, 128.9, 128.0, 122.9, 108.2, 100.9, 87.0, 81.1, 71.3, 53.0. IR (neat) νmax 3499, 3391, 3354, 3087, 2359, 2042, 2204, 1697, 1614, 1506, 1300, 1239, 1094, 1002, 886, 740, 731, 696, 612 cm^{-1}.

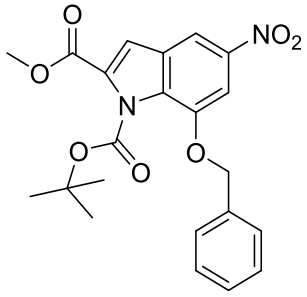

2.5

2.4 (15 g, 48.1 mmol) in anhydrous THF (215 mL) was treated with 1M TBAF in THF solution (95.5 mL, 96 mmol) and refluxed at 66°C for 1 h. After cooling to room temperature the THF was removed by rotary evaporation under reduced pressure. The residue was dissolved in ethyl acetate (250 mL) and washed three times with water (250 mL). Concentration of the ethyl acetate followed by co-evaporation of the residue with DCM afforded crude **2.4a** as a dark purple foam. The foam was dissolved in DCM (250 mL) and treated with Boc_2O (20.9 g, 95 mmol) and DMAP (5.83 g, 4.8 mmol) at room temperature for 2 h. Removal of the DCM gave crude **2.5** as a dark foam. The reaction was then repeated on the same scale and the foam dry loaded onto

silica and purified using column chromatography (10% ethyl acetate in hexane). Removal of the solvent gave 6.21 g of **2.5** as a bright yellow solid (15%). Rf 0.31 (20% ethyl acetate in hexane); mp 166-168 °C (lit.[123] 168–171 °C). ^{1}H NMR ($CDCl_3$, 400 MHz) δ 8.26 (1H, d, J = 1.9), 7.67 (1H, d, J = 1.9), 7.48–7.44 (2H, m), 7.42–7.35 (3H, m), 7.33 (1H, s) 5.33 (2H, s), 3.94 (3H, s), 1.47 (9H, s). ^{13}C NMR ($CDCl_3$, 100 MHz) δ 160.4, 149.2, 145.5, 143.5, 135.1, 130.1, 128.8, 128.6, 128.1, 126.3, 112.6, 112.3, 102.1, 86.4, 71.2, 52.4, 27.8, 27.2. IR (neat) νmax 3308, 3127, 2981, 2523, 2161, 1765, 1721, 1586, 1511, 1325, 1251, 1225, 1152, 982, 875, 841, 822, 742, 730, 697, 606 cm^{-1}.

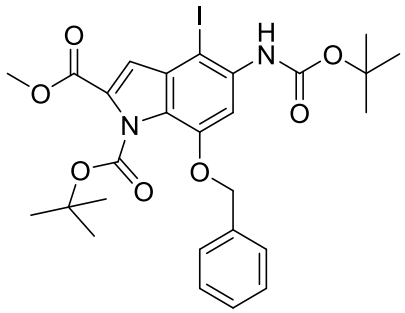

2.6

2.5 (6.2 g, 14.4 mmol) was dissolved in THF (260 mL) and treated with zinc powder (14.0 g, 215 mmol) NH_4Cl (7.7 g, 143.7 mmol), Boc_2O (9.36 g, 43.1 mmol), DMAP (175 mg, 1.4 mmol) and water (25 mL). The resulting suspension was stirred vigorously at room temperature overnight. After removal of the THF under pressure, the residue was dissolved in Et_2O (200 mL) and washed three times with water (100 mL) and dried with $MgSO_4$. Removal of the ether gave crude **2.5a** as a yellow foam. Crude **2.5a** was dissolved in DMF (80 mL) and treated with H_2SO_4 (76 μL, 1.4 mmol) before portionwise addition of NIS (4.9 g, 21.5 mmol). The solution was stirred for 3 h at room temperature. The reaction was then diluted with Et_2O (200 mL) and washed once with 50% saturated brine in water (200 mL), twice with water (200 mL), and once with saturated brine (200 mL). The first wash was back extracted three times with Et_2O (100 mL) and washed twice with saturated brine (200 mL). All the Et_2O was combined and concentrated to give a dark red foam. The foam was purified by column chromatography (10% ethyl acetate in hexane) to give **2.6** (5.0 g, 57%) as an off white solid. Rf 0.32 (20% ethyl acetate in hexane); mp 160-161 °C (lit.[123] 158–161 °C). ^{1}H

NMR ($CDCl_3$, 400 MHz) δ 7.78 (1H, brs), 7.49–7.44 (2H, m), 7.29–7.38 (3H, m), 7.09 (1H, s), 6.76 (1H, brs), 5.24 (2H, s), 3.91 (3H, s), 1.53 (9H, s), 1.40 (9H, s). ^{13}C NMR ($CDCl_3$, 100 MHz) δ 160.8, 152.9, 149.7, 146.4, 135.8, 134.5, 131.4, 128.5, 128.4, 128.2, 127.6, 123.6, 114.4, 102.4, 85.5, 80.9, 70.9, 52.2, 28.4, 27.1. IR (neat) νmax 3391, 2973, 1764, 1730, 1715, 1615, 1576, 1539, 1450, 1359, 1232, 1216, 1150, 1076, 982, 878, 843, 723, 693 cm^{-1}.

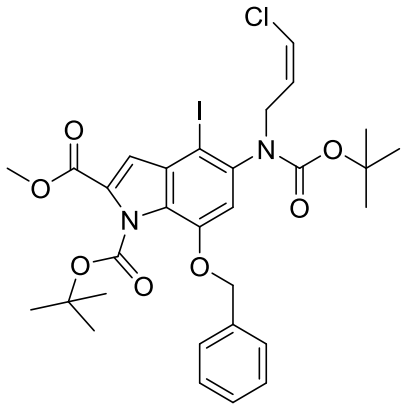

2.7

2.6 (5.0 g, 8 mmol) was dissolved in DMF (85 mL) and treated with t-BuOK (1.9 g, 17 mmol) and 1,3-dichloropropene as a mixture of *cis* and *trans* isomers (3.0 mL, 25 mmol). The resulting solution was stirred for 1.5 h submerged in a room temperature water bath. The reaction was then cooled to 0 °C before being quenched with saturated aqueous NH_4Cl (4 mL). The mixture was then diluted with Et_2O (200 mL) and washed twice with 50% saturated brine in water (200 mL) and once with saturated brine (200 mL). The Et_2O was then dried over $MgSO_4$ and concentrated before co-evaporation with DCM to give a brown foam. The crude foam was absorbed onto silica and purified by silica gel chromatography (5% ethyl acetate in hexane increasing up to 10% ethyl acetate until complete elution of the product) to give **2.7** as a light brown foam (4.1 g, 73 %). Rf 0.29 (20% ethyl acetate in hexane); mp 103-105 °C (lit.[123] 104–106 °C). ^1H NMR ($CDCl_3$, 400 MHz, mixture of E/Z isomers) δ 7.28–7.44 (5H, m) 7.18 (1H, s), 6.65–6.47 (1H, m), 5.80–6.00 (2H, m), 5.17–5.28 (2H, m), 4.46 and 4.18 (1H, m), 4.33 and 3.73 (1H, m), 3.93 (3H, s), 1.53 (9H, s), 1.29 and 1.27 (9H, s). ^{13}C NMR ($CDCl_3$, 100 MHz) δ 160.7, 154.1, 149.9, 145.5, 138.6, 138.3 135.8, 132.1, 128.7, 128.3, 127.95, 127.5, 127.3, 125.3, 121.7, 120.6, 115.1, 109.7 85.8, 83.8, 80.5, 70.6,

52.3, 49.3, 46.1, 28.2, 27.2. IR (neat) νmax 2923, 1775, 1735, 1702, 1695, 1572, 1535, 1463, 1435, 1372, 1299, 1251, 1227, 1077, 978, 845, 784, 764, 739, 731, 698 cm^{-1}.

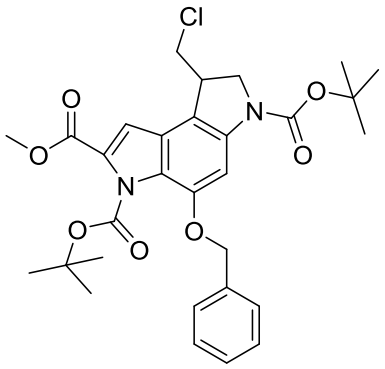

2.8

2.7 (4.1 g, 5.9 mmol) was dissolved in anhydrous toluene and degassed with a stream of nitrogen for 45 minutes prior to addition of AIBN (0.24 g, 1.5 mmol) and TTMSS (2.0 mL, 6.5 mmol). The resulting solution was refluxed at 90°C under nitrogen for 2 h. The reaction was then left to cool to room temperature before being concentrated and subjected directly to silica gel column chromatography. 2% ethyl acetate in hexane was initially run before increasing up to 5% ethyl acetate until complete elution of the product. Removal of the solvent gave **2.8** (2.4 g, 71%) as a colourless foam. Rf 0.35 (20% ethyl acetate in hexane); mp 116-119 °C (lit.[123] 115–118 °C). ^{1}H NMR (DMSO-d_6, 400 MHz) δ 7.69 (1H brs), 7.48–7.29 (6H, m), 5.27 (2H, s), 4.13 (1H, t, J = 9.7), 4.06–3.89 (4H, m), 3.87 (3H, s), 1.48 (9H, s), 1.38 (9H, s). ^{13}C NMR (DMSO-d_6, 100 MHz) δ 160.8, 151.9, 150.0, 145.5, 136.6, 128.5, 128.3, 128.2, 124.0, 113.2, 108.9, 97.4, 85.4, 80.3, 70.2, 52.7, 52.6, 48.0, 40.7 (obscured by DMSO peak observed by HSQC), 28.4, 27.2, 22.5. IR (neat) νmax 2998, 2974, 2921, 1782, 1698, 1593, 1538, 1494, 1439, 1417, 1381, 1343, 1241, 1216, 1141, 1089, 1022, 918, 836, 763, 747, 699, 691 cm^{-1}.

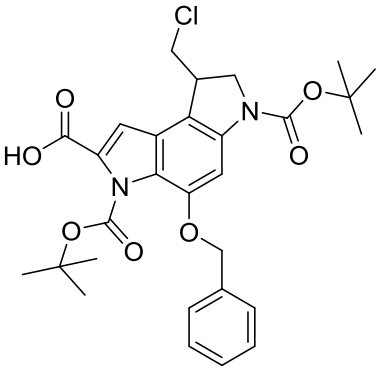

2.9

2.8 (2.4 g, 4.2 mmol) was dissolved in a mixture of THF (45 mL) and MeOH (30 mL) and treated with a saturated aqueous solution of LiOH (17 mL) dropwise. After 4 h the THF and MeOH was removed under reduced pressure, and the residue diluted with water (30 mL). Acidification with 5 M HCl promoted the precipitation of **2.9** (2.3 g, 100%) as a green foam. Rf 0.46 (10% MeOH in CH_2Cl_2); mp 177-180 °C (lit.[123] 174–178 °C). ^{1}H NMR (DMSO-d_6, 400 MHz) δ 13.45 (1H, brs), 7.66 (1H, brs), 7.47–7.31 (6H, m), 5.26 (2H, s), 4.12 (1H, t, J = 9.7), 4.05–3.86 (4H, m), 1.49 (9H, s), 1.37 (9H, s). ^{13}C NMR (DMSO-d_6, 100 MHz) δ 161.9, 151.7, 149.4, 136.4, 129.9, 128.8, 128.4, 127.9, 123.8, 123.8, 122.9, 107.9 97.6, 85.0, 80.5, 70.0, 52.6, 47.9, 41.0 (obscured by DMSO peak observed by HSQC), 28.5, 26.8, 22.5. IR (neat) νmax 2972, 2926, 2358, 2321, 1765, 1690, 1682, 1592, 1536, 1495, 1393, 1251, 1142, 1084, 1015, 942, 747, 695, 669 cm^{-1}.

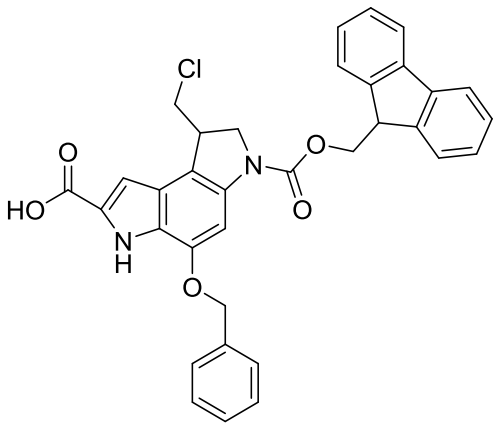

2.10

2.9 (2.4 g, 4.3 mmol) was dissolved in 4 M HCl in dioxane (45 mL) and stirred at room temperature overnight. Upon removal of the dioxane under reduced pressure, the residue was dissolved in THF (65 mL) and the solution

cooled to 0 °C. The solution was then treated with $NaHCO_3$ (1.08 g, 12.9 mmol) in H_2O (22 mL) followed by Fmoc-Cl (1.11 g, 4.3 mmol) in THF (24 mL) and left to stir for 5 minutes. After quenching with MeOH (1 mL) the THF and MeOH were removed under reduced pressure. The resulting mixture was then acidified with 2 M HCl and extracted three times with 2-MeTHF (100 mL). The organic layer was dried over $MgSO_4$ and the 2-Me-THF removed under reduced pressure. The crude was dried loaded onto silica and purified by silica gel chromatography. 100% DCM was initially run gradually increasing up to 5% MeOH in DCM until complete elution of the product. Upon removal of the solvent, **2.10** (2.1 g, 84%) was obtained as a light green foam. Rf 0.42 (10% MeOH in CH_2Cl_2); mp 122-125 °C (lit.[123] 125–128 °C). ^{1}H NMR (DMSO-d_6, 400 MHz) δ 12.97 (1H, brs), 11.90 (1H, s), 7.90 (2H, d, J = 6.7), 7.74–7.68 (2H, m), 7.67–7.57 (2H, m), 7.53–7.23 (8H, m), 7.20 (1H, d, J = 1.8), 5.35–5.84 (2H, brs, [rotameric coalescence observed at 333 K, δ 5.17, 2H, s]), 4.74– 4.31 (3H, m, [rotameric coalescence observed at 333 K, δ 4.55, 2H, app quin, δ 4.39, 1H, t, J = 6.6]), 4.23–4.14 (1H, m), 4.10–3.94 (3H, m), 3.93–3.84 (1H, m). ^{13}C NMR (DMSO-d_6, 100 MHz) δ 162.9, 152.0, 146.0, 143.9, 141.2, 137.2, 130.3, 128.6, 128.2, 128.0, 127.9, 127.6, 126.0, 125.4, 124.1, 120.6, 113.0, 106.2, 95.9, 70.0, 67.0, 51.9, 47.9, 47.1, 41.5, 34.9. IR (neat) νmax 3031, 2359, 2320, 1733, 1601, 1594, 1539, 1444, 1417, 1311, 1243, 1218, 1172, 1130, 1056, 827, 753, 737, 667 cm^{-1}. HRMS (ES-) calcd. for $C_{34}H_{27}N_2O_5Cl$ (M - H)-,577.1530; found, 577.1325.

2.5.3 Synthesis of Fmoc Substituted Binding Subunit (2.14)

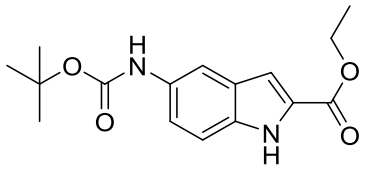

2.15

Ethyl-5-nitro-indole-2-carboxylate (0.5 g, 2.1 mmol) was dissolved in THF (10 mL) and treat with zinc (2.1 g, 31.8 mmol), NH_4Cl (1.13 g, 21.2 mmol), Boc_2O (1.36 g, 6.3 mmol) DMAP (26 mg, 0.2 mmol) and water (3.5 mL). The resulting mixture was stirred vigorously overnight at room temperature. Upon removal of the THF under reduced pressure the residue was taken up in diethyl ether (200 mL) and washed with water (3 x 200 mL). The organic

layer was concentrated to give crude **2.15**. The reaction was repeated on a 1 g scale and the crudes combined before purification by silica gel column chromatography (10% ethyl acetate in hexane). Upon removal of the solvent **2.15** (1.7 g, 88%) was obtained as a colourless solid. Rf 0.35 (20% ethyl acetate in hexane); mp 187–188 °C. ^{1}H NMR (DMSO-d_6, 400 MHz) δ 11.71 (1H, s), 9.17 (1H, s), 7.80 (1H, s), 7.23-7.33 (2H, m), 7.05 (1H, d, J = 1.5), 4.32 (2H, q, J = 6.9), 1.48 (9H, s), 1.33 (3H, t, J = 7.2). ^{13}C NMR (DMSO-d_6, 100 MHz) δ 161.7, 153.6, 134.2, 133.0, 128.1, 127.2, 119.0, 112.9, 110.7, 107.9, 79.0, 60.8, 28.7, 14.8. IR (neat) νmax 3379, 3339, 2976, 2354, 1702, 1682, 1525, 1230, 1165, 1050, 1024, 808, 769, cm^{-1}. HRMS (ES-) calcd. for $C_{16}H_{20}N_2O_4$ (M - H)- , 303.1343; found, 303.1365.

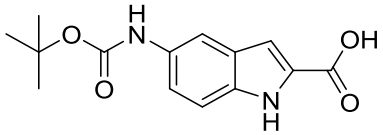

2.16

2.15 (1.7 g, 5.6 mmol) was dissolved in THF (50 mL), and MeOH (30 mL) and treated with a saturated aqueous solution of LiOH (16 mL) dropwise. The solution was left to stir at room temperature for 4 h before removal of the THF and MeOH under reduced pressure. The residue was diluted with water (100 mL) and acidified using 5 M HCl. The resulting precipitate was collected using vacuum filtration and recovered from the sinter by dissolution in ethyl acetate. Removal of the solvent under reduced pressure gave **2.16** (1.45 g, 93%) as an off white solid. Rf 0.35 (10% MeOH in CH_2Cl_2); mp 206-208 °C. ^{1}H NMR (DMSO-d_6, 400 MHz) δ 12.81 (1H, brs), 11.59 (1H, s), 9.15 (1H, s), 7.77 (1H, s), 7.22-7.31 (2H, m), 6.97 (1H, d, J = 1.5), 1.48 (9H, s). ^{13}C NMR (DMSO-d_6, 100 MHz) δ 163.2, 153.6, 134.1, 132.8, 129.3, 127.3, 118.5, 112.8, 110.7, 107.5, 79.0, 28.7. IR (neat) νmax 3352, 2978, 2346, 1697, 1538, 1468, 1428, 1242, 1201, 1180, 1165, 1050, 1029, 802, 769 cm^{-1}. HRMS (ES-) calcd. for $C_{14}H_{16}N_2O_4$ (M - H)- , 275.1030; found, 275.1109

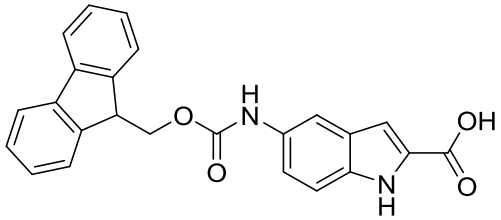

2.14

2.16 (1.4 g, 5.2 mmol) was dissolved in 4 M HCl in dioxane (25 mL) and stirred overnight at room temperature. The dioxane was removed under reduced pressure and the resulting residue taken up in THF (45 mL). The solution was cooled to 0 ºC before being treated with $NaHCO_3$ (1.30 g, 15.5 mmol) in water (25 mL) followed by Fmoc-Cl (1.34 g, 5.2 mmol) dropwise in THF (28 mL). After 5 mins the reaction was quenched with MeOH (1 mL) and the THF and MeOH removed under reduced pressure. The remaining mixture was acidifed using 2 M HCl and extracted three times with 2-MeTHF before being dried over $MgSO_4$. Crude 2.14 was purified by silica gel chromatography (100% DCM increasing up to 5% MeOH in DCM until complete elution of the product). Upon removal of the solvent, **2.14** (1.07 g, 55%) was obtained as a colourless solid. Rf 0.38 (10% MeOH in CH_2Cl_2); mp 255-257 °C. ^{1}H NMR (DMSO, 400 MHz) δ 12.88 (1H, s), 11.64 (1H, s), 9.56 (1H, s), 7.91 (2H, d, J = 7.5), 7.73-7.80 (2H, m), 7.39-7.45 (3H, m), 7.29-2.738 (4H, m), 4.47 (2H, d, J = 6.9), 4.31 (1H, t, J = 6.6). ^{13}C NMR (DMSO-d_6, 100 MHz) δ 163.2, 154.2, 144.3, 141.3, 134.3, 132.3, 129.4, 128.1, 127.6, 127.3, 125.6, 120.6, 118.7, 113.0, 111.1, 107.6, 65.9, 47.2, 23.0. IR (neat) νmax 3327, 2962, 2364, 1699, 1670, 1534, 1434, 1293, 1232, 1177, 1293, 1232, 1048, 741 cm^{-1}. HRMS (ES+) calcd. for $C_{24}H_{18}N_2O_4$ (M - H)- , 398.1186; found, 397.1281.

2.5.4 Synthesis of PMB Protected Fmoc-DSA-OH

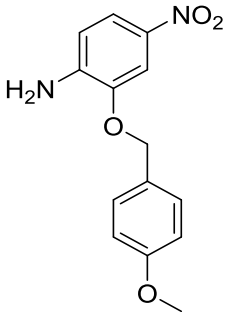

2.2-PMB

4-Methoxybenzyl chloride (12.8 mL, 96.0 mmol) was added dropwise to a stirring suspension of 2-amino-5-nitrophenol (15.0 g, 96 mmol) and K_2CO_3 (26.5 g, 192 mmol) in DMF (150 mL) at room temperature. After 3 h, the reaction mixture was poured over crushed ice and allowed to rest for 30 minutes. The precipitate was collected by filtration and triturated with cold water before drying under vacuum. This yielded 26.53 g of **2.2-PMB** as a yellow/brown solid (99%). Rf 0.15 (20% ethyl acetate in hexane); mp 132-133 °C. ^{1}H NMR ($CDCl_3$, 400 MHz) δ 7.82 (1H, dd, J = 2.4, 8.6), 7.78 (1H, d, J = 2.4), 7.34–7.40 (2H, m), 6.91-6.95 (2H, m), 6.64 (1H, d, J = 8.7), 5.07 (2H, s), 3.83 (3H, s). ^{13}C NMR ($CDCl_3$, 100 MHz) δ 144.7, 143.2, 136.2, 134.2, 129.7, 128.2, 127.7, 119.3, 114.1, 107.3, 70.7, 55.3. IR (neat) νmax 3491, 3352, 3218, 3188, 2947, 2852, 1625, 1569, 1510, 1482, 1468, 1386, 1282, 1194, 1176, 1091, 950, 870, 782, 754, 646 cm^{-1}.

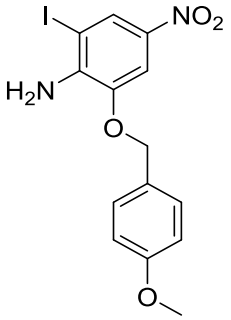

2.3-PMB

H_2SO_4 (507 µL, 9.60 mmol) was added to a stirring solution of **2.2-PMB** (26.50 g, 96.0 mmol) in DMF (420 mL), followed by portionwise addition of NIS (32.0 g, 144 mmol) at room temperature. After 2 h the reaction mixture was poured over crushed ice and left to rest for 30 minutes. The precipitate was collected by filtration and triturated with cold water, followed by cold hexane before drying under vacuum. This yielded 37.10 g of **2.3-PMB** as a

bright yellow solid (93%). Rf 0.28 (20% ethyl acetate in hexane); mp 138-140 °C. ^{1}H NMR ($CDCl_3$, 400 MHz) δ 8.28 (1H, d, J = 2.2), 7.74 (1H, d, J = 2.2), 7.34–7.48 (2H, m) 6.92-6.97 (2H, m), 5.08 (2H s), 4.99 (2H, brs), 3.84 (3H, s). ^{13}C NMR ($CDCl_3$, 100 MHz) δ 160.0, 144.0 143.3, 138.7, 129.8, 128.1, 127.3, 114.2, 106.6, 78.3, 71.2, 55.4. IR (neat) νmax 3469, 3387, 3242, 3056, 3045, 2332, 1612, 1569, 1492, 1444, 1282, 1205, 1145, 1032, 869, 849, 810, 758, 652 cm^{-1}. HRMS (ES-) calcd. for $C_{14}H_{13}N_2O_4I$ (M - H)- , 398.9841; found, 398.9945.

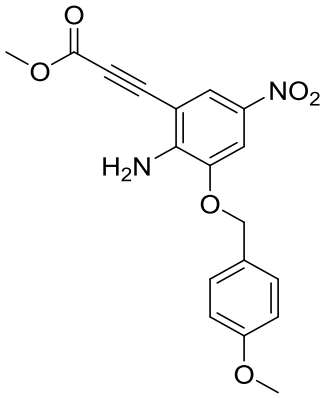

2.4-PMB

2.3-PMB (15.0 g, 32 mmol) was dissolved in anhydrous DMF (220 mL). The resulting solution was degassed with a stream of N_2 for 50 minutes prior to addition of methyl propiolate (11.38 mL, 128.0 mmol), $Pd(PPh_3)_2Cl_2$ (1.12 g, 1.6 mmol), $ZnBr_2$ (28.82 g, 128.0 mmol) and DIPEA (22.29 mL, 128.0 mmol). The reaction mixture was then heated to 66 °C and stirred overnight under N_2. After cooling to room temperature the reaction was poured over crushed ice, and the resulting chocolate colour precipitate collected by filtration. The precipitate was then absorbed on to silica. Elution through a silica plug with 50% ethyl acetate and hexane afforded 6.73 g of **2.4-PMB** as an orange solid (60%). Rf 0.20 (20% ethyl acetate in hexane); mp 146-147 °C. ^{1}H NMR ($CDCl_3$, 400 MHz) δ 8.04 (1H, d, J = 2.3), 7.76 (1H, d, J = 2.3), 7.34–7.38 (2H, m), 6.93-6.97 (2H, m), 5.28 (2H, brs), 5.09 (2H, s), 3.86 (3H, s), 2.84 (3H, s). ^{13}C NMR ($CDCl_3$, 100 MHz) δ 160.1, 154.0, 146.7, 144.4, 137.5, 129.9, 127.1, 122.8, 114.3, 108.1, 100.7, 86.9, 81.1, 71.2, 55.3, 53.0. IR (neat) νmax 3488, 3384, 3256, 3101, 3024, 3015, 2902, 2226, 1699, 1608, 1475, 1398, 1297, 1281, 1230, 1158, 1099, 1010, 882, 749, 735, 690, 650, 620

cm^{-1}. HRMS (ES-) calcd. for $C_{18}H_{16}N_2O_6$ (M - H)- , 355.0930; found, 355.0917.

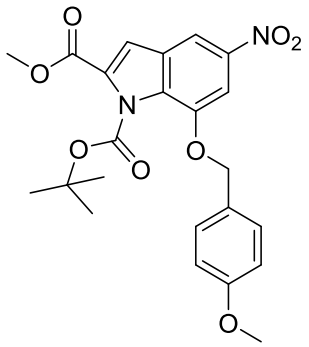

2.5-PMB

2.4-PMB (7.52 g, 21.1 mmol) in anhydrous THF (110 mL) was treated with 1 M TBAF in THF solution (47 mL, 47.2 mmol) and refluxed at 66°C for 1 h. After cooling to room temperature the THF was removed by rotary evaporation under reduced pressure. The residue was dissolved in ethyl acetate (125 mL) and washed three times with water (125 mL). Concentration of the ethyl acetate followed by co-evaporation of the residue with DCM afforded crude **2.4a-PMB** as a dark purple foam. The foam was dissolved in DCM (125 mL) and treated with Boc_2O (9.17 g, 42.2 mmol) and DMAP (2.58 g, 21.1 mmol) at room temperature for 2 h. Removal of the DCM gave crude **2.5-PMB** as a dark foam which was dry loaded onto silica and purified using column chromatography (10% ethyl acetate in hexane). Removal of the solvent gave 5.22 g of **2.5-PMB** as a bright yellow solid (54%). Rf 0.37 (20% ethyl acetate in hexane); mp 154-156 °C. ^{1}H NMR ($CDCl_3$, 400 MHz) δ 8.25 (1H, d, J = 1.9), 7.69 (1H, d, J = 1.9), 7.41–7.37 (2H, m), 7.33 (1H, s), 6.92-6.89 (2H, m) 5.25 (2H, s), 3.93 (3H, s), 3.81 (3H, s), 1.47 (9H, s). ^{13}C NMR ($CDCl_3$, 100 MHz) δ 161.0, 149.6, 145.9, 143.8, 135.6, 130.4, 129.2, 128.8, 128.3, 126.5, 113.1, 113.0, 101.9, 86.7, 71.4, 54.2, 52.6, 27.8, 27.2. IR (neat) νmax 3135, 3106, 3092, 2812, 1762, 1715, 1594, 1503, 1399, 1310, 1246, 1178, 1003, 954, 852, 842, 811, 766, 729, 703, 618 cm^{-1}.

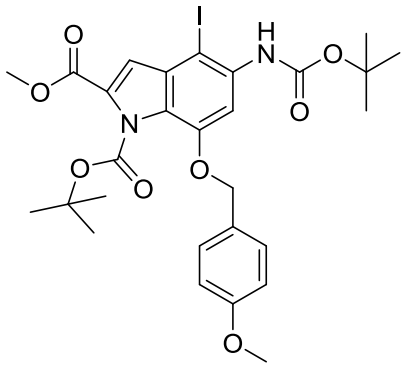

2.6-PMB

2.5-PMB (5.22 g, 11.4 mmol) was dissolved in THF (110 mL) and treated with zinc powder (11.17 g, 171.7 mmol) NH_4Cl (6.12 g, 114.3 mmol), Boc_2O (7.46 g, 34.3 mmol), DMAP (139 mg, 1.14 mmol) and water (21 mL). The resulting suspension was stirred vigorously at room temperature overnight. After removal of the THF under pressure, the residue was dissolved in Et_2O (200 mL) and washed three times with water (100 mL) and dried with $MgSO_4$. Removal of the ether gave crude **2.5a-PMB** as a yellow foam. Crude **2.5a-PMB** was dissolved in DMF (70 mL) and treated with H_2SO_4 (60 μL, 1.14 mmol) before portionwise addition of NIS (7.72 g, 34.3 mmol). The solution was stirred for 3 h at room temperature. The reaction was then diluted with Et_2O (200 mL) and washed once with 50% saturated brine in water (200 mL), twice with water (200 mL), and once with saturated brine (200 mL). The first wash was back extracted three times with Et_2O (100 mL) and washed twice with saturated brine (200 mL). All the Et_2O was combined and concentrated to give a dark red foam. The foam was purified by column chromatography (10% ethyl acetate in hexane) to give **2.6-PMB** (2.43 g, 33%) as an off white solid. Rf 0.38 (20% ethyl acetate in hexane); mp 110-112 °C. ^{1}H NMR ($CDCl_3$, 400 MHz) δ 7.79 (1H, brs), 7.41–7.37 (2H, m), 7.08 (1H, s), 6.90-6.86 (2H, m), 6.77 (1H, brs), 5.17 (2H, s), 3.90 (3H, s), 3.80 (3H, s), 1.54 (9H, s), 1.40 (9H, s). ^{13}C NMR ($CDCl_3$, 100 MHz) δ 159.7, 152.9, 149.8, 146.5, 135.8, 134.5, 131.3, 130.2, 128.0, 127.6, 121.5, 114.4, 113.9, 85.5, 80.9, 70.7, 55.3, 52.1, 28.4, 27.1. IR (neat) νmax 3355, 2910, 2325, 1755, 1736, 1702, 1652, 1529, 1485, 1401, 1365, 1312, 1239, 1209, 1172, 1042, 971, 852, 767, 753, 682 cm^{-1}.

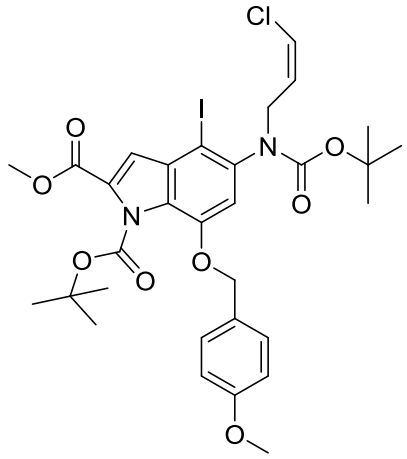

2.7-PMB

2.6-PMB (2.43 g, 3.7 mmol) was dissolved in DMF (50 mL) and treated with NaH (0.18 g, 7.4 mmol) and 1,3-dichloropropene as a mixture of *cis* and *trans* isomers (1.03 mL, 11.1 mmol). The resulting solution was stirred for 2 h submerged in a room temperature water bath. The reaction was then cooled to 0 °C before being quenched with saturated aqueous NH_4Cl (2 mL). The mixture was then diluted with Et_2O (150 mL) and washed twice with 50% saturated brine in water (150 mL) and once with saturated brine (150 mL). The Et_2O was then dried over $MgSO_4$ and concentrated before co-evaporation with DCM to give a brown foam. The crude foam was absorbed onto silica and purified by silica gel chromatography (5% ethyl acetate in hexane increasing up to 10% ethyl acetate until complete elution of the product) to give **2.7-PMB** as a light brown foam (1.05 g, 40%). Rf 0.34 (20% ethyl acetate in hexane); mp 87-89 °C. ^{1}H NMR ($CDCl_3$, 400 MHz, mixture of E/Z isomers) δ 7.41–7.30 (2H, m) 7.17 (1H, s), 6.93–6.83 (2H, m), 5.79–6.46 (1H, m), 6.05–5.83 (2H, m), 5.16 (1H, m), 4.52-4.15 (1H, m), 2.94-3.89 (3H, m), 3.81-3.77 (3H, s), 1.57-1.46 (9H, m), 1.41-1.24 (9H, m). ^{13}C NMR ($CDCl_3$, 100 MHz) δ 160.7, 159.7, 153.8, 149.6, 145.9, 142.7, 138.4, 135.2, 132.5, 129.3, 128.7, 128.2, 127.9, 127.8, 127.7, 121.5, 120.4, 115.2, 109.5, 85.9, 83.4, 79.8, 70.4, 55.3, 52.2, 46.3, 28.2, 27.2. IR (neat) νmax 2984, 1762, 1720, 1699, 1679, 1571, 1449, 1429, 1413, 1296, 1278, 1162, 1099, 969, 853, 845, 764, 705 cm^{-1}. HRMS (ES-) calcd. for $C_{31}H_{36}N_2O_8ClI$ (M - H)- , 725.1126; found, 725.1216.

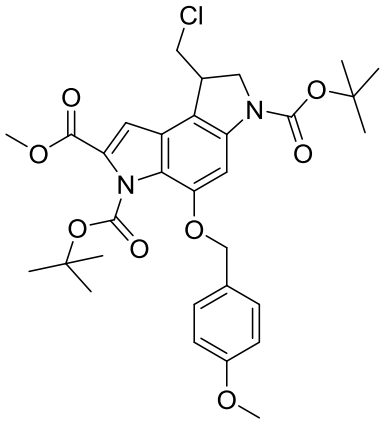

2.8-PMB

2.7-PMB (1.05 g, 1.5 mmol) was dissolved in anhydrous toluene (10 mL) and degassed with a stream of nitrogen for 45 minutes prior to addition of AIBN (60 mg, 0.36 mmol) and TTMSS (490 μl, 1.59 mmol). The resulting solution was refluxed at 90°C under nitrogen for 2 h. The reaction was then left to cool to room temperature before being concentrated and subjected directly to silica gel column chromatography. 2% ethyl acetate in hexane was initially run before increasing up to 5% ethyl acetate until complete elution of the product. Removal of the solvent gave **2.8-PMB** (0.74 g, 55%) as a colourless foam. Rf 0.35 (20% ethyl acetate in hexane); mp 108.120 °C. ^{1}H NMR ($CDCl_3$, 400 MHz) δ 7.80 (1H, brs), 7.45–7.34 (2H, m), 7.07 (1H, s), 6.91-6.86 (2H, m), 5.16 (2H, m), 4.01-4.18 (2H, m), 3.89 (3H, s), 3.87-3.81 (2H, m), 3.80 (3H, s), 3.50 (1H, t, J = 8.8), 1.56 (9H, s), 1.40 (9H, s). ^{13}C NMR (DMSO-d^{6}, 100 MHz) δ 160.9, 159.7, 150.0, 148.2, 145.7, 135.2, 130.1, 130.0, 129.9, 128.6, 128.0, 124.7, 124.0, 129.9, 114.3, 108.2, 97.0, 85.5, 80.6, 70.1, 55.6.3, 52.8, 48.1, 40.7, 28.5, 27.2, 22.5. IR (neat) νmax 3016, 2982, 2416, 1771, 1735, 1703, 1610, 1509, 1482, 1405, 1299, 1254, 1152, 1102, 998, 876, 749, 736, 705, cm^{-1}. HRMS (ES-) calcd. for $C_{31}H_{37}N_2O_8Cl$ (M - H)- , 599.2160; found, 599.2042.

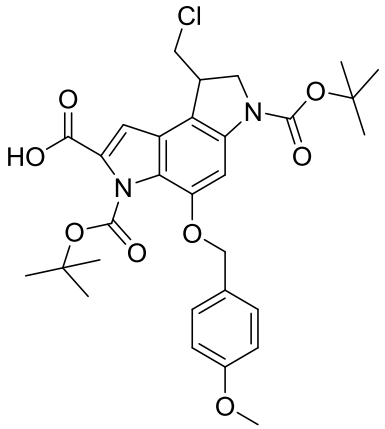

2.19

2.8-PMB (0.47 g, 0.8 mmol) was dissolved in a mixture of THF (5 mL) and MeOH (3 mL) and treated with a saturated aqueous solution of LiOH (1.7 mL) dropwise. After 4 h the THF and MeOH was removed under reduced pressure, and the residue diluted with water (10 mL). Acidification with 5 M HCl promoted the precipitation of **2.19** (0.46 g, 99%) as a green foam. Rf 0.52 (10% MeOH in CH_2Cl_2); mp 158.159 °C. ^{1}H NMR ($CDCl_3$, 400 MHz) δ 7.81 (1H, brs), 7.42–7.30 (2H, m), 7.18 (1H, brs), 6.90-6.84 (2H, m), 5.14 (2H, s), 4.17-4.00 (2H, m), 2.89-3.80 (2H, m), 3.79 (3H, m), 3.48 (1H, t, J = 8.8), 1.56 (9H, s), 1.34 (9H, s) ^{13}C NMR (DMSO-d_6, 100 MHz) δ 162.5, 159.6, 152.1, 150.7, 145.5, 136.2, 130.0, 128.7, 128.0, 127.2, 124.3, 123.4, 122.4, 114.2, 106.1, 98.3, 84.4, 80.0, 69.9, 55.6, 52.7, 48.1, 40.6, 28.5, 27.3, 22.4. IR (neat) νmax 2958, 2912, 2299, 1782, 1683, 1652, 1599, 1515, 1402, 1384, 1248, 1206, 1165, 969, 912, 758, 705, cm^{-1}. HRMS (ES-) calcd. for $C_{30}H_{35}O_8N_2Cl$ (M - H)-, 585.2009; found, 585.1995.

2.5.5 Synthesis of PCIB Protected Fmoc-DSA-OH (2.21)

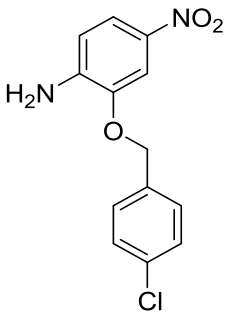

2.2-PCIB

4-chlorobenzyl chloride (1.15 g, 7.2 mmol) was added dropwise to a stirring suspension of 2-amino-5-nitrophenol (1.0 g, 6.5 mmol) and K_2CO_3 (1.45 g, 10.5 mmol) in DMF (10 mL) at room temperature. After 3 h, the reaction mixture was poured over crushed ice and allowed to rest for 30 minutes. The precipitate was collected by filtration and triturated with cold water before drying under vacuum. This yielded 1.8 g of **2.2-PCIB** as a yellow/brown solid (99%). Rf 0.20 (20% ethyl acetate in hexane); mp 127-128.5 °C. ^{1}H NMR ($CDCl_3$, 400 MHz) δ 7.82 (1H, dd, J = 2.3, 8.8), 7.73 (1H, d, J = 2.3), 7.38 (4H, s), 6.66 (1H, d, J = 8.7), 5.11 (2H, s). ^{13}C NMR ($CDCl_3$, 100 MHz) δ 144.3, 143.2, 138.7, 134.5, 134.2, 129.2, 129.0, 119.5, 112.2, 107.3, 70.1. IR (neat) νmax 3492, 3299, 3124, 3055, 2986, 1682, 1512, 1471, 1399, 1372, 1284, 1171, 950, 918, 856, 832, 820, 765, 744, 697 cm^{-1}. HRMS (ES-) calcd. for $C_{13}H_{11}N_2O_3Cl$ (M - H)-, 277.0379; found, 277.0385.

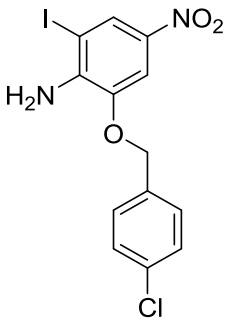

2.3-PCIB

H_2SO_4 (300 µL, 0.65 mmol) was added to a stirring solution of **2.2-PCIB** (1.8 g, 6.5 mmol) in DMF (20 mL), followed by portionwise addition of NIS (2.19 g, 9.8 mmol) at room temperature. After 2 h the reaction mixture was poured over crushed ice and left to rest for 30 minutes. The precipitate was collected by filtration and triturated with cold water, followed by cold hexane before drying under vacuum. This yielded 2.52 g of **2.3-PCIB** as a bright yellow solid (93%). Rf 0.35 (20% ethyl acetate in hexene); mp 142-143 °C. ^{1}H NMR ($CDCl_3$, 400 MHz) δ 8.29 (1H, d, J = 2.3), 7.71 (1H, d, J = 2.3), 7.42–7.34 (4H, m) 5.12 (2H, s), 5.01 (2H brs). ^{13}C NMR (CDCl3, 100 MHz) δ 143.9, 142.9, 138.7, 134.7, 133.7, 129.3, 129.1, 128.3, 106.6, 78.5, 70.5. IR (neat) νmax 3452, 3265, 3110, 3028, 3002, 2592, 1631, 1592, 1482, 1431, 1392, 1267, 1241, 1063, 1009, 891, 823, 812, 764 cm^{-1}. HRMS (ES-) calcd. for $C_{13}H_{10}N_2O_3ClI$ (M - H)-, 403.9424; found, 403.9355.

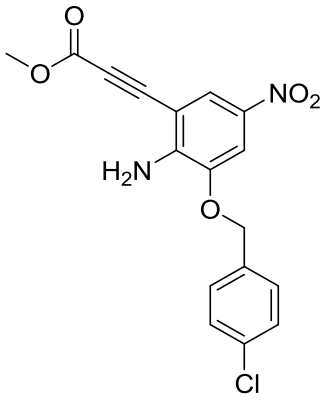

2.4-PCIB

2.3-PCIB (2.52 g, 6.2 mmol) was dissolved in anhydrous DMF (50 mL). The resulting solution was degassed with a stream of N_2 for 50 minutes prior to addition of methyl propiolate (2.2 mL, 24.9 mmol), $Pd(PPh_3)_2Cl_2$ (0.22 g, 0.31 mmol), $ZnBr_2$ (5.6 g, 24.9 mmol) and DIPEA (4.3 mL, 24.9 mmol). The reaction mixture was then heated to 66 °C and stirred overnight under N_2. After cooling to room temperature the reaction was poured over crushed ice, and the resulting chocolate colour precipitate collected by filtration. The precipitate was then absorbed on to silica. Elution through a silica plug with 50% ethyl acetate and hexane afforded 1.3 g of **2.4-PCIB** as an orange solid (58%). Rf 0.19 (20% ethyl acetate in hexane); mp 120-122 °C. ^{1}H NMR ($CDCl_3$, 400 MHz) δ 8.06 (1H, d, J = 2.4), 7.73 (1H, d, J = 2.4), 7.41–7.35 (4H, m), 5.29 (2H, brs), 5.14 (2H, s), 3.86 (3H, s). ^{13}C NMR ($CDCl_3$, 100 MHz) δ 153.7, 146.3, 144.1, 137.4, 134.8, 129.4, 129.2, 128.6, 123.5, 108.4, 101.4, 87.2, 81.3, 71.0, 53.4. IR (neat) νmax 3483, 3353, 3120, 3058, 2876, 2115, 1706, 1626, 1503, 1421, 1403, 1304, 1285, 1198, 1120, 998, 874, 752, 726, 712, 657, 608 cm^{-1}.

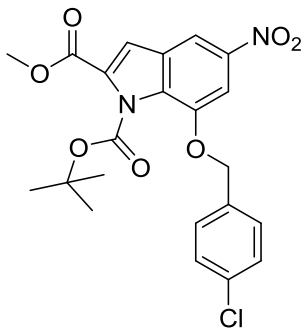

2.5-PCIB

2.4-PCIB (1.3 g, 3.6 mmol) in anhydrous THF (20 mL) was treated with 1 M TBAF in THF solution (7.2 mL, 7.2 mmol) and refluxed at 66°C for 1 h. After cooling to room temperature the THF was removed by rotary evaporation under reduced pressure. The residue was dissolved in ethyl acetate (40 mL) and washed three times with water (40 mL). Concentration of the ethyl acetate followed by co-evaporation of the residue with DCM afforded crude **2.4a-PCIB** as a dark purple foam. The foam was dissolved in DCM (40 mL) and treated with Boc_2O (1.6 g, 7.2 mmol) and DMAP (441 mg, 3.61 mmol) at room temperature for 2 h. Removal of the DCM gave crude **2.5-PCIB** as a dark foam which was dry loaded onto silica and purified using column chromatography (10% ethyl acetate in hexane). Removal of the solvent gave 0.47 g of **2.5-PCIB** as a bright yellow solid (29%). Rf 0.36 (20% ethyl acetate in hexane); mp 152-153 °C. ^{1}H NMR ($CDCl_3$, 400 MHz) δ 8.27 (1H, d, J = 1.8), 7.65 (1H, d, J = 1.8), 7.43–7.35 (4H, m), 7.34 (1H, s), 5.28 (2H, s) 3.90 (3H, s), 1.48 (9H, s). ^{13}C NMR ($CDCl_3$, 100 MHz) δ 160.1, 148.8, 145.2, 143.1, 134.9, 130.0, 129.4, 129.0, 128.7, 126.1, 112.2, 112.0, 101.9, 86.3, 71.0, 52.4, 27.5, 27.0. IR (neat) νmax 3135, 3026, 3012, 1752, 1736, 1592, 1499, 1420, 1399, 1368, 1301, 1236, 1210, 1105, 1062, 996, 852, 812, 735, 721, 705, 684 cm^{-1}.

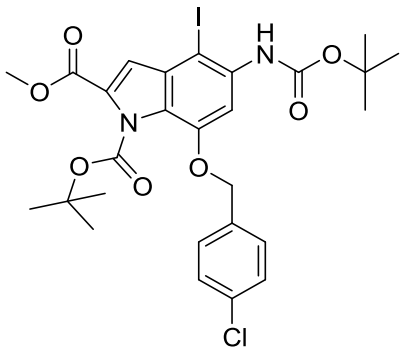

2.6-PCIB

2.5-PCIB (0.47 g, 1.0 mmol) was dissolved in THF (10 mL) and treated with zinc powder (1.0 g, 15.3 mmol) NH_4Cl (0.55 g, 10 mmol), Boc_2O (0.66 g, 3.03 mmol), DMAP (13 mg, 0.10 mmol) and water (2 mL). The resulting suspension was stirred vigorously at room temperature overnight. After removal of the THF under pressure, the residue was dissolved in Et_2O (20 mL) and washed three times with water (10 mL) and dried with $MgSO_4$.

Removal of the ether gave crude **2.5a-PCIB** as a yellow foam. Crude **2.5a-PCIB** was dissolved in DMF (10 mL) and treated with H_2SO_4 (6 μL, 0.1 mmol) before portionwise addition of NIS (0.35 g, 1.5 mmol). The solution was stirred for 3 h at room temperature. The reaction was then diluted with Et_2O (20 mL) and washed once with 50% saturated brine in water (20 mL), twice with water (20 mL), and once with saturated brine (20 mL). The first wash was back extracted three times with Et_2O (10 mL) and washed twice with saturated brine (20 mL). All the Et_2O was combined and concentrated to give a dark red foam. The foam was purified by column chromatography (10% ethyl acetate in hexane) to give **2.6-PCIB** (0.4 g, 60%) as an off white solid. Rf 0.32 (15% ethyl acetate in hexane); mp 160-161 °C. ^{1}H NMR ($CDCl_3$, 400 MHz) δ 7.78 (1H, brs), 7.44–7.40 (2H, m), 7.35–7.31 (2H, m), 7.09 (1H, s), 6.79 (1H, brs), 5.21 (2H, s), 3.91 (3H, s), 1.54 (9H, s), 1.43 (9H, s). ^{13}C NMR ($CDCl_3$, 100 MHz) δ 161.3, 153.4, 149.5, 146.1, 135.8, 134.2, 131.1, 129.2, 129.0, 128.9, 128.1, 123.8, 114.5, 103.1, 85.2, 80.6, 70.5, 52.4, 28.3, 27.0. IR (neat) νmax 3410, 3001, 2956, 1759, 1731, 1706, 1625, 1590, 1562, 1510, 1382, 1306, 1249, 1218, 1078, 922, 896, 821, 825, 754, 722 cm^{-1}. HRMS (ES-) calcd. for $C_{27}H_{30}N_2O_7Cl$ (M - H)-, 529.1741; found, 529.1756.

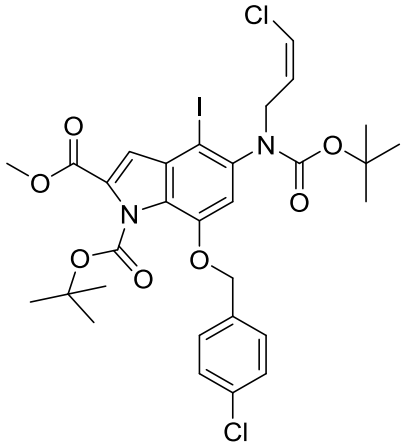

2.7-PCIB

2.6-PCIB (1.3 g, 1.9 mmol) was dissolved in DMF (30 mL) and treated with NaH (0.16 g, 3.9 mmol) and 1,3-dichloropropene as a mixture of *cis* and *trans* isomers (551 μL, 5.94 mmol). The resulting solution was stirred for 2 h submerged in a room temperature water bath. The reaction was then cooled to 0 °C before being quenched with saturated aqueous NH_4Cl (0.8 mL). The mixture was then diluted with Et_2O (50 mL) and washed twice with 50%

saturated brine in water (50 mL) and once with saturated brine (50 mL). The Et_2O was then dried over $MgSO_4$ and concentrated before co-evaporation with DCM to give a brown foam. The crude foam was absorbed onto silica and purified by silica gel chromatography (5% ethyl acetate in hexane increasing up to 10% ethyl acetate until complete elution of the product) to give **2.7-PCIB** as a light brown foam (1.16 g, 80%). Rf 0.35 (20% ethyl acetate in hexane); mp 111-113 °C. ^{1}H NMR ($CDCl_3$, 400 MHz, mixture of E/Z isomers) δ 7.41–7.38 (4H, m) 7.16 (1H, s), 6.67–6.47 (1H, m), 6.10–5.98 (2H, m), 5.22–5.08 (2H, m), 4.56-4.20 (1H, m), 4.32 and 3.75 (1H, m), 3.95 (3H, s), 1.61-1.21 (18H, m). ^{13}C NMR ($CDCl_3$, 100 MHz) δ 161.2, 154.6, 150.5, 145.2, 138.2, 135.5, 132.0, 129.3, 128.9, 128.5, 128.0, 125.0, 121.9, 120.3, 115.6, 110.0, 86.1, 83.7, 80.3, 70.1, 52.3, 49.5, 46.1, 28.4, 27.2. IR (neat) νmax 2910, 2905, 1782, 1720, 1699, 1682, 1555, 1502, 1478, 1415, 1381, 1315, 1274, 1110, 1096, 1052, 946, 876, 836, 819, 720, 702 cm^{-1}. HRMS (ES-) calcd. for $C_{30}H_{33}N_2O_7Cl_2I$ (M - H)-, 729.0631; found, 729.0704.

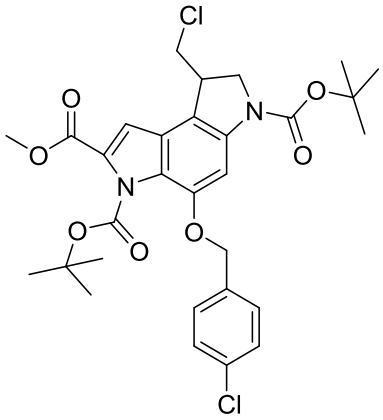

2.8-PCIB

2.7-PCIB (1.14 g, 1.60 mmol) was dissolved in anhydrous toluene (20 mL) and degassed with a stream of nitrogen for 45 minutes prior to addition of AIBN (64 mg, 0.39 mmol) and TTMSS (543 µl, 1.7 mmol). The resulting solution was refluxed at 90°C under nitrogen for 2 h. The reaction was then left to cool to room temperature before being concentrated and subjected directly to silica gel column chromatography. 2% ethyl acetate in hexane was initially run before increasing up to 5% ethyl acetate until complete elution of the product. Removal of the solvent gave **2.8-PCIB** (0.81 g, 82%) as a colourless foam. Rf 0.33 (20% ethyl acetate in hexane); mp 124-126 °C. ^{1}H

NMR (DMSO-d_6, 400 MHz) δ 7.67 (1H brs), 7.50–7.43 (5H, m), 5.26 (2H, s), 4.13 (1H, t, J = 9.7), 4.07–3.89 (4H, m), 3.87 (3H, s), 1.49 (9H, s), 1.38 (9H, s). ^{13}C NMR (DMSO-d_6, 100 MHz) δ 160.8, 151.1, 149.0, 144.9, 136.0, 128.9, 128.5, 128.2, 123.1, 113.0, 108.1, 97.1, 84.6, 80.0, 69.3, 52.0, 51.9, 47.5, 40.6 (obscured by DMSO peak, observed by HSQC), 28.1, 26.8, 22.2. IR (neat) νmax 3010, 2986, 2265, 1764, 1699, 1682, 1601, 1582, 1502, 1499, 1399, 1359, 1321, 1256, 1199, 1136, 1012, 992, 896, 799, 705, 701, 625 cm^{-1}. HRMS (ES-) calcd. for $C_{30}H_{34}N_2O_7Cl_2$ (M - H)-, 603.1665; found, 603.1681.

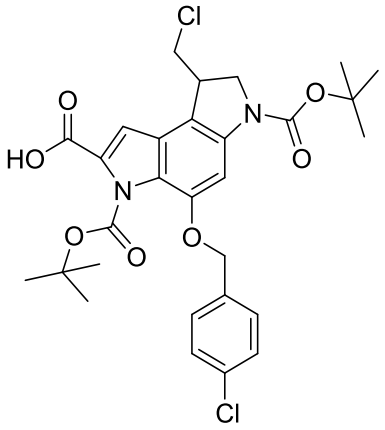

2.9-PCIB

2.8-PCIB (0.81 g, 1.3 mmol) was dissolved in a mixture of THF (9 mL) and MeOH (5 mL) and treated with a saturated aqueous solution of LiOH (2.9 mL) dropwise. After 4 h the THF and MeOH was removed under reduced pressure, and the residue diluted with water (15 mL). Acidification with 5 M HCl promoted the precipitation of **2.9-PCIB** (0.75 g, 97%) as a green foam. Rf 0.45 (10% MeOH in CH_2Cl_2); mp 177-180 °C. ^{1}H NMR (DMSO-d_6, 400 MHz) δ 13.62 (1H, brs), 7.62 (1H, brs), 7.53–7.41 (4H, m), 7.25 (1H, brs), 5.24 (2H, s), 4.13 (1H, t, J = 9.7), 4.05–3.85 (4H, m), 1.48 (9H, s), 1.36 (9H, s). ^{13}C NMR (DMSO-d_6, 100 MHz) δ 161.3, 151.1, 148.7, 135.9, 129.1, 128.9, 128.5, 128.1, 123.8, 123.7, 122.1, 108.5, 96.8, 84.1, 79.6, 69.2, 52.0, 47.2, 40.4 (obscured by DMSO peak, observed by HSQC), 28.0, 26.7, 22.2. IR (neat) νmax 3002, 2956, 2327, 1771, 1682, 1683, 1545, 1512, 1399, 1372, 1352, 1104, 1092, 924, 897, 810, 789, 702 cm^{-1}. HRMS (ES-) calcd. for $C_{29}H_{32}N_2O_7Cl_2$ (M - H)-, 589.1508; found, 589.1547.

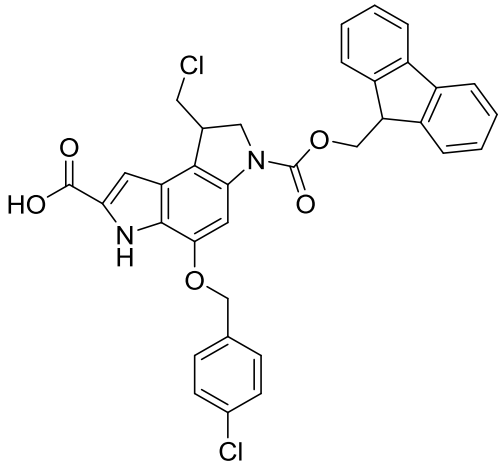

2.21

2.9-PCIB (0.75 g, 1.3 mmol) was dissolved in 4 M HCl in dioxane (15 mL) and stirred at room temperature overnight. Upon removal of the dioxane under reduced pressure, the residue was dissolved in THF (21 mL) and the solution cooled to 0 °C. The solution was then treated with $NaHCO_3$ (0.32 g, 3.8 mmol) in H_2O (6 mL) followed by Fmoc-Cl (0.33 g, 1.3 mmol) in THF (6.5 mL) and left to stir for 5 minutes. After quenching with MeOH (0.5 mL) the THF and MeOH were removed under reduced pressure. The resulting mixture was then acidified with 2 M HCl and extracted with 2-MeTHF (3 x 10 mL). The organic layer was dried over $MgSO_4$ and the 2-Me-THF removed under reduced pressure. The crude was dried loaded onto silica and purified by silica gel chromatography. 100% DCM was initially run gradually increasing up to 5% MeOH in DCM until complete elution of the product. Upon removal of the solvent, **2.21** (0.62 g, 78%) was obtained as a light green foam. Rf 0.42 (10% MeOH in CH_2Cl_2); mp 131-135 °C. ^{1}H NMR (DMSO-d_6, 400 MHz) δ 12.95 (1H, brs), 11.94 (1H, s), 7.91 (2H, d, J = 6.7), 7.73–7.68 (2H, m), 7.48–7.31 (8H, m), 7.18 (1H, d, J = 1.8), 5.23 (2H, s), 4.58-4.33 (3H, m), 4.18 (1H, t, J = 6.6), 4.09-3.86 (5H, m). ^{13}C NMR (DMSO-d_6, 100 MHz) δ 162.9, 152.4, 146.1, 144.2, 141.3, 137.3, 130.3, 128.7, 128.2, 128.1, 127.8, 127.6, 126.0, 125.5, 124.6, 120.7, 110.4, 106.2, 95.9, 69.9, 67.0, 52.4, 48.1, 47.1, 30.9, 25.6. IR (neat) νmax 2965, 2321, 2306, 1704, 1691, 1594, 1538, 1436, 1389, 1302, 1265, 1242, 1202, 1106, 1045, 1009, 978, 899, 814, 730, 624, 613 cm^{-1}. HRMS (ES–) calcd. for $C_{34}H_{26}O_5N_2Cl_2$ (M – H)–, 611.1141; found, 611.1149.

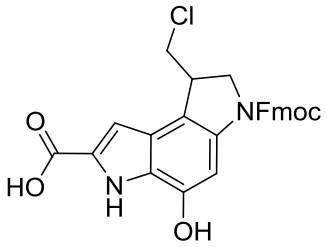

2.17

2.10 (20 mg, 0.04 mmol) was suspended in DCM (5 mL) and the mixture cooled to -78 °C. To this, a 1 M solution of BBr_3 in DCM (35 µL, 0.04 mmol) was added and the resulting suspension stirred under N_2 for 1 h. Subsequently, the reaction was quenched with crushed ice and the organic layer washed with water (3 x 10 mL). The DCM solution was concentrated before being subjected directly to silica gel column chromatography (10% MeOH in DCM). Removal of the solvent gave **2.17** (11 mg, 64%) as a light brown solid. Rf 0.15 (10% MeOH in CH_2Cl_2); mp 134-136°C. ^{1}H NMR (DMSO-d_6, 400 MHz) δ 12.84 (1H, brs), 11.36 (1H, s), 7.91 (2H, d, J = 8.3), 7.76–7.68 (2H, m), 7.43 (2H, t, J = 7.5), 7.38–7.31 (3H, m), 7.09 (1H, s), 4.55– 4.33 (3H, m), 4.28–4.08 (1H, m), 4.04–3.90 (3H, m), 3.93–3.84 (1H, m). δ ^{13}C NMR (DMSO-d_6, 100 MHz) δ 162.9, 152.0, 146.0, 137.2, 130.3, 128.6, 127.6, 126.0, 125.4, 124.1, 120.6, 113.0, 106.2, 95.9, 70.0, 67.0, 51.9, 47.9, 47.1, 41.5. HRMS (ES–) calcd. for $C_{27}H_{21}O_5N_2Cl$ (M – H)–, 487.1066; found, 487.1068.

2.5.6 General Benzyl Deprotection Conditions

1. 10% Pd/C + Ammonium Formate

The benzyl protected DSA analogue was dissolved in MeOH/THF and the resulting solution degassed with a stream of N_2 for 45 mins. A slurry of 10% palladium on carbon (2 mg per 1 mg of benzyl protected compound) was prepared with 25% aqueous ammonium formate (25 µL per 1 mg of palladium on carbon) and introduced into the benzyl protected compound solution. The resulting heterogeneous reaction was stirred for 1 h under nitrogen before the palladium on carbon was removed via filtration through a celite plug. The MeOH/THF was removed from the supernatant under

reduced pressure. The resulting benzyl deprotected compound was purified using reverse-phase preparative HPLC.

2. BBr_3

The benzyl protected DSA analogue was suspended in DCM (5 mL per 10 mg of benzyl protected compound) and the resulting suspension cooled to -78 ^{0}C. A 1 M solution of BBr_3 in DCM (1 equiv.) was added and the reaction stirred for 1 h at -78 ^{0}C. The mixture was stirred for a further hour and allowed to warm to room temperature before being quenched with crushed ice. The solution was then washed with water (3 x 10 mL) before the solvent was removed from the organic layer under reduced pressure. The crude benzyl deprotected compound was then purified using reverse-phase preparative HPLC.

3. On Resin Benzyl Deprotection Using BBr_3

20 mg of resin, containing the benzyl protected DSA analogue, was suspended in DCM (5 mL) and the resulting suspension cooled to -78 ^{0}C. A 1 M solution of BBr_3 in DCM (1 equiv. in relation to resin loading) was added to the mixture before being stirred at -78 ^{0}C under N_2 for 1 h and then for a further hour warming to room temperature. The suspension was then filtered and the resin washed with DCM (6 x 10 mL). The crude benzyl deprotected peptide was then cleaved from the resin using standard TFA based cleavage conditions before being purified using reverse-phase preparative HPLC.

Chapter 3 -Investigations into the Conjugation of DSA-based Analogues to Jacalin for Targeted Delivery to the Thomsen-Friedenreich Antigen

3.1 Introduction

3.1.1 The Thomsen-Friedenreich Antigen

The cancer phenotype is commonly associated with aberrant glycosylation patterns. One glycan that is directly linked to cancer is the Thomsen-Friedenreich antigen (T-antigen) also known as the TF antigen, the core 1 glycan or CD176.[149, 150] The T-antigen is a disaccharide composed of a galactose β1-3 *N*-acetylgalactosamine, O-linked to a glycoprotein through serine or threonine residues or more commonly written as Galβ1-3GalNAc-α-O-ser/thr. A chemical structure of the T antigen is shown in Figure 3.1.

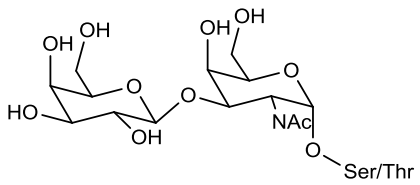

Figure 3.1: Chemical structure of the Thomsen-Friedenreich antigen (T-antigen).

The T-antigen is considered therapeutically attractive due to its oncofetal nature. This means that it is usually cryptic in normal cells but shows exposure in embryonic and cancer cells.[151] In fact, the expression of the T-antigen has been demonstrated in 90% of primary human carcinomas, including in the lung, the breast and the pancreas.[95, 152] Additionally, cancer initiating cells or cancer stem cells in the lung, liver and colon have been found to express the T-antigen, further cementing its potential as a target for therapeutic purposes.[153]

The reason for the exposure of the T-antigen within cancer cells has been attributed to the differing glycosylation mechanisms that are observed between healthy cells and cancer cells. Within normal cells, the T-antigen is often concealed by sulfate molecules, sialic acid, fucose or *N*-acetylglucosamine residues.[154] However, within cancer cells, the T-antigen is more exposed. The biosynthetic pathway to the T-antigen is shown in Figure 3.2 and demonstrates how the expression of the T-antigen arises from a further cancer associated α-linked *N*-acetylgalactosamine glycan called the Tn-antigen. This conversion from the Tn-antigen to the T-antigen is mediated by the enzyme core 1 β3- galactose transferase.[155] Deficiencies in

β3-galactose transferase activity are suggested to be responsible for the exposure of the Tn-antigen and hence a possible route to the exposure of the T-antigen. In addition to an increase in the T-antigen exposure, colon cancer cells have also shown a decrease in the expression of the core 3 glycan.[156] Decreased synthesis of core 3 glycans in colon cancer cells has been attributed to a marked decrease in core 3 β3-*N*-acetylglucosamine transferase activity, leading to the prevalence of T-antigen synthesis.

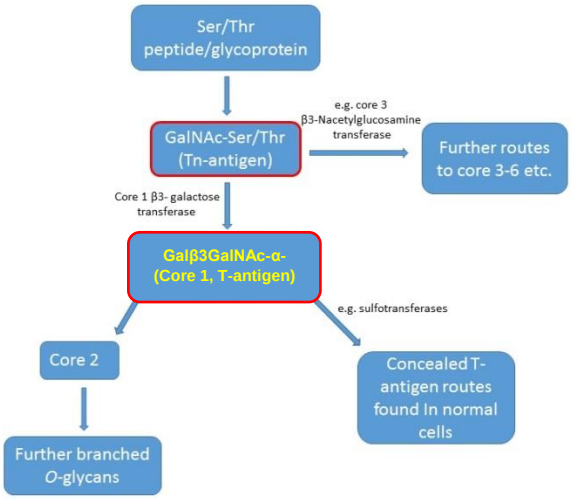

Figure 3.2: Biosynthetic pathway towards the T-antigen used to decipher possible causes of over exposure of the T-antigen within cancer cells.

Further proposals for the increased expression of the T-antigen in cancer cells have included a link to the decreased expression of carbohydrate sulfotransferases.[151] These enzymes are responsible for concealing the T-antigen through sulfation and hence a lack of activity could lead to its exposure. Furthermore, in breast and colorectal cancer cells, T antigen expression was found to be highly dependent on the pH of the Golgi apparatus. An increase of ca. 0.2 pH units in the Golgi apparatus was sufficient to elevate the expression of the T antigen.[151, 157]

The role of the T-antigen within cancer cells has been proposed to be significant in metastasis and cell adhesion. This is due to the existence of T-antigen-mediated adhesion of highly metastatic murine lymphoma cells and hepatocytes.[158] In addition, the participation of the T-antigen in human breast carcinoma cell adhesion to the endothelium has been discovered and

this process has been found to be critical in early stages of cancer metastasis.[159] Despite these revelations, more research is required to develop and further understand the molecular underpinnings of the T-antigen within cancer. This in turn may aid in the potential use of this target within the therapeutic world.

Although the expression patterns of the T-antigen make it an ideal target for therapeutic purposes, the biosynthetic pathway demonstrates the intricate discrepancies that exist between the T-antigen and other related, non-cancer associated antigens. Highly selective and specific targeting ligands are therefore required for these targets to be useful for therapeutic purposes.

3.1.2 Jacalin – a T-antigen Selective Lectin

Jacalin is a plant based lectin which is derived from the seeds of the Jack fruit (*Artocarpus heterophyllus*) and was isolated towards the end of the 1970s.[160] This lectin has been shown to selectively bind to the T-antigen and hence presents itself as an ideal agent for targeted delivery to tumour cells.[161]

Structurally, jacalin consists of two chains termed the α-chain and the β-chain. The α-chain is much larger with a molecular weight of around 14.5 kDa whilst the β-chain has a molecular weight of 2.1 kDa. The total molecular mass of jacalin has been reported to be between 65-66 kDa suggesting that the quaternary structure of this lectin comprises a tetramer composed of four α-chains and between two and four β-chains (Figure 3.3).[160, 162]

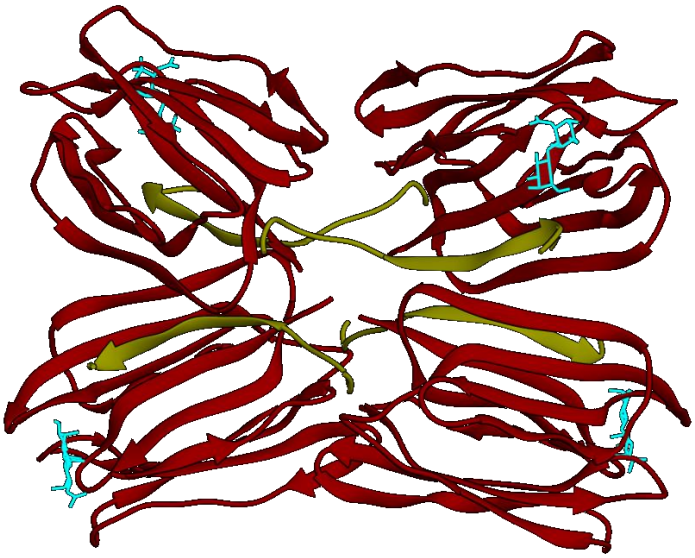

Figure 3.3: Chimera generated image of the crystal structure of jacalin-T-antigen complex (PDB ID 1M26). In red is shown the four α-subunits, in yellow are four β- subunits and in green is the T-antigen bound at the α-subunit based binding site.[110]

Whilst other T-antigen specific lectins exist, jacalin separates itself from others in the biological response it elicits upon binding. Whilst lectins such as peanut agglutinin increase cell proliferation through an interaction with c-Met and mitogen-activated protein kinase, jacalin has been shown to inhibit cell proliferation upon binding. This was demonstrated in HT-29 colon cancer cells with the inhibition shown to be reversible and non-toxic.[109, 163] In the same cell line, jacalin was shown to bind to the T-antigen with a dissociation constant (K_d) of 500 ± 50 nM, reaching maximum binding in 20 minutes at 4 °C.[112]

The ability of jacalin to specifically recognise and bind to the T-antigen was demonstrated by Kumar and co-workers who used it to detect the antigen on precancerous and cancerous colonic tissue.[164] Histological examination of T-antigen expression was made using a comparison of jacalin, an anti-T antigen antibody and the galactose oxidase-Schiff (GOS) reaction. The latter is a reaction which colourimetrically labels tissue expressing the T antigen, following oxidation of the terminal galactose residue of the disaccharide and treatment with Schiff's reagent. Although jacalin didn't show the highest specificity of these agents, the results showed that jacalin had the highest sensitivity of 84.3% for cancerous and precancerous tissue, as compared to the GOS reaction (75.7%) and immunostaining (50%). Although, the reduced

specificity towards the T-antigen may at first seem detrimental for targeted delivery, an 80% selectivity can be viewed as impressively high. This is due to the fact the other 20% is likely to be caused by jacalin's ability to also recognise the cancer associated sialylated version of the T-antigen albeit with a much lower binding affinity.[165]

The use of lectins in targeted drug delivery has been reported on numerous occasions. Gabor and co-workers demonstrated the use of wheat germ agglutinin for the targeted delivery of doxorubicin to caco-2 cell lines.[166] Additionally, Ohkohchi and co-workers utilised a recombinant bacterial C-type lectin (rBC2LC-N) to successfully deliver a bacterial exotoxin to a human PDAC cell line (Capan-1).[167] Despite this, the use of jacalin to achieve targeted delivery of cytotoxic payloads to cancer cells has been relatively scarce although some do exist. One such study completed by Russell and co-workers involved the formation of jacalin capped nanoparticles functionalised with a photosensitiser.[111] The group found that in comparison to non-jacalin capped nanoparticles, the jacalin nanoparticles were delivered and taken up much more readily by HT-29 colon cancer cells through a specific interaction with the T-antigen. This was demonstrated by an increase in cell death post irradiation, from 8% up to 95% when the particles were conjugated with jacalin in comparison to when they were not. This specific interaction was confirmed using inhibition studies with and asialofetuin which has been shown to express the T-antigen on its surface.

Following on from this study, Anbazhagan and co-workers utilised jacalin in the formation of silver nanoparticles carrying the anticancer phytomolecules, acetylshikonin and β,β-dimethylacrylshikonin.[168] Again, improved cytotoxicity's were demonstrated for the drugs loaded onto jacalin capped silver nanoparticles. The acetylshikonin attached to the jacalin capped particle showed induced maximum cytotoxicity effects on human chronic myeloid leukaemia (CML) cell line, K562 at 100 nM, whereas for a similar effect about 500 nM of pure acetylshiknin was required. This can be attributed to the ability of jacalin to recognise the T-antigen expressed on the cell line studied and hence allow for improved cellular uptake of the drug molecule.

With evidence that jacalin shows desirable specificity and sensitivity for the T-antigen and also a proven ability to enhance the delivery of cytotoxic warheads, further research is warranted to establish the potential use of this lectin in antibody-drug like systems. It could be that jacalin provides the necessary properties that may help to achieve the targeted delivery of a duocarmycin based analogue and hence help this family of agents realise their potential as therapeutic agents.

3.2 Aims of the Research in this Chapter

The aim of the research in this chapter is to introduce investigations carried out to attach a duocarmycin based analogue, synthesised on the solid phase, to jacalin.

The chapter will begin with a brief overview of the mass spectrometry analysis of jacalin which was completed to aid characterisation of the conjugates. The use of LC-MS and MALDI mass spectrometry were investigated as tools to try and decipher whether conjugation had occurred within our system and also to measure the degree of conjugation.

Following on from this initial section, the chapter will then move to focus on the various conjugation strategies employed in order to achieve the desired conjugates. These strategies are broadly classified into EDC/NHS chemistry, maleimide/thiol chemistry and click chemistry.

3.3 Results and Discussion

3.3.1 Mass Spectrometry Analysis of Jacalin

For the work carried out in this chapter, a method of deducing the level of conjugation obtained to the jacalin structure was required. Mass spectrometry presented an ideal way to deduce this characteristic and is used frequently for similar purposes within ADC like systems. For this reason, investigations to decipher the most efficient way to study jacalin using the mass spectrometry equipment available were conducted.

As an initial strategy the use of liquid chromatography-mass spectrometry (LC-MS) was explored. Figure 3.4 shows the results of the LC-MS which were obtained for unlabelled jacalin.

Figure 3.4: A: shows the α-subunit of jacalin, B: shows the α'-subunit of jacalin and C: the β-subunit of jacalin. See page 177 for LCMS details.

From Figure 3.4, the three characteristic subunits of jacalin are evident. Figure 3.4A represents the α-subunit. What is also evident from the peak observed for this subunit is a series of masses with subsequent additions of 162 Da. This indicates some glycosylation caused by additions of hexose moieties. Figure 3.4B represents the α'-chain of jacalin. The α and α'-

subunits, existing in a 1:3 ratio, are almost identical in their primary amino acid sequence except for one valine for isoleucine substitution.[169] Although the α-chain shows some evidence of hexose glycosylation, the extent of glycosylation in the α'-chain is much greater than that in the α-subunit. In the α'-polypeptide, all molecules contain an N-linked oligosaccharide at position 74 and some contain a sugar at position 43 as verified by threonine resonance in the ^{1}H-NMR spectrum of the jacalin glycopeptide.[170] Figure 3.4C shows the smaller β-subunit at around 2.1 kDa. This subunit is composed of 20 amino acids and is bound in a non-covalent manner to the α-subunits.[169]

The presence of the 162 Da increments in the mass spectrum of the jacalin α-subunit was expected given the numerous literature reports demonstarting the binding of jacalin to a number of hexose units.[169] The presence of these increments in the jacalin mass spectrum however does raise the question as to whether the jacalin used in this body of work will still readily bind the T-antigen given that it is clearly interacting with some other hexose units. However, it has been reported that jacalin is able to recognise the GalNAc moiety in the T-antigen structure more extensively that for example a Gal moiety.[170] As such, this inferred that the jacalin used here would still demonstrate some binding towards the T-antigen. Despite this, the above was still a consideration to take forward for later experiments in this body of work.

The LC-MS results above present an ideal way to analyse conjugation to the jacalin structure. The majority of the conjugation strategies attempted as part of this thesis utilised a route via the lysine residues of the jacalin. With the α-subunit containing the majority of the lysine residues, an increase in mass to this subunit, depending on the duocarmycin peptide analogue used, would represent conjugation occurring.

Whilst the LC-MS results present an accurate method of establishing conjugation, due to time constraints and equipment availability, the use of matrix assisted laser desorption ionisation (MALDI) was also explored for analysing conjugates. MALDI mass spectrometry presents itself as an ideal

method for analysing protein mass due to its mild ionisation technique.[171] In addition, the method itself is relatively easy and time efficient.

One of the most crucial aspects for a successful MALDI analysis is the choice of matrix. This can greatly affect the level of ionisation of the sample and hence the quality of the resulting spectra.[172] In order to find the best MALDI matrix for jacalin, a variety of matrices were studied. These were α-cyano-4-hydroxycinnamic acid (αCHCA), trans-ferulic acid, sinapinic acid, 2,5 dihydroxybenzoic acid (DHB) and picolinic acid. It was found that trans-ferulic acid was able to give the clearest and sharpest spectra for jacalin, especially in the α-subunit mass range. In addition to the matrix, other features which were found to greatly affect the spectra quality were matrix solvent system, sample buffer desalting, TFA introduction and sample preparation. Details of these key components are shown in Table 3.1 along with an example MALDI spectra using the discovered, ideal conditions in Figure 3.5.

Table 3.1: standard conditions utilised for MALDI based analysis of jacalin and the resulting conjugates.

MALDI variable	**Ideal conditions**
Matrix	*Trans*-ferulic acid shown to give best ionisation. Sinapinic acid also shown to be a good alternative.
Matrix solvent	70:30 mixture of acetonitrile (ACN) to H_2O shown to give the best results.
Mode	A linear mode on the MALDI was used for all samples.
Sample desalting	All samples in buffer were desalted prior to sample plating using Dowex® MB Mixed Ion Exchange Resin.
TFA introduction	Introduction of 0.1% TFA to matrix solution was made for all samples.
Sample preparation	A 'sandwich' technique was utilised for all sample preparations. This involved spotting the matrix onto the plate and allowing it to dry. The sample was then spotted before drying and then finally another layer of the matrix.

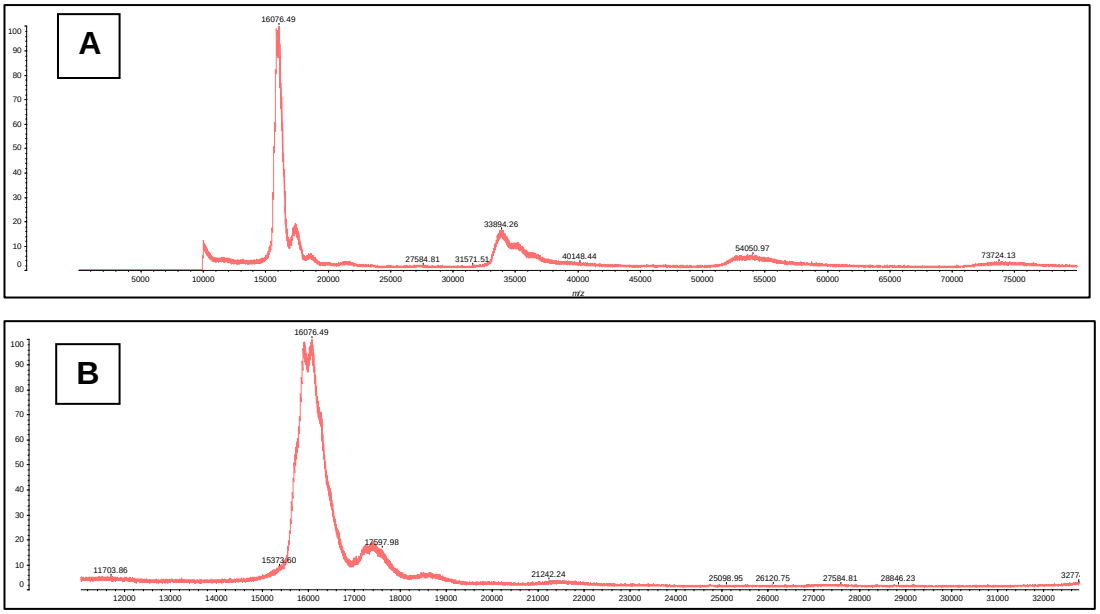

Figure 3.5: MALDI mass spectrometry spectra conducted in linear mode with a laser power of 180 of the α-subunit of jacalin, A: shows the full spectrum whilst B: shows the main peak at higher resolution.

Figure 3.5A demonstrates the sharp peak of the jacalin α-subunit under the investigated conditions. The presence of a 2M peak at around 34 kDa is also evident. Figure 3.5B presents a higher resolution version of this α-subunit peak. Similar to the LC-MS, a shoulder off this main peak is likely to be caused by the presence of the glycosylated α'-subunit. Although the main α-subunit peak is sharp, slight broadening maybe present due to glycosylation of 162 Da as seen in the LC-MS data presented in Figure 3.4.

It should be noted however that a relatively large difference (~ 1.2 kDa) exists between the mass of the α-subunit and the α'-submit found in MALDI mass spectrometry in comparison with that found via electrospray ionisation in the LCMS spectra (see Figure 3.4). This also constitutes a mass difference of 1.4 kDa between the calculated mass of the α-subunit and that obtained using MALDI mass spectrometry. The reason for such a large difference is unknown. However, this may be due to the MALDI mass spectrometer not functioning at optimal capacity and failing to be sufficiently calibrated. However, since the purpose of obtaining the mass of the jacalin α- and α'-subunits in this chapter was to observe any increase in the mass of said subunits, it was decided that the MALDI spectrometer still provided an ideal qualitative tool which would be useful within this body of work. However, it

should be fully appreciated that in order to obtain a more concrete picture of any conjugations observed using the MALDI mass spectrometer, a more accurate mass analysis would be required.

With two methods of analysis optimised and in hand for assessing the level of conjugation to the jacalin structure, work could begin on attempting to achieve the desired conjugation. The next sections will detail the various strategies utilised in order to achieve this.

3.3.2 EDC/NHS Chemistry

The carbodiimide, *N*-(3-Dimethylaminopropyl)-*N'*-ethylcarbodiimide hydrochloride (EDC), is the most commonly used coupling agent for achieving conjugation between an amine and a carboxylic acid. The reason for this popularity stems from the water soluble nature of this reagent and also of the isourea by-product. This feature means that post reaction, these impurities can be removed with relative ease using techniques such as dialysis.[173] A general route to the stable amide linkage formed from an EDC mediated reaction is demonstrated in Scheme 3.1.

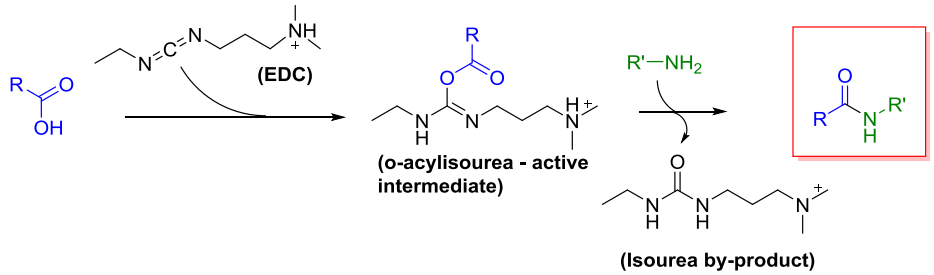

Scheme 3.1: general scheme showing the reaction between an amine and a carboxylic acid using EDC. The carboxylic acid reacts with EDC to form an active ester intermediate which can go on to react with an amine to form a stable amide bond.

Whilst there is no doubt about the utility of this reaction for achieving conjugations, it also has a number of drawbacks. Firstly, EDC itself is particularly labile in the presence of water and hence decomposition of the reagent prior to reaction is not uncommon. In order to avoid this, optimal pH ranges for the reaction have been established.[174] A more detrimental drawback for this reaction however, is the instability of the o-acylisoura active intermediate (Scheme 3.1). This intermediate can hydrolyse in aqueous solutions with rate constants of only a few seconds.[27] Therefore, if the relative

concentrations of the intermediate and amine are not optimised for the coupling to occur, the resulting reaction is likely to be hindered leading to greatly reduced yields. This is a particular problem when reagents are in low concentration compared to water which is often the case for protein conjugations.

In order to avoid these problems, it was discovered that the addition of *N*-hydroxysuccinimde (NHS) to an EDC mediated reaction can greatly increase yields.[175] The addition of NHS pushes the reaction via an active NHS ester intermediate which has been shown to react rapidly with amines. Additionally, this NHS ester intermediate shows improved stability in aqueous solutions in comparison to the o-acylisourea intermediate. This is particularly the case when the pH is ~ 5. A scheme representing this NHS based EDC coupling is demonstrated in Scheme 3.2.

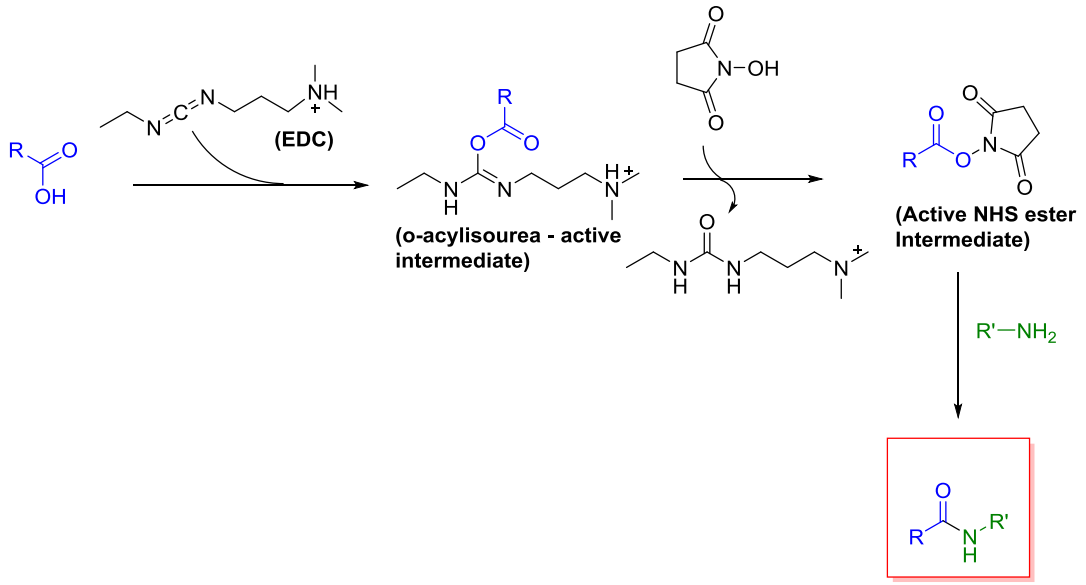

Scheme 3.2: efficiency of the EDC mediated coupling can be improved through the addition of NHS. This forms a more stable NHS ester intermediate for reaction with the amine.

3.3.2.1 In-situ EDC/NHS Activation

With this reaction showing great applicability and with literature procedures being extensive, it was chosen as a first strategy for the conjugation between jacalin and a duocarmycin based analogue. What was also ideal about this reaction is the abundance of amine containing lysine residues on the jacalin α-subunit. These can be utilised in the reaction with a carboxylic acid. As mentioned in Chapter 2, the use of 2-cltrt resin with the DSA unit has shown

advantageous results. This is also ideal in this situation since cleavage from this resin results in the formation of a carboxylic acid at the C-terminus of the peptide sequence. The required amine and carboxylic acid functionalities would therefore be in hand without significant chemical manipulation.

For the synthesis of the duocarmycin peptide, it was decided that a cleavable peptide sequence would be incorporated. This would allow for cleavage of the duocarmycin moiety from the jacalin upon cellular internalisation. From a brief literature search, a Phe-Leu sequence was found which has demonstrated cleavage by cellular enzymes.[176, 177] This sequence was desirable since it would be easy to incorporate using SPPS. Compound **3.1** shown in Figure 3.6 was therefore synthesised.

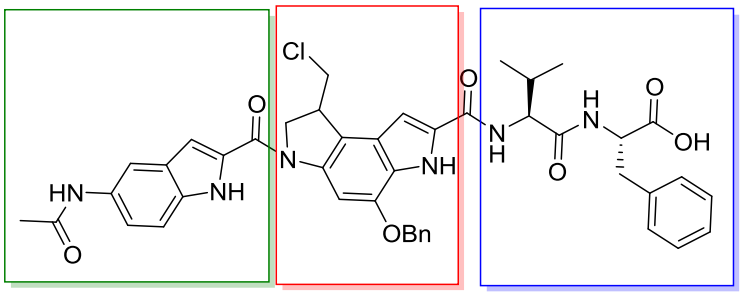

3.1

Figure 3.6: structure of compound **3.1** synthesised for the attempted conjugation to jacalin. In green is the DNA binding subunit, in red is the alkylating subunit and in blue a possible cleavable peptide sequence.

Following the general solid phase conditions presented in Chapter 2, Section 2.3.3.2, the above peptide was successfully synthesised. Subsequent to cleavage from the resin, the peptide was purified using preparative high performance liquid chromatography (HPLC). Post purification, analytical HPLC demonstrated >95% purity of **3.1** and an overall yield of 48% was obtained. MALDI was used to confirm the desired molecular weight of **3.1**. For the initial conjugation investigation it was decided to leave the benzyl group in place to reduce handling of the potentially dangerous cytotoxic agents.

Now that a duocarmycin based peptide containing a carboxylic acid functionality was in hand, attempts could be made to conjugate this to the lysine residues of jacalin. Initial attempts focused on an in-situ based EDC/NHS activation method using a one pot mixture of jacalin, **3.1**, EDC and NHS. This method is advantageous in that since jacalin, and hence the amine residues are present within the mixture, rapid reaction with the NHS ester intermediate of **3.1** should proceed.

Notable during the development of these reactions was the insolubility of **3.1** in aqueous solutions. For this reason, stock solutions of **3.1** were made in DMSO before dilution into the specific reaction buffer being used. A relative concentration of 20 molar equivalents of **3.1** was selected as an initial starting point in the reaction since it was known there were 8 lysine residues per α-subunit in jacalin and hence 32 overall. Since a drug-jacalin ratio of around 4 was targeted, this concentration ratio of **3.1** to jacalin was deemed an acceptable starting point.

The reaction buffer chosen for the conjugation presented above was HEPES buffer saline at pH 6.5. This was chosen for two reasons. Firstly, HEPES buffer saline pH 7.4 was recommended by the company from which the jacalin was purchased and hence deviation from this buffer system was undesirable. Secondly, slightly acidic pH's promote the formation of the NHS ester and also reduce the likelihood of hydrolysis.[174] Scheme 3.3 demonstrates the reaction undertaken as described above.

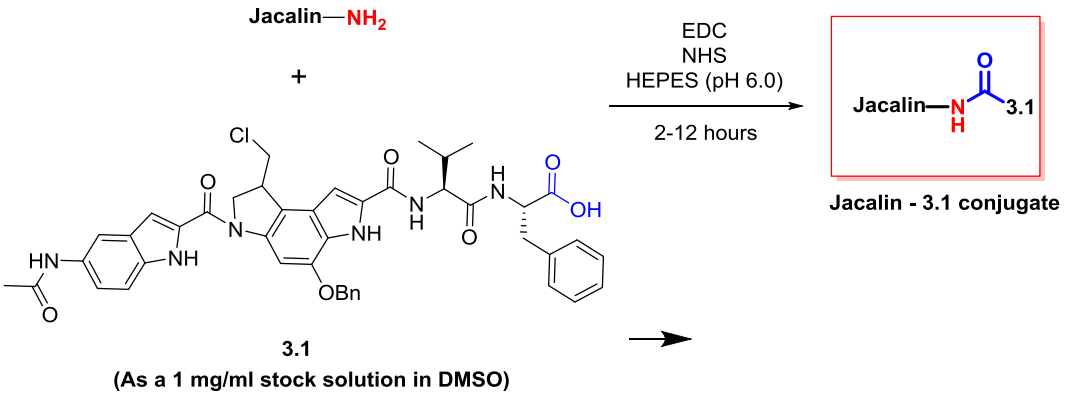

Scheme 3.3: in-situ EDC/NHS activation of **3.1** was utilised as an initial attempt at making the jacalin-duocarmycin conjugates.

Upon leaving the mixture to react for between 2 and 12 h, the reaction was purified using dialysis to remove the small molecule components. Using a specific molecular weight cut off (MWCO), the conjugated jacalin or any unlabelled jacalin should remain as the sole component. After this procedure, the solution was analysed using the mass spectrometry strategies presented in Section 3.3.1. What was observed here was no conjugation occurring with the masses obtained being identical to that of the unlabelled jacalin. One possibility for the lack of reaction came from the observation that a precipitate had formed during the reaction. After analysis of the precipitate through HPLC and MALDI mass spectrometry, it was found that **3.1** was precipitating from the reaction buffer, this could therefore be preventing the formation of the conjugate. Secondly, since EDC and NHS are included in the presence of the jacalin, it is possible that jacalin cross-linking may occur. This is because of the presence of exposed amine residues (lysine) and carboxylic acid residues (glutamic/aspartic acid) on the jacalin structure. EDC/NHS based activation of the carboxylic functionality of the glutamic/aspartic acid could therefore occur which in turn could react with the lysine residues. Although these cross-linked structures were absent from the MALDI spectra, this was expected since ionisation and hence detection of these can be difficult.

In order to address the issue surrounding the hydrophobicity of **3.1**, a further duocarmycin analogue was synthesised that contained more hydrophilic amino acid residues. The chosen residues were arginine amino acids and the structure of this peptide (**3.2**) is shown in Figure 3.7. For the ease and speed of synthesis, the DNA binding subunit and the cleavable sequence were omitted from this analogue. The removal of the DNA binding unit has previously been shown to have some effect on the biological activity of analogues although for these early stage conjugation investigations it was decided that this was acceptable.

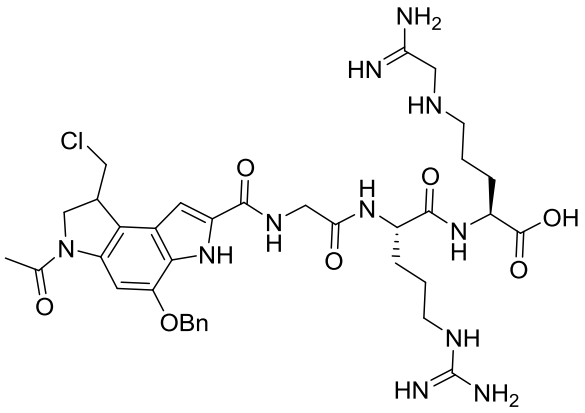

3.2

Figure 3.7: structure of peptide **3.2** synthesised to improve the hydrophilicity and hence eliminate the issues with peptide precipitation.

The water soluble compound, **3.2**, was included in the in-situ EDC/NHS reaction with jacalin. Again, upon purification, mass analysis demonstrated no conjugation occurring. With the issue of peptide solubility now eliminated, it appeared that possible jacalin cross-linking might be preventing the desired reaction from occurring. In order to address this issue, the EDC/NHS molar ratios were adjusted. This has been shown in previous work to have an effect on promoting the intermolecular reaction as opposed to protein cross-linking in conjugation reactions.[178] Additionally, the utilisation of sulfo-N-hydroxysuccinimide (sulfo-NHS) was attempted in our system as this analogue of NHS has demonstrated effects on conjugation efficiencies.[175] A summary of the attempted conditions to promote conjugation using the in-situ EDC/NHS activation method are demonstrated in Table 3.2.

Table 3.2: conditions employed for the conjugation of 3.2 to jacalin. The conditions were selected based on attempts to reduce the precipitation of the jacalin and achieve the desired coupling

Jacalin concentration [a]	**3.2 equivalents**	**EDC equivalents** [b]	**NHS**[c] **and equivalents**[b]	**Results**
2 mg/mL	20	20	NHS - 25	Precipitation and no conjugation
1 mg/mL	20	20	NHS - 20	Precipitation and no conjugation
1 mg/mL	10	10	NHS - 10	Less precipitation and no conjugation
1 mg/mL	20	20	sulfo-NHS - 25	Precipitation and no conjugation
1 mg/mL	10	10	sulfo-NHS - 10	Less precipitation but no conjugation

[a] *concentration within a 10 mM HEPES buffer* [b] *molar equivalents in relation to jacalin* [c] *type of NHS ester (NHS or sulfo-NHS)*

Since a lack of conjugation was still being observed it was decided to investigate whether the issues were jacalin or peptide specific. Bovine serum albumin (BSA) is a model protein that is relatively inexpensive and available in reasonable quantities. Also, the molecular weight of BSA is very similar to that of jacalin so it was hoped that results could be applicable to both species. **3.2** was reacted with BSA in the presence of EDC (0.1 mg per mg of protein). NHS was omitted and a 0.1 M MES buffer at pH 5 was used. After reacting for 90 minutes at room temperature, the BSA was purified through a 7K MWCO spin column and analysed by MALDI mass spectrometry. The resulting spectrum demonstrated a mass increase of around 3200 Da which suggest a conjugation of around four units of **3.2** to the BSA structure (Figure 3.8).

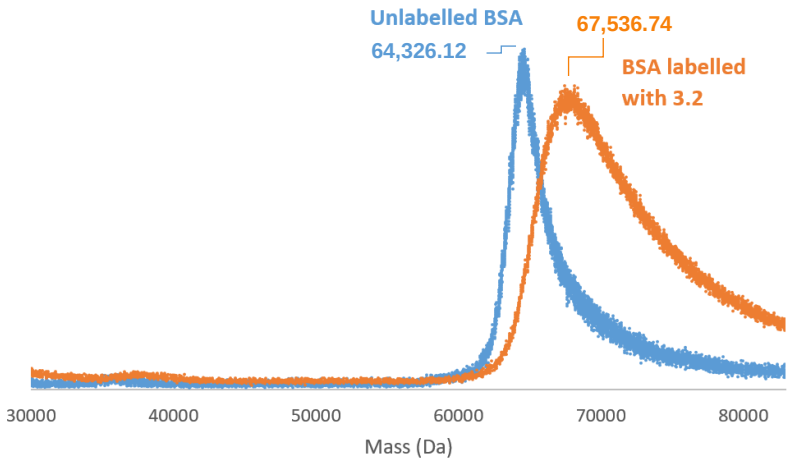

Figure 3.8: MALDI mass spectrometry spectrum of unlabelled BSA in blue and **BSA-3.2** conjugate in orange. A clear increase in the mass of BSA is evident after subjection to the conjugation conditions. N.b. the masses shown in the figure are taken from the data points at the apex of the respective peak.

This result suggested there was no issue occurring with the EDC activation of our duocarmycin peptides. When the above conditions were repeated with jacalin however, no conjugation upon mass analysis was visible. It is possible that the lysine residues on the jacalin structure could be more concealed and hence less likely to react with the activated esters formed in-situ before they hydrolyse.

3.3.2.2 Ex-situ NHS Ester Formation of Duocarmycin Analogues

Since attempts using the in situ activation of duocarmycin peptides with EDC/NHS were unsuccessful, attention turned to an ex-situ formation of duocarmycin-based NHS esters. These esters could then be added into a buffer containing jacalin in order to achieve conjugation. This strategy would allow for greater control over the degree of conjugation to jacalin since specific molar ratios of the active NHS esters could be added. Additionally, with EDC and NHS being absent from the reaction mixture, any problems due to jacalin crosslinking could be avoided.

The utility of this strategy for conjugation to jacalin was first demonstrated using a number of commercially available NHS esters. For these reactions, jacalin in HEPES buffer at pH 7.4, was reacted with 20 molar equivalents of the NHS esters. The MALDI results of these conjugations are demonstrated in Figure 3.9.

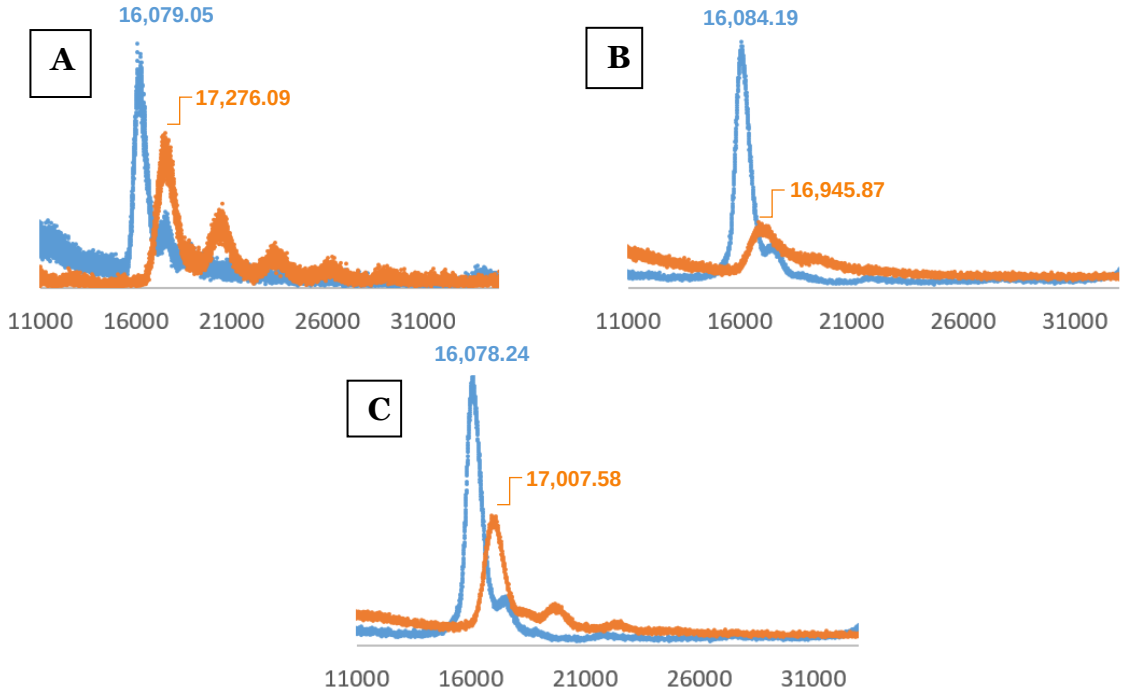

Figure 3.9: MALDI mass spectrometry results of conjugations to jacalin. In Blue is the MALDI spectra of the unlabelled jacalin α-subunit. In orange is the MALDI of the respective conjugates post reaction with a; DBCO-NHS b: SMCC, c: Biotin-NHS. All reactions show an increase in mass of the α-subunit with each increase representing around four additions of the NHS ester to the jacalin. N.b. the masses shown in the figure are taken from the data points at the apex of the respective peak.

What can be seen from the above figure is that an increase in mass to the α-subunit of the jacalin is achieved through reaction with a pre-made NHS ester. These results therefore confirm that this strategy is a viable option to achieve conjugation to the structure of jacalin. Some of the conjugates formed in these reactions precipitated from the solution and were resuspended in acetonitrile and water in order to generate the MALDI results. This suggested that the precipitation of the jacalin upon conjugation was a general phenomenon and not necessarily associated just with duocarmycin conjugation

Following on from the above model reaction, the synthesis of the NHS ester of peptide **3.1** was attempted. This was carried out using N,N'-dicyclohexylcarbodiimide (DCC) and NHS. The conditions utilised for this manipulation are demonstrated in Scheme 3.4.

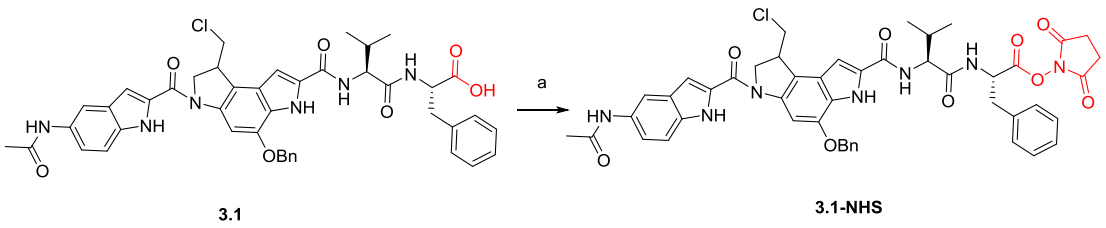

Scheme 3.4: a: DCC, NHS, Anhydrous DMF, 16 h

Post reaction, MALDI mass spectrometry showed a mass representing only **3.1** rather than **3.1-NHS,** which suggested that the reaction had been unsuccessful. To assess the presence of the NHS ester the proposed **3.1-NHS** was reacted with N,N-dimethylaminopropylamine. However, HPLC and MALDI analysis demonstrated no coupling reaction occurring suggesting, again, that the NHS formation had been unsuccessful. These findings coincided with the observation that no dicyclohexylurea (DCU) had precipitated during the reaction. DCU is the by-product from the DCC based coupling reactions and is insoluble in DMF. Therefore, a sign of the reaction proceeding is the precipitation of DCU as a colourless solid.[173]

A possible reason for the lack of reactivity of **3.1** was the steric hindrance around the C-terminus carboxylic acid caused by the phenylalanine amino acid. This could prevent the formation of the active O-acylisourea intermediate and therefore stop the reaction from occurring. In order to test this theory compound **3.3** was made. For ease of synthesis the binding-subunit and cleavable sequence were again removed and a short β-alanine sized linker was introduced. It was proposed that with less steric hindrance around the C-terminus carboxylic acid, the DCC based coupling reaction with NHS is more likely to proceed (Scheme 3.5).

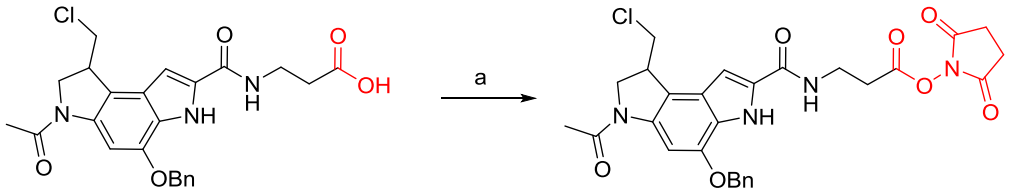

3.3 **3.3-NHS**

Scheme 3.5: a: DCC, NHS, Anhydrous DMF, 16 h. Formation of the NHS ester of **3.3** using DCC proceeded successfully. This was proposed to be due to the lack of steric hindrance around the C-terminus carboxylic acid.

Although compound **3.3-NHS** (Scheme 3.5) was not isolated, the presence of the NHS ester was confirmed using LC-MS which showed a peak indicative of the desired mass. Additionally, upon reaction of **3.3-NHS** with N,N-dimethylaminopropylamine, HPLC and MALDI mass spectrometry showed coupling had occurred which was further indicative of the NHS ester being formed. These findings were consistent with the observation that in this reaction, DCU did precipitate.

For the conjugation of **3.3-NHS** to jacalin, **3.3-NHS** was prepared freshly in anhydrous DMF. The resulting DCU was removed by centrifugation and the DMF evaporated. **3.3-NHS** was then resuspended in DMSO before being added to jacalin in HEPES buffer at 20 molar excess (Scheme 3.6). This followed the conditions utilised for the results in Figure 3.9.

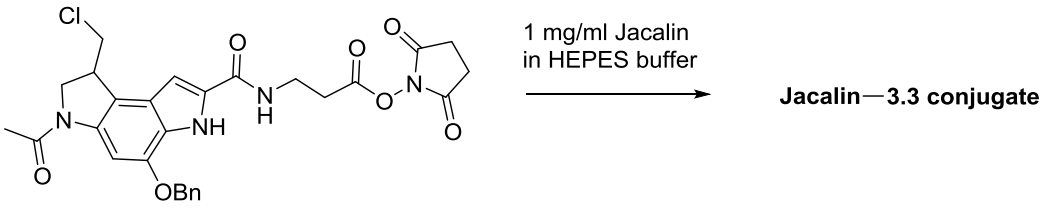

3.3-NHS

Scheme 3.6: reaction of **3.3-NHS** with jacalin in HEPES buffer gave successful conjugation to the jacalin structure albeit with resulting precipitation of the jacalin.

During the reaction, it was again observed that a precipitate was forming. After the required reaction time, the precipitate was removed via centrifugation and resuspended in acetonitrile and water and analysed using MALDI mass spectrometry (Figure 3.10).

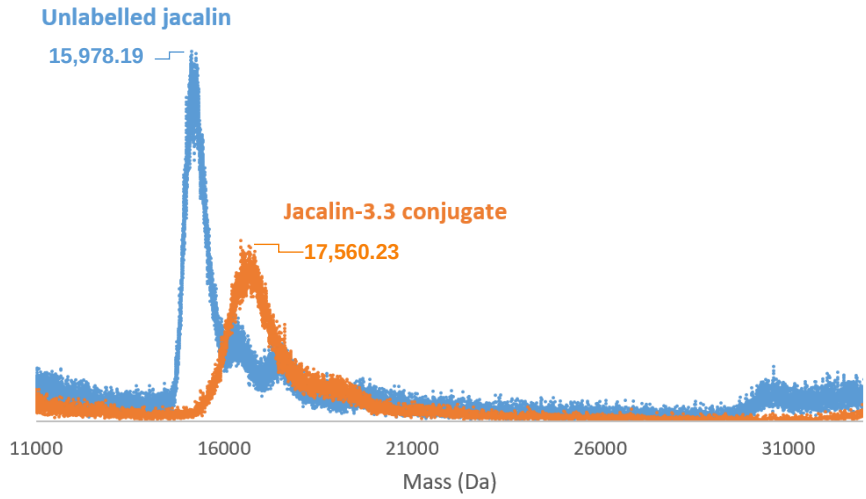

Figure 3.10: MALDI mass spectrometry result for the reaction of jacalin with **3.3-NHS**. The precipitate from the reaction was removed and resuspended in acetonitrile to obtain the above spectrum. In blue is the unlabelled jacalin α-subunit and in orange, the labelled α-subunit. N.b. the masses shown in the figure are taken from the data points at the apex of the respective peak.

The precipitate from the reaction was the labelled jacalin species, as demonstrated in orange in the above MALDI spectrum. The mass increase of around 1500 Da suggested the addition of between 3 and 4 molecules of **3.3** to the jacalin α-subunit. The precipitation of jacalin which had been observed on multiple occasions was a concern due to potential issues with the quaternary structure of the protein and potential effects on biological assays. In addition, the precipitation made the characterisation of the conjugates difficult as it was observed that mass spectral analysis of the conjugate following precipitation was problematic. It could be that the masking of the lysine residues (a point of possible ionisation during MALDI) via the conjugation of **3.3** could be hindering the characterisation process.

Benzyl deprotection of **3.3** would give the active duocarmycin which could be converted to the NHS ester for conjugation to the jacalin. Benzyl deprotection of **3.3** was achieved using transfer hydrogenation with 10% palladium on carbon and ammonium formate as detailed in Chapter 2, Section 2.3.4. The resulting active duocarmycin unit, **3.4**, was then reacted with DCC and NHS (Scheme 3.7).

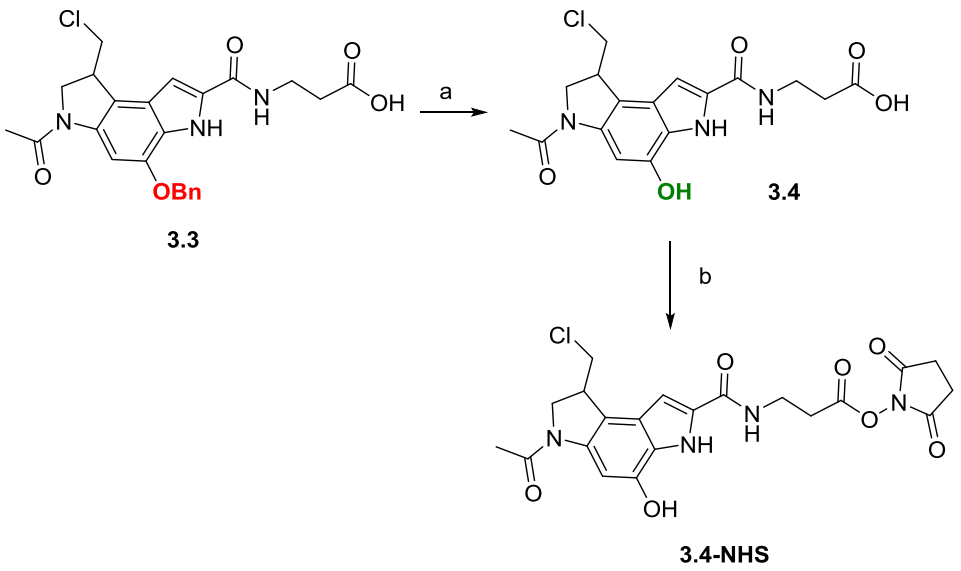

Scheme 3.7: a: 10% Pd/C, 25% Aq. Ammonium formate, MeOH, 1h, rt b: DCC, NHS, anhydrous DMF, 16 h, rt.

Crude **3.4-NHS** was redissolved in DMSO and reacted with jacalin in a 20 molar excess. Precipitation was again observed during the reaction time course. After 20 h, the precipitate was collected and resuspended in acetonitrile and water. It was noted this time that it was harder to get the precipitate back into solution. Despite this, the precipitate was analysed via MALDI mass spectrometry (

Figure 3.11). The spectra obtained for this conjugate were less clear, possibly due to the dissolution issues, but did seem to suggest conjugation occurring through an increase in mass of the α-subunit.

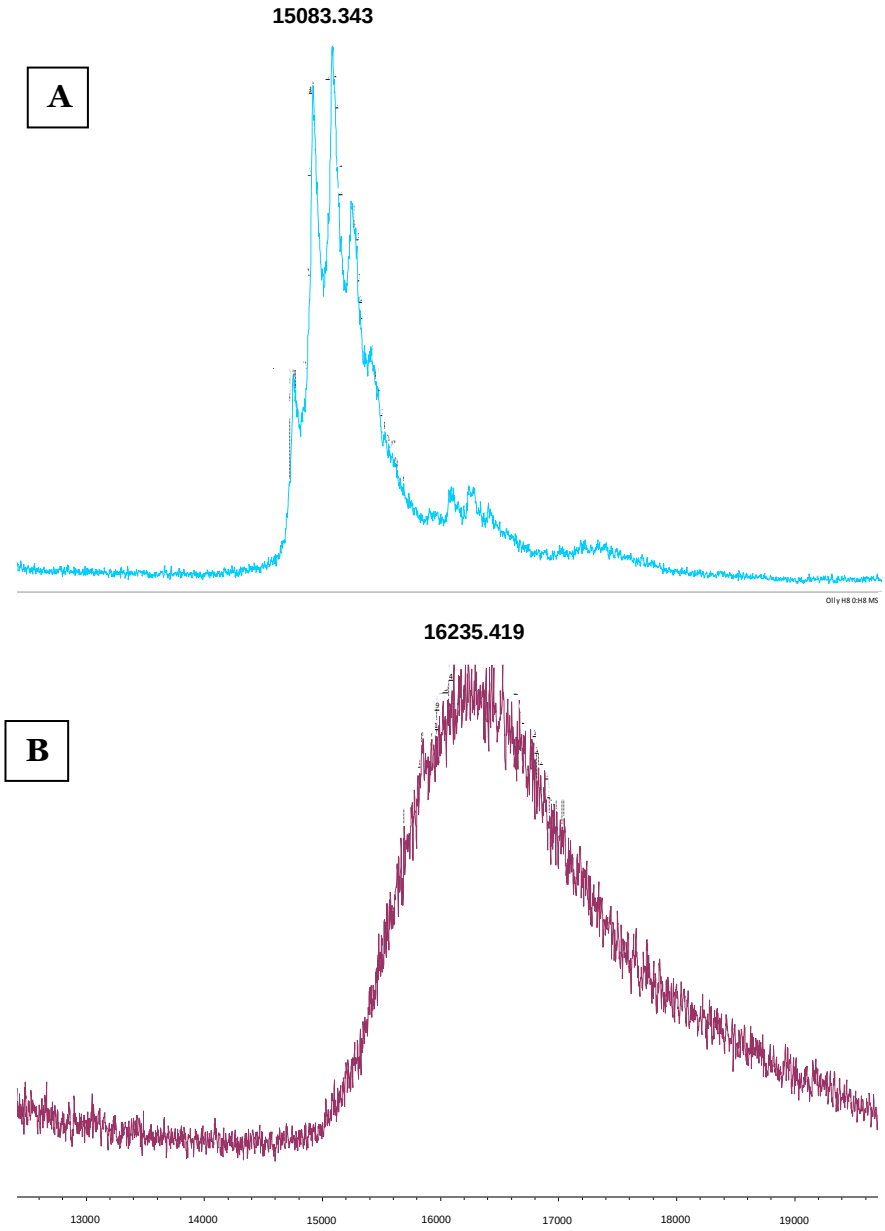

Figure 3.11: A: MALDI mass spectrometry result for unlabelled α-subunit of jacalin. B: MALDI of α-subunit after reaction with **3.4-NHS**. What is evident here is the shifting of the subunit to a higher mass indicating conjugation occurring. The spectrum however of this conjugate is less clear possibly due to dissolution issues of the conjugate. N.b. the masses shown in the figure are taken from the data points at the apex of the respective peak.

The addition of duocarmycin based units onto antibodies and proteins has previously been described as difficult due to problems with precipitation.[87] This is likely to be due to the unfavourable covering of the protein surface with hydrophobic units in aqueous conditions. It was this reason which drove ImmunoGen to investigate the use of phosphate groups to aid dissolution.[87] It is notable, however, that jacalin, at least in our hands, seemed to be

particularly prone to precipitation, even in the model reactions described above. Attempts to reduce precipitation by controlling the levels of conjugation occurring to the jacalin structure by reducing the molar equivalents of the NHS-esters were unsuccessful. Addition of hydrophilic amino acids into the sequence could potentially prevent precipitation. Peptide **3.5** was synthesised using SPPS, however, the formation of **3.5-NHS** was unsuccessful (Scheme 3.8). It seems likely that the basicity of the arginine unit may affect the DCC/NHS reaction preventing formation of the reactive ester.

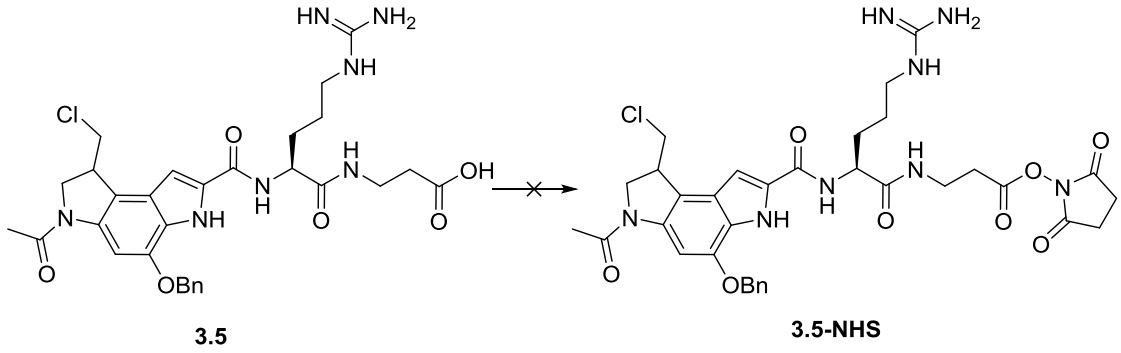

Scheme 3.8: attempted NHS ester formation of **3.5** was found to be unsuccessful under our previously used conditions.

Although the use of the EDC/NHS route was successful in forming a protected jacalin-DSA conjugate (jacalin-3.3) and an active analogue (jacalin-3.4), issues with precipitation and the lack of solubility of these conjugates suggested that alternative methods for conjugation might be more appropriate and, as such, investigations into the potential of the maleimide/thiol conjugation route were initiated.

3.3.3 Maleimide/Thiol Conjugation Strategy

The reaction between a thiol and maleimide has been studied extensively for use within protein bioconjugation reactions as a non-cleavable linkage.[173] The reaction involves a Michael type addition of a thiol to the activated alkene of a maleimide (Scheme 3.9). The activation of this position is a direct result of the electron-withdrawing ability of the adjacent carbonyl groups. Release of ring strain also contributes to the driving force of this reaction. The efficiency

and ease of this manipulation has contributed to its classification as a click chemistry reaction.[179]

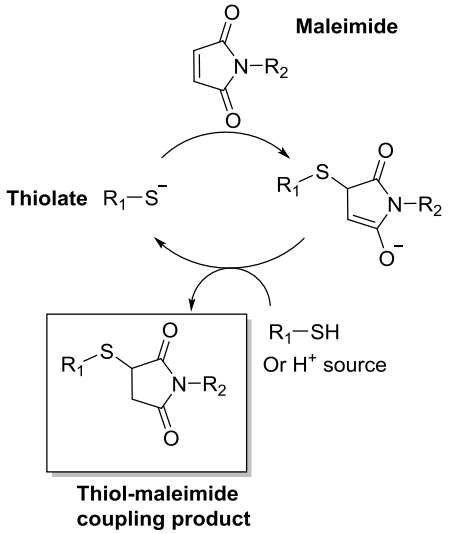

Scheme 3.9: the thiol-maleimide coupling reaction is thought to proceed through attack of a thiolate anion to the activated alkene of the maleimide.

It is this efficiency that has led to the utilisation of this reaction in the bioconjugation field. Cysteine residues on proteins can be utilised for the reaction with maleimides introduced onto small molecules. Mixing of the two species within an appropriate buffer system was shown to give favourable conjugation results.[173] The use of this technique has more recently been utilised in ADC like systems since selective disulfide bridge reduction on antibodies can allow for selective conjugations to these sites.[180] This in turn gives some control over the resulting drug-antibody ratio and hence a move to more homogenous product mixtures. This strategy was utilised in the synthesis of the approved ADC, Adcetris® (Figure 3.12).

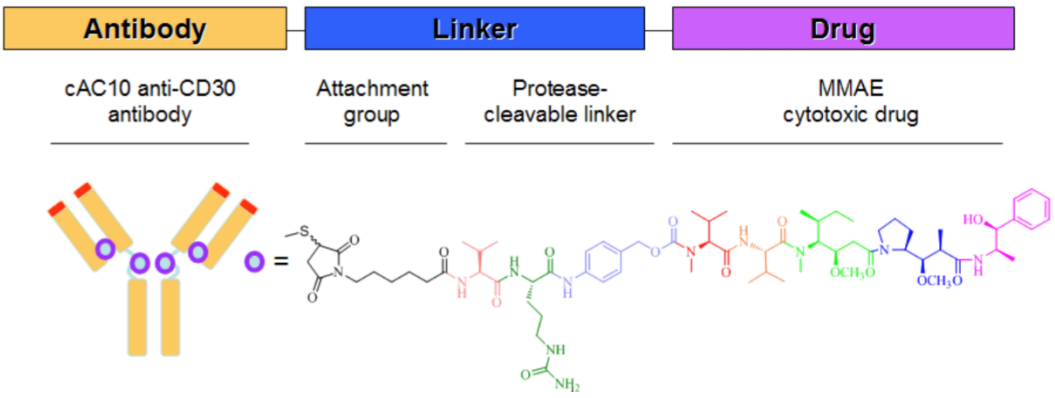

Figure 3.12: structure of the clinically approved Adcetris® which utilises a strategy where a reduced disulphide on the antibody is coupled to a maleimide moiety which is integrated into the MMAE drug payload.[181]

In the reverse manner, the formation of linkers that allow the functionalisation of a protein with a maleimide have also been introduced. This allows thiol containing small molecules to be conjugated to these sites. One such linker which has been used extensively within ADC development and bioconjugation reactions is succinimidyl 4-(N-maleimidomethyl)cyclohexane-1-carboxylate (SMCC) (Figure 3.13).[182] This bifunctional linker contains a NHS ester functionality and a maleimide functionality. These are held apart by a cyclohexane ring which has been shown to confer added stability to the linker.

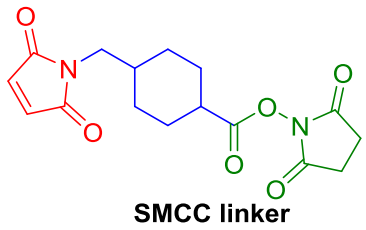

Figure 3.13: chemical structure of SMCC. In red is the maleimide moiety, in blue is the cyclohexane ring spacer and in green the NHS functionality.

Careful control over pH can ensure that thiol addition occurs selectively at the maleimide (pH 6.5-7.5) whilst amine residues react with the NHS ester functionality (pH 7-9).[173] This strategy is utilised in the formation of Kadcyla® (Figure 3.14).[36]

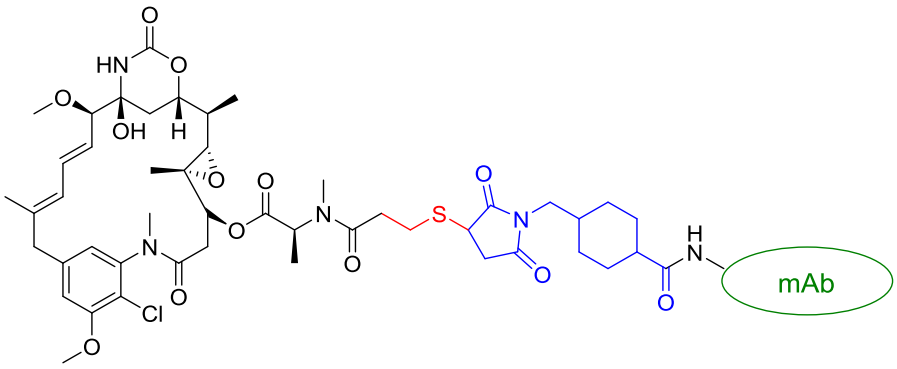

Figure 3.14: structure of Kadcyla where mAb = trastuzumab. In blue is the SMCC linker with the antibody attached through reaction with the NHS ester functionality. In red is the thiol introduced onto the DM1 payload for reaction with the maleimide of SMCC.

The use of the SMCC linker within our system can be seen as favourable for a number of reasons. Firstly, jacalin does not contain any cysteine residues in its primary amino acid sequence.[169] This means that regioselective reactions of the SMCC with jacalin can be achieved as only lysine residues are available for reaction with the NHS ester of the linker. This results in jacalin being functionalised with a maleimide moiety. In addition to this, with the DSA system being utilised on the solid phase, the introduction of a cysteine residue, and hence a thiol, into a specific peptide sequence should proceed with relative ease. This means that both components of the desired click reaction should be simple to synthesise.

In order to attempt this conjugation, the solid phase synthesis of a duocarmycin peptide containing a thiol functionality was completed. The peptide was based on peptide **3.1** from earlier but with a cysteine residue introduced. This gives **3.5** as shown in Figure 3.15.

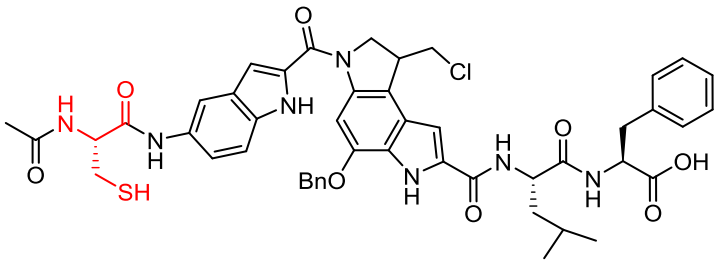

3.5

Figure 3.15: chemical structure of peptide **3.5**. In red is shown the cysteine residue which was introduced into the sequence on the solid phase.

Peptide **3.5** was synthesised on a 2-Cltrt resin. Typically, cysteine residues utilised in Fmoc based SPSS contain a trityl protecting group on the thiol. However, this group requires high TFA concentrations for removal so a methoxytrityl thiol protecting group, which can be removed in only 1% TFA, was utilised.[183] The synthetic strategy employed for this peptide was very similar to those described in Chapter 2, Section 2.3.3.2. However, one difference is within the cleavage cocktail utilised - for peptide **3.5**, ethanedithiol (EDT) at 2.5% was introduced. EDT has been shown to aid in the cleavage of peptides containing cysteine residues since it acts as an ideal scavenger for the trityl and methoxytrityl groups as well as a reducing agent to avoid intermolecular disulphide bond formation.[184] Evidence of the successful synthesis of **3.5** was provided by MALDI with the expected mass being clearly shown. Preparative HPLC was used to purify the peptide and a reasonable purity of 92% was found post purification using analytical HPLC. It was decided that for a proof of concept reaction, the benzyl group would be left in to reduce handling of the highly cytotoxic analogues.

It was then necessary to attempt the maleimide functionalisation of the jacalin lectin. For this, the lyophilized protein was reconstituted into HEPES buffer saline at pH 7.4 at a 2 mg/mL concentration. A 2 mg/mL solution of SMCC in DMSO was then made and added to the jacalin to give a 20 molar excess of the linker. After 2 h, the functionalised jacalin was purified through a 7K MWCO spin column and the resulting solution analysed by LC-MS. The results of the LCMS are shown in Figure 3.16.

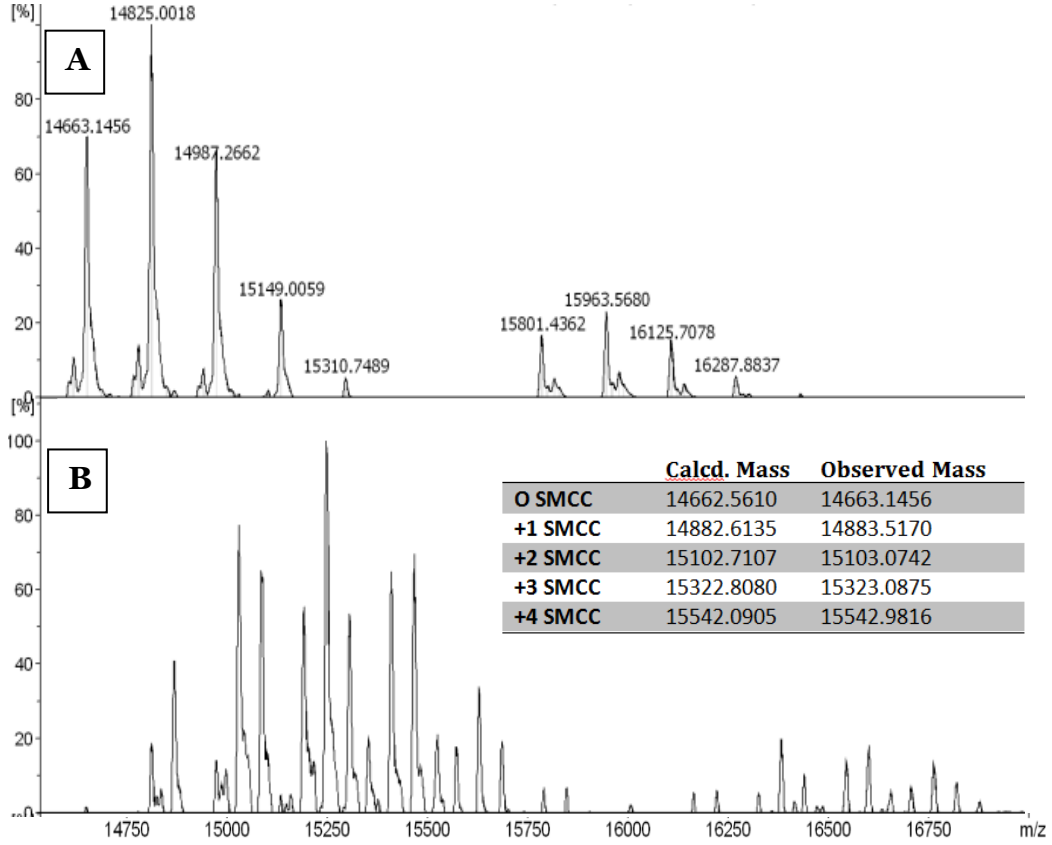

	Calcd. Mass	Observed Mass
O SMCC	14662.5610	14663.1456
+1 SMCC	14882.6135	14883.5170
+2 SMCC	15102.7107	15103.0742
+3 SMCC	15322.8080	15323.0875
+4 SMCC	15542.0905	15542.9816

Figure 3.16: LCMS results of the coupling of jacalin to the SMCC linker. A: Results of unlabelled jacalin, B: Results of jacalin labelled with SMCC. See page 177 for LCMS method details

From these results it is evident that the coupling of the SMCC linker has occurred with the addition of up to four linkers per α-subunit. The complexity of the labelled jacalin spectrum is a result of the glycosylation of the jacalin structure and the various levels of conjugation present in the mixture. However, thorough deconvolution and analysis can show that each peak is shifted by 220 Da (up to four times) which is consistent with the addition of an SMCC linker. The data provided in the table of Figure 3.16 relates to the jacalin α-subunit without any addition of a hexose moiety. The other peaks present in the spectrum relate to the masses of the jacalin α-subunit with differing levels of hexose conjugation. Also noteworthy here is the lack of precipitation upon SMCC conjugation. It could be the smaller size of this unit aids in keeping this jacalin conjugate in solution.

With the maleimide functionalised jacalin now in hand. Attempts could be made to react this with peptide **3.5**. For this, the SMCC functionalised jacalin

was mixed with 20 molar equivalents of **3.5** in HEPES buffer. After 2 h, a precipitate was evident within the reaction mixture. This was removed and the resulting supernatant passed through a spin column. Both the precipitate and the supernatant were then analysed through LC-MS. Whilst the supernatant seemed to contain only jacalin and SMCC labelled jacalin, the LC-MS result of the precipitate which was dissolved in DMSO/Buffer showed a more promising result (Figure 3.17).

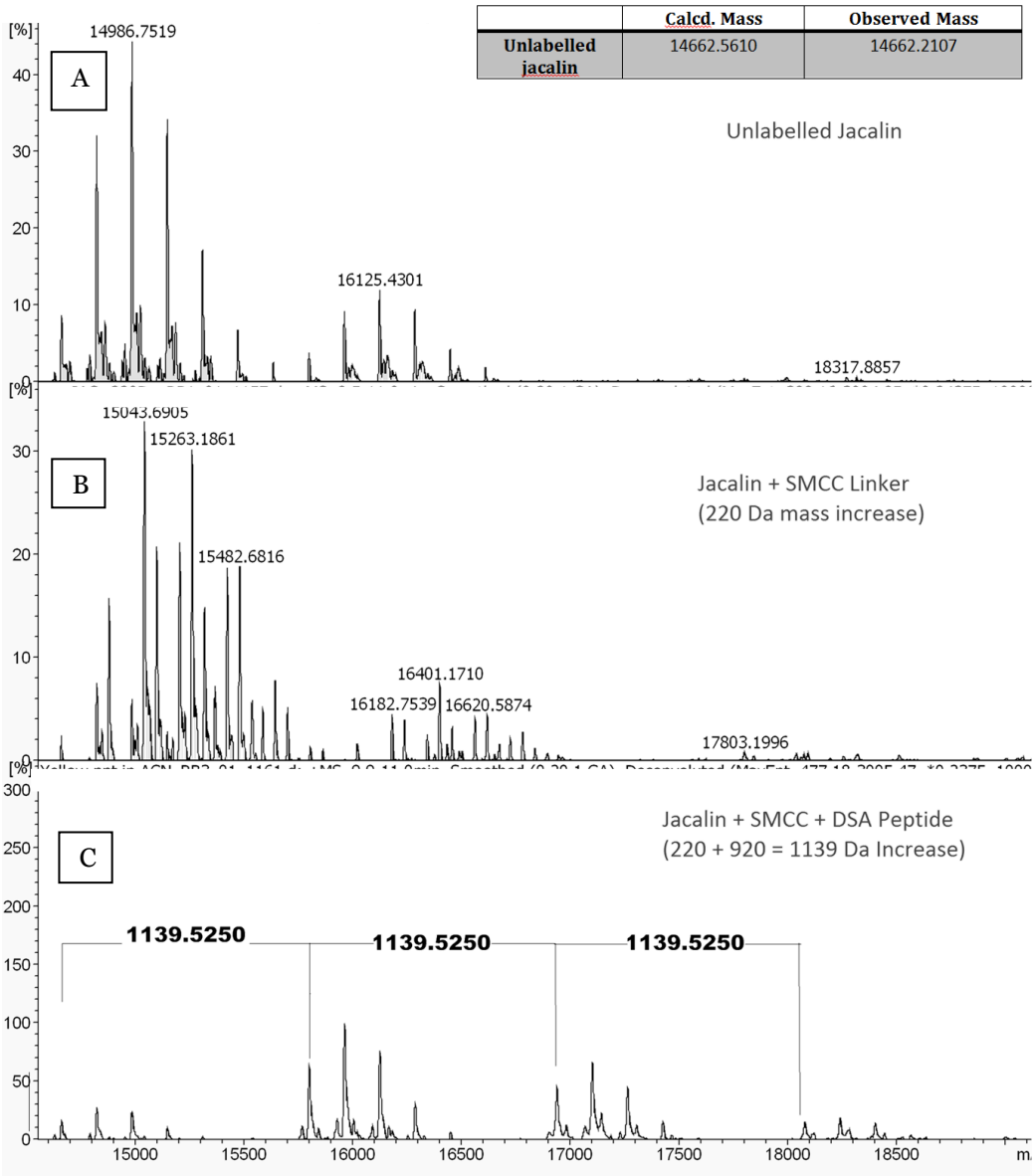

Figure 3.17: LC-MS results of A: unlabelled jacalin, b: SMCC labelled jacalin, c: jacalin labelled with SMCC and peptide **3.5**. See page 177 for LCMS method details.

The above results show that the precipitate from the reaction mixture contains the desired conjugate with between 1-3 units of SMCC-3.5 per α-

subunit. This was pleasing since a DAR of between 3 and 4 has previously been shown to be desirable in ADC like systems.[185] Precipitation was again observed and the effect this could have on the potential of the conjugates as targeted agents was of some concern.

To investigate the conjugation reaction with the benzyl deprotected, active form of peptide **3.5**, Initial studies involved the transfer hydrogenation reaction using palladium and ammonium formate introduced in Chapter 2 (Scheme 3.10).

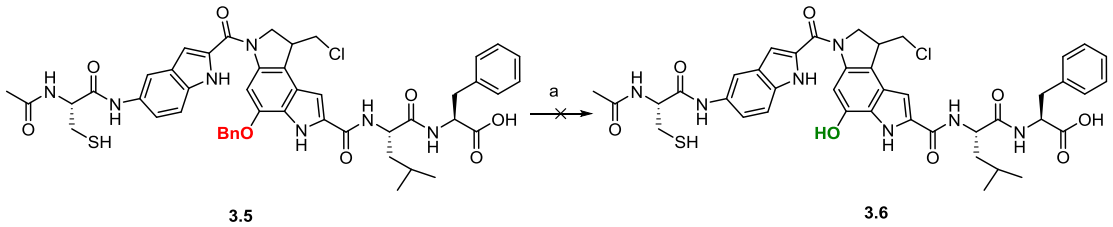

Scheme 3.10: a: 10% Pd/C, 25% Aq. Ammonium formate, MeOH, rt, 1 h

HPLC analysis after 1 h showed that no reaction had occurred via the presence of the starting material peak. For this reason, the reaction was left for an extended amount of time. When HPLC still presented no reaction occurring, further additions of palladium and ammonium formate were made but no reaction occurred. Other Palladium based catalysts for the transfer hydrogenation also returned no favourable results.

This lack of reactivity could be due to the poisoning of the palladium catalyst via the sulphur of the cysteine residue. This process has previously been shown to occur in a number of reaction conditions.[186, 187]

Benzyl deprotection was also attempted using aluminium chloride and BBr_3 (see Chapter 2, Section 2.3.4.), which has also shown promise in previous studies.[131] However, neither of these conditions returned the desired product.

As an alternative approach, peptide **3.1** could again be synthesised and benzyl deprotected. Following on from this, a thiol moiety could be added via the C-terminus carboxylic acid which could then be used for maleimide coupling. For this it was decided cysteamine could act as an ideal bifunctional

linker for the system. Cysteamine was coupled to the benzyl deprotected form of **3.1**, numbered here as **3.7** (Scheme 3.11).

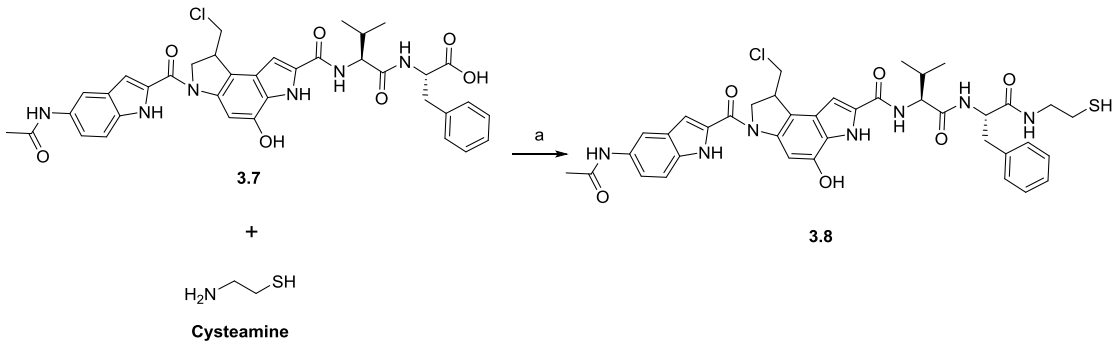

Scheme 3.11: a: HATU, DIPEA, DMF, rt, 2 h

Post reaction HPLC demonstrated the presence of two main peaks in the reaction mixture and these were identified using mass spectrometry as **3.8** and also 3.8 but with cysteamine as a disulphide. Both of the peaks were isolated and could be utilised in parallel as within the reaction buffer during the conjugation to the maleimide jacalin, TCEP would be included to reduce the disulphide to give solely **3.8**.[188] However, when this was attempted and the resulting conjugate analysed by LC-MS, only SMCC labelled jacalin was evident, indicating that **3.8** had not reacted with the maleimide. As an alternative approach, prior to jacalin conjugation, the **3.8** mixture was passed through a TCEP containing resin- the resulting eluent then added directly into the jacalin SMCC containing buffer. However, post reaction LC-MS again indicated that no coupling had occurred.

An alternative approach involved the reversal of the reactivity employed above i.e. introduce a maleimide functionality onto a duocarmycin agent and a thiol onto the protein. Since jacalin does not contain a cysteine residue, artificial introduction of a thiol moiety is required. The use of 2-iminothiolane, also known as Traut's reagent, (Scheme 3.12) provides a simple, one step conversion of amines to sulfhydryl's and is therefore ideal for the introduction of thiols onto lysine resides of jacalin.[173] A further advantage of this reagent is that it maintains the charge properties of the original lysine residue and should therefore not result in any solubility issues for the jacalin in aqueous solutions.

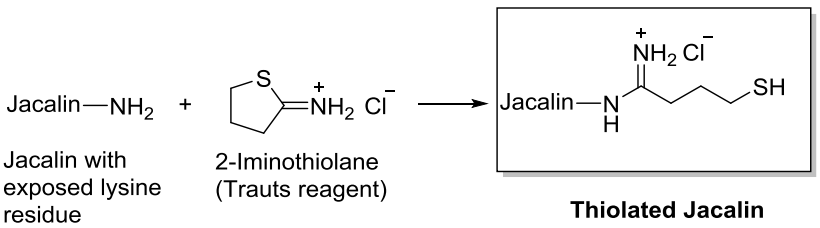

Scheme 3.12: 2-Iminothiolane can be used to introduce sulfhydryl residues into proteins via reaction with exposed lysine residues.

For this reaction, jacalin was dissolved in HEPES buffer at pH 7.4 and treated with 2-iminothiolane at a 20 molar excess. After 2 h, the reaction mixture was purified to remove excess 2-iminothiolane. This was achieved by spinning the mixture through a 7K MWCO spin column. In order to confirm the presence of thiols on jacalin, an Ellman's assay was completed. The observed colour change from colourless to yellow upon introduction of the Ellman's reagent provided evidence of a successful reaction.[189]

Compound **3.9** (Figure 3.18) represents a duocarmycin analogue containing a maleimide moiety. The DNA binding subunit is not present and the peptide was synthesised on a rink amide resin to cap the C-terminus with an amide. A maleimide functionality was introduced onto the N-terminus through use of N-ε-maleimidocaproic acid.

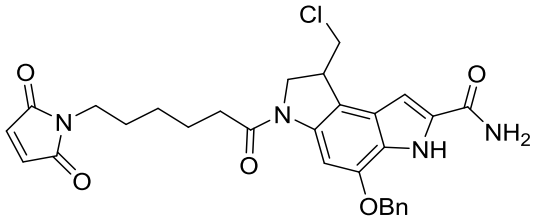

3.9

Figure 3.18: chemical structure of compound 3.13 containing a maleimide functionality

Upon the successful synthesis of crude **3.9** as determined by mass spectrometry the benzyl deprotection of **3.9** was realised. For this manipulation, the BBr_3 benzyl deprotection conditions were used as opposed to the transfer hydrogenation reactions to avoid reduction of the required maleimide functionality. ^1H NMR confirmed the formation of **3.10** (Scheme 3.13) via the absence of peaks representing the benzyl group. Mass spectrometry also confirmed the formation of **3.10**.

What remained now was for **3.10** to be reacted with the thiolated jacalin. This was done using a 20 molar excess of **3.10** to the jacalin (Scheme 3.13).

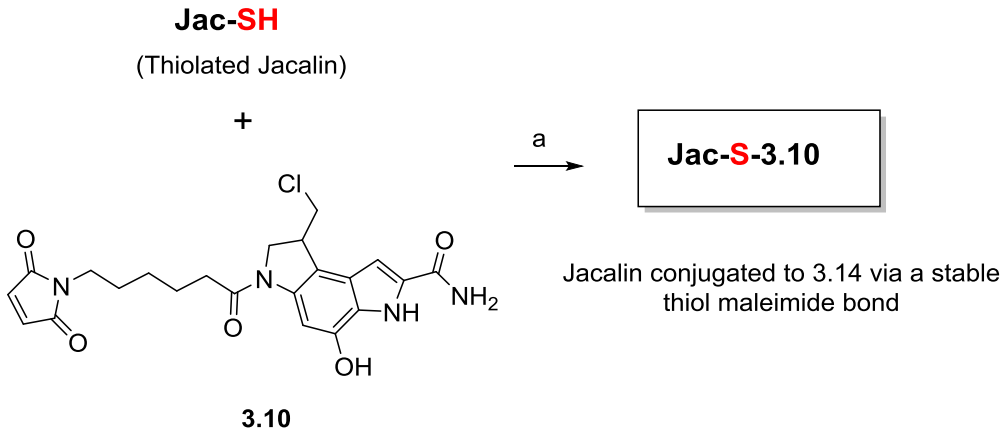

Scheme 3.13: reaction of thiolated Jacalin with compound 3.10 to form a jacalin-3.10 conjugate. A: 10 Mm HEPES buffered saline, 2 h, rt.

After the 2 h reaction time, a precipitate was again evident within the reaction mixture which was in turn removed by centrifugation and analysed via MALDI mass spectrometry (Figure 3.19).

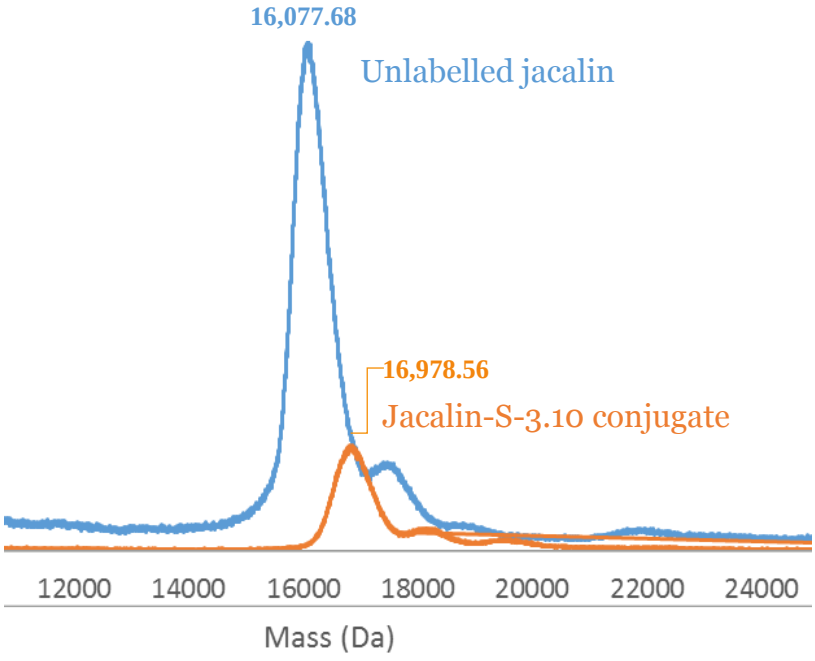

Figure 3.19: MALDI mass spectrometry spectrum of unlabelled jacalin (blue) and jacalin labelled with 3.10 (orange). N.b. the masses shown in the figure are taken from the data points at the apex of the respective peak.

Again this precipitate was difficult to get back into solution and hence analysis using MALDI mass spectrometry was problematic. The MALDI

spectrum however, did indicate a mass increase suggesting the addition of between two and three **3.10** units per jacalin α-subunit. With this conjugate only re-dissolving in large quantities of DMSO, investigations into its use as a possible active conjugate for our studies were discontinued.

After the promising results obtained for the coupling of **3.5** to jacalin functionalised with SMCC, it was particularly disappointing that troubles with the subsequent benzyl deprotection and thiol introduction were encountered. Despite this, it is worth noting that this conjugation strategy along with the reverse reactivity strategy had also promoted the precipitation of jacalin. It maybe that therefore, this conjugation route was also going to result in issues when it came to the biological analysis of these conjugates. The work in this section therefore further supports those findings from Section 3.3.2 of this chapter in that jacalin may be very difficult to conjugate with small molecules without causing its precipitation and hence an alteration to its quaternary structure. To further confirm whether this is the case a further conjugation strategy was explored.

3.3.4 Alkyne-Azide Cycloaddition Click Chemistry

The Huisgen 1,3-dipolar cycloaddition reaction, also termed the [3 + 2] azide-alkyne cycloaddition has manifested itself as the most popular click reaction founded to date.[173] This reaction involves the formation of five-membered triazole-based heterocycles, from the reaction between an azide and an alkyne (Scheme 3.14).

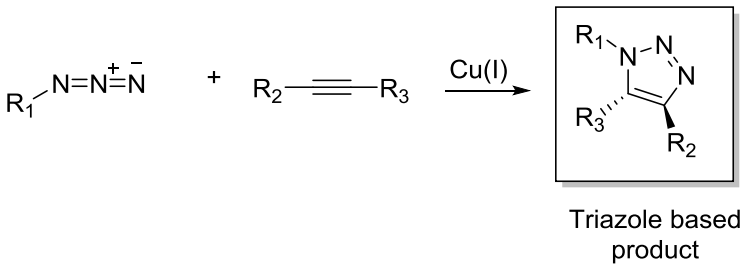

Scheme 3.14: the Huisgen 1,3-dipolar cycloaddition reaction between an azide and an alkyne to form a stable triazole based product.

Whilst most commonly used within the area of organic synthesis and drug discovery, this click reaction has found multiple uses within bioconjugation chemistry.[173] The popularity in this area can be attributed to a number of

factors. Firstly, the azide moiety is absent in almost all naturally existing compounds, and lacks reactivity with natural biomolecules. This means, that the azide itself can be used for highly selective bioconjugation reactions. In addition to this, the click chemistry reaction allows for mild reaction conditions, high yields, simple work-ups and specificity, all of which are ideal in bioconjugation. These advantages for bioconjugation reactions were brought about by the realisation that a Cu(I) catalyst could lower the activation energy to reaction between the azide and alkyne and therefore both speed up the reaction and allow for more mild conditions. This is of course vital when using biomolecules such as proteins. In addition to this, the Cu(I) catalyst was also found to promote the formation of 1,4-disubstituted 1,2,3-triazole products therefore improving the selectivity of the reaction.[173]

More recently, the utility of the azide-alkyne click reaction has been broadened through the development of strain-promoted azide-alkyne cycloaddition.[190] This reaction uses a highly strained alkyne which allows the reaction to proceed without the need for a copper catalyst. This is particularly advantageous within living systems where the toxicity of the copper catalyst can cause issues. Not only this, but the simplicity of the strained promoted click reaction, in that the two reagents simply need to be mixed, means it presents itself as a good tool within bioconjugation reactions.

The utility of this reaction within ADC like systems has been demonstrated by Zhou et al. who conjugated azide functionalised sulfonate agents to monoclonal antibodies via a strained dibenzocyclooctyl (DBCO) alkyne (Figure 3.20).[191]

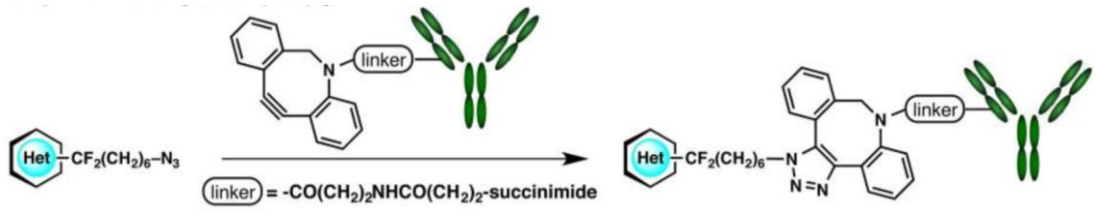

Figure 3.20: work by Zhou et al. used the strain-promoted azide-alkyne cycloaddition to from antibody-drug conjugates.

As an initial start point for the jacalin-duocarmycin based system it was expected that a duocarmycin-based peptide containing an azide moiety could

be made with relative ease. An alkyne-NHS compound could then be utilised to functionalise jacalin following conditions previously employed. The two moieties could then be coupled together under copper catalyst conditions. A copper catalyst promoted reaction formed the initial investigation since protocols using this technique were extensive within the literature.

When considering the formation of the duocarmycin based peptide containing an azide, a more hydrophilic compound could be useful to reduce the precipitation of jacalin previously observed. Azide **3.11** (Scheme 3.15) contained an amine moiety connected to an azide via a PEG chain. This linker combines a hydrophilic PEG chain and an amine which can be coupled to the C-terminus of the duocarmycin-based peptides. Coupling of azide **3.11** to peptide **3.12** (a simplified version of **3.1** for speed and ease of synthesis) via a stable amide bond was achieved in good yield (Scheme 3.15).

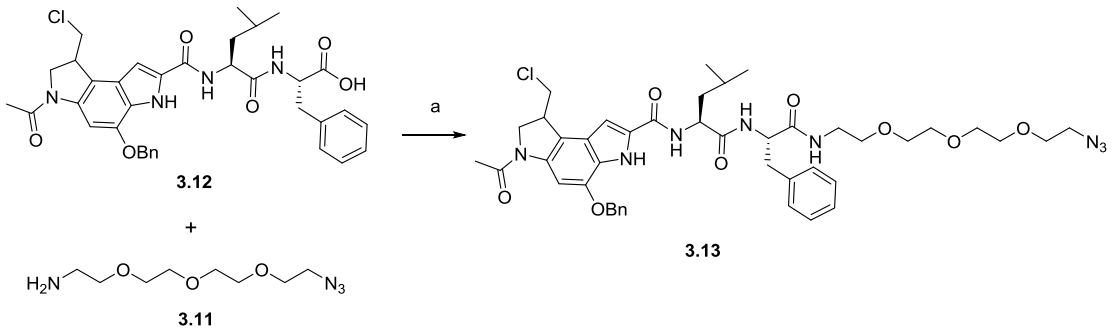

Scheme 3.15: a: HATU, DIPEA, DMF, 2 h, rt.

The successful synthesis of **3.13** was confirmed via MALDI which demonstrated M+Na and M+K adducts of **3.13**. Analytical HPLC also demonstrated a purity of >90% which was adequate for the proof of concept coupling reactions. As previously, the click reactions were investigated with the benzyl protected **3.13** so as to reduce the handling of potentially cytotoxic agents.

Jacalin functionalisation with an alkyne utilised propargyl-*N*-hydroxysuccinimidyl ester. This was reacted with jacalin in HEPES buffer at room temperature for 2 h. After this, excess alkyne was removed from the reaction mixture. Successful coupling of the alkyne to the jacalin was demonstrated through MALDI which showed a clear increase in the mass of

the α-subunit. This increase suggested the coupling of around four alkynes per α-subunit.

With both components now in hand, the click reaction between the two could be attempted. For the required Cu(I) catalyst a mixture of $CuSO_4$ and sodium ascorbate was utilised. The ascorbate is able to reduce the Cu(II) to Cu(I) in situ.[173] This is desirable since the direct use of Cu(I) can cause the reaction to be extremely susceptible to oxygen, which in turn can dramatically reduce the yield. The azide and jacalin-alkyne conjugate were mixed in HEPES buffer before addition of the $CuSO_4$-ascorbate mixture. Following a protocol published by Weil and co-workers the reaction was left to proceed for four days at room temperature.[192] After this time course, a precipitate was evident within the reaction mixture. This precipitate was removed before being analysed by MALDI. The resulting spectrum suggested that no conjugation had occurred with a peak similar to that of the jacalin-alkyne being observed. The MALDI spectrum of the supernatant also seemed to present no indication of a successful coupling. To further investigate this click chemistry reaction, an alternative catalyst was employed which has previously shown success in click reactions within our laboratory. $Cu(MeCN)_4.PF_6$ and DIPEA were used within a repeated reaction but again, no coupling occurred.

What was different with this reaction was that the jacalin precipitation was occurring without actual coupling to its structure. This suggested that the lectin was unstable within the reaction conditions utilised. This could be as a result of a pH change that may occur within the buffer system with the specific reaction components utilised here. For this reason a brief investigation of the strain-promoted click reaction was carried out. In theory, the azide and alkyne can simply be mixed together simplifying the reaction conditions and hence hopefully maintaining the jacalin within solution.

For this alternative the coupling of dibenzocyclooctyl-NHS (DBCO-NHS) to the jacalin was attempted. From this reaction a precipitate was obtained but it was easily re-dissolved in a H_2O/ACN mixture. This allowed us to easily obtain a MALDI mass spectrum for this conjugate (Figure 3.21).

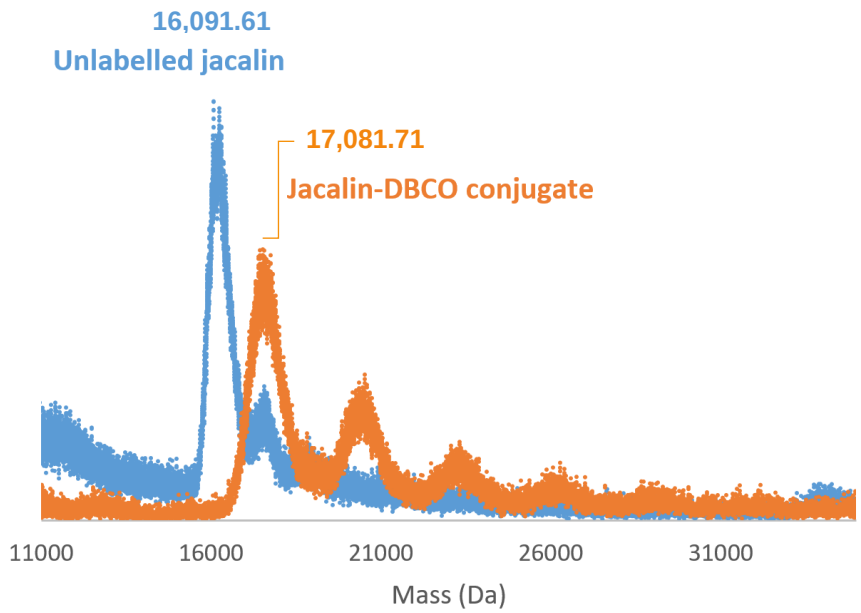

Figure 3.21: MALDI mass spectrometry spectrum of unlabelled jacalin (blue) and jacalin-DBCO (orange). A clear mass increase in the α-subunit is observed for jacalin-DBCO. N.b. the masses shown in the figure are taken from the data points at the apex of the respective peak.

The precipitation of jacalin in this reaction was unsurprising due to the large, hydrophobic nature of DBCO. However, upon analysis of the MALDI spectrum it can be seen that an addition of two DBCO units per α-subunit was enough to cause this precipitation. This was more surprising since it was not expected that this would be enough to cause the instability or aggregation of the jacalin within the aqueous solution.

The coupling of jacalin-DBCO to **3.13** was attempted by simply mixing the two reactants in HEPES buffer/ACN mixture and allowing the reaction to proceed for four days. After the reaction time course, the mixture was analysed by MALDI mass spectrometry. Disappointingly, this spectrum suggested that no coupling of the azide of **3.13** had occurred to the DBCO. Whilst this was disheartening, it can be seen as unsurprising since the reaction of DBCO with azides has previously been described as challenging and nontrivial. This has been proposed to be due to low yields, a lack of reactivity and extended reaction times.[173]

With these results further backing up our proposition of jacalin being a difficult lectin to conjugate to, it was decided to spend no further time investigating the coupling of duocarmycin to this lectin. It is clear that jacalin

is a lectin that is extremely sensitive to additions to its surface. This has been observed here on numerous occasions with a variety of ligands. Even with careful control over the level of conjugation being made, the precipitation of the lectin is observed. This property of jacalin therefore means that it does not suit itself for use within ADC like systems, where surface modifications are required. This of course could be solely attributed to the hydrophobic nature of the duocarmycin unit employed within the conjugations, however the precipitation has also been observed with various other NHS esters used within this body of work.

It is for this reason a further route to achieve the targeted delivery of duocarmycin agents to cancer cells via the Thomsen-Friedenreich T-antigen was investigated. With this antigen presenting itself as a viable and potentially efficacious moiety to achieve targeted delivery, further research was warranted. The following chapter presents an alternative method to achieve this.

3.4 Conclusion

The aim of the research within this chapter was to investigate the conjugation of duocarmycin based moieties to the T-antigen binding lectin, jacalin. An exploration into various methods of conjugation, often mimicking those utilised in approved ADCs, was proposed to ascertain which was the most advantageous for our specific system.

As an initial method the commonly employed EDC/NHS chemistry was utilised. The coupling of the exposed lysine residues of jacalin with the C-terminus carboxylic acid of our duocarmycin analogues was attempted. Both in-situ and ex-situ formation of the NHS ester of our duocarmycin analogues was investigated. Whilst the ex-situ NHS formation gave the most consistent results, jacalin precipitation with these conditions was common and occurred on numerous occasions. This was potentially concerning due to the possible alterations to the jacalin quaternary that led to aggregation and precipitation from the buffer system.

As an additional attempt to achieve the conjugation, thiol/maleimide chemistry was investigated. Initial attempts involved the formation of a

maleimide functionalised jacalin and a duocarmycin analogue containing a cysteine residue. The coupling of these two proceeded with ease. However, it became clear that the benzyl deprotection of the thiol containing duocarmycin analogues was difficult and was not successful. The reverse of this chemical reactivity whereby the jacalin was functionalised with a thiol and a duocarmycin-maleimide analogue was synthesised demonstrated an ability to conjugate the two species together. However, precipitation and difficulties with re-dissolution of the conjugate again suggested that jacalin may be sensitive to surface modification with the duocarmycin based units utilised within this body of work.

As a final conjugation strategy the azide-alkyne click reaction was attempted. Jacalin was functionalised with an alkyne, and an azide containing duocarmycin analogue was synthesised. However, the coupling of the two using a copper catalyst demonstrated no conjugation. As a further attempt, DBCO was utilised to try a strain promoted click reaction. Jacalin was functionalised with DBCO and reacted with our azide-duocarmycin unit. Under these conditions, no conjugation was observed.

What was common throughout all the above strategies was the precipitation of jacalin upon conjugation or within the reaction conditions employed. This has been attributed to both the sensitivity of the lectin to certain conditions and also the sensitivity to surface modifications. This can be seen as a particular problem due to the hydrophobic nature of the DSA units employed within this chapter. It is for this reason that we concluded that jacalin may not be suitable for investigations within ADC like systems incorporating our duocarmycin analogues. However, the directed targeting to the T-antigen is an area which warrants further research.

3.5 Experimental

3.5.1 General Procedures

Reagents and Solvents

All chemicals were reagent grade and were purchased from Sigma Aldrich, Fisher Scientific and Tokyo Chemical Industry. Fmoc-amino acids and coupling reagents were purchased from Novabiochem, Fluorochem or AGTC

Bioproducts. Anhydrous solvents were bought from Sigma Aldrich and assumed to conform to specification. Jacalin was purchased from Vector laboratories. Zeba™ spin desalting columns (7K MWCO, 0.5 mL) were purchased from Fisher scientific.

Physical Characterisation and Spectroscopic Techniques

^{1}H- and ^{13}C-NMR spectra were recorded on a Bruker spectrometer operating at 400 MHz (^{1}H) or 100 MHz (^{13}C) using the specified deuterated solvent. The chemical shifts for both ^{1}H- and ^{13}C were recorded in ppm and were referenced to the residual solvent peak of DMSO at 2.50 ppm (^{1}H) and 39.7 ppm (^{13}C). Multiplicities in the NMR spectra are described as s = singlet, d = doublet, t = triplet, q = quartet, m = multiplet, br = broad, and combinations thereof; coupling constants are reported in Hz. Low resolution mass spectra were recorded using a Shimadzu LCMS 2010EV operated under electrospray ionisation in positive (ES+) mode. Accurate mass spectra were recorded at the EPSRC National Mass Spectroscopy Service Centre, Swansea or The John Innes Centre, Norwich Research Park. Melting points were recorded using open capillary tubes on a Mel-Temp electrothermal melting point apparatus, melting points are uncorrected. Infrared spectra were recorded using a PerkinElmer Spectrum BX with ATR attachment.

Chromatographic Techniques

Analytical RP-HPLC was performed on an Agilent 1200 using an Agilent eclipse XDB-C18 column, 4.6 x 150 mm, 5 μM and a flow rate of 1 mL/min. Solvent A = Water + 0.05% TFA and Solvent B = MeOH + 0.05% TFA. Gradient 5% B up to 95% B over 20 minutes. Detection wavelength 214 nm and 254 nm. Semi-preparative RP-HPLC was performed on an Agilent 1200 using an Agilent eclipse XDB-C18 column, 9.4 x 250 mm, 5 μM and a flow rate of 4 mL/min. Solvent A = Water + 0.05% TFA and Solvent B = MeOH + 0.05% TFA. Gradient 5% B up to 95% B over 20 minutes. Detection wavelength 214 nm and 254 nm. Preparative RP-HPLC was performed on an Agilent 1200 using an Agilent eclipse XDB-C18 column, 21.2 x 150 mm, 5 μM and a flow rate of 20 mL/min. Solvent A = 95% H_2O + 5% MeOH + 0.05% TFA and Solvent B = 95% MeOH + 5% H_2O + 0.05% TFA. Gradient 5% B up to 95% B over 20 minutes.

Protein MALDI Mass Spectrometry

MALDI mass spectrometry of proteins and peptides was performed on Kratos Analytical Axima MALDI-TOF. For peptides, α-cyano-4-hydroxycinnamic acid was utilised as a matrix and for proteins, trans-ferulic acid was used. MALDI sample preparation for jacalin/BSA MALDI involved a sandwich method where matrix was first applied to the plate followed by a desalted sample of protein followed by a further layer of matrix. MALDI mass spectrometry profiles were recorded in linear mode with a laser power between 150 and 180 for jacalin and BSA. Reflectron mode was used for the obtainment of MALDI spectra for peptides.

Protein LCMS

Samples were injected onto a ProSwift reversed phase RP-1S column (4.6 × 50 mm; Thermo Scientific) at 25 °C using an UltiMate 3000 HPLC system (Dionex). Gradient elution was performed at a flow rate of 0.2 mL/min using a linear gradient (15 min) from 2 to 100% (vol/vol) acetonitrile and 0.1% (vol/vol) formic acid. The eluent was continuously infused into a Bruker micrOTOF-QIII mass spectrometer running Hystar (Bruker Daltonics) using positive mode ESI. The mass spectrometer was calibrated with ESI-L tuning mix (Agilent Technologies). MS acquisition parameters were as follows: dry gas flow of 8 L/min, nebulizer gas pressure of 1.8 Bar, dry gas at 240 °C, capillary voltage of 4,500 V, offset of 500 V, and collision RF of 650 Vpp. Processing and analysis of MS experimental data were carried out using Compass DataAnalysis, version 4.1 (Bruker Daltonik). Neutral mass spectra were generated using the ESI Compass, version 1.3 Maximum Entropy deconvolution algorithm over a mass range of 2,000–30,000 Da for the α-subunit. Exact masses are reported from peak centroids representing the isotope average neutral mass.

3.5.2 Solid Phase Chemistry

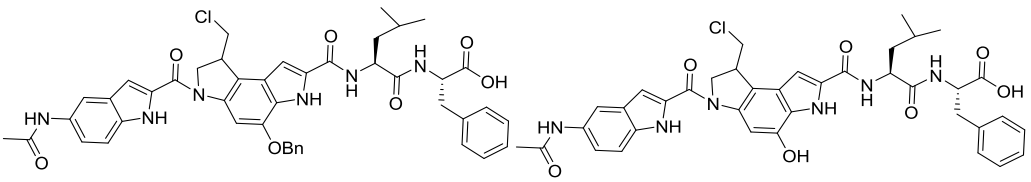

3.1

3.11

H-Phe-2ClTrt resin (100 mg, 0.09 mmol, [manufacturer's resin loading 0.9 mmol/g]) was prepared for coupling by swelling in DCM for 30 mins followed by DMF for 30 mins. Fmoc-Val-OH (152 mg, 0.45 mmol) was dissolved in 2 mL of DMF and treated with HATU (171 mg, 0.45 mmol) and DIPEA (156 μL, 0.90 mmol). After 10 secs the resulting solution was added to the resin and the mixture shaken for 1 h. Subsequently, the resin was washed with DMF (6 x 10 mL) and the coupling repeated. The resin was washed 6 times with DMF (10 mL) before removal of the valine Fmoc using piperidine in DMF (6 mL 40% 10 mins, 6 mL 20% 5 mins twice). Following Fmoc deprotection, the resin was washed with DMF (6 x 10 mL). Next, **2.10** (78 mg, 0.14 mmol) was dissolved in 2 mL of DMF and treated with HATU (51 mg, 0.14 mmol) and DIPEA (47 μL, 0.27 mmol). After 10 secs the resulting solution was added to the resin and the mixture shaken overnight. The resin was subsequently washed with DMF (6 x 10 mL) before the Fmoc group on the indoline nitrogen of **2.10** removed using piperidine in DMF (6 mL 40% 10 mins, 6 mL 20% 5 mins twice). The resin was then washed again with DMF (6 x 10 mL) before being treated with **2.14** (143 mg, 0.36 mmol) HATU (136 mg, 0.36 mmol) and DIPEA (125 μL, 0.72 mmol). The mixture was shaken for 6 h before the resin was with DMF (6 x 10 mL) and the coupling repeated. The resin was then washed with DMF (6 x 10 mL) before the Fmoc group of **2.14** was removed using piperidine in DMF (6 mL 40% 10 mins, 6 mL 20% 5 mins twice). Upon washing of the resin with DMF (6 x 10 mL) the resin was treated with AcCl (32 μL, 0.45 mmol) and DIPEA (156 μL, 0.9 mmol) in DMF (2 mL). After shaking for 1 h the resin was washed with DMF (6 x 10 mL) followed by DCM (6 x 10 mL). Cleavage of **3.1** from the resin was affected by addition of a solution of 2% TFA, 10% TIPS in DCM (10 mL). After 3 h of shaking the cleavage mixture was filtered. The resin was rinsed with DCM (2 x 3 mL) and the combined filtrates were concentrated to dryness by rotary evaporation under vacuum. Crude **3.1** was then analysed via analytical RP-HPLC (RT = 18.2 min) and HRMS (ES+) calcd. for $C_{45}H_{45}ClN_6O_7$ (M + H)+, 317.3111; found, 317.3112. Crude **3.1** (10 mg, 0.01 mmol) was dissolved in MeOH (1 mL) and the resulting solution degassed with a gentle stream of N_2 for 30 mins. To this solution was added a slurry of 10% Pd/C (20 mg) in 25% aq. Ammonium formate (500 μL) and the

resulting suspension stirred under N_2 for 1 h. The reaction mixture was then filtered through a pad of celite before the MeOH was removed under reduced pressure. Crude **3.11** was then purified using preparative HPLC to give pure **3.11** (4.1 mg, 47%) as a light brown solid which was analysed via RP-HPLC (RT + 16.5 min) and HRMS (ES+) calcd. for $C_{38}H_{39}ClN_6O_7$ (M + H)+, 727.2642; found, 727.2639.

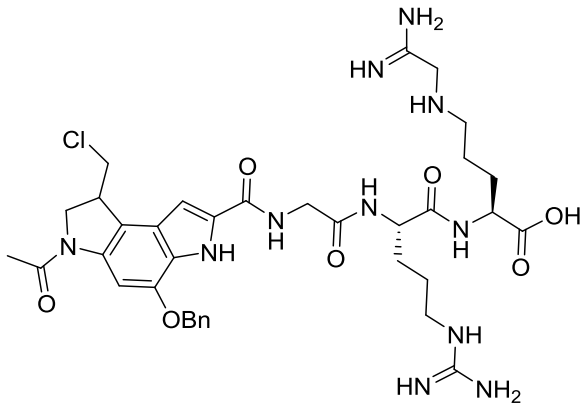

3.2

H-Arg(Pbf)-2ClTrt resin (100 mg, 0.067 mmol, [manufacturer's resin loading 0.67 mmol/g]) was prepared for coupling by swelling in DCM for 30 mins followed by DMF for 30 mins. Fmoc-Arg(Pbf)-OH (217 mg, 0.34 mmol) was dissolved in 2 mL of DMF and treated with HATU (127 mg, 0.34 mmol) and DIPEA (116 µL, 0.67 mmol). After 10 secs the resulting solution was added to the resin and the mixture shaken for 1 h. Subsequently, the resin was washed with DMF (6 x 10 mL) and the coupling repeated. The resin was washed with DMF (6 x 10 mL) before removal of the arginine Fmoc using piperidine in DMF (6 mL 40% 10 mins, 6 mL 20% 5 mins twice). Following Fmoc deprotection, the resin was washed with DMF (6 x 10 mL). Next, Fmoc-Gly-OH (99 mg, 0.34 mmol) was dissolved in 2 mL of DMF and treated with HATU (127 mg, 0.34 mmol) and DIPEA (116 µL, 0.67 mmol). After 10 secs the resulting solution was added to the resin and the mixture shaken for 1 h before being washed with DMF (6 x 10 mL) and the coupling with Fmoc-Gly-OH repeated. The resin was subsequently washed with DMF (6 x 10 mL) before the Fmoc group on the glycine was removed using piperidine in DMF (6 mL 40% 10 mins, 6 mL 20% 5 mins twice). The resin was then washed again with DMF (6 x 10 mL) before being treated with **2.10** (57 mg, 0.1

mmol) HATU (38 mg, 0.1 mmol) and DIPEA (34 μL, 0.2 mmol). The mixture was shaken overnight before the resin was with DMF (6 x 10 mL). The indoline Fmoc group of **2.10** was removed using piperidine in DMF (6 mL 40% 10 mins, 6 mL 20% 5 mins twice). Upon washing with DMF (6 x 10 mL), the resin was treated with AcCl (23 μL, 0.34 mmol) and DIPEA (116 μL, 0.67 mmol) in DMF (2 mL). After shaking for 1 h the resin was washed with DMF (6 x 10 mL) followed by DCM (6 x 10 mL). Cleavage of **3.2** from the resin was affected by addition of a solution of 47% TFA, 10% TIPS in DCM (10 mL). After 3 h of shaking the cleavage mixture was filtered. The resin was rinsed with DCM (2 x 3 mL) and the combined filtrates were concentrated to dryness by rotary evaporation under vacuum to give 3.2 which was analysed using reverse phase HPLC (RT = 14.3 min) and HRMS (ES+) calcd. for $C_{36}H_{48}ClN_{11}O_7$ (M + Na)+, 804.3324; found, 804.3336.

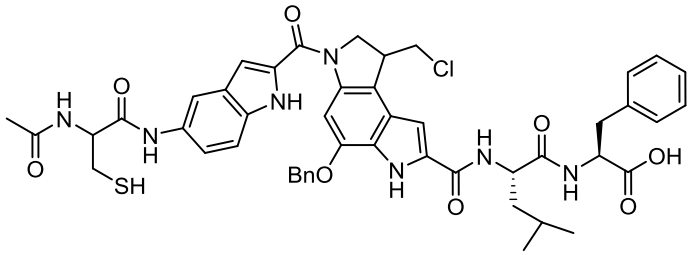

3.5

H-Phe-2ClTrt resin (100 mg, 0.09 mmol, [manufacturer's resin loading 0.9 mmol/g]) was prepared for coupling by swelling in DCM for 30 mins followed by DMF for 30 mins. Fmoc-Leu-OH (152 mg, 0.45 mmol) was dissolved in 2 mL of DMF and treated with HATU (171 mg, 0.45 mmol) and DIPEA (156 μL, 0.9 mmol). After 10 secs the resulting solution was added to the resin and the mixture shaken for 1 h. Subsequently, the resin was washed with DMF (6 x 10 mL) and the coupling repeated. The resin was washed 6 times with DMF (10 mL) before removal of the leucine Fmoc using piperidine in DMF (6 mL 40% 10 mins, 6 mL 20% 5 mins twice). Following Fmoc deprotection the resin was washed with DMF (6 x 10 mL). Next, **2.10** (78 mg, 0.14 mmol) was dissolved in 2 mL of DMF and treated with HATU (51 mg, 0.135 mmol) and DIPEA (47 μL, 0.27 mmol). After 10 secs the resulting solution was added to the resin and the mixture shaken overnight. The resin was subsequently washed with DMF (6 x 10 mL) before the Fmoc group on

the indoline nitrogen of **2.10** removed using piperidine in DMF (6 mL 40% 10 mins, 6 mL 20% 5 mins twice). The resin was then washed again with DMF (6 x 10 mL) before being treated with **2.14** (143 mg, 0.36 mmol) HATU (136 mg, 0.36 mmol) and DIPEA (125 μL, 0.72 mmol). The mixture was shaken for 6 h before the resin was with DMF (6 x 10 mL) and the coupling repeated. The resin was then washed with DMF (6 x 10 mL) before the Fmoc group of **2.14** was removed using piperidine in DMF (6 mL 40% 10 mins, 6 mL 20% 5 mins twice). Upon washing of the resin with DMF (6 x 10 mL) The resin was treated with Fmoc-Cys(mtt)-OH (269 mg, 0.45 mmol), HATU (171 mg, 0.45 mmol) and DIPEA (156 μL, 0.9 mmol) in DMF (2 mL). After 10 seconds, the solution was added to the resin and the mixture shaken for 1 h. Subsequently the resin was washed with DMF (6 x 10 mL) and the Fmoc-Cys(mtt)-OH coupling repeated. The resin was then again washed with DMF (6 x 10 mL) and the cysteine Fmoc group removed using piperidine in DMF (6 mL 40% 10 mins, 6 mL 20% 5 mins twice). Following washing of the resin with DMF (6 x 10 mL), the resin was treated with AcCl (32 μL, 0.45 mmol) and DIPEA (156 μL, 0.9 mmol) in DMF (2 mL). After shaking for 1 h the resin was washed with DMF (6 x 10 mL) followed by DCM (6 x 10 mL). Cleavage of **3.5** from the resin was affected by addition of a solution of 2% TFA, 10% TIPS in DCM (10 mL). After 3 h of shaking the cleavage mixture was filtered. The resin was rinsed with DCM (2 x 3 mL) and the combined filtrates were concentrated to dryness by rotary evaporation under vacuum. Crude **3.5** was then purified using prep-HPLC to give **3.5** (2.1 mg, 42%) as a light brown solid which was analysed using reversed phase HPLC (RT = 18.6 min) and HRMS (ES-) calcd. for $C_{48}H_{50}ClN_7O_8S$ (M - H)-, 918.3034; found, 918.3057.

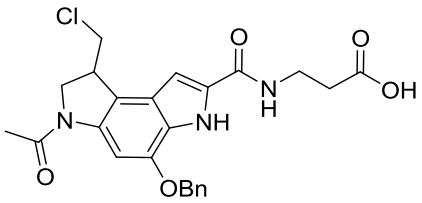

3.3

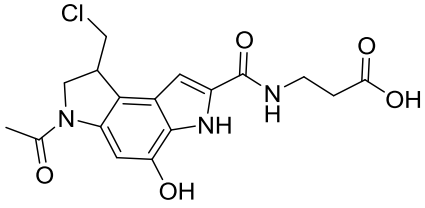

3.4

H-β-Ala-2ClTrt resin (100 mg, 0.075 mmol, [manufacturer's resin loading 0.75 mmol/g]) was prepared for coupling by swelling in DCM for 30 mins

followed by DMF for a further 30 mins. **2.10** (65 mg, 0.11 mmol) was dissolved in 2 mL of DMF and treated with HATU (42 mg, 0.11 mmol) and DIPEA (39 μL, 0.22 mmol). After 10 secs the resulting solution was added to the resin and the mixture shaken overnight. The resin was with DMF (6 x 10 mL) and removal of the Fmoc group from the indoline nitrogen of **2.10** affected with piperidine in DMF (3 mL 40% 10 mins, 3 mL 20% 5 mins twice). Following Fmoc deprotection the resin was washed with DMF (6 x 10 mL) before being treated with anhydrous DMF (2 mL), DIPEA (130 μL, 0.75 mmol), and AcCl (26 μL, 0.375 mmol). After 1 h of shaking the resin was washed with DMF (6 x 10 mL) and the acetylation repeated. Subsequently the resin was washed with DMF (6 x 10 mL) and then DCM (6 x 10 mL). Cleavage was affected by addition of a solution of 1% TFA, 10% TIPS in DCM (10 mL). After 2 h of shaking the cleavage mixture was filtered. The resin was rinsed 3 times with DCM (3 mL) and the combined filtrates were evaporated to dryness under reduced pressure to give crude **3.3**. Crude **3.3** (10 mg, 0.02 mmol) was dissolved in MeOH (1 mL) and the resulting degassed with a gentle stream of N_2 for 30 mins. To this solution was added a slurry of 10% Pd/C (20 mg) in 25% aq. ammonium formate (500 μL) and the resulting suspension stirred under N_2 for 1 h. The reaction mixture was then filtered through a pad of celite before the MeOH was removed under reduced pressure. Crude **3.4** was then purified using preparative HPLC to give **3.4** (3.2 mg, 38%) as a light brown solid. ^{1}H NMR (DMSO-d_6, 400 MHz) δ 12.29 (1H, brs), 11.18 (1H, s), 9.68 (1H, s), 8.46 (1H, brs), 7.66 (1H, s), 7.09 (1H, s), 4.30–4.25 (1H, m), 4.11–4.00 (3H, m), 3.87–3.81 (1H, m), 3.48 (2H, m), 2.53 (2H, obscured by DMSO peak, observed by HSQC and COSY), 2.11 (3H, s). HRMS (ES+) calcd. for $C_{17}H_{19}ClN_3O_5$ (M + H)+, 380.1008; found, 380.1010.

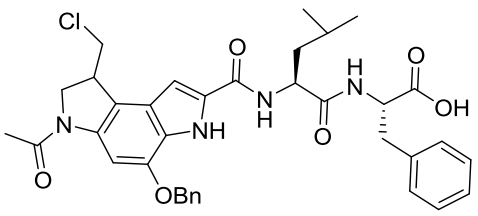

3.12

H-Phe-2ClTrt resin (100 mg, 0.09 mmol, [manufacturer's resin loading 0.9 mmol/g]) was prepared for coupling by swelling in DCM for 30 mins

followed by DMF for 30 mins. Fmoc-Val-OH (152 mg, 0.45 mmol) was dissolved in 2 mL of DMF and treated with HATU (171 mg, 0.45 mmol) and DIPEA (156 μL, 0.90 mmol). After 10 secs the resulting solution was added to the resin and the mixture shaken for 1 h. Subsequently, the resin was washed with DMF (6 x 10 mL) and the coupling repeated. The resin was washed 6 times with DMF (10 mL) before removal of the valine Fmoc using piperidine in DMF (6 mL 40% 10 mins, 6 mL 20% 5 mins twice). Following Fmoc deprotection the resin was washed with DMF (6 x 10 mL). Next, **2.10** (78 mg, 0.14 mmol) was dissolved in 2 mL of DMF and treated with HATU (51 mg, 0.14 mmol) and DIPEA (47 μL, 0.28 mmol). After 10 secs the resulting solution was added to the resin and the mixture shaken overnight. The resin was subsequently washed with DMF (6 x 10 mL) before the Fmoc group on the indoline nitrogen of **2.10** removed using piperidine in DMF (6 mL 40% 10 mins, 6 mL 20% 5 mins twice). Upon washing with DMF (6 x 10 mL) the resin was treated with AcCl (32 μL, 0.45 mmol) and DIPEA (156 μL, 0.9 mmol) in DMF (2 mL). After shaking for 1 h the resin was washed with DMF (6 x 10 mL) followed by DCM (6 x 10 mL). Cleavage of **3.12** from the resin was affected by addition of a solution of 2% TFA, 10% TIPS in DCM (10 mL). After 3 h of shaking the cleavage mixture was filtered. The resin was rinsed with DCM (2 x 3 mL) and the combined filtrates were concentrated to dryness by rotary evaporation under vacuum. **3.12** was then analysed using reversed phase HPLC (RT = 14.8 min) and MALDI mass spectrometry for 3.12 (M + H)+, 659.2730.

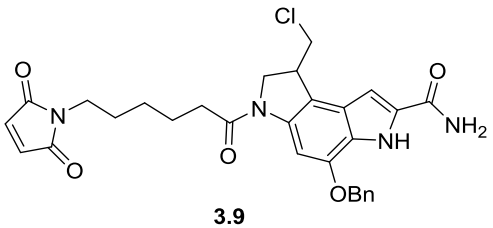

3.9

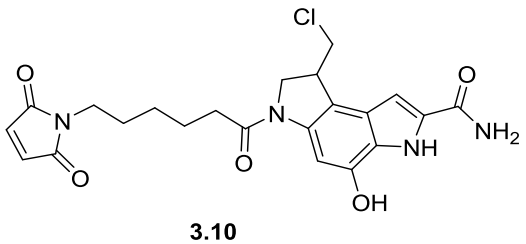

3.10

NovaPEG Rink Amide resin (100 mg, 0.049 mmol [manufacturer's resin loading 0.49 mmol/g]) was prepared for coupling by swelling in DMF for 30 mins. **2.10** (42 mg, 0.0735 mmol) was dissolved in 2 mL of DMF and treated with HATU (27 mg, 0.0735 mmol) and DIPEA (25 μL, 0.147 mmol). After 10 secs the resulting solution was added to the resin and the mixture shaken

overnight. The resin was washed 6 with DMF (6 x 10 mL) and removal of the Fmoc group from the indoline nitrogen of **2.10** affected with piperidine in DMF (3 mL 40% 10 mins, 3 mL 20% 5 mins twice). Following Fmoc deprotection the resin was washed with DMF (6 x 10 mL) before being treated with N-ε-maleimidocaproic acid (51 mg, 0.245 mmol), HATU (93 mg, 0.245 mmol) and DIPEA (85 μL, 0.49 mmol) in DMF. The resin was shaken for 6 h before being washed and the coupling with N-ε-maleimidocaproic acid repeated. Subsequently, the resin was washed with DMF (6 x 10 mL) and then DCM (6 x 10 mL). Cleavage was affected by addition of a solution of 47% TFA, 10% TIPS in DCM (10 mL). After 2 h of shaking, the cleavage mixture was filtered. The resin was rinsed 3 times with DCM (3 mL) and the combined filtrates were concentrated to dryness by rotary evaporation under vacuum to give crude **3.9**. Crude **3.9** (10 mg, 0.018 mmol) was dissolved in MeOH (1 mL) and the resulting degassed with a gentle stream of N_2 for 30 mins. To this solution was added a slurry of 10% Pd/C (20 mg) in 25% aq. ammonium formate (500 μL) and the resulting suspension stirred under N_2 for 1 h. The reaction mixture was then filtered through a pad of celite before the MeOH was removed under reduced pressure. Crude **3.10** was then purified using preparative HPLC to give **3.10** (3.7 mg, 45%) as a light brown solid. ^{1}H NMR (DMSO-d_6, 400 MHz) δ 11.09 (1H, s), 7.72 (1H, s), 7.39 (2H, brs), 7.12 (2H, s), 6.99 (1H, d, J = 2.1), 4.30–4.25 (1H, m), 4.11–4.00 (3H, m), 3.87–3.81 (1H, m), 3.37 (2H, t, J = 6.8), 2.17 (2H, t, J = 7.2), 1.52-1.43 (4H, m), 1.16-1.24 (2H, m). HRMS (ES-) calcd. for $C_{22}H_{23}ClN_4O_5$ (M - H)-, 457.1279; found, 457.1281.

3.5.3 Solution Phase Chemistry

NHS Esters formations

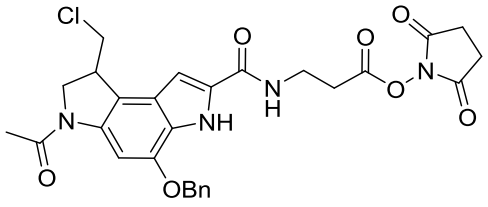

3.3-NHS

3.3 (2 mg, 0.004 mmol) was dissolved in anhydrous DMF (200 μL) and treated with DCC (1 mg, 0.005 mmol) and NHS (0.7 mg, 0.006 mmol). The resulting reaction was allowed to stir overnight at room temperature. Subsequently, the precipitated DCU was removed from the mixture by centrifugation at 14,000 rpm for 10 mins. The supernatant containing **3.3-NHS** was then evaporated to dryness under reduced pressure and washed with diethyl ether (3 x 5 mL). The presence of the NHS ester was then confirmed via reaction with 3-(dimethylamino)-1-propylamine and subsequent HPLC and Mass spectrometry.

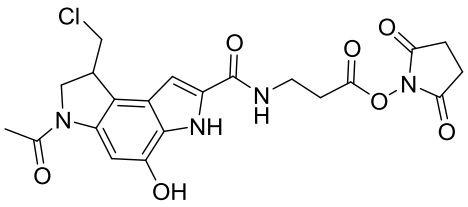

3.4-NHS

3.4 (2 mg, 0.005 mmol) was dissolved in anhydrous DMF (200 μL) and treated with DCC (1.3 mg, 0.006 mmol) and NHS (0.8 mg, 0.007 mmol). The resulting reaction was allowed to stir overnight at room temperature. Subsequently, the precipitated DCU was removed from the mixture by centrifugation at 14,000 rpm for 10 mins. The supernatant containing crude **3.4-NHS** was then evaporated to dryness under reduced pressure and washed with diethyl ether (3 x 5 mL). The presence of the NHS ester was then confirmed via reaction with 3-(dimethylamino)-1-propylamine and subsequent HPLC and Mass spectrometry.

NHS Presence Confirmation Using 3-(dimethylamino)-1-propylamine Coupling

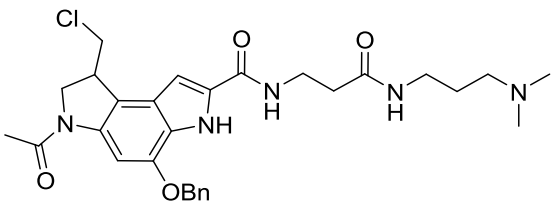

3.3-Amino tail

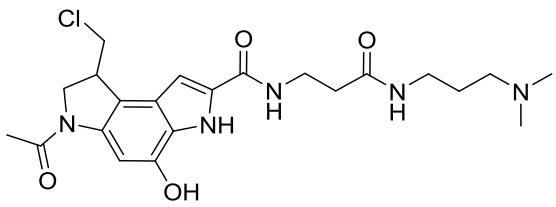

3.4-Amino tail

Presence of the NHS on **3.3-NHS** and **3.4-NHS** was confirmed via reaction with 3-(dimethylamino)-1-propylamine and subsequent analysis via MALDI mass spectrometry and analytical HPLC. Briefly, crude **3.3-NHS/3.4-NHS**

(2 mg) was dissolved in anhydrous DMF (200 µL) and treated with 3-(dimethylamino)-1-propylamine (1 equiv.). The reaction was left to stir for 1 h at room temperature. Subsequently, the DMF was removed under reduced pressure and the resulting solid dissolved in MeOH (1 mL) and analysed via analytical HPLC and MALDI mass spectrometry. **3.3-Amino tail** RT = 15.2 min, MALDI for **3.3-Amino tail** (M - H)-, 552.35. **3.4-Amino tail** RT = 13.8 min, MALDI for **3.4-Amino tail** (M - H)-, 463.32.

Off Resin C-terminus Couplings

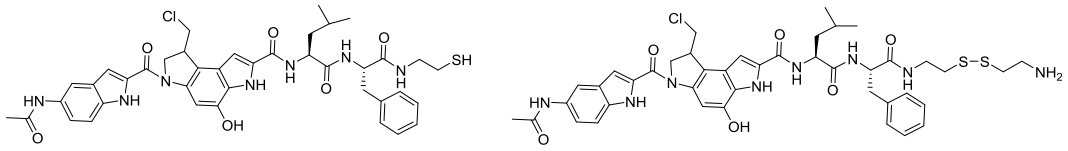

3.8

3.7 (4 mg, 0.007 mmol) was dissolved in DMF (200 µL) and treated with HATU (2.6 mg, 0.007 mmol) and DIPEA (2 µL, 0.014 mmol). After stirring for 10 secs, cysteamine (1 mg, 0.014 mmol) was added and the resulting solution left to stir for 2 h at room temperature. Subsequently, the reaction mixture was diluted with MeOH (5 mL) and subjected directly to reverse phase Prep-HPLC where **3.8** (2.2 mg, 37%) was isolated as a mixture of disulphide and non-disulfide products as analysed via analytical HPLC (RT = 16.8 min and 17.1 min) and MALDI mass spectrometry for **3.8** (M + Na)+, 808.35.

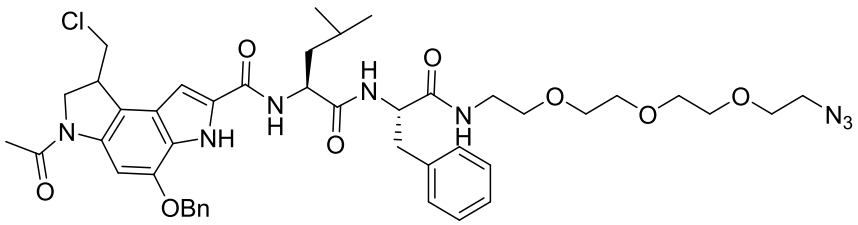

3.13

3.12 (10 mg, 0.015 mmol) was dissolved in DMF (300 µL) and treated with HATU (6 mg, 0.015 mmol) and DIPEA (5 µL, 0.03 mmol). After stirring for 10 secs, 11-Azido-3,6,9-trioxaundecan-1-amine (**3.11**) (6 µL, 0.03 mmol) was added and the resulting solution left to stir for 2 h at room temperature. Subsequently, the reaction mixture was diluted with MeOH (5 mL) and

subjected directly to reverse phase Prep-HPLC where **3.13** (5.1 mg, 39%) was isolated as a light brown solid. **3.13** was subsequently analysed using reverse phase HPLC (RT = 13.7 min) and MALDI mass spectrometry for **3.13** (M + Na)+, 881.2789.

3.5.4 Protein bioconjugations

Jacalin-NHS Ester Conjugations;

The following experimental relates to the conjugation of jacalin to the following NHS esters; succinimidyl 4-(N-maleimidomethyl) cyclohexane-1-carboxylate (SMCC), dibenzocyclooctyne-*N*-hydroxysuccinimidyl ester (DBCO), propargyl-*N*-hydroxysuccinimidyl ester, (+)-biotin N-hydroxysuccinimide ester, 3.3-NHS and 3.4-NHS.

Jacalin (2 mg/mL) was reconstituted in 10 mM HEPES buffered saline (pH 7.4, 150 mM NaCl, 100 μM $CaCl_2$) and treated with a solution of the respective NHS-ester (1 mg/mL, 20 equiv.) in DMSO. The resulting solution was left to react for 1 h at room temperature and then for a further 1 h at 4 °C. Any precipitate was removed from the solution via centrifugation at 1,000 rpm for 5 mins at 4 °C. The resulting supernatant was then transferred to equilibrated Zeba™ spin desalting columns (7K MWCO, 0.5 mL) and centrifuged at 1500 xg for 2 min at 4 °C. For MALDI mass spectrometry, the centrifuged pellet was resuspended in ACN/H_2O and the purified supernatant analysed directly from water. Resulting conjugates were stored frozen at -20 °C.

Coupling of Peptide 3.5 to Jac-SMCC

To a solution of Jac-SMCC (1 mL, 2mg/mL) in 10 mM HEPES buffered saline (pH 7.4, 150 mM NaCl, 100 μM $CaCl_2$) was added peptide **3.5** (0.5 mg, 0.54 μmol) in DMSO (100 μL). The resulting reaction was incubated for 2 h at 4 °C. Subsequently, the formed precipitate was removed from the solution via centrifugation (3000 xg, 3 min, 4 °C). Excess **3.5** was then removed from the supernatant through spinning the mixture through an equilibrated Zeba™ spin desalting columns (7K MWCO, 0.5 mL) at 1500 xg for 2 min at 4 °C. The precipitated pellet was then resuspended in 50% ACN:H_2O and analysed via LCMS along with the purified supernatant.

Functionalisation of Jacalin with 2-Iminothiolane

Jacalin (1 mL, 2mg/mL) was reconstituted in 10 mM HEPES buffered saline (pH 7.4, 150 mM NaCl, 100 μM $CaCl_2$, 5 mM EDTA) and treated with 2-Iminothiolane (22 μL, 14 mM) in water. The resulting solution was incubated for 1 h at room temperature before being transferred to Zeba™ spin desalting columns (7K MWCO, 0.5 mL) and centrifuged at 1500 xg for 2 min at 4 °C. The thiol functionalised jacalin was subjected to Ellmans reagent assay conditions to confirm the presence of the thiol on the protein. The thiol functionalised jacalin was stored frozen at -20 °C until required for reaction.

Conjugation of 3.2 to Bovine Serum Albumin (BSA)

Bovine serum albumin (3 mg) was reconstituted in MES buffer (0.1 M, pH 5). To this was added **3.2** (0.8 mg, 0.001 mmol) and EDC (25 μL, 10 mg/mL) and the resulting mixture incubated at room temperature for 90 min. Subsequently, the reaction mixture was transferred to an equilibrated Zeba™ spin desalting columns (7K MWCO, 0.5 mL) and centrifuged at 1500 xg for 2 min at 4 °C. The resulting solution was then analysed using MALDI mass spectrometry.

Chapter 4 –The Design and Synthesis of Peptide-duocarmycin Conjugates for Targeted Delivery to the Thomsen-Friedenreich Antigen

4.1 Introduction

4.1.1 Peptides as Targeting Molecules.

Whilst ADCs have dominated the targeted therapeutic landscape over previous years, this strategy does not come without significant drawbacks. For example, the synthetic routes to these agents are very difficult, increasingly so when the need for homogenous product mixtures has been identified.[34] Being able to create ADCs with constant and repeatable drug-antibody ratios (DARs) has been identified as non-trivial on numerous occasions.[34] This lack of synthetic accessibility has therefore led to many setbacks within a clinical trial setting for ADCs. In addition to this, the development or discovery of antibodies to target particular antigens is also not a trivial process and difficulties within this area have been a continuous hindrance within the area of ADCs. Finally, for ADCs to show significant efficacy in solid tumour models, it has been recognised that they must be able to successfully penetrate the tumour.[42] Due to the large size of the antibody employed within ADCs, this has been shown to be difficult and, as a result, poor efficacies within these models are not uncommon.

It is these disadvantages of ADCs that have expedited the search for alternative strategies to achieve the targeted delivery of cytotoxic agents to cancer cells. One such strategy is the use of peptides rather than antibodies. The rationale behind this approach is that due to the smaller size of peptides, the penetration into solid tumours will be improved, resulting in enhanced efficacies. This improved penetration has been established for numerous targeting peptides.[193] In addition to this, the design, synthesis and characterisation of peptides used for targeting purposes is much easier than for antibodies. Synthetic methodologies to generate peptides are well established and automated systems have been developed. In relation to this, the coupling of drug molecules to peptides also allows for complete control over the drug ratio within the resulting conjugates and their full structural characterisation. This in turn allows for more homogenous product mixtures to be made in comparison to ADC systems. Not only this, but due to their smaller size, the purification of these systems is more accessible with preparative HPLC systems being commonly utilised. Finally, and of

particular importance for the development of peptides for therapeutic purposes, comes the advantage that a greater ease of modification to peptides in relation to antibodies can be obtained. These modifications can be to add functionality for conjugation purposes or for imparting improved physiochemical properties into the peptide sequence. For example, the incorporation of specific amino acids into a targeting sequence can be utilised to improve stability or water solubility.[194] These advantages of peptide based systems has meant that research into their use for therapeutic purposes has increased significantly over recent years and this has led to over 60 of these systems now being approved by the FDA with many more in clinical development.[195]

4.1.2 Peptide-Drug Conjugates

As alluded to in the previous section, the use of peptides for therapeutic purposes and hence their potential use in peptide-drug conjugates (PDCs) could hold many advantages. PDCs combine the cytotoxic activity of a drug warhead with the targeting ability of a specific peptide sequence.[194] As in ADC systems, linker technologies between the cytotoxic drug and the peptide can be employed to allow for efficient release of the warhead once at the desired site of action whilst ensuring stability during circulation. Additionally, the individual components of a PDC must hold certain properties in order for the overall system to achieve success within a clinical setting. These are summarised briefly in Figure 4.1.

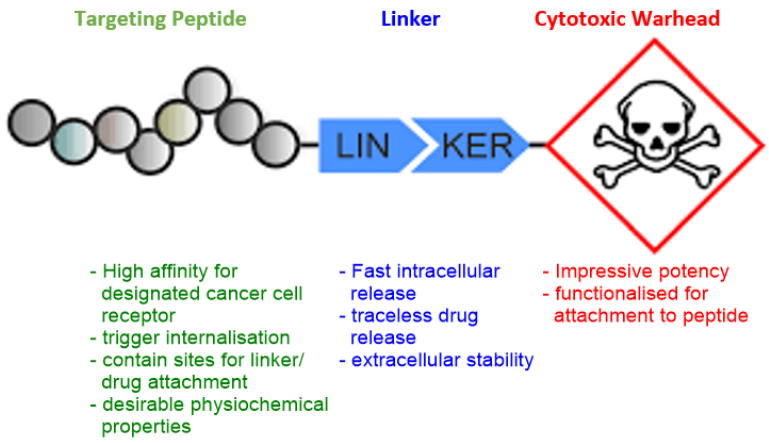

Figure 4.1: Schematic representation of a peptide-drug conjugate and descriptions of ideal characteristics of each individual component.

Taking the above into consideration, a number of PDCs have been developed. One example involves a doxorubicin payload and was designed by Cui and co-workers.[196] In this work, various numbers of doxorubicin-based units were coupled to a cell penetrating Tat peptide via a cathepsin B cleavable linker. The group showed that the number of doxorubicin units utilised in the peptide had an effect on the rate of drug release from the PDC and that a balance of these two factors was vital. In their system, two doxorubicin units was found to give the most desirable results with this PDC showing favourable accumulation and drug release.

In another study, Mezo and co-workers utilised peptides containing the asparagine-glycine-arginine (NGR) motif that is recognised by CD13 receptor isoforms that are selectively overexpressed in tumour neovasculature.[197] A daunomycin warhead was conjugated to these peptides in a variety of different orientations and the resulting conjugates tested for their biological activity. The results of the study showed low micromolar activity in some of the structural analogues and a lack of activity in others. This demonstrates the importance of the drug positioning within a peptide sequence. Improved activity of the PDCs within CD13 positive cell lines in relation to CD13 negative cell lines was also obtained demonstrating the targeting ability of the conjugates synthesised in this study.

PDCs to combat prostate cancer have also been established. Cheng and co-workers synthesised a PDC based on a highly potent phosphoinositide 3-kinase β (PI3Kβ) inhibitor (TGX-D1) which has previously shown cytotoxicity in prostate cancer cell lines (Figure 4.2).[198]

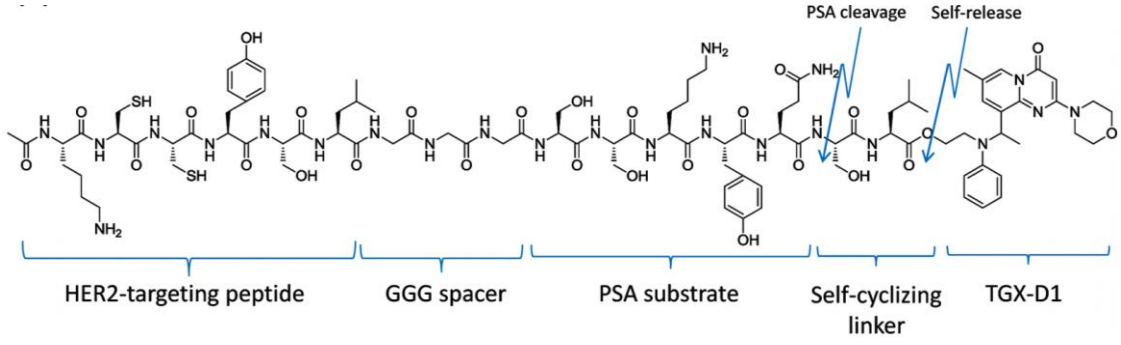

Figure 4.2: chemical structure of the PDC synthesised by Cheng and co-workers based on a PI3Kβ inhibitor.[198]

In order to improve the poor solubility and lack of specificity, which limit its therapeutic applications, the group conjugated this warhead to a HER2 targeting peptide via a cleavable linker. The results from the study showed significantly higher cellular uptake of the PDC in prostate cancer cells compared to the parent drug. In addition, both the PDC and its cleaved products demonstrated comparable cytotoxic activity to the parent drug.

These studies highlight the potential of PDCs to help improve upon some of the drawbacks of current cytotoxic agents. Therefore, it is possible that the use of such a system implementing a duocarmycin unit could potentially allow for an improved therapeutic index of this cytotoxic warhead. In addition to this, with the more favourable synthetic accessibility of PDCs, it is possible that a number of the issues addressed within Chapter 3 of this thesis could be overcome.

4.2 Aims of the Research in this Chapter

The aim of the research presented in this chapter was to investigate the design and synthesis of a duocarmycin based peptide-drug conjugate. The synthesis of this conjugate could aid in overcoming many of the issues faced with the attachment of duocarmycin to jacalin as presented in Chapter 3 of this thesis. In addition to this, it was expected that the advantages brought about by peptide based therapeutics would help realise the potential of duocarmycin as a possible future clinical candidate.

The chapter will begin by addressing the synthesis of a number of peptide conjugates which incorporate a T-antigen binding peptide sequence and a duocarmycin warhead. The incorporation of a cleavable sequence into the conjugate is also discussed.

Following on from this, the chapter provides a comparison between the biological activities of these peptide conjugates including analysis of their T-antigen binding properties and also their cytotoxicity within T-antigen expressing cell lines.

4.3 Results and Discussion

4.3.1 Design and Synthesis of Duocarmycin Based PDCs.

4.3.1.1 T-antigen Binding Peptides

A series of peptides have been shown to specifically bind the Thomsen-Friedenreich antigen.[199] Quinn and co-workers established these peptides from a 15 amino acid random peptide bacteriophage display library and characterised them for their binding affinities and specificities. The group found that synthetic peptides identified from the bacteriophage display library had reasonable affinities (K_d ~ 1 μM) and specificities for human tumour cells that present the T-antigen on their surface. Sequence analysis of these peptides revealed that many of them shared homology with sugar recognition sites in several carbohydrate-binding proteins. A comparison of the affinity selected sequences from the libraries also yielded a common motif (W-Y-A-W/F-S-P) rich in aromatic amino acids.[200] The group also demonstrated the importance of tyrosine within these sequences after an iodination of this residue was shown to greatly reduce the affinity of the peptides to the T-antigen. The ability and significance of the peptides disclosed by Quinn and co-workers is evidenced by their ability to inhibit melanoma cell aggregation *in vitro,* which has previously been shown to have a direct relationship to T-antigen expression.[159] Additionally, the ability of these peptides to compete with peanut lectin for binding to the T-antigen displayed on the surface of MDA-MB-435 breast carcinoma cells in situ was observed.[199]

One of the major attractions to the investigation of a PDC based system as part of this work was the fact that the duocarmycin unit (Fmoc-DSA-OH or **2.10** from Chapter 2) was already functionalised for solid phase peptide synthesis. Thus, the synthesis of conjugates could proceed without any functional group modifications to the duocarmycin unit for its coupling to the peptide. In addition to this, it is possible that with the Fmoc-DSA-OH unit in hand, numerous additions of this warhead could be incorporated into the peptide sequence in order to achieve optimised cytotoxic activity. The combination of these two factors indicated that the synthesis of a conjugate should be attempted.

4.3.1.2 Synthesis of PDC 4.3

The literature by Quinn and co-workers disclosed a peptide (**4.1**) capable of binding the T antigen and competing with the T-antigen specific peanut lectin (Figure 4.3).[199, 200] Also of note was the fact that this peptide had been used in consequent studies by the group to further investigate the roles of the T-antigen within cancer.[159] It was proposed therefore that this peptide would provide a good starting point for the synthesis of a PDC. As an initial strategy, it was proposed that PDC **4.2** (Figure 4.3) could be synthesised.

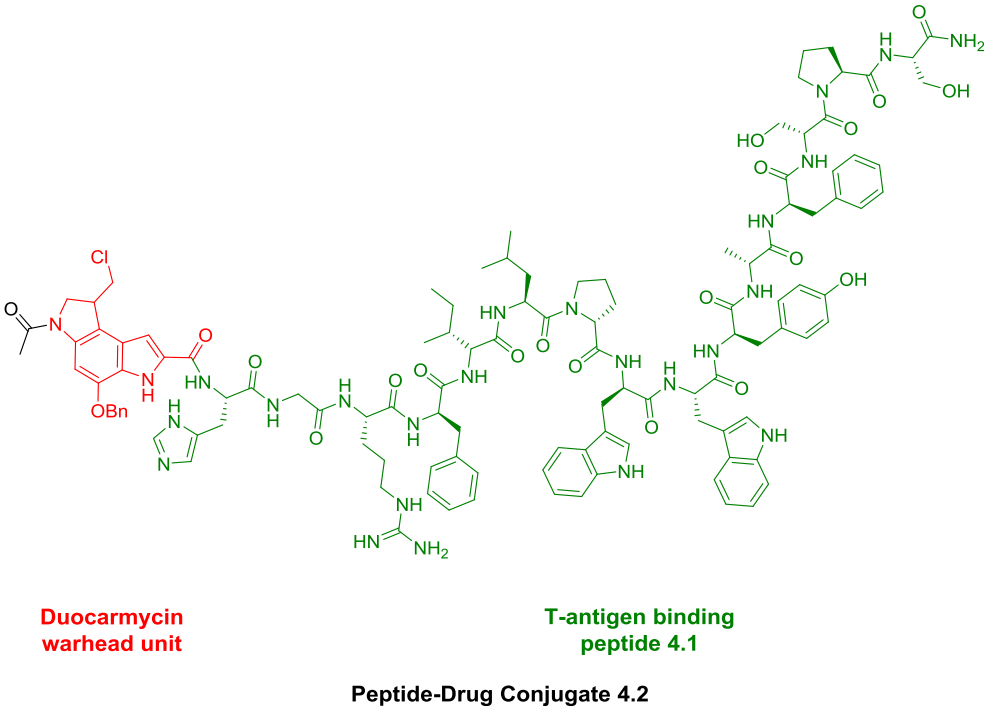

Figure 4.3: chemical structure of PDC **4.2**. T-antigen binding peptide **4.1** (green) is coupled to the DSA based warhead (red).

For the ease of synthesis of this PDC, it was proposed that a single duocarmycin alkylating subunit could be coupled directly to the peptide without a linker. It was proposed that an analogue of this PDC containing a cleavable linker between the peptide and warhead could be synthesised for comparative purposes and this will be discussed later in this chapter. The synthesis of **4.2** started with automated SPPS of peptide **4.1**. This was completed using a rink amide resin and HOBt/HBTU couplings. Following on from the successful formation of the 15 amino acid sequence, as deciphered by a test cleavage and mass analysis, the duocarmycin unit was coupled manually using HATU/DIPEA, and the N-terminus capped with an

acetyl group. After cleavage from the resin, analytical HPLC indicated the presence of one major product peak indicating a clean synthesis (Figure 4.4). MALDI mass spectrometry of crude **4.2** also suggested successful synthesis of the PDC with the desired mass being found.

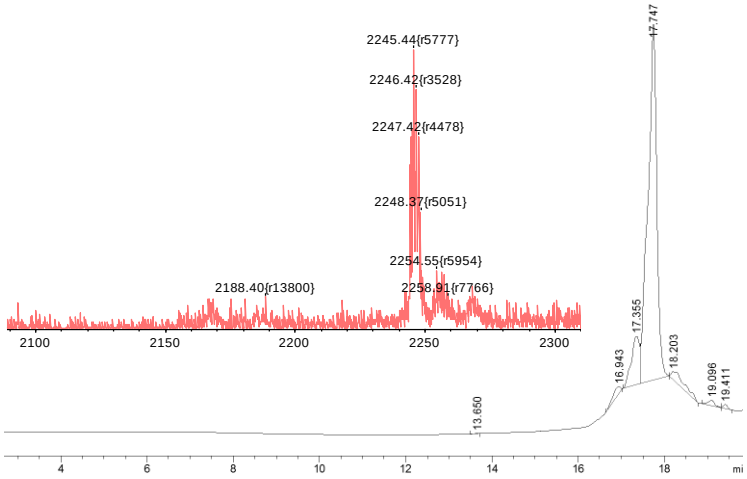

Figure 4.4: analytical HPLC and MALDI of the crude PDC **4.2** isolated directly from the resin. Expected mass 2244.98 $gmol^{-1}$. HPLC - Agilent Eclipse XDB-C18 column, 4.8 x 150 mm, 5 µm. Solvent A: [Water and 0.05 % TFA], Solvent B: [MeOHand 0.05 % TFA]. Gradient: 0% [B] to 95 % [B], from 0 min to 15 mins, 95 % [B] to 0 % [B] from 15to 20 mins. Monitored UV 254 nm. Flow rate 1 mL/min. Column temperature 40 ^{o}C.

In order to undertake the biological studies and evaluate the cytotoxicity of PDC **4.2**, it was necessary to achieve the benzyl deprotection of the duocarmycin warhead within the sequence to give PDC **4.3** (Scheme 4.1). Initial attempts to achieve this manipulation were made using transfer hydrogenation reaction involving Pd/C and ammonium formate as introduced in Chapter 2, Section 2.3.4.

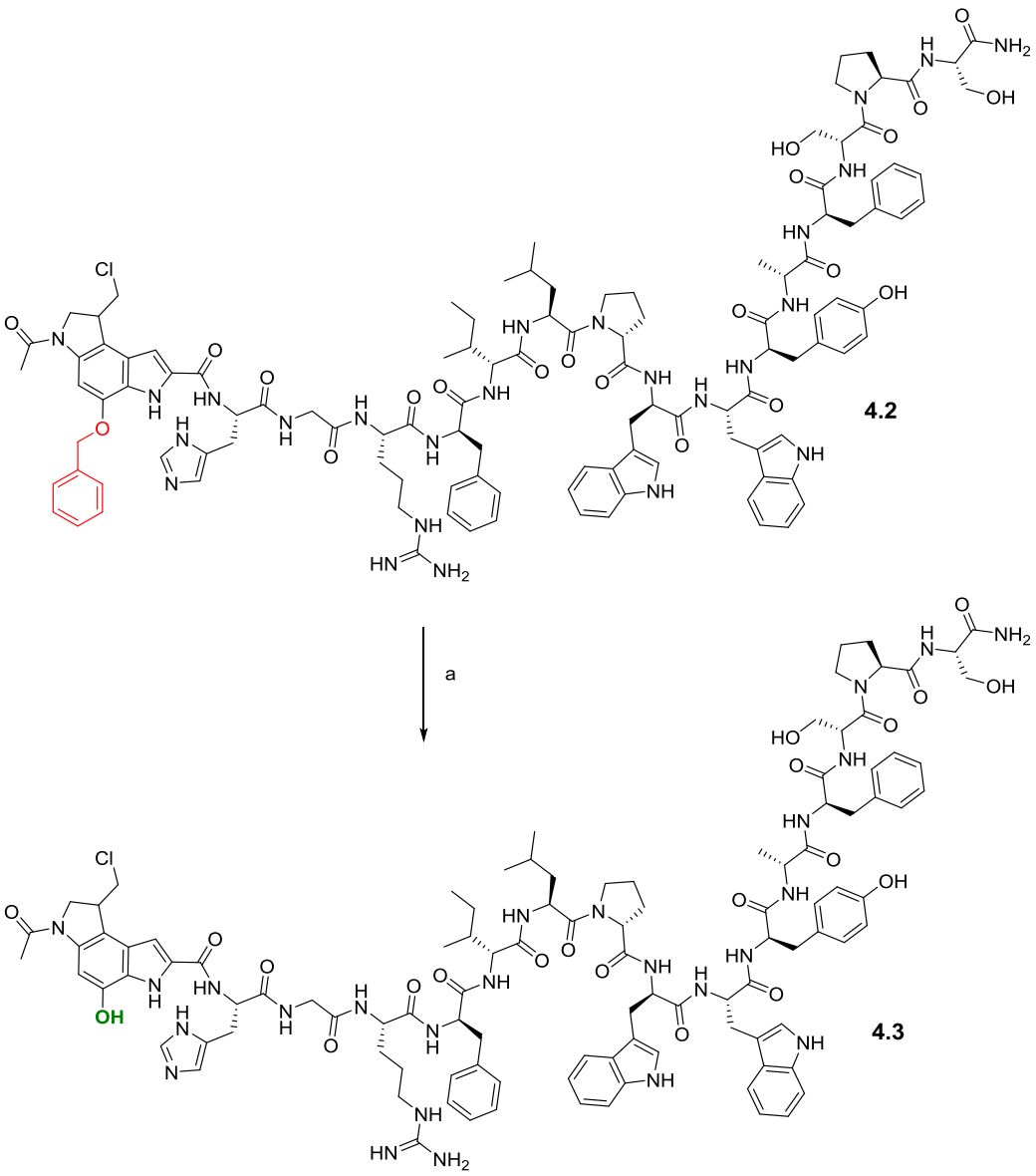

Scheme 4.1: benzyl deprotection of PDC **4.2**. a: 10% Pd/C, 25% Aq. ammonium formate, MeOH, 1 h, rt, 32%.

After the specified time, the reaction was analysed by HPLC and MALDI mass spectrometry. The HPLC of the reaction mixture showed the presence of new peaks but also clear retention of the starting material peak. Similarly, MALDI mass spectrometry indicated retention of the starting material yet no evidence of **4.3**. After prolonging the reaction times and adding further equivalents of Pd/C and ammonium formate, the required manipulation was still not obtained. It was proposed that under these reaction conditions, the possible positions for the Pd to insert itself/bind are extensive and hence insertion at the required benzylic position may not proceed as the most likely.

As a further attempt to obtain PDC **4.3**, the BBr_3 conditions introduced during Chapter 2, Section 2.3.4. were employed. Compound **4.2** was suspended in dichloromethane (DCM) and treated with a 1 M solution of BBr_3 at -78 °C. After the 1 h reaction time, the mixture was analysed via HPLC which showed the presence of a new peak and also evidence of existing starting material. For this reason, the reaction time was extended for a further hour and the solution allowed to warm to room temperature. Subsequent to this, analytical HPLC was again used to analyse the reaction progress which this time showed complete consumption of the starting material and evidence of a new major peak at an earlier retention time. This was promising since such a shift in retention time is expected for a benzyl deprotection reaction. Following on from this, the product was purified using preparative HPLC and analysed through MALDI mass spectrometry. Evident from the MALDI spectrum was a clear peak representing the mass of **4.3**. Post purification analytical HPLC also demonstrated a purity of >90% for the PDC (Figure 4.5). These results meant that investigations into the cytotoxicity of the PDC within cell lines could be made.

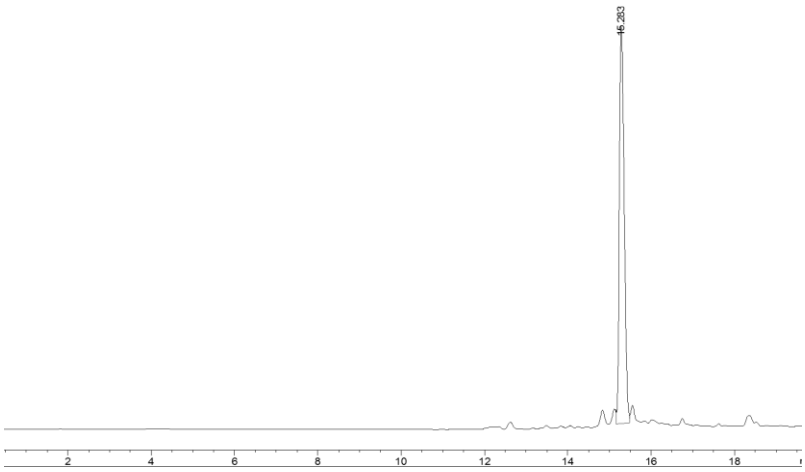

Figure 4.5: analytical HPLC trace of **4.3** post purification using preparative HPLC. Agilent Eclipse XDB-C18 column, 4.8 x 150 mm, 5 μm. Solvent A: [Water and 0.05 % TFA], Solvent B: [MeOHand 0.05 % TFA]. Gradient: 0% [B] to 95 % [B], from 0 min to 15 mins, 95 % [B] to 0 % [B] from 15 to 20 mins. Monitored UV 214 nm. Flow rate 1 mL/min. Column temperature 40 °C.

A clear advantage for the synthesis of duocarmycin/peptide hybrids on solid phase would be the ability to remove the benzyl group on the resin so that on cleavage, the active compound is obtained, as noted in Chapter 2, Section

2.3.6. For this reaction, the resin containing PDC **4.2** was suspended in DCM and treated with a 1 M solution of BBr_3 at -78 °C. The reaction was left for 2 h and allowed to warm to room temperature. The peptide was cleaved from the resin and the resulting product analysed via analytical HPLC (Figure 4.6 - blue) and MALDI mass spectrometry. Evident from this analysis was the presence of **4.3**.

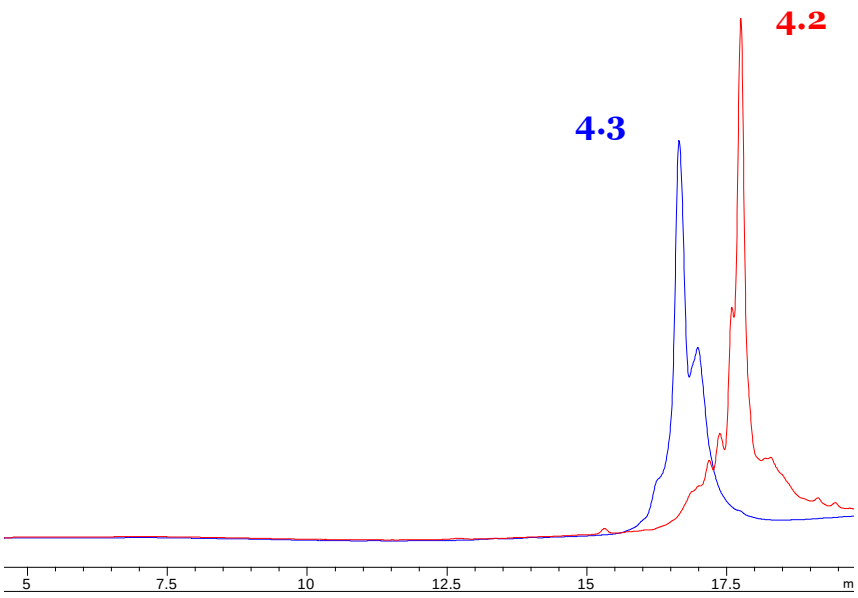

Figure 4.6: HPLC spectrum of two crude samples taken from the same batch of resin-peptide construct. Treatment of the resin with cleavage cocktail gives **4.2** in red, whilst resin treatment with BBr_3 and subsequently cleavage cocktail, gives **4.3** in blue. Agilent Eclipse XDB-C18 column, 4.8 x 150 mm, 5 µm. Solvent A: [Water and 0.05 % TFA], Solvent B: [MeOHand 0.05 % TFA]. Gradient: 0% [B] to 95 % [B], from 0 min to 15 mins, 95 % [B] to 0 % [B] from 15 to 20 mins. Monitored UV 254 nm. Flow rate 1 mL/min. Column temperature 40 °C.

Notable was the synthetic simplicity of the on resin benzyl deprotection strategy, in comparison to the post cleavage benzyl deprotection route. This also reduced handling of the cytotoxic **4.3** as simple cleavage and removal of the solvent under reduced pressure yielded the active PDC for biological evaluation.

4.3.1.3 Introduction of a Cleavable Sequence into PDC 4.3

As part of this work a comparison between PDCs which include a cleavable linkage and those which do not was proposed. Previously within this thesis (see Chapter 3), a Phe-Leu peptide sequence has been used that has shown to act as a cleavable linker.[177] More recently however, the use of a citrulline-

valine (Cit-Val) cleavable sequence has become far more common and has shown desirable stability-lability profiles for use as a linker in targeted delivery systems.[201] This includes within duocarmycin based systems, and for this reason the incorporation of this unit within a PDC system was explored.[90] The Cit-Val unit is often accompanied by a benzyl group spacer to allow for efficient cleavage via a cathepsin B enzyme. This cleavage occurs between the benzyl group spacer and the citrulline residue. With cathepsin B also being overexpressed within cancer cells, this cleavable sequence further presents itself as an ideal linker strategy in targeted delivery systems.[202] In order to test the suitability of the Cit-Val sequence in the duocarmycin based PDC system, the synthesis of a short peptide (**4.4** - Figure 4.7) was proposed which incorporates the duocarmycin unit, a p-aminobenzoic acid spacer and a Cit-Val sequence. A lysine residue at the C-terminus was also included in order to add a possible conjugation point for other systems synthesised in this body of work (see Chapter 5).

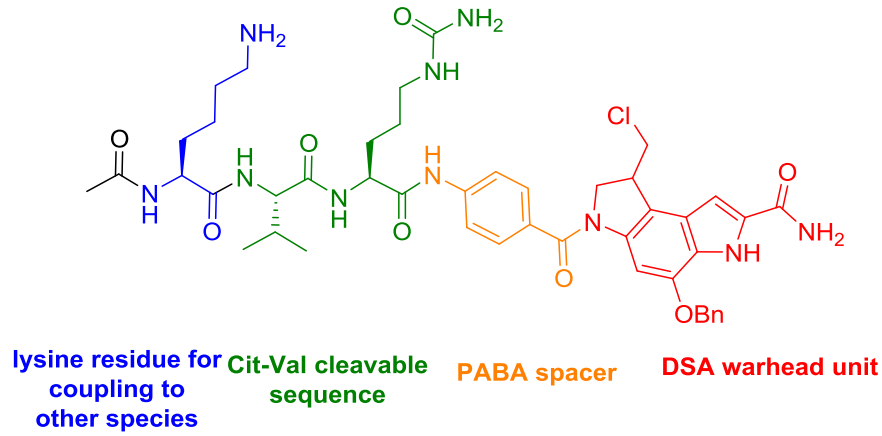

Peptide 4.4

Figure 4.7: chemical structure of peptide **4.4**. In red is the DSA unit, in orange is the PABA spacer connected to the Cit-Val cleavable linker in green. In blue is a lysine residue used elsewhere in this thesis for attachment to other moieties.

Peptide **4.4** was synthesised on rink amide which was initially loaded with the Fmoc-DSA-OH unit (**2.10**) synthesised in Chapter 2. This placed the unit at the C-terminus to allow the PABA unit to be introduced before addition of the citrulline, valine and lysine, finally capping the N-terminus with an acetyl group. Cleavage of **4.4** from the resin was achieved using 47% TFA, 10%

TIPS in DCM. Post cleavage HPLC of the crude material demonstrated one sharp major peak and MALDI mass spectrometry analysis showed the desired mass of **4.4**. This indicated that the PABA-Cit-Val linker was applicable to the synthetic conditions used with the duocarmycin unit.

Subsequent to this it was necessary to remove the benzyl group from **4.4** to give **4.5** (Scheme 4.2). This would yield an active species that could be analysed biologically to see what cytotoxicity could be obtained. The benzyl deprotection of **4.4** was shown to proceed smoothly under the standard transfer hydrogenation conditions. The resulting peptide **4.5** was purified using preparative HPLC to give a pure compound ready to be tested (Figure 4.8).

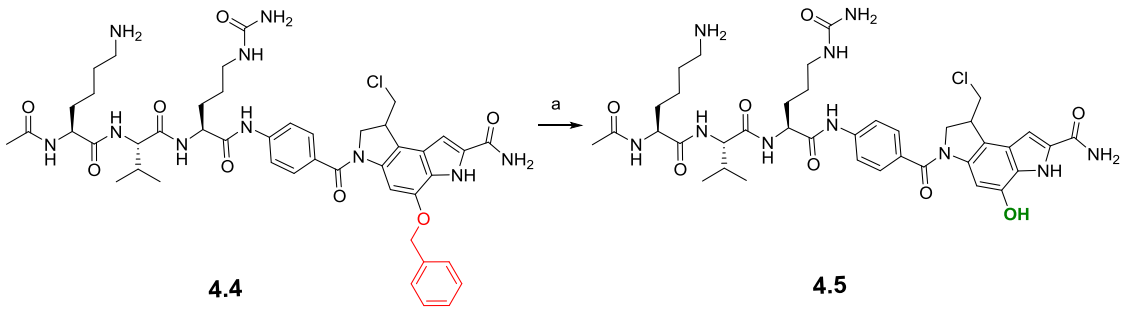

Scheme 4.2: benzyl deprotection of peptide **4.4** to give **4.5**. a: 10% Pd/C, 25% aq. Ammonium formate, MeOH, 1 h, rt.

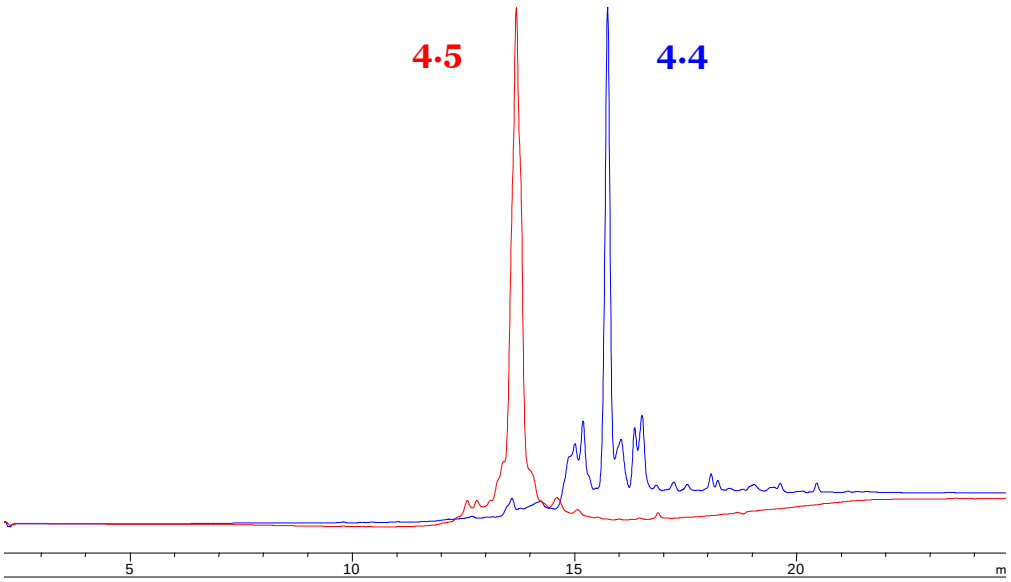

Figure 4.8: HPLC traces of crude **4.4** (in blue) and pure **4.5** (in red). Agilent Eclipse XDB-C18 column, 4.8 x 150 mm, 5 µm. Solvent A: [Water and 0.05 % TFA], Solvent B: [MeOHand

0.05 % TFA]. Gradient: 0% [B] to 95 % [B], from 0 min to 15 mins, 95 % [B] to 0 % [B] from 15 to 20 mins. Monitored UV 254 nm. Flow rate 1 mL/min. Column temperature 40 °C.

As a control, the cathepsin B cleavage product of **4.5** was also synthesised. This would give an indication of the activity expected when this DSA-PABA-Cit-Val unit is utilised within our PDC systems and subjected to cellular conditions. Compound **4.6** (Scheme 4.3) was synthesised following conditions utilised for the synthesis of **4.4**. Following cleavage from the resin, **4.6** was benzyl deprotected, also using transfer hydrogenation conditions to give **4.7** (Scheme 4.3).

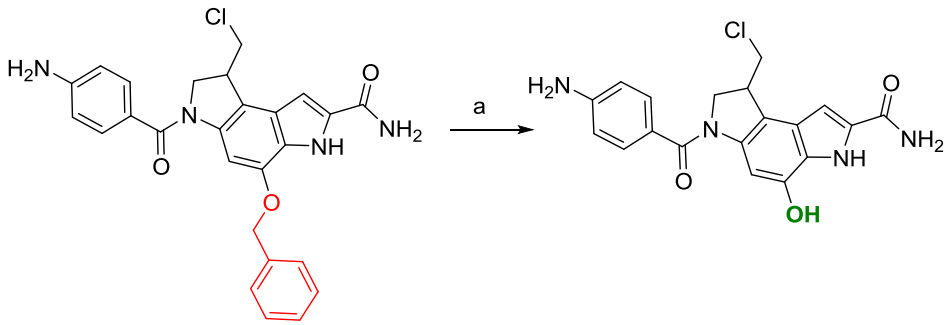

4.6 **4.7**

Scheme 4.3: benzyl deprotection of **4.6** to give **4.7**. a: 10% Pd/C, 25% aq. Ammonium formate, MeOH, 1 h, rt, 38%.

The desired benzyl deprotection was confirmed using high resolution mass spectrometry and also ^{1}H NMR. The smaller molecule size of **4.7** allowed for easy analysis via ^{1}H NMR where removal of the 5 aromatic protons and also the benzylic CH_2 was evident.

In order to further investigate the potential of this duocarmycin-cleavable sequence combination, a cathepsin B cleavage assay was completed following a procedure reported by LaBelle and co-workers.[203] This would help to confirm that the sequence in **4.5** is indeed cleaved by the enzyme to release compound **4.7**. For this assay, a stock solution of **4.5** was dissolved in DMSO and diluted into a cathepsin B activation buffer (0.25 μM HEPES in PBS (pH 5) with 0.25 μM DTT) which mimics the environment of the lysosome where the cathepsin B is found. To this solution, cathepsin B from human liver was added before the reaction was incubated at 37 °C for 72 h. After this time course, the reaction was diluted with methanol to precipitate the protein

which was then removed. The resulting mixture was then analysed via analytical HPLC and MALDI mass spectrometry. The HPLC trace indicated complete consumption of **4.5**. The new peak formed had a shorter retention time but only by a marginal time difference. It was discovered however, that the retention times of **4.5** and **4.7** are very similar and so this small retention time difference was expected. MALDI mass spectrometry also suggested complete consumption of **4.5** with no peak for this mass being observed. A peak suggesting the formation of **4.7** was however identified providing further evidence of successful cleavage of **4.5** by the cathepsin B.

For a comparison between PDC **4.3**, which does not contain a cleavable linker, and a PDC which does contain a cleavable linker, the synthesis of PDC **4.8** was proposed (Figure 4.9). This PDC makes use of the cleavable sequence found in **4.5**. With the DSA unit now on the C-terminus and the Cit-Val cleavable sequence being towards the N-terminus, a shift in the positioning of the targeting peptide **4.1** was required in the design of the PDC. This is to ensure that that cleavable sequence acts to separate the duocarmycin unit from the targeting peptide moiety.

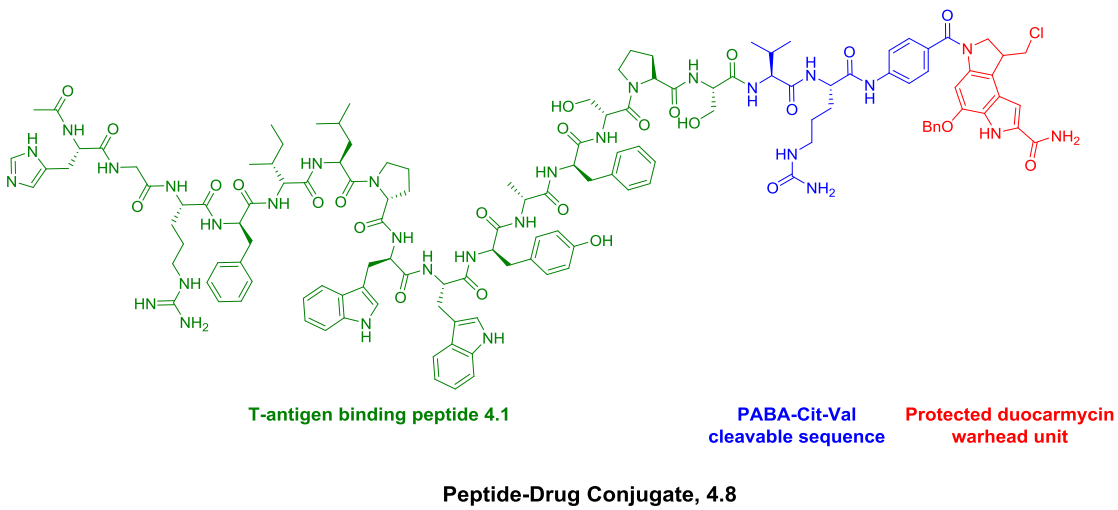

Figure 4.9: chemical structure of PDC **4.8**. In red is the DSA based warhead unit, in blue is the PABA-Cit-Val cleavable sequence obtained from peptides **4.4** and **4.5** and in green is the T antigen binding peptide, **4.1**.

The synthesis of PDC **4.8** began with the manual synthesis of the DSA-PABA-Cit-Val sequence as above in **4.5**. The Fmoc-DSA-OH unit was first loaded onto a rink amide resin using HATU/DIPEA chemistry and the

subsequent couplings of the PABA, Cit and Val proceeded in the same manner. Upon removal of the Fmoc group from the valine unit, the remaining peptide **4.1** sequence was synthesised on the automatic peptide synthesiser using HOBt/HBTU coupling chemistries. The final histidine unit was then capped using an acetyl group. Upon cleavage from the resin, crude PDC **4.8** was treated with BBr_3 in order to achieve the required benzyl deprotection to give PDC **4.9** (Figure 4.10).

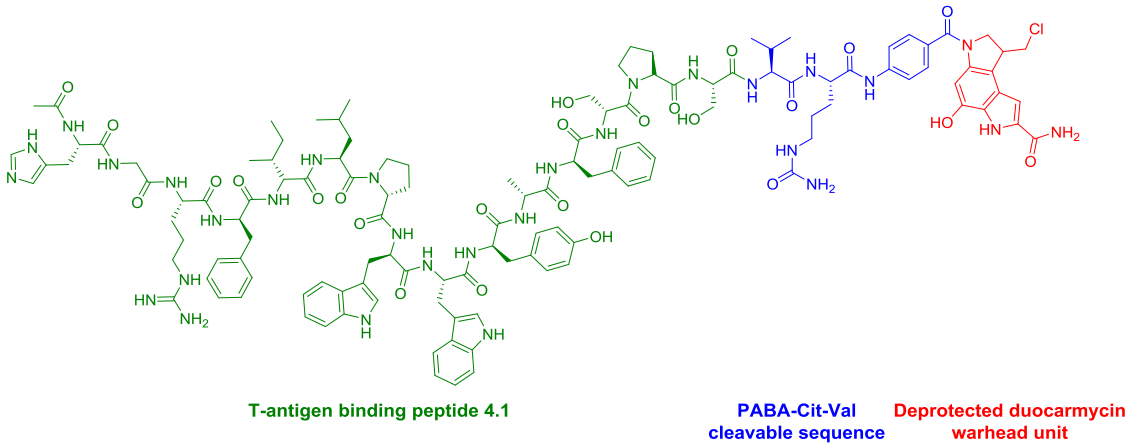

Figure 4.10: chemical structure of the debenzylated PDC **4.9.**

After 2 h, the mixture was analysed by HPLC which suggested the required benzyl deprotection had occurred. Subsequently, the mixture was purified and again analysed by HPLC and MALDI mass spectrometry to confirm the presence of PDC **4.9** (Figure 4.11).

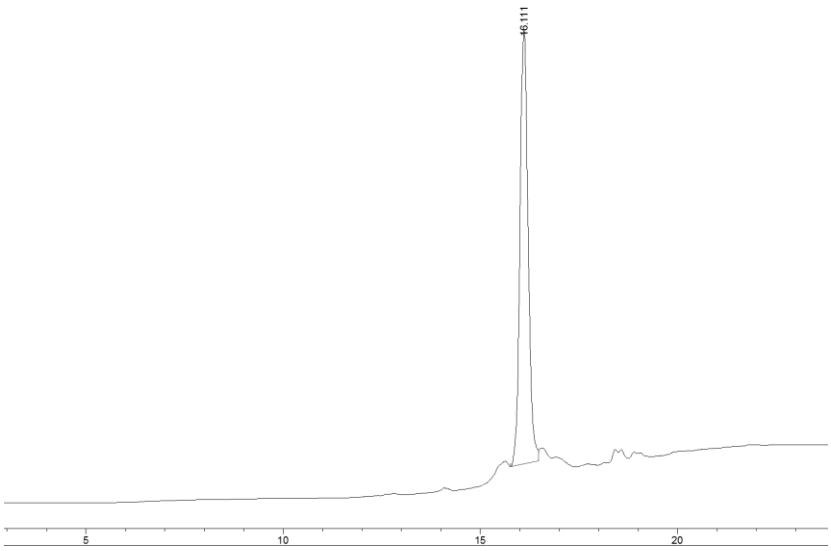

Figure 4.11: HPLC chromatogram of a pure sample of PDC **4.9**. Agilent Eclipse XDB-C18 column, 4.8 x 150 mm, 5 µm. Solvent A: [Water and 0.05 % TFA], Solvent B: [MeOHand 0.05 % TFA]. Gradient: 0% [B] to 95 % [B], from 0 min to 15 mins, 95 % [B] to 0 % [B] from 15 to 20 mins. Monitored UV 214 nm. Flow rate 1 mL/min. Column temperature 40 °C.

The formation of **4.9** meant that two PDC constructs had now been successfully synthesised to allow a direct comparison between the two. This in turn would provide an analysis on the requirement of a cleavable linker between warhead and peptide in these conjugates.

To further establish the biological activity of this PDC construct, a cathepsin B cleavage assay was again completed. It was hoped that after reaction with the cathepsin B a clear release of the **4.7** would be observed. The conditions by LaBelle and co-workers discussed earlier were repeated but this time on PDC **4.9**. After 72 hours analytical HPLC and MALDI mass spectrometry were used to analyse the data. This time however, there was no observed degradation of **4.9** to release **4.7**. Efforts are currently ongoing to optimise this assay in order to try and observe the release of **4.7**.

4.3.1.4 Synthesis of a Fluorescent Analogue of Peptide 4.1.

A fluorescein isothiocyanate (FITC) analogue based on **4.1** would allow for assessment of the binding of this peptide to the T-antigen expressed on cell lines during biological evaluation. For this **4.1-FITC** analogue, peptide **4.1** was again synthesised on the automated peptide synthesiser. To this peptide, FITC isomer I was directly coupled onto the final histidine residue using

pyridine in DMF/DCM. Post cleavage HPLC of **4.1-FITC** demonstrated a number of signals on the chromatogram suggesting a problem specifically with the FITC coupling since the synthesis of **4.1** had been shown to proceed smoothly previously. It is not uncommon for the FITC and the terminal amino acid residue to undergo an elimination reaction under the acidic conditions utilised during cleavage (Scheme 4.4).[204] In order to avoid this issue, it has been suggested that a spacer should be utilised between the N-terminal amino acid and the FITC.

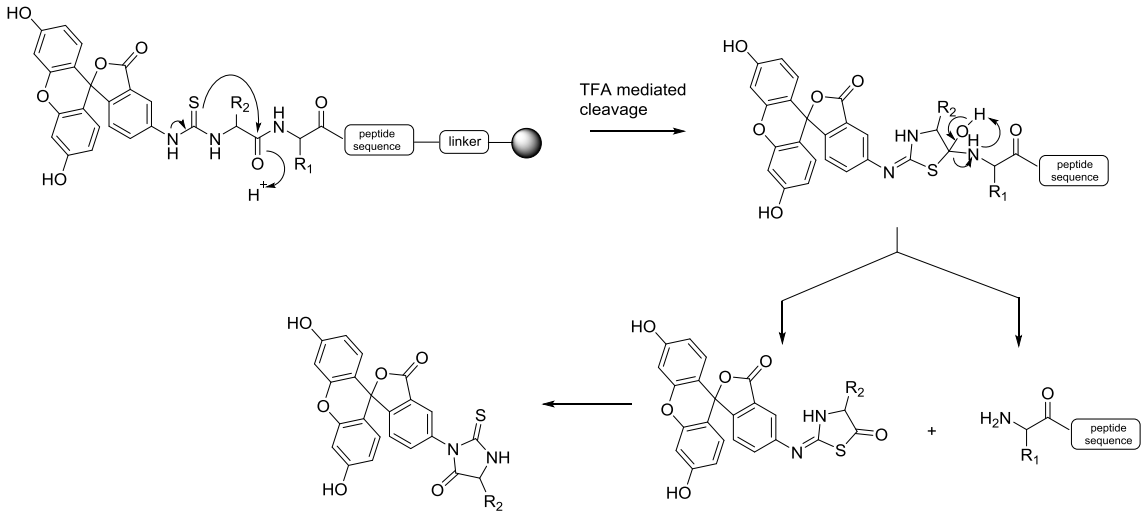

Scheme 4.4: elimination of the FITC module from the N-terminus of a peptide sequence during TFA mediated cleavage from the resin. Without a spacer after the N-terminal amino acid, this process is likely to occur causing a number of unwanted side products within the cleavage mixture.

For this reason, peptide **4.1** was synthesised incorporating a β-alanine unit after the final histidine residue. Subsequently, FITC was coupled onto the β-alanine again using pyridine in DMF to give **4.1-βAla-FITC** (Figure 4.12).

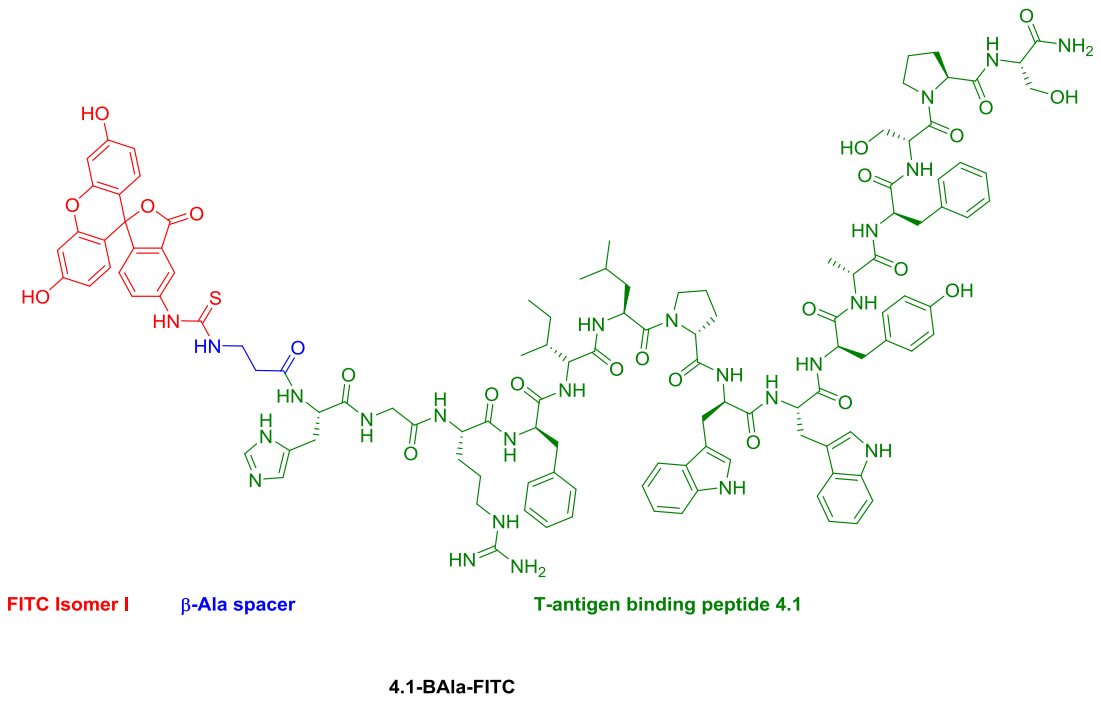

Figure 4.12: chemical structure of **4.1-βAla-FITC**, synthesised to study the interaction of 4.3 with cell lines used for biological evaluation.

HPLC and MALDI mass spectrometry analysis of the resulting cleavage product demonstrated the successful synthesis of **4.1-βAla-FITC**. The HPLC indicated a major product peak (Figure 4.13) and the MALDI mass spectrum showed the expected mass for the peptide. With this analogue in hand, investigations into the interaction of this peptide with T-antigen expressing cell lines could be made.

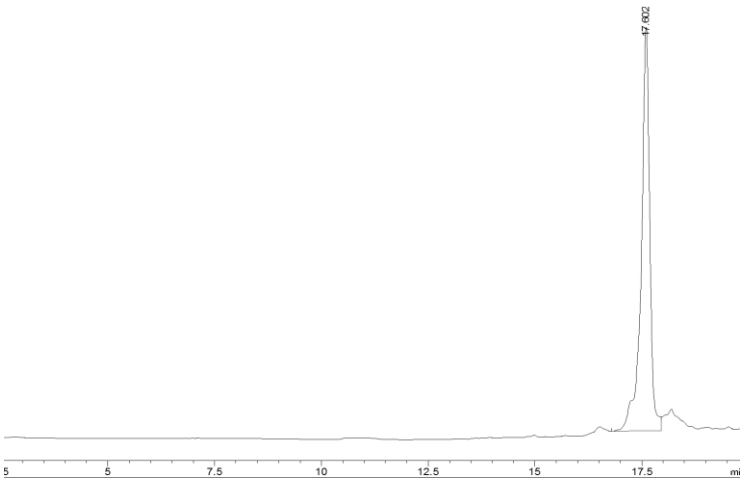

Figure 4.13: HPLC trace of pure **4.1-βAla-FITC.** Agilent Eclipse XDB-C18 column, 4.8 x 150 mm, 5 μm. Solvent A: [Water and 0.05 % TFA], Solvent B: [MeOHand 0.05 % TFA]. Gradient: 0% [B] to 95 % [B], from 0 min to 15 mins, 95 % [B] to 0 % [B] from 15 to 20 mins. Monitored UV 214 nm. Flow rate 1 mL/min. Column temperature 40 °C.

4.3.2 Biological Evaluation of T-antigen Targeting PDCs

4.3.2.1 βAla-FITC Cell Binding Assays

As a starting point for the biological analysis of the synthesised peptide conjugates, investigations into the interaction of the T-antigen binding peptide (**4.1**) with a cell line which has previously been shown to express the antigen were proposed. The MCF-7 human breast cancer cell line has previously been shown to demonstrate high levels of T-antigen expression and hence were used within these studies.[151] For this work **4.1-βAla-FITC** was utilised. As an initial investigation, MCF-7 cells were incubated with **4.1-βAla-FITC** for 4 h, after which, the cells were visualised using fluorescence microscopy (Figure 4.14).

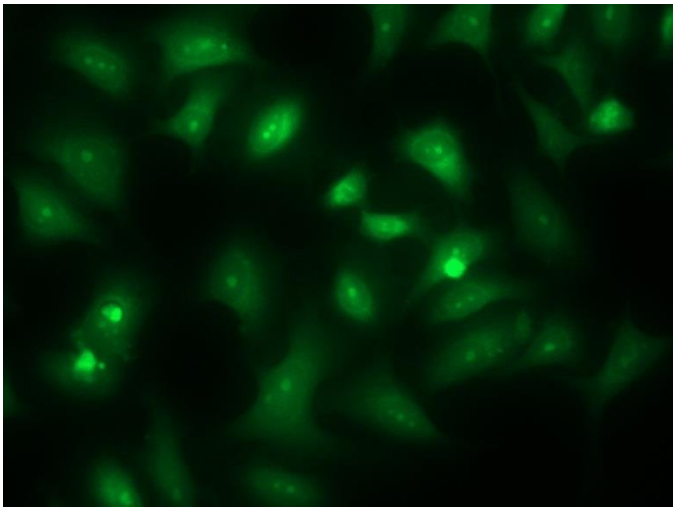

Figure 4.14: fluorescence microscopy images of MCF-7 cells post incubation with **4.1-βAla-FITC**.

The above microscopy images demonstrate the localisation of **4.1-βAla-FITC** on the MCF-7 cell line. This is presumed to be due to the interaction of peptide **4.1** with the T-antigen expressed on these cells. This result indicates that the delivery of the DSA unit in the synthesised conjugates to the cancer cell lines should occur. Of course, further studies would be required to determine the selectivity of this delivery.

4.3.2.2 Cell Viability Assays

As an initial screen for activity of **4.3**, it was decided to investigate the viability of MCF-7 human breast cancer cells post exposure to this PDC. The MCF-7 cells were treated with PDC **4.3** at final concentrations of 100 μM, 10 μM and 1 μM and incubated for 72 h. Post incubation, an MTS assay was used to deduce the levels of cell death within the wells. Disappointingly, it was evident from the results of this assay that no cell death had occurred even at the highest concentration of **4.3**. Whilst we have found in our laboratory that MCF-7 cells can be relatively resistant to cell death, it was still expected that with the active duocarmycin unit present, and at the concentrations examined, biological activity of some sort would be observed.

With this lack of biological activity being obtained within the MCF-7 cell line, it was suggested that the lack of a cleavable sequence between peptide **4.1** and the duocarmycin unit could have been the cause. With the duocarmycin warhead having a specific site of action within the cell nucleus, it can be

envisioned how when the unit is attached to a large peptide such as **4.1**, accessibility to the DNA could be an issue. Although cellular degradation of the peptide via proteolysis may be expected, this may not occur at a great enough extent to achieve the desired release of the duocarmycin unit and hence biological activity. With peptide **4.5** and a PDC incorporating this cleavable sequence, **4.9**, in hand, a comparison of the biological activities of these to PDC **4.3** could be made in order to confirm the above as a possible reason for the inactivity observed.

Initially, an assessment of the biological activity of **4.5** and **4.7** was proposed to establish whether these units themselves hold any activity and hence may demonstrate cytotoxicity when utilised alongside the T-antigen targeting peptide **4.1**. For activity screening purposes, a set of T-antigen expressing cell lines commonly used within the laboratory were chosen.[149, 151] The cells were treated with **4.5** and **4.7** for 72 h before an MTS assay was used to assess cell viability. Table 4.1 gives a summary of the cell lines studied along with the respective IC_{50}'s obtained for **4.5** and **4.7**.

Table 4.1: IC_{50} results obtained for compounds **4.5** and **4.7** with MCF-7. HL-60 and HCT116 cell lines.

Cell Lines	4.5 IC_{50} (μM)	4.7 IC_{50} (μM)
MCF-7	0.784	0.178
HL-60	4.384	0.059
HCT116	0.343	0.032

The nanomolar IC_{50}'s obtained within these investigations were some of the lowest that have been observed for the particular duocarmycin unit used within this thesis. This was somewhat surprising considering the lack of a binding subunit on these molecules which has been shown previously to cause a reduction in the activity obtained for duocarmycin units.[205] However, it could be that the PABA group present is acting in a similar way to a binding subunit and hence could be a key component in achieving these biological results.

Although peptide **4.5** should be cleaved by cathepsin B to give **4.7**, quite different IC_{50}'s were obtained here, with **4.5** showing a reduced biological

activity. However, this could be explained by a reduced cellular uptake of the larger **4.5** unit by the cell lines. Alternatively, incomplete cathepsin B cleavage of **4.5** may mean that the concentration of **4.7** obtained *in vitro* may be smaller than that used in the assays where the cells were directly exposed to **4.7**. Despite this slight discrepancy, the activity of **4.5** was still relatively high. Therefore, these studies demonstrated that this cleavable sequence unit has potential to obtain high activities when incorporated into a duocarmycin based sequence and hence warranted further investigation. Also worth noting here is the applicability of the **4.5** unit to be introduced into a variety of systems for various targeted therapeutic purposes.

Biological analysis of the whole PDC construct containing this cleavable sequence (**4.9**) was completed in order to determine its cytotoxic activity. MCF-7 cells were treated with 8 different concentrations of PDC **4.9** and incubated for 72 h. Post incubation, cells were treated with MTS to assess cell viability. The results from this assay provided an IC_{50} of 2 μM for PDC **4.9**. Importantly, the inactive, protected PDC **4.8** demonstrated no activity at 100 μM confirming that the activity observed in **4.9** is due to the active duocarmycin unit. This result indicates that **4.9** provides a promising starting point for the generation of a successful duocarmycin-based PDC. Despite this promising result, further investigations are required to help fully realise the potential of this PDC construct. Foremost, a thorough assessment of the selectivity of the duocarmycin warhead delivery is required. This would ensure that the T-antigen binding peptide, **4.1**, is successfully delivering the duocarmycin warhead to cancerous, T-antigen expressing cells.

What can be deduced from this comparative assessment of biological activity is the advantage of including a cleavable sequence between the duocarmycin unit and **4.1**. Little activity was obtained for the PDC without a cleavable sequence (**4.3**) yet with a cleavable sequence, low micromolar activity was obtained. This suggests that release of the duocarmycin unit from the PDC construct is required for this warhead to exert its biological activity. Of course, these PDC constructs differ in the positioning of the duocarmycin unit (N terminus in **4.3** and C terminus in **4.9**) and so this could also be playing a role within the activities obtained.

4.4 Conclusions

The aim of the research within this chapter was to develop a duocarmycin-based peptide-drug conjugate for targeted delivery to cancer cells via the T-antigen.

The discovery of a 15 amino acid peptide sequence (**4.1**) which has been shown to selectively and specifically bind the T-antigen provided an ideal starting point for the formation of this PDC construct. The binding of this peptide sequence to the T-antigen on MCF-7 cells was confirmed through the synthesis of a fluorescent analogue of this peptide. **4.1-βAla-FITC** was shown, using fluorescence microscopy studies, to bind to MCF-7 cells which have been previously reported to express the T-antigen.

Following on from this, two PDCs based on **4.1** were synthesised. One PDC (**4.3**) was synthesised without a cleavable sequence between peptide and duocarmycin warhead and the other PDC (**4.9**) was synthesised containing a cathepsin B cleavable PABA-Cit-Val sequence. Biological analysis of the cathepsin B cleavable sequence (**4.5**) and its respective cleavage product (**4.7**) demonstrated the potential of this unit after IC_{50}s in the low to mid nanomolar range in MCF-7, HL60 and HCT116 cell lines were obtained. The design and synthesis of this DSA-PABA-Cit-Val sequence also provides scope for further studies involving targeted delivery due to its ease of synthesis on the solid phase, and its applicability in terms of incorporation into numerous other targeting systems. To confirm the cleavage of PDC **4.9** and therefore release of **4.7**, the PDC was subjected to cathepsin B cleavage assay conditions. Unfortunately, whilst **4.7** was observed to be released from **4.5**, no signs of this occurring from **4.9** were observed. However, efforts to optimise this assay for the **4.9** system are on-going.

During biological analysis, PDC **4.3** demonstrated no cytotoxic activity at concentrations of 100 μM and lower in MCF-7 cell lines. This was assumed to be due to the lack of cellular degradation of the PDC construct thereby preventing the duocarmycin warhead from exerting its DNA alkylation based activity. On the other hand, PDC **4.9,** containing the cleavable sequence, demonstrated an IC_{50} of 2 μM. This dramatic improvement in activity is

assumed to be due to the addition of the cleavable sequence which allows the duocarmycin unit to be released. Release of **4.7** specifically from the construct is thought to be desirable since the PABA unit in this compound may act in a similar way to a DNA binding subunit. This could explain the low nanomolar activity obtained for **4.7** in cellular assays.

Investigations are now required to establish the potential of this promising PDC construct (**4.9**). Studies which aim to ascertain whether this PDC can selectively target and hence show greater efficacies in cell lines which show an elevated level of T-antigen expression are essential. The literature reports a number of cells lines that show a reduced T-antigen expression which these studies could be completed with. Additionally, scrambling of the T-antigen peptide **4.1**, and specifically the aromatic region thought to be essential for T-antigen binding, could be used to establish whether the targeting capabilities of **4.1** are enabling the activity of PDC construct **4.9**. Should the scrambled sequence PDC show a lower cytotoxicity, then this would suggest that the binding of **4.1** to the T-antigen is crucial for the observed activity within **4.9**. The literature surrounding the use of **4.1** also describes how a simple iodination of the tyrosine residue can result in complete loss of binding to the T-antigen. This strategy could therefore also be employed to further investigate the behaviour of **4.9**.

Following on from studies which aid in understanding the binding and targeting behaviour of **4.9**, investigations which aim to improve upon the current cytotoxic activity of this PDC could be made. Of particular interest here would be additions of further duocarmycin units into the PDC sequence. By adding additional warheads, a greater level of DNA alkylation may be achieved which in turn could result in greater cytotoxicity. This strategy has shown success within other unpublished analogues from our laboratory and so may also prove successful within this system.

4.5 Experimental

4.5.1 General Procedures

Reagents and Solvents

All chemicals were reagent grade and were purchased from Sigma Aldrich, Fisher Scientific, FluoroChem and Tokyo Chemical Industry. Fmoc-amino acids and coupling reagents were purchased from Novabiochem or AGTC Bioproducts. Anhydrous solvents were bought from Sigma Aldrich and assumed to conform to specification.

Physical Characterisation and Spectroscopic Techniques

^{1}H- and ^{13}C-NMR spectra were recorded on a Bruker spectrometer operating at 400 MHz (^{1}H) or 100 MHz (^{13}C) using the specified deuterated solvent. The chemical shifts for both ^{1}H- and ^{13}C were recorded in ppm and were referenced to the residual solvent peak of DMSO at 2.50 ppm (^{1}H) and 39.52 ppm (^{13}C). Multiplicities in the NMR spectra are described as s = singlet, d = doublet, t = triplet, q = quartet, m = multiplet, br = broad, and combinations thereof; coupling constants are reported in Hz. MALDI was performed on Kratos Analytical Axima MALDI-TOF using α-cyano-4-hydroxycinnamic acid as a matrix. Low resolution mass spectra were recorded using a Shimadzu LCMS 2010EV operated under electrospray ionisation in positive (ES+) mode. Accurate mass spectra were recorded at the EPSRC National Mass Spectroscopy Service Centre, Swansea or at The John Innes Centre, Norwich Research Park.

Chromatographic Techniques

Analytical RP-HPLC was performed on an Agilent 1200 using an Agilent eclipse XDB-C18 column, 4.6 x 150 mm, 5 μM and a flow rate of 1 mL/min. Solvent A = Water + 0.05% TFA and Solvent B = MeOH + 0.05% TFA. Gradient 5% B up to 95% B over 20 minutes. Detection wavelength 214 nm and 254 nm. Semi-preparative RP-HPLC was performed on an Agilent 1200 using an Agilent eclipse XDB-C18 column, 9.4 x 250 mm, 5 μM and a flow rate of 4 mL/min. Solvent A = water + 0.05% TFA and Solvent B = MeOH + 0.05% TFA. Gradient 5% B up to 95% B over 20 minutes. Detection wavelength 214 nm and 254 nm. Preparative RP-HPLC was performed on an Agilent 1200 using an Agilent eclipse XDB-C18 column, 21.2 x 150 mm, 5 μM and a flow rate of 20 mL/min. Solvent A = 95% H_2O + 5% MeOH + 0.05%

TFA and Solvent B = 95% MeOH + 5% H_2O + 0.05% TFA. Gradient 5% B up to 95% B over 20 minutes.

4.5.2 Synthesis

Synthesis of PDC-4.2

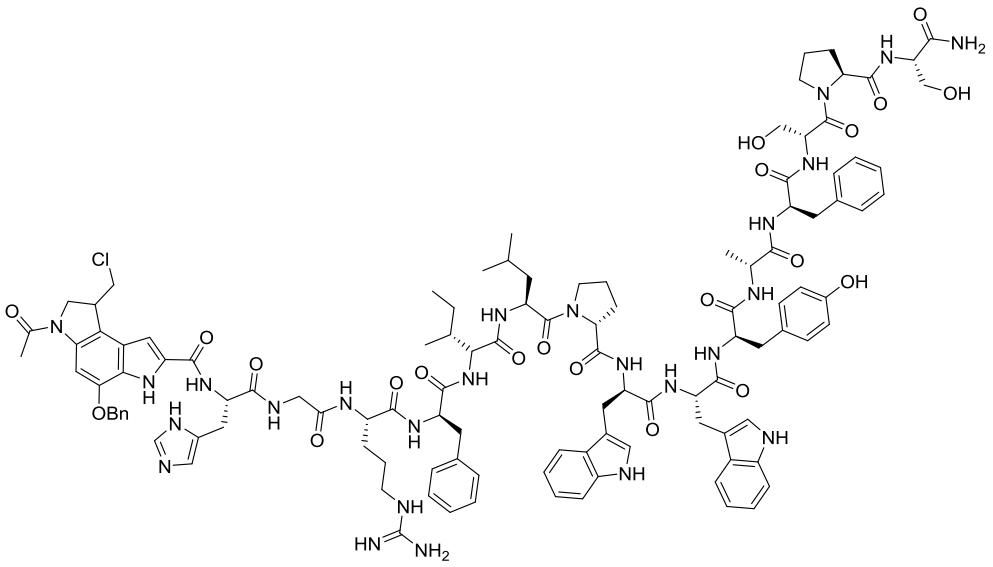

Peptide-Drug Conjugate 4.2

The 15 amino acid T-antigen binding peptide **4.1** (HGRFILPWWYAFSPS) was synthesised on NovaPEG Rink amide resin (resin loading 0.49 mmol/g) using an automated peptide synthesiser. 100 mg of NovaPEG Rink Amide resin (0.049 mmol) was suspended in DMF (2 mL) and was allowed to swell for 30 minutes. The DMF was drained from the peptide vessel and the resin was treated with a solution of Fmoc-Ser(tBu)-OH (4 equiv. compared to resin loading), to which HBTU (3.9 equiv.), HOBt (4 equiv.) and DIPEA (8 equiv.) in DMF were added. The mixture was then vortexed for 30 min. The vessel was drained and the resin washed with DMF (3 x 2 mL). The coupling reaction was then repeated followed by Fmoc deprotection (2 x 2 mL 40% piperidine in DMF, 10 min) and finally the resin was washed with DMF. Subsequent amino acids were coupled in an identical fashion. After the final amino acid coupling reaction (histidine) and Fmoc deprotection, the resin was treated with **2.10** (1.5 equiv.), HATU (1.5 equiv.) and DIPEA (3 equiv.) and reacted overnight. Subsequent Fmoc deprotection (3 mL 40% piperidine

in DMF, 10 min, 3 mL 20% piperidine in DMF, 5 min x 2) was followed by coupling with AcCl (5 equiv.) and DIPEA (10 equiv.) in DMF for 1 h. The resin was washed with DMF (6 x 10 mL) followed by DCM (6 x 10 mL). The peptide was cleaved from the resin using 47% TFA, 10% TIPS in DCM (10 mL) and shaken for 3 h after which the cleavage cocktail was drained into a round bottom flask. The resin was washed with TFA (x 3) and the solutions combined and concentrated under reduced pressure. The peptide was precipitated using cold diethyl ether and filtered. PDC **4.2** was purified using automated reversed phase Prep HPLC and lyophilised from water to yield a brown solid. This was subsequently analysed using RP-HPLC (RT = 17.6 min) and MALDI mass spectrometry for **4.2** (M + H)+, 2244.46.

Synthesis of PDC - 4.3

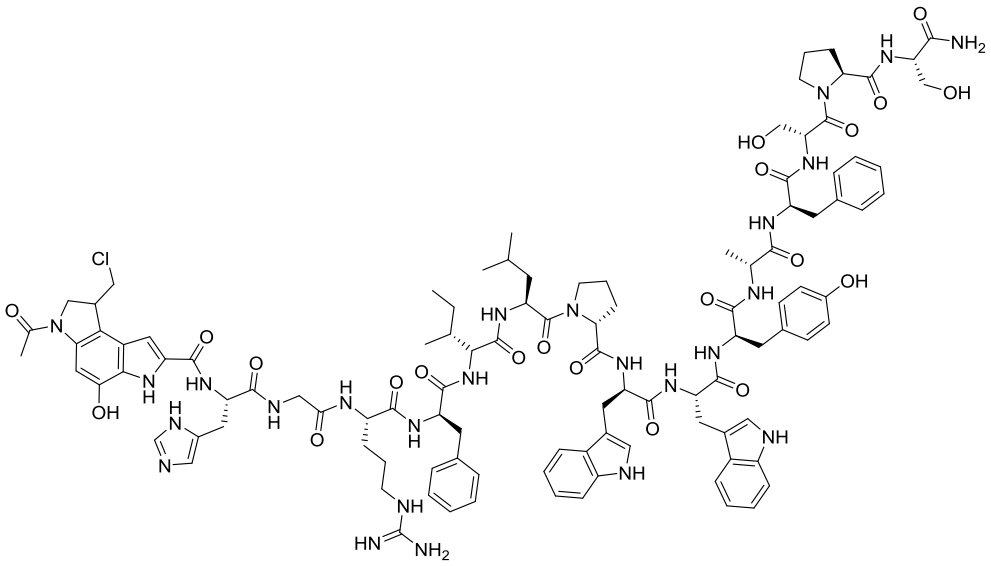

Peptide-Drug Conjugate 4.3

PDC **4.2** (10.0 mg, 0.004 mmol) was suspended in anhydrous DCM (5 mL) and cooled to -78 °C under an atmosphere of N_2. To this was added a 1 M solution of BBr_3 in DCM (9 µL, 0.009 mmol) and the resulting reaction stirred at –78 °C for 1 h. Subsequently, the reaction was allowed to warm to room temperature and stir for a further 1 h before being quenched with crushed ice. The mixture was then evaporated to dryness under reduced pressure before being resuspended in MeOH (5 mL) for purification by

reverse-phase Prep HPLC. This yielded PDC **4.3**, (3.1 mg, 32%) as a light brown solid which was analysed via using RP-HPLC (RT = 16.5 min) and MALDI mass spectrometry for **4.3** (M + H)+, 2152.56.

On Resin Benzyl Deprotection of PDC – 4.2

The resin-4.2 construct (30 mg, 0.015 mmol as determined from resin loading) was washed with DCM (6 x 5 mL) and suspended in anhydrous DCM (5 mL) under an atmosphere of N_2. The resulting mixture was cooled to -78 °C and treated with a 1 M solution of BBr_3 in DCM (28 μL, 0.028 mmol) before stirring for 1 h at -78 °C. The mixture was allowed to warm to room temperature and then stirred for a further 1 h. Subsequently, the reaction was quenched with crushed ice and the resin filtered off and washed with DCM (5 x 5 mL). The benzyl deprotected PDC, **4.3**, was cleaved from the resin through treatment with 47% TFA, 10% TIPS in DCM for 3 h, after which the cleavage cocktail was drained into a round bottom flask. The resin was washed with TFA (x 3) and the solutions combined and evaporated to dryness under reduced pressure. The peptide was precipitated using cold diethyl ether and filtered. PDC **4.3** was purified using automated reversed phase Prep-HPLC and lyophilised from water to yield a light brown solid. This was subsequently analysed using RP-HPLC (RT = 16.5 min) and MALDI mass spectrometry for **4.3** (M + H)+, 2152.68).

Synthesis of Peptide 4.4 and 4.5

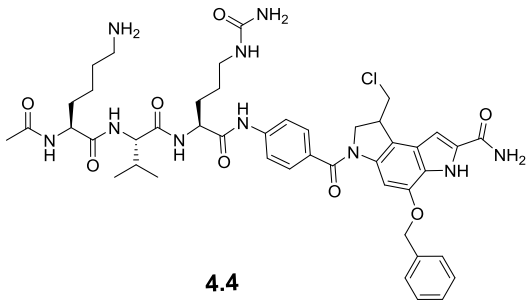

4.4

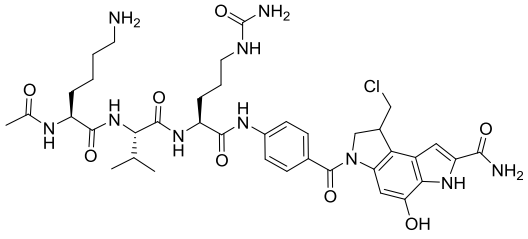

4.5

NovaPEG Rink Amide resin (150 mg, 0.0735 mmol, [manufacturer's resin loading 0.49 mmol/g]) was prepared for coupling by swelling in dichloromethane (DCM) for 30 mins followed by N,N-dimethylformamide (DMF) for 30 mins. **2.10** (64 mg, 0.11 mmol) was dissolved in 2 mL of DMF

and treated with HATU (42 mg, 0.11 mmol) and DIPEA (39 μL, 0.22 mmol). After 10 secs the resulting solution was added to the resin and the mixture shaken overnight. Subsequently, the resin was washed with DMF (6 x 10 mL) before removal of the indoline Fmoc using piperidine in DMF (6 mL 40% 10 mins, 6 mL 20% 5 mins twice). Following Fmoc deprotection the resin was washed with DMF (6 x 10 mL). Next, Fmoc-PABA-OH (132 mg, 0.368 mmol) was dissolved in 2 mL of DMF and treated with HATU (140 mg, 0.368 mmol) and DIPEA (129 μL, 0.735 mmol). After 10 secs the resulting solution was added to the resin and the mixture shaken for 2 h. The resin was subsequently washed with DMF (6 x 10 mL) and the coupling with Fmoc-PABA-OH repeated. Next, the Fmoc group on the PABA was removed using piperidine in DMF (6 mL 40% 10 mins, 6 mL 20% 5 mins twice). The resin was then washed again with DMF (6 x 10 mL) before being treated with Fmoc-Cit-OH (146 mg, 0.368 mmol) HATU (140 mg, 0.368 mmol) and DIPEA (129 μL, 0.735 mmol). The mixture was shaken for 2 h before the resin was washed with DMF (6 x 10 mL). The citrulline Fmoc group was removed using piperidine in DMF (6 mL 40% 10 mins, 6 mL 20% 5 mins twice). Upon washing of the resin with DMF (6 x 10 mL), the resin was treated with Fmoc-Val-OH (125 mg, 0.368 mmol), HATU (140 mg, 0.368 mmol) and DIPEA (129 μL, 0.735 mmol) and shaken for 2 h. Upon Fmoc deprotection of the valine residue with piperidine (6 mL 40% 10 mins, 6 mL 20% 5 mins twice), the resin was treated with Fmoc-Lys(Boc)-OH (172 mg, 0.368 mmol) HATU (140 mg, 0.368 mmol) and DIPEA (129 μL, 0.735 mmol) and left to react for 2 h. Subsequently the resin was washed with DMF (6 x 10 mL) and the lysine Fmoc group removed using piperidine in DMF (6 mL 40% 10 mins, 6 mL 20% 5 mins twice). Following on from this, the resin was washed with DMF (6 x 10 mL) and treated with AcCl (26 μL, 0.37 mmol) and DIPEA (129 μL, 0.735 mmol) in DMF (2 mL) for 2 h. Subsequently, the resin was washed with DMF (6 x 10 mL) and the AcCl coupling conditions repeated. The resin was washed with DMF (6 x 10 mL) and then DCM (6 x 10 mL). Cleavage of **4.4** from the resin was affected by addition of a solution of 47% TFA, 10% TIPS in DCM (10 mL). After 3 h of shaking, the cleavage mixture was filtered. The resin was rinsed with DCM (2 x 3 mL) and the combined filtrates were evaporated to dryness under reduced pressure to

give crude **4.4** which was analysed using RP-HPLC (RT = 15.9 min) and MALDI mass spectrometry for **4.4** (M + H)+, 901.50). Crude **4.4** (10 mg, 0.011 mmol) was dissolved in MeOH (1 mL) and treated with a slurry of 10% Pd/C (20 mg) in a 25% aq. ammonium formate (500 μL) under N_2. After 1 h the Pd/C was removed by filtering through a plug of celite. Purification by Prep-HPLC yielded **4.5** (4.1 mg, 45%) as a light brown solid which was analysed by RP-HPLC (RT = 13.7 min) and HRMS (ES+) calcd. for $C_{38}H_{51}ClN_{10}O_8$ (M + H)+, 811.3658; found, 811.3652).

Synthesis of 4.6 and 4.7

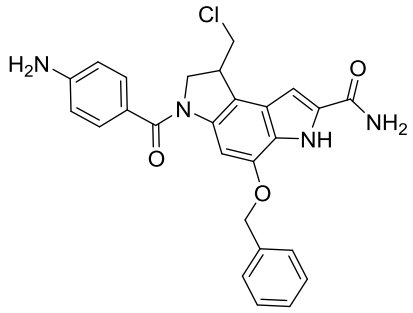

4.6

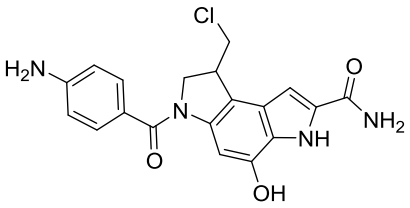

4.7

NovaPEG Rink Amide resin (150.0 mg, 0.0735 mmol, [manufacturer's resin loading 0.49 mmol/g]) was prepared for coupling by swelling in dichloromethane (DCM) for 30 mins followed by N,N-dimethylformamide (DMF) for 30 mins. **2.10** (64 mg, 0.11 mmol) was dissolved in 2 mL of DMF and treated with HATU (42 mg, 0.11 mmol) and DIPEA (39 μL, 0.22 mmol). After 10 secs the resulting solution was added to the resin and the mixture shaken overnight. Subsequently, the resin was washed with DMF (6 x 10 mL) before removal of the indoline Fmoc using piperidine in DMF (6 mL 40% 10 mins, 6 mL 20% 5 mins twice). Following Fmoc deprotection the resin was washed with DMF (6 x 10 mL). Next, Fmoc-PABA-OH (132 mg, 0.368 mmol) was dissolved in 2 mL of DMF and treated with HATU (140 mg, 0.368 mmol) and DIPEA (129 μL, 0.735 mmol). After 10 secs the resulting solution was added to the resin and the mixture shaken for 2 h. The resin was subsequently washed with DMF (6 x 10 mL) and the coupling with Fmoc-PABA-OH repeated. Next, the Fmoc group on the PABA was removed using piperidine in DMF (6 mL 40% 10 mins, 6 mL 20% 5 mins twice). The resin was then washed again with DMF (6 x 10 mL) and then with DCM (6 x 10

mL) before cleavage from the resin using 47% TFA, 10% TIPS in DCM (10 mL) for 3 h. **4.6** was isolated via filtration of the cleavage mixture and subsequent washing of the resin with DCM (3 x 5 mL). The combined filtrates were evaporated to dryness under reduced pressure to give crude **4.6** as a dark green solid. Crude **4.6** (10 mg, 0.021 mmol) was dissolved in MeOH (1 mL) and treated with a slurry of 10% Pd/C (20 mg) in a 25% aq. ammonium formate (500 μL) under N_2. After 1 h the Pd/C was removed by filtering through a plug of celite. Purification by Prep-HPLC yielded **4.7** (3.1 mg, 38%) as a light brown solid. RP-HPLC (RT = 11.9 min). ^{1}H NMR (DMSO-d_6, 400 MHz) δ 11.12 (1H, s), 7.85 (1H, s), 7.33 (2H, d, J = 8.1), 7.26 (1H, s), 7.14 (1H, s), 7.00 (1H, s), 6.64 (2H, s, J = 8.2), 4.33-4.24 (1H, m), 4.01-3.93 (3H, m), 4.87-3.81 (1H, m). HRMS (ES+) calcd. for $C_{19}H_{17}O_3N_4Cl$ (M + H)+, 385.1067; found, 385.1058.

Synthesis of PDC – 4.8

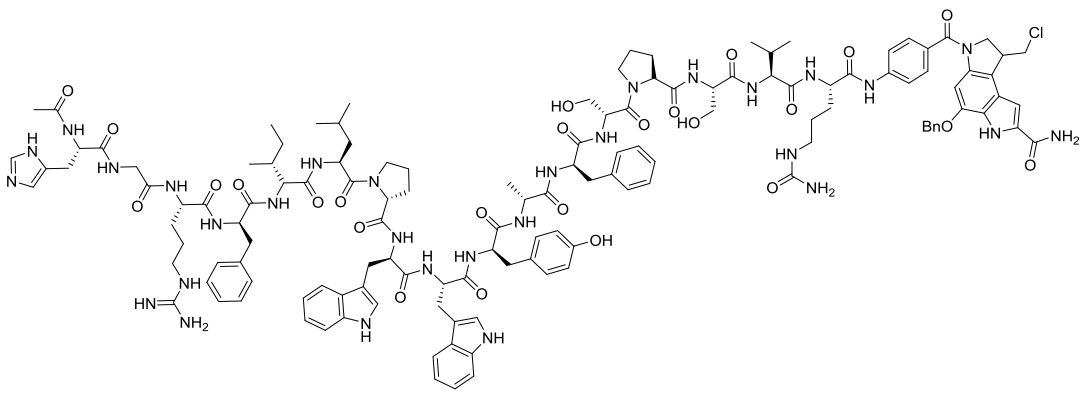

Peptide-Drug Conjugate, 4.8

The synthesis of PDC **4.8** began with a repeat synthesis of peptide **4.4**. This was completed on 100 mg (0.049 mmol substitution) NovaPEG Rink Amide resin (resin loading 0.49 mmol/g). Unlike in peptide **4.4**, following on from the coupling of the valine unit and subsequent Fmoc deprotection, the resin was transferred to the automated peptide synthesiser where peptide **4.1** was built on the valine unit following the same method above, as synthesised in PDC **4.2**. Upon completion of the final amino acid coupling in peptide **4.1** (histidine) and subsequent Fmoc deprotection, the N-terminus was capped via a coupling with AcCl (5 equiv.) and DIPEA (10 equiv.) in DMF (2 mL).

The resin was washed with DMF (6 x 10 mL) followed by DCM (6 x 10 mL). The peptide was cleaved from the resin using 47% TFA, 10% TIPS in DCM (10 mL) and shaken for 3 h after which the cleavage cocktail was drained into a round bottom flask. The resin was washed with TFA (3 x 3 mL) and the solutions combined and concentrated under reduced pressure. The peptide was precipitated using cold diethyl ether and filtered. PDC **4.8** was purified using automated reversed phase Prep-HPLC and lyophilised from water to yield a brown solid. This was subsequently analysed using RP-HPLC (RT = 17.1 min) and MALDI mass spectrometry for **4.2** $(M + H)^+$, found, 2618.50).

Synthesis of PDC – 4.9

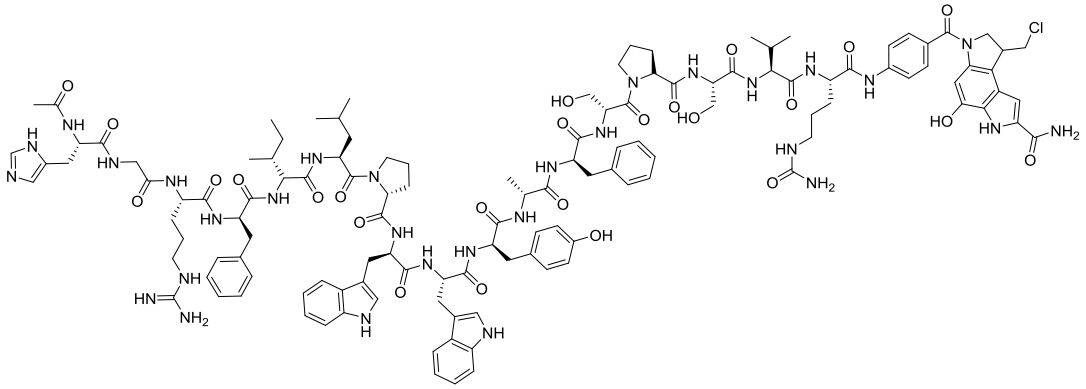

Peptide-Drug Conjugate, 4.8

PDC **4.8** (10 mg, 0.0038 mmol) was suspended in anhydrous DCM (5 mL) and cooled to -78 °C under an atmosphere of N_2. To this was added a 1 M solution of BBr_3 in DCM (8 µL, 0.007 mmol) and the resulting reaction stirred at – 78 °C for 1 h. Subsequently, the reaction was allowed to warm to room temperature and stir for a further 1 h before being quenched with crushed ice. The mixture was then evaporated to dryness under reduced pressure before being resuspended in MeOH (5 mL) for purification by reverse-phase Prep HPLC. This yielded PDC **4.9**, 4.1 mg (43%) as a light brown solid which was analysed via using RP-HPLC (RT = 16.1 min) and MALDI mass spectrometry for **4.9** (M + H)+, found, 2528.37.

Synthesis of 4.1-βAla-FITC

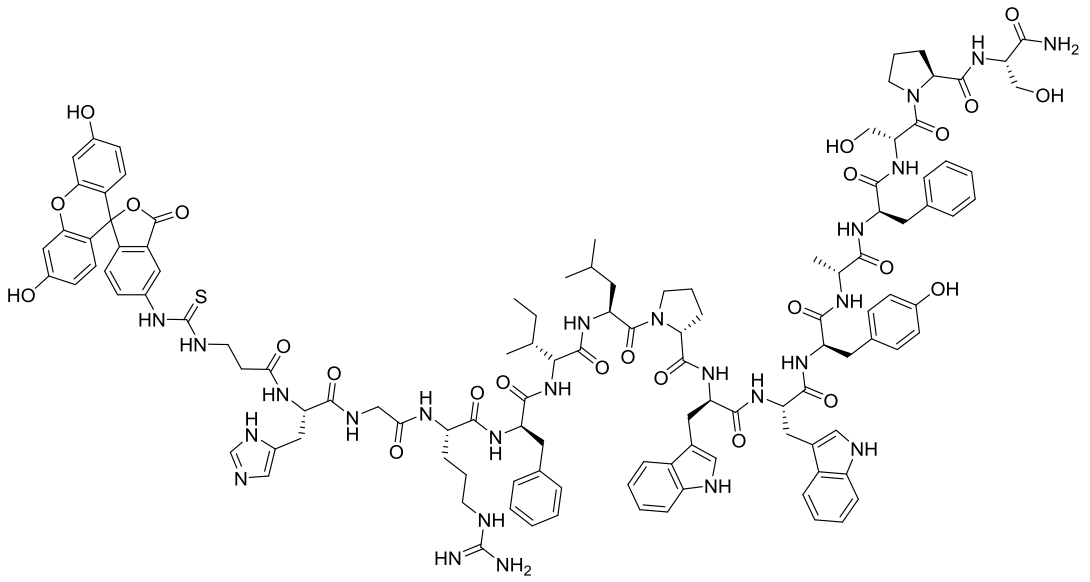

4.1-BAla-FITC

The 15 amino acid T-antigen binding peptide **4.1** (HGRFILPWWYAFSPS) was synthesised as above for PDC **4.2**. After the final amino acid coupling reaction (histidine) and Fmoc deprotection, the resin was this time treated with Fmoc-βAla-OH (5 equiv.), HATU (5 equiv.) and DIPEA (10 equiv.) and reacted for 2 h. Subsequent Fmoc deprotection (3 mL 40% piperidine in DMF, 10 min, 3 mL 20% piperidine in DMF, 5 min x 2) was followed by coupling with FITC isomer I (1.1 equiv.) in pyridine:DMF:DCM (2.4:1.4:1) overnight in the dark. The resin was washed with DMF (6 x 10 mL) followed by DCM (6 x 10 mL). The peptide was cleaved from the resin using 47% TFA, 10% TIPS in DCM (10 mL) and shaken for 3 h after which the cleavage cocktail was drained into a round bottom flask. The resin was washed with TFA (x 3) and the solutions combined and concentrated under reduced pressure. The peptide was precipitated using cold diethyl ether and filtered. Peptide **4.1-βAla-FITC** was purified using automated reversed phase Prep-HPLC and lyophilised from water to yield a yellow solid. This was subsequently analysed using RP-HPLC (RT = 17.6 min) and MALDI mass spectrometry for **4.1-βAla-FITC** (M + Na)+, found, 2245.08).

4.5.3 Biological Assays

Cell culture: The HL60, MCF-7 and HCT116 cell lines was purchased from ECACC (Porton Down, UK). Cells were cultured in RPMI 1640 medium supplemented with 10% foetal calf serum and 2 mM L-glutamine. HL-60, MCF-7 and HCT116 cells were passaged twice weekly and maintained between 1-9 x 10^5 cells/mL at 37 °C and 5% CO_2.

4.1-βAla-FITC Fluorescent Microscopy Binding Assay

MCF-7 human breast cancer cells were seeded in clear 96- well plates at 5 x 10^3 cells/well and treated with a 10 mM stock of **4.1-βAla-FITC** and incubated for 4 h at 37 °C. The cells were subsequently washed three times with PBS and fluorescence microscopy was used to examine cells and pictures taken with an inverted Leica DMII fluorescence microscope at 10x magnification.

Antiproliferative Assays

Antiproliferative assay: Antiproliferative activity was determined by MTS assay using the CellTiter 96 Aqueous One Solution Cell Proliferation Assay (Promega) and following the manufacturer's instructions. Briefly, HL-60, MCF-7 and HCT116 cells (3 x 10^4 /100 μL) were seeded in 96-well plates and left untreated or treated with DMSO (vehicle control), duocarmycins, or doxorubicin hydrochloride in triplicate for 72 h at 37 °C with 5% CO_2. Following this, MTS assay reagent was added for 4 h and the absorbance measured at 490 nm using the Polarstar Optima microplate reader (BMG Labtech). IC_{50} values were calculated using GraphPad Prism Version 5.0 software. Concentrations tested: Compound **4.3** in MCF-7 cells (100 μM, 10 μM, 1 μM). Compounds **4.5** and **4.7** in MCF-7, HL60 and HCT116 cell lines (100 μM, 10 μM, 1 μM, 0.1 μM, 0.01 μM, 0.001 μM, 0.0001 μM, 0.00001 μM) and **4.8** and **4.9** in MCF-7 cells (100 μM, 10 μM, 1 μM, 0.1 μM, 0.01 μM, 0.001 μM, 0.0001 μM, 0.00001 μM).

Chapter 5 - The Design and Synthesis of Targeted Gold Nanoparticles Functionalised with a Duocarmycin SA-based Analogue.

5.1 Introduction

5.1.1 Nanoparticles as Drug Delivery Platforms

Despite a century of continuous discovery and development, current formulations leave many drugs with poor pharmacokinetic profiles and incapable of localising specifically at sites of interest. Drug molecules simply diffuse and distribute freely throughout the body, resulting in undesirable side effects and a lack of efficacious responses. This inability to reach target sites contributes to exceptionally high attrition rates of new chemical entities across all therapeutic areas.[1]

Nanoparticle-based drug delivery platforms have emerged as suitable vehicles for overcoming some of the pharmacokinetic limitations associated with conventional drug formulations. Nanoparticles have proven advantageous at solubilising therapeutic cargos and substantially prolonging their circulation lifetimes. In addition to this, high drug loading within or on the surface of nanoparticles has shown great potential for improving the efficacy of drugs.[206-208] Maeda and co-workers, with their discovery of the enhanced permeability and retention (EPR) effect, demonstrated the potential for increased accumulation of long-circulating macromolecules by extravasation through fenestrated blood vessels in tumours (Figure 5.1).[26] Consequently, over the past two decades, this characteristic of solid tumours has been a major motivation for extensive research efforts aimed at applying nanoparticles to chemotherapy.

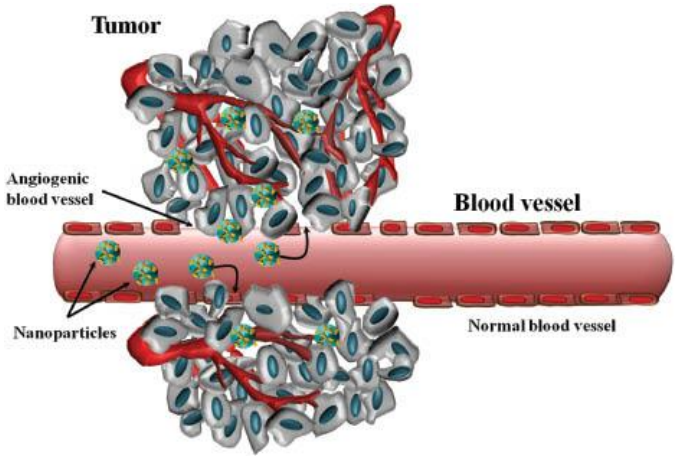

Figure 5.1: a schematic representation demonstrating how the enhanced permeability and retention effect leads to the natural accumulation of nanoparticles within tumorous tissue.[209]

The safety and tolerability of nanoparticle-formulated drugs are largely improved due to their ability to localise at disease sites.[210] This is best shown by the reduced cardiotoxicity observed in patients after administration of liposomal doxorubicin compared to that of those undergoing treatment with the conventional formulation.[211] These improvements in patient morbidity led to the FDA approval of liposomal doxorubicin (Doxil®) for the treatment of Kaposi's sarcoma in 1995 as well as approval of nanoparticle albumin-bound paclitaxel (Abraxane®) 10 years later.[212]

Whilst the EPR effect presents itself as a successful passive targeting strategy for nanoparticle systems, the ability to actively target these nanoparticles to specific disease locations is also possible. This is achieved through the functionalisation of nanoparticles with targeting moieties such as antibodies, proteins and small molecules. These agents are able to specifically recognise antigens on the surface of cancerous tissues allowing the nanoparticles to accumulate in these regions. This strategy has also been shown to improve cellular uptake, thereby further increasing the systems efficacy within studies.[213] This active targeting approach has been demonstrated using liposome nanoparticles conjugated to folic acid for the targeted delivery of doxorubicin to folate expressing tumour cells.[214, 215] Not only did these particles show improved tumour accumulation in comparison to free doxorubicin but they also showed evidence of evading multidrug-resistance efflux pumps.

5.1.2 Gold Nanoparticles as Drug Delivery Platforms

Among the many nanomaterials being developed for nanomedicine applications, gold nanoparticles (AuNPs) have shown potential as tumour sensors and drug delivery agents.[216-218] The use of AuNPs gained popularity in these areas of research for several reasons. Firstly, AuNPs are considered to be relatively biologically non-reactive and therefore suitable for *in vivo* applications compared to the very toxic cadmium and silver NPs.[219] Other advantageous qualities include the strong optical properties of AuNPs due to localised surface plasmon resonance (LSPR), easily controllable surface chemistry, and also, the ease of control over particle size and shape during synthesis.[217] AuNPs may be considered to be fully multifunctional, with the

possibility of combining different desired functionalities in one molecular-sized package.

A prominent application of AuNPs is their use as vehicles for the delivery of molecules into cells; AuNPs have been described as "promising nanocarriers for therapeutics".[220] However, as with other drug delivery systems such as ADCs, various factors need to be considered in designing an effective nanoparticle drug delivery system. The properties of AuNPs such as their size, charge and surface chemistry have been shown to affect their uptake into cells as well as their subsequent intracellular fate and pharmacokinetic profiles.[221]

If AuNPs are used solely as carriers into cells, it is critical to monitor any toxic effects of residual materials in the cell after delivery; a biodegradable nanoparticle vector whose lifespan is limited to the therapeutic window of the drug would be ideal. If the nanoparticle vector is cleared from the system once its purpose is reached, it will reduce exposure and limit its toxic effects in the body. Another area of concern is the penetration rate of AuNPs into tumours and their specificity for target sites. This issue is dependent on the choice of targeting moiety used within active targeting strategies and also on the receptor being targeted.

As with ADC systems, drug attachment and release from nanoparticles is another challenging area. While the ease of surface modification is what makes AuNPs attractive for drug delivery, the strength of drug attachment and timing of the release needs to be suitably controlled to produce the highest therapeutic efficacy. Foremost, the method of release, if necessary, at the tumour site is dependent on how the drug is attached to the AuNP, whether covalently or non-covalently.

Despite the potential of AuNP drug delivery systems, an agent of this kind has yet to be approved for use within the clinic. However, there have been several reports that have demonstrated the potential of these agents for this purpose. The effects of AuNPs conjugated with methotrexate (MTX) for inducing cytotoxicity *in vitro* and anti-tumorigenic effects *in vivo* have been reported.[222] It was observed that accumulation of Au-MTX in tumour cells

occurred more rapidly and at higher concentrations than those treated with free MTX. As a result, enhanced cytotoxic effects were also present in several tumour cell lines compared with an identical dosage of free MTX. These results warrant further investigation as they suggest that the conjugation of AuNPs with a chemotherapeutic drug such as MTX is more efficacious than the administration of free drug alone. In addition, with this study only relying on a passive targeting strategy, an active targeting strategy could further improve the efficacy of this system.

In another study, a phase I clinical trial on a PEGylated colloidal gold–tumour necrosis factor (TNF) construct (CYT-6091) conducted in patients with advanced stage solid cancers has shown potential (Figure 5.2).[223] The CYT-6091 complex was well-tolerated in this first clinical trial on human subjects. What was also evident was that the AuNP-TNF construct produced less adverse reactions than the TNF alone even at the highest drug-AuNP concentrations in the pre-clinical findings. AuNPs were found in the tumour as well as in the liver biopsies but no toxic adverse effects were observed. The authors concluded that the clinical results correlated well with the preclinical data, which bodes well for future translational studies for AuNPs. This nanoparticle construct has now been involved in studies where the central CYT-6091 unit has been functionalised with small molecule drugs such as paclitaxel for anticancer treatment.[224]

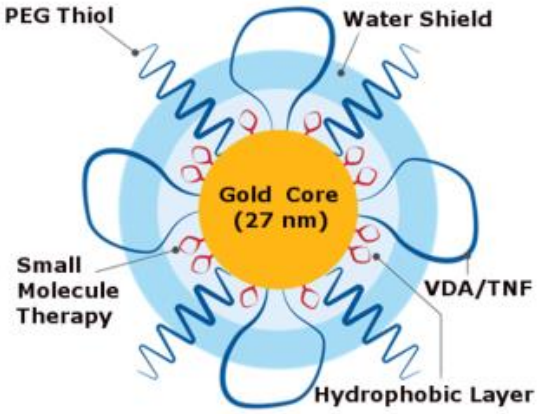

Figure 5.2: schematic representation of CYT-6091 – An AuNP functionalised with TNF-α, PEG chains and a small molecule drug therapeutic.

What is evident from the above brief summary, is the ability of AuNP systems to dramatically improve the pharmacokinetic and toxicity profiles of known

cytotoxic agents. The nanoparticle based systems have shown improved solubility, cellular uptake, selectivity and circulatory properties in comparison to the free drug. Since these issues have been attributed to the lack of success for the duocarmycin family of compounds, it could be that the nanoparticle based systems hold the ability to help this family realise their potential as clinically successful antitumour agents.

5.2 Aims of the Research in this Chapter

The work presented in this chapter encompasses efforts towards the synthesis of a gold nanoparticle system functionalised with a cytotoxic duocarmycin-based analogue. The design of this system, along with various strategies employed to functionalise the gold nanoparticle with the duocarmycin analogue will be discussed. Efforts towards the characterisation of these gold nanoparticle-duocarmycin conjugates will then be addressed.

The chapter will also look at attempts to further advance the nanoparticle system via an active targeting strategy utilising the jacalin lectin introduced in Chapter 3. This was made to allow these gold nanoparticles to specifically bind to the T-antigen disaccharide and hence achieve targeted delivery to cancerous tissues.

Finally, the biological assessment of these nanoparticles within various cell lines will be addressed which provides considerations for future work.

5.3 Results and Discussion

5.3.1 Initial Design of the Nanoparticle Systems

One of the vital considerations when designing a gold nanoparticle drug delivery system is the size of the nanoparticle core. The importance of this has been discussed in great detail within the literature and has been shown to have a great effect on pharmacokinetic and distribution parameters.[221] Additionally, the functionalisation of the nanoparticle with various molecules has also been shown to have an impact on these parameters.[225] Thus, the design of a duocarmycin-AuNP system had to take into consideration these two factors.

In a study by De Jong and co-workers, AuNPs of various size were detected in various bodily locations after intravenous injection of male rats with different sized AuNPs.[226] After 24 h, the highest amount of Au was detected in the blood, liver and spleen with lower amounts in the lungs, kidneys, testis, thymus, heart and brain. When AuNPs are functionalised with PEG, different trends are observed; after tail vein injection of white rats, the accumulation of Au in the liver and spleen appears to decrease with decreasing nanoparticle size from 50 to 15 nm.[227] Conversely, the blood showed the greatest amount of Au after 24 h when 15-nm PEG–AuNPs were administered. Having a higher concentration in the blood, the 15-nm nanoparticles have a greater probability of recirculating and accumulating into the reticuloendothelial system, as well as inflamed and/or malignant disease sites.

It was these findings that led to an initial proposed synthesis of a duocarmycin-AuNP conjugate involving a 16 nm gold nanoparticle core functionalised with PEG. A PEG monolayer on the particle, which is functionalised with a terminal carboxylic acid, can be coupled to an amine on a duocarmycin peptide. Additionally, the carboxylic acid functionality can be utilised for an active targeting strategy whereby jacalin is coupled onto this position via a lysine residue yielding AuNP-duocarmycin/jacalin conjugates. This strategy is outlined in Scheme 5.1.

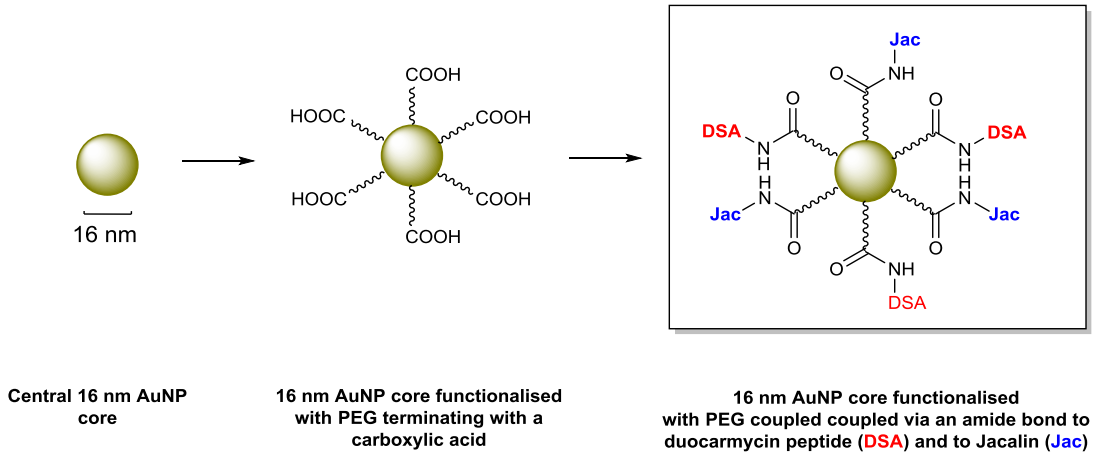

Scheme 5.1: a schematic representation of the initial strategy envisioned for the synthesis of a AuNP-duocarmycin/jacalin conjugate.

Russell and co-workers have utilised 4 nm AuNPs to target phthalocyanine analogues to tumours in the development of agents for photodynamic therapy.[111] As these have shown promising cellular activity, a second set of compounds were designed using 4 nm AuNPs conjugated to DSA and to jacalin. The proposed structures and routes to these compounds were:

a) A 4 nm AuNP with DSA directly attached to the AuNP and targeted by jacalin attached to PEG (Scheme 5.2).

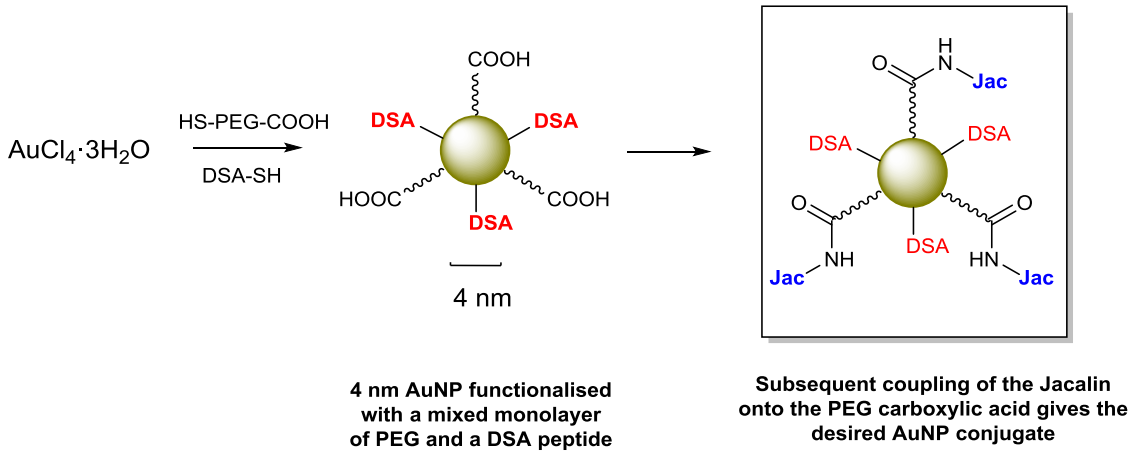

Scheme 5.2: envisioned synthesis of a 4 nm AuNP core functionalised with a mixed monolayer of a DSA peptide and PEG, followed by coupling of jacalin to the carboxylic terminated PEG.

b) A DSA peptide attached to PEG and then incorporated into the 4 nm AuNP conjugate (Scheme 5.3).

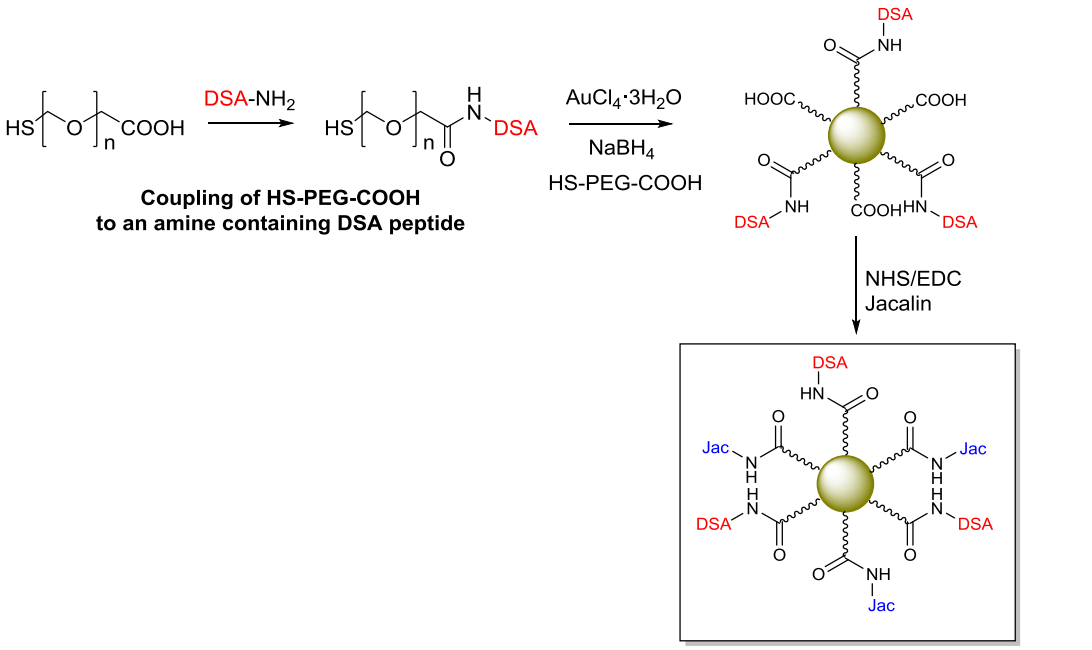

Scheme 5.3: schematic representation of a route to a AuNP-DSA-Jac conjugate utilising an initial coupling of HS-PEG-COOH to an amine containing DSA peptide.

c) A cleavable DSA peptide sequence attached to PEG and then incorporated into the 4 nm AuNP conjugate.

The synthesis of these four systems are described below.

5.3.2 Synthesis of 16 nm AuNP Functionalised with PEG, a Duocarmycin Peptide and Jacalin

The synthesis of the AuNP conjugate began with the 16 nm central AuNP core, which has been disclosed in the literature and proceeds via the reduction of gold tetrachloride trihydrate using sodium citrate.[228] The citrate also acts as a stabiliser of the gold core preventing the formation of aggregates. The success of this step was demonstrated through characterisation via Ultraviolet–visible spectroscopy (UV-Vis) (Figure 5.3). The 16 nm AuNPs have previously been shown to display a surface plasmon absorption band at 523 nm and this value was also obtained for the particles synthesised here.[228] Additionally, the deep red colour of the nanoparticles in solution suggested a successful synthesis of particles of the desired size. The

citrate-reduced gold nanoparticles were then decorated with a monolayer of PEG (3000 Da). The PEG utilised here was functionalised at one end with a thiol, for attachment to the gold nanoparticle core, and with a carboxylic acid at the other end to allow further functionalisation. For this, the citrate AuNPs were stirred with the HS-PEG-COOH in water prior to removal of excess PEG via passing the solution through a 100K MWCO spin column. The functionalisation of the gold nanoparticle core was confirmed via UV-Vis, which demonstrated the expected 3 nm red-shift in the plasmon absorption band of the nanoparticles post functionalisation (Figure 5.3).

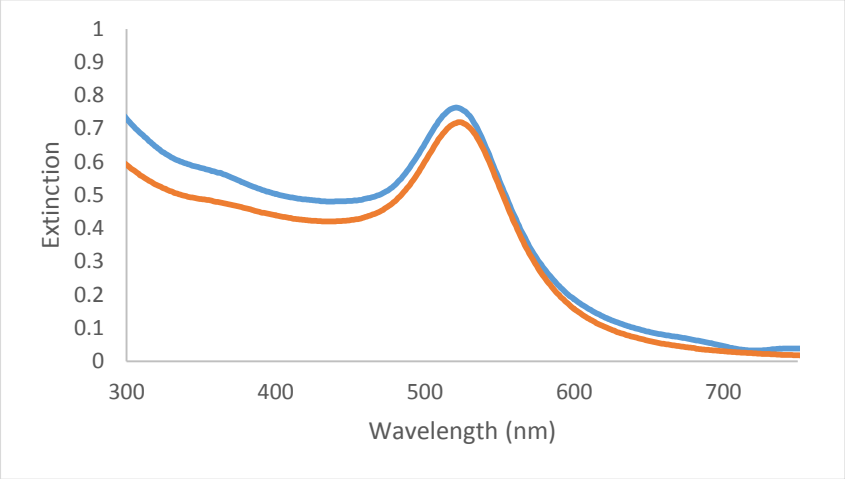

Figure 5.3: extinction spectrum of AuNP stabilised with citrate (blue) and AuNPs functionalised with a monolayer of HS-PEG-COOH (orange). The plasmon absorption band at 525 nm of the PEG functionalised particles is red shifted in comparison to citrate AuNPs (522 nm).

In order to further confirm that the correctly sized PEG functionalised AuNPs had been synthesised, transmission electron microscopy (TEM) was utilised. The images produced confirmed the particles had an average size of 15.7 ± 2.8 nm (n = 25) (Figure 5.4).

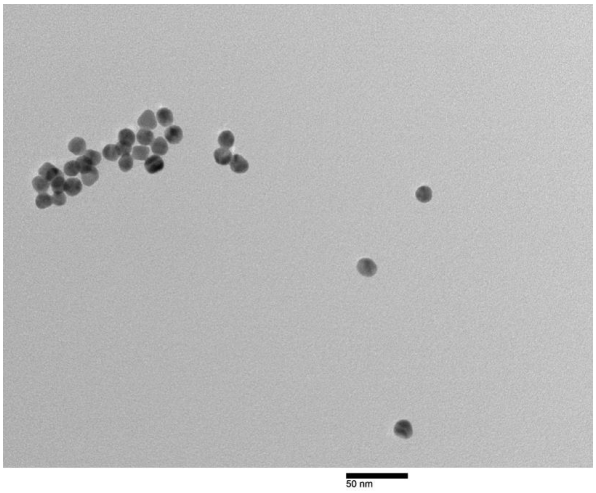

Figure 5.4: TEM image of 16 nm AuNP functionalised with a monolayer of HS-PEG-COOH. An average particle size of 15.7 nm was observed for these particles.

Next, investigations turned to the coupling of a peptide to the carboxylic acid residue of the PEG chain. It was projected that this could be achieved via the activation of the carboxylic acid of the PEG with EDC/NHS and then subsequent coupling with an amine residue on the peptide. In order to test this strategy, a short peptide sequence was synthesised containing a lysine residue – peptide **5.1** (Figure 5.5). Arginine residues were included in the sequence to aid the water solubility of this peptide since the nanoparticles are soluble, and stable, in water. A fluorescein isothiocyanate (FITC) tag was also included in the sequence as it was hoped this would help us to confirm the presence of the peptide on the AuNP using UV-Vis spectroscopy. For this early stage proof of concept study, and to reduce the use of the Fmoc-DSA-OH unit, (see Chapter 2, compound **2.10**) this warhead was omitted from the sequence.

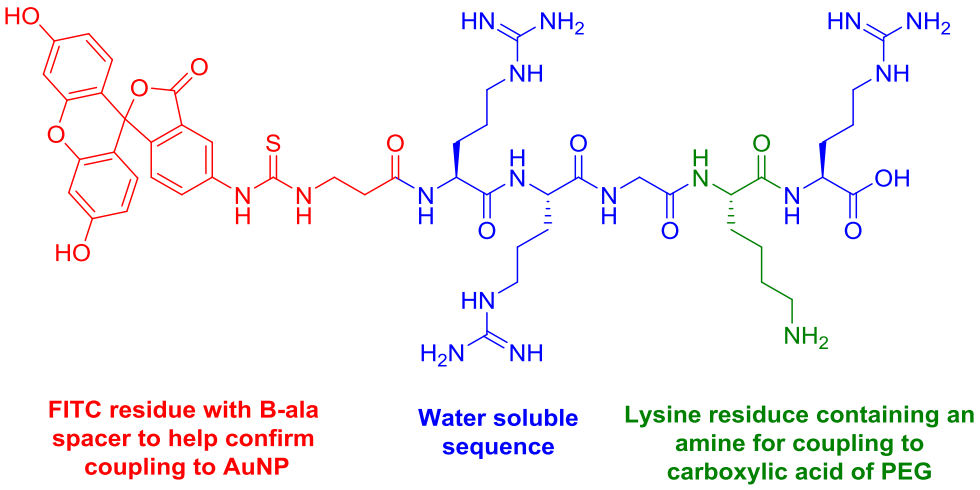

Peptide 5.1

Figure 5.5: chemical structure of peptide 5.1. In green is the lysine residue, in blue is a water soluble sequence and in red is the FITC tag.

The successful synthesis of this peptide sequence, following the standard SPPS conditions discussed in Chapter 2, Section 2.3.3.2 was confirmed using MALDI mass spectrometry and HPLC. The purity obtained for this peptide (>80%) was deemed acceptable for this initial investigation. With the amine containing peptide and the PEG functionalised AuNPs in hand, investigations began into the coupling of the two via an amide bond. For this, the 16 nm AuNP-PEG were suspended in MES buffer pH 5 and treated with EDC and NHS. After 30 mins, excess EDC and NHS were removed, and NHS activated particles resuspended in HEPES buffer at pH 7.4. Peptide **5.1** in water, was then added into the solution and the mixture stirred overnight (Scheme 5.4).

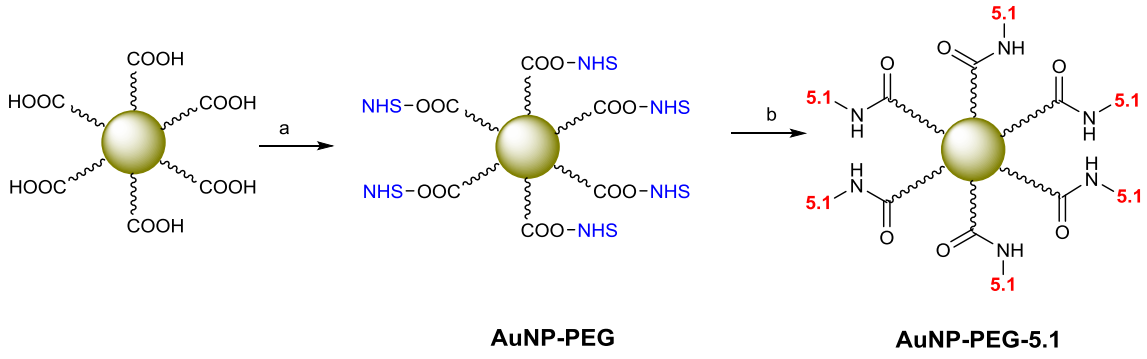

Scheme 5.4: attempted coupling of PEG-AuNP with peptide **5.1**. a: MES buffer (pH 5), NHS, EDC, 30min, rt, b: HEPES buffer (pH 7.4), peptide **5.1**, 24 h, rt

It was observed that a dark precipitate had formed in the reaction mixture and this was attributed to the aggregation of the gold nanoparticles. This suggested that the particles were either unstable within the HEPES buffer or were unstable to the coupling of **5.1**. After confirming that the HEPES buffer was not the cause of this instability, it appeared that the coupling, or interaction of the particles with **5.1** was undesirable. Despite this, the aggregate was removed and the supernatant was characterised to see if any of the **AuNP-PEG-5.1** conjugates remained in solution. Upon running the UV-Vis spectrum, it was evident that the concentration of particles remaining in solution was very low suggesting the amount of aggregation occurring was substantial. Additionally, it was apparent that the 16 nm particles presented another issue; the characteristic plasmon absorption band of 16 nm particles lies in the same region as the absorption of FITC (495 nm). Due to the intensity of the extinction from the particles, the peak from the FITC was masked and hence it was very difficult to characterise the coupling of the peptide to the particle surface. Without the FITC tag, the absorption of the peptide sequence itself, even with the duocarmycin unit is also likely to be masked by the particles extinction in the region below 300 nm. As a result, further characterisation techniques to confirm the presence of **5.1** on the gold nanoparticle were attempted. Both NMR and MALDI mass spectrometry however, returned inconclusive results.

The observed aggregation and characterisation issues presented here indicated that this initial strategy employed for the synthesis of a duocarmycin-AuNP conjugate may not be appropriate. Whilst further efforts, with other fluorescent tags with differing absorptions, such as those beyond 530 nm, may have resulted in a successful way to characterise these conjugates an alternative nanoparticle construct was investigated.

5.3.3 Synthesis of 4 nm AuNP Functionalised with a Mixed Monolayer of PEG, a Duocarmycin Peptide and Jacalin

It is possible that 4 nm AuNPs could present themselves as an advantageous alternative for the desired duocarmycin-AuNP system. This was the case for various reasons. Firstly, the synthesis of functionalised 4 nm particles has been completed within organic solutions.[111] This is ideal for a duocarmycin-

based construct since duocarmycin based peptides are often very hydrophobic and so an organic based synthetic procedure would aid in the solubility and stability of these agents during the particle assembly. Additionally, the characteristic UV-Vis extinction spectrum of 4 nm AuNPs does not show a strong plasmon absorption band at a wavelength similar to FITC unlike 16 nm particles.[111] This means that a FITC tagging strategy could be used to easily confirm the successful coupling of ligands onto the particle surface. These factors prompted the design of a strategy for the synthesis of a 4 nm AuNP-duocarmycin conjugate. Whilst the pharmacokinetic profile of these smaller particles may not be fully understood, this size would allow for the formation of workable system, which could then be scaled accordingly to achieve a desired set of properties. Additionally, with previous successful cellular studies being completed by other groups, the 4 nm systems presented themselves as an attractive alternative to a 16 nm core.

Following a procedure reported by Russell and co-workers, it was proposed that a 4nm AuNP core could be functionalised with a mixed monolayer of duocarmycin and PEG.[111] The PEG could then be used to couple jacalin for the active targeting to the T-antigen disaccharide. For this, Gold tetrachloride trihydrate can be reduced using sodium borohydride in the presence of HS-PEG-COOH and a thiol containing DSA peptide. This gives a mixed monolayer on a central 4 nm AuNP core. A thiol is required on the duocarmycin peptide to allow for formation of a Au-S bond and therefore functionalisation of the core. In a separate step, jacalin is then coupled onto the exposed carboxylic acid of the PEG via the lysine residue on the lectin.

In order for this strategy to be attempted, peptide **3.5** (Figure 5.6) was utilised, the synthesis and characterisation of which was discussed in Chapter 3, Section 3.3.3.

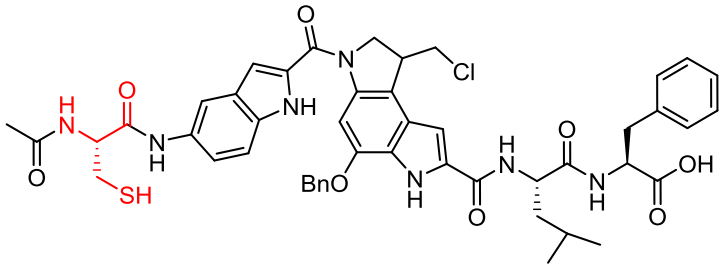

3.5

Figure 5.6: chemical structure of peptide **3.5** which contains a thiol residue for the formation of a Au-thiol bond.

This peptide was chosen as a proof of concept approach to the use of a cysteine-labelled duocarmycin analogue to build the nanoparticle. As noted in chapter 3, removal of the benzyl group from this system could prove problematic, but this was a not a consideration at this point.

The synthesis of the 4 nm AuNP conjugates containing PEG and DSA peptide proceeded via the reduction of gold tetrachloride trihydrate with sodium borohydride in water and THF. The stronger reducing agent used here, in comparison to sodium citrate, allows for the formation of smaller gold nanoparticles.[229] This reduction was performed in the presence of a 1:1 ratio of HS-PEG-COOH and **3.5** ligands that also help to stabilise the particles from aggregation (Scheme 5.5).

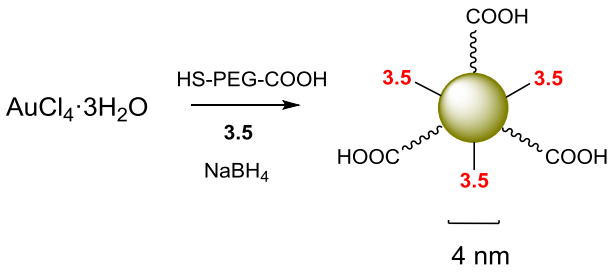

4 nm AuNP functionalised with a mixed monolayer of PEG and 3.5

Scheme 5.5: Synthesis of a 4 nm AuNP core functionalised with a mixed monolayer of SH-PEG-COOH and peptide **3.5**.

Upon completion of this step, excess ligands were removed from the solution by spinning through a 100K MWCO spin column and a UV-Vis extinction spectrum obtained for characterisation (Figure 5.7). The less intense surface

plasmon absorption band observed in the UV-Vis spectrum suggested a much smaller particle size than those synthesised in Section 5.3.2. In addition to the UV-Vis, TEM images showed that a mean particle diameter of 3.7 ± 1.2 nm (n = 45) had been synthesised (Figure 5.8).

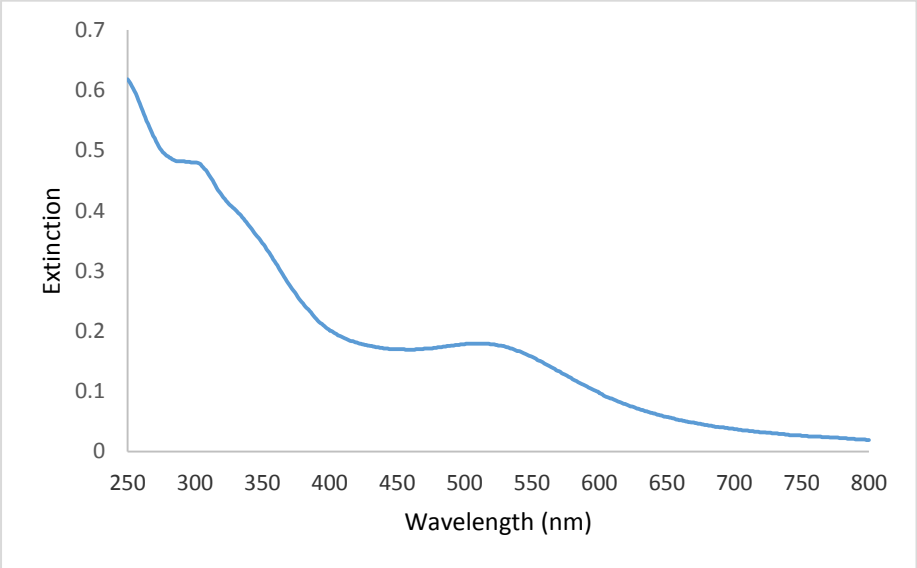

Figure 5.7: UV-Vis extinction spectrum of 4 nm AuNPs functionalised with PEG and DSA peptide **3.5** obtained after reaction of $AuCl_4 \cdot 3H_2O$, $NaBH_4$, HS-PEG-COOH and **3.5.**

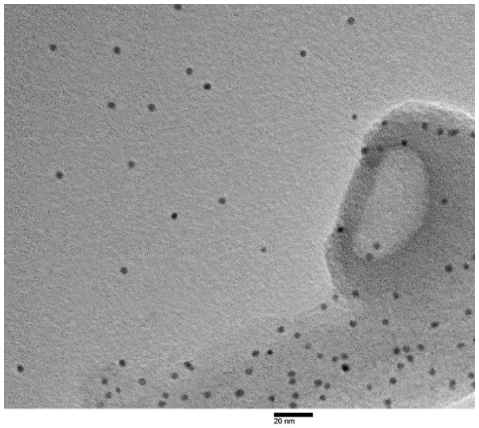

Figure 5.8: TEM image of AuNP functionalised with a mixed monolayer of PEG and peptide 3.5. An average particle size of 3.7 nm was observed for these particles.

The unusual shaped band at 300 nm suggested a possible coupling of **3.5** to the surface of the AuNP. Further evidence was required to indicate whether peptide **3.5** was coupled onto the surface of the nanoparticle. However, the attachment of the DSA peptide directly to the gold core, within a matrix of PEG, could prove to be problematic as this may restrict access to, for example, peptidases that could breakdown the peptide or the nucleic acid

target of the DSA. On this basis, coupled with the problematic nature of the benzyl deprotection of the thiol-containing DSA system, a second PEG-DSA 4 nm particle was designed.

5.3.4 Coupling of a DSA Peptide to PEG and Subsequent AuNP Conjugate Assembly

The new design involved the direct coupling of a DSA peptide to HS-PEG-COOH via an amide bond strategy and utilisation of this DSA-PEG conjugate and free HS-PEG-COOH in the assembly of the 4 nm AuNP. This would give a nanoparticle that was decorated with both DSA and free carboxylic acids for derivatisation to a targeting protein or peptide (such as jacalin).

Peptide **5.2** (Figure 5.9) was synthesised with a lysine residue for coupling to the carboxylic acid of the PEG and a FITC unit for confirmation of attachment to the particle surface. For the initial AuNP assembly, the benzyl protection of the DSA unit was kept in place to reduce handling of the cytotoxic agents.

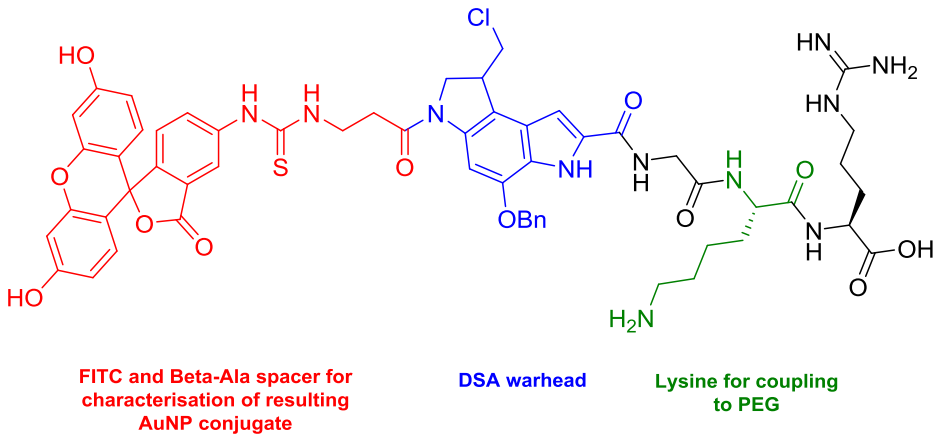

Figure 5.9: chemical structure of peptide **5.2**. In red is the FITC unit, in blue is the DSA warhead and in green the lysine residue for coupling to PEG prior to AuNP synthesis.

Following the conditions outlined in Chapter 2, Section 2.3.3.2, peptide **5.2** was successfully synthesised and characterised using MALDI mass spectrometry and HPLC. Following on from this, the peptide was coupled onto the HS-PEG-COOH using HATU/DIPEA coupling chemistry. A MALDI of the PEG was run post reaction, which showed a visible increase in the mass indicating a successful coupling to give the PEG-DSA conjugate (**PEG-**

5.2). Subsequently, $AuCl_4 \cdot 3H_2O$, in the presence of $NaBH_4$, was reacted with **PEG-5.2** along with HS-PEG-COOH in a 1:1 ratio. This reaction mixture was stirred overnight in the dark. Upon removal of excess ligand by centrifugation through a 100K MWCO spin column, the particles, in water, were characterised via UV-Vis spectroscopy. The resulting spectrum showed the characteristic shape of a 4 nm particle along with the presence of a band characteristic of FITC at 495 nm (Figure 5.10). This provided an indication that peptide **5.2** was present on the AuNP core.

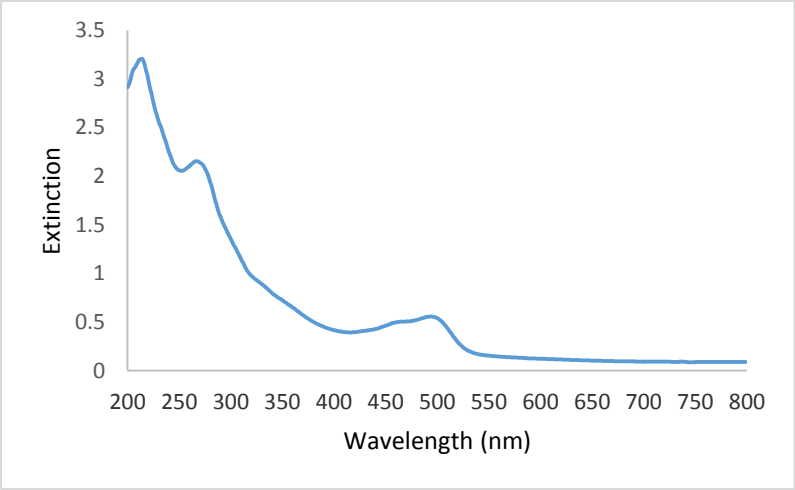

Figure 5.10: UV-Vis extinction spectrum of AuNP functionalised with **PEG-5.2**. Evident is the characteristic band of FITC at 495 nm suggesting successful coupling of the peptide onto the particle surface.

The next step was to test whether the jacalin could be coupled onto the free PEG that was also included in the reaction mixture. In order to do this, the synthesis was repeated with peptide **5.3** (Scheme 5.6), whose structure resembles **5.2** but without the FITC unit**.** This was so that a jacalin-FITC analogue could be used in the synthesis of the construct to ascertain whether the lectin had coupled onto the free PEG. The jacalin-FITC was synthesised through the stirring of jacalin in HEPES buffer with 20 equivalents of FITC isomer I. After 2 h, the excess FITC was removed through a 7K MWCO spin column and the presence of FITC on the jacalin surface confirmed using UV-Vis spectroscopy. Once the synthesis of the **AuNP-PEG-5.3** conjugate had been completed, the carboxylic acid of the PEG chains was activated with EDC and NHS. Subsequently, the jacalin-FITC was added into the solution and left to stir overnight in the dark. Following on from the removal of excess

jacalin by passing the reaction mixture through a 100K MWCO spin column, the **AuNP-PEG-5.3-Jac(FITC)** conjugate was characterised through UV-Vis spectroscopy and TEM. Evident here was the presence of the FITC band at 495 nm within the spectrum (Figure 5.11). Additionally, TEM (Figure 5.12) showed that an average particle size of 4.1 nm ± 1.4 (n = 50) had been obtained. This indicated the successful coupling of jacalin to the nanoparticle and hence suggested that the entire desired nanoparticle system had been synthesised.

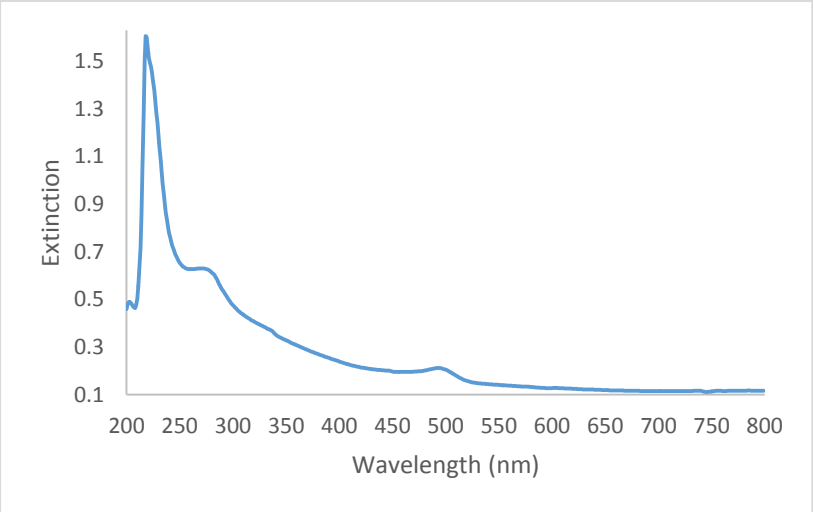

Figure 5.11: UV-Vis spectra of AuNP functionalised with PEG, 5.3 and jacalin-FITC. Evident is the FITC peak here, suggesting the successful coupling of the jacalin onto the free PEG carboxylic acid.

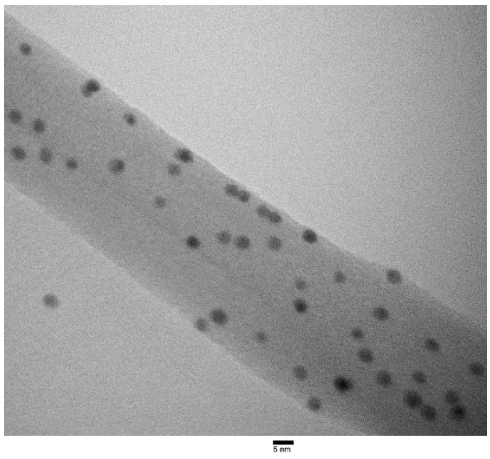

Figure 5.12: TEM images of AuNP-PEG-5.3-Jac(FITC) showing an average particle size of 4.1 nm.

With a method for building the entire construct in hand, it was next required to repeat the above synthesis but with the benzyl deprotected peptide of **5.3**.

This would provide the active AuNP conjugates for biological evaluation. The benzyl deprotection was achieved via the standard palladium on carbon, aqueous ammonium formate route introduced in Chapter 2, Section 2.3.4. (Scheme 5.6).

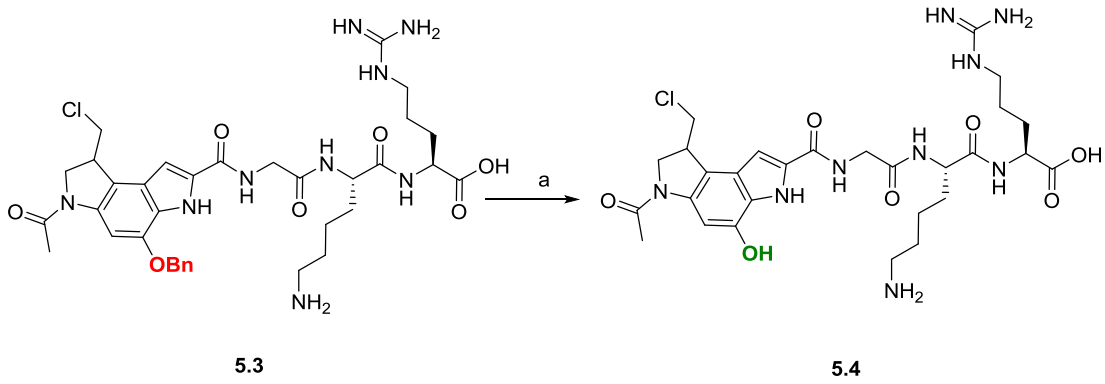

5.3 5.4

Scheme 5.6: benzyl deprotection of **5.3** to give the biologically active **5.4**. a: 10% Pd/C, 25% Aq. ammonium formate, MeOH, rt, 1 h

With this deprotection proceeding successfully as determined by the obtainment of the desired mass of 650.28 (calcd. (M+H)+, 650.27) for **5.4**, the repetition of the synthesis of the AuNP construct above could be completed. Peptide **5.4** was coupled onto the PEG unit and MALDI mass spectrometry again confirmed the increase in mass to the polymer backbone. The AuNP core was then synthesised as previously using PEG and **PEG-5.4** at a 1:1 ratio, before jacalin was coupled onto the free PEG carboxylic acid groups. This gave an overall structure termed here **AuNP-PEG-5.4-Jac**, as presented schematically in Figure 5.13 along with the UV-Vis extinction spectrum shown in Figure 5.14.

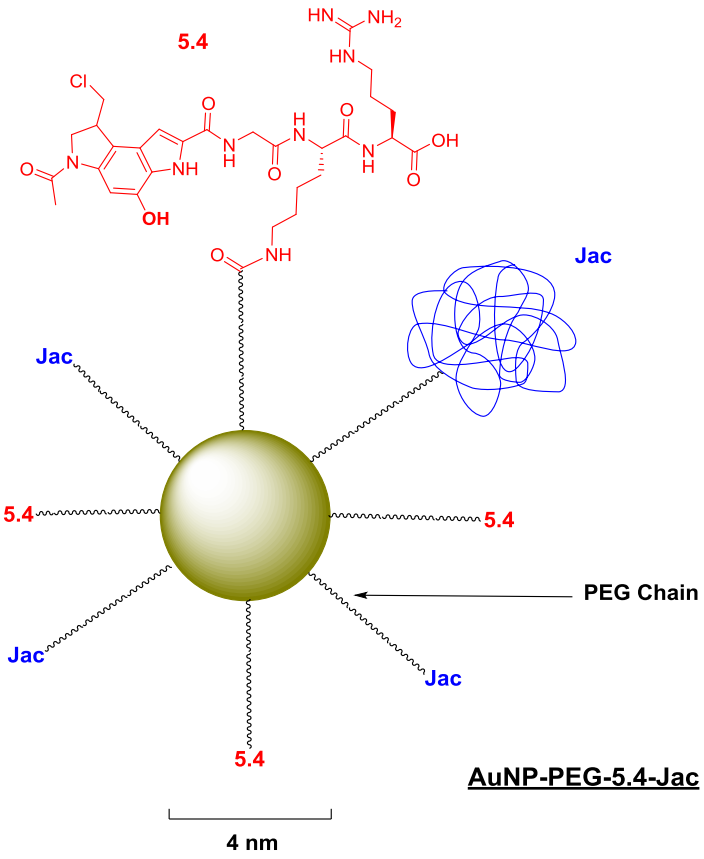

Figure 5.13: schematic representation of the synthesised **AuNP-PEG-5.4-Jac** conjugate.

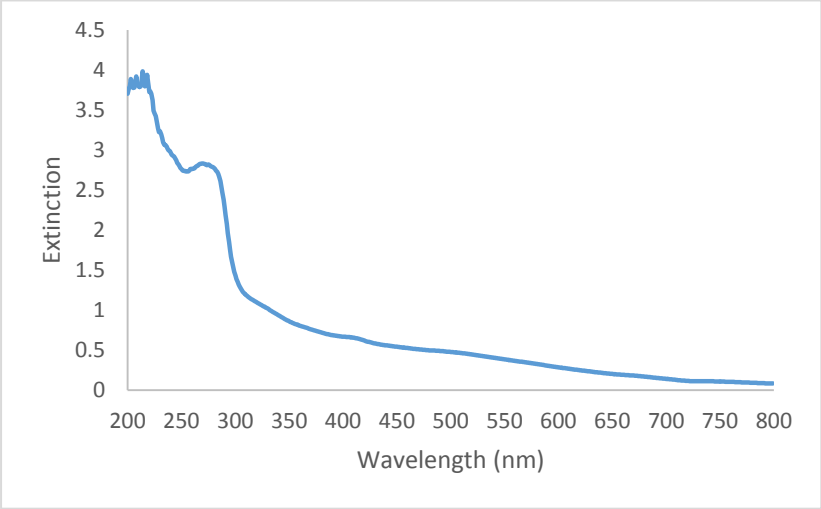

Figure 5.14: UV-Vis extinction spectrum of **AuNP-PEG-5.4-Jac** in water.

5.3.5 Synthesis of a Duocarmycin-AuNP Construct Containing a Cleavable Sequence

As a final AuNP construct for investigation, it was proposed that a cleavable sequence could be introduced into the **AuNP-PEG-5.4-Jac** conjugates.

Upon cellular internalisation, it was projected that the cleavable sequence could be used to release the duocarmycin unit from the AuNP more efficiently, allowing it to enter the nucleus and alkylate the DNA. This could in turn demonstrate improved cellular activity in comparison to the **AuNP-PEG-5.4-Jac** construct. It was this proposition that led to investigations into peptide **4.7** (Figure 5.15) as a potential peptide for introduction into the AuNP construct. This peptide was introduced in Chapter 4, Section 4.3.1.3 of this thesis where its design, synthesis and characterisation were discussed in detail.

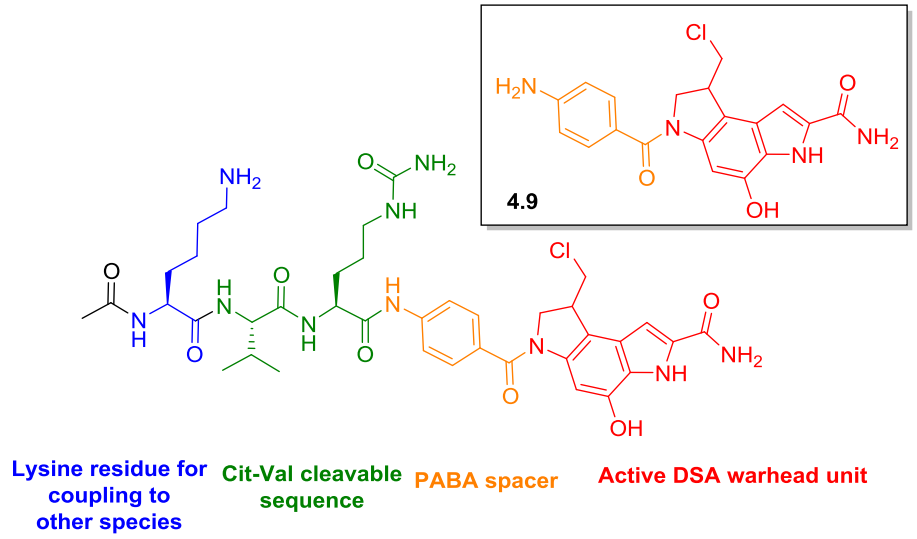

Figure 5.15: chemical structure of 4.7 and 4.9.

In Chapter 4, the biological activity of **4.7** along with its cleavage product (**4.9**) was presented. It was this activity that prompted investigations into this peptide within an AuNP construct. The possibility that the activity of **4.7** might be lower than expected due to poorer cellular internalisation in comparison to its cleavage product (**4.9**) was previously discussed. However, with proven ability to be taken up by the cells, it could be that the AuNP construct could help this peptide show more potent activity than that observed in Chapter 4. Peptide **4.7** also contains the required amine handle on the lysine residue to be attached to the PEG prior to AuNP assembly.

With **4.7** in hand, the assembly of the AuNP construct, in the same manner as detailed in Section 5.3.4, was completed to give **AuNP-PEG-4.7-Jac** (Figure 5.16).

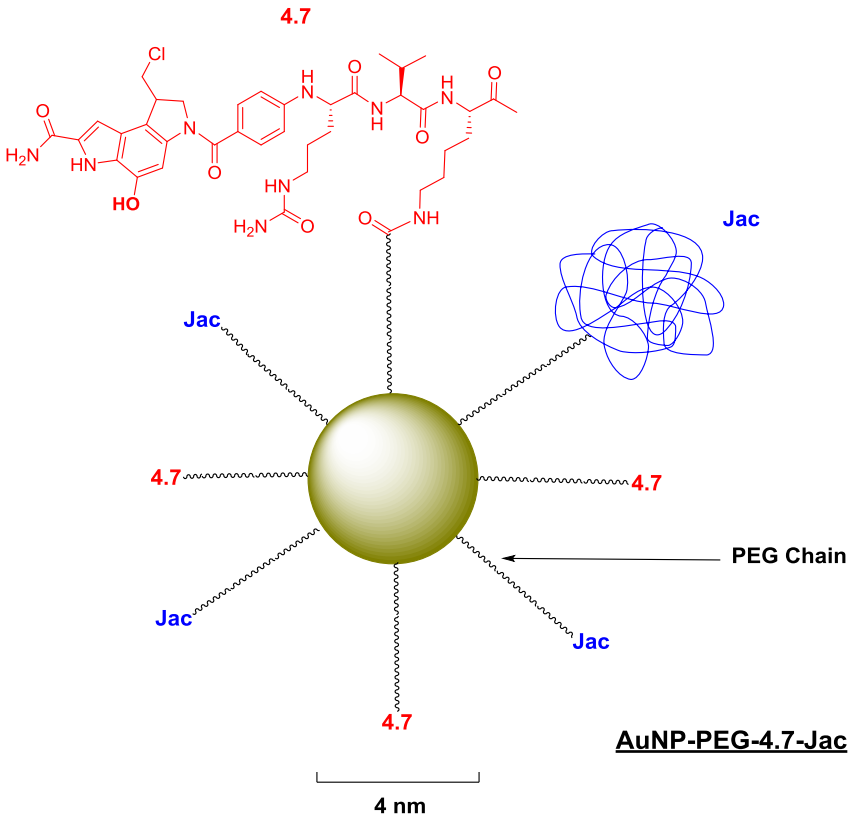

Figure 5.16: schematic representation of the AuNP-PEG-4.7-Jac construct. A cleavable sequence is included to test whether efficient release of the DSA warhead from the AuNP conjugate results in improved activity.

The UV-vis extinction spectrum and TEM images of these particles are shown in Figure 5.17 and Figure 5.18 respectively.

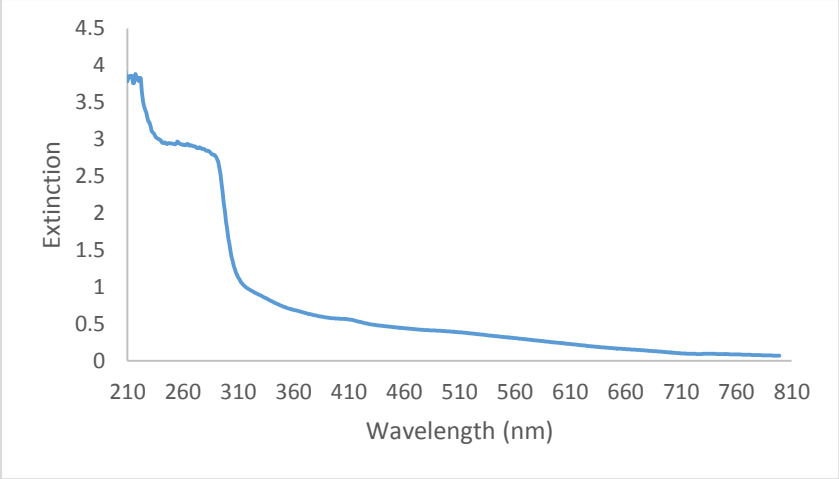

Figure 5.17: extinction spectrum of **AuNP-PEG-4.7-Jac**

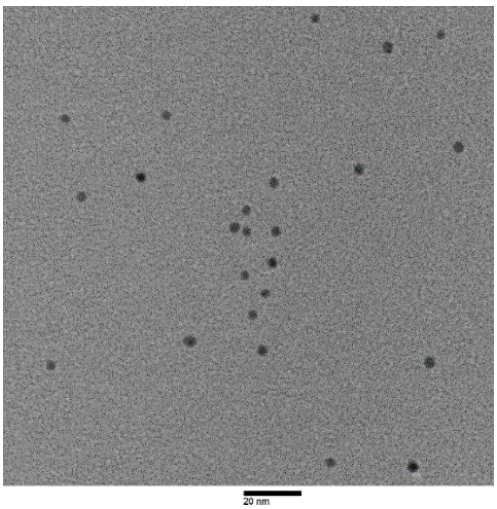

Figure 5.18: TEM image of **AuNP-PEG-4.7-Jac** showing an average particle size of 4.4 nm ± 1.3 (n = 50).

5.3.6 Biological Evaluation of AuNP-PEG-DSA-Jac Conjugates

5.3.6.1 Biological Evaluation of AuNP-PEG-5.4-Jac

For these studies the **AuNP-PEG-5.4-Jac** were tested on an MCF-7 human breast cancer cell line due to its high T-antigen expressing properties.[149, 151] It was also decided that the same nanoparticle construct but without the jacalin unit attached would be assessed here to see if any differing activity was obtained.

The concentration of a stock solution of particles was determined using the particle UV-Vis extinction absorption at 450 nm and an extinction coefficient of 3.62×10^6 M cm^{-1} as suggested in a report by Fernig and co-workers.[230]

Dilutions of this stock were then made to give final well concentrations of 18.2 nM, 1.82 nM, and 0.182 nM.

The MCF-7 cells were incubated for 72 h after treatment with **AuNP-PEG-5.4-Jac** and **AuNP-PEG-5.4**. **AuNP-PEG** and **AuNP-PEG-Jac** were also synthesised and included in the assay as controls. Following the incubation period, the cell viability was analysed via an MTS assay. Upon analysis, it became evident that none of the nanoparticle constructs tested in the assay had caused cell death, even at the highest concentrations. The lack of activity obtained was attributed to two possible factors. Firstly, it could be that the particles themselves were not able to enter the cells and hence the duocarmycin warhead was unable to reach the nucleus to exert its biological activity. Alternatively, it could be that since the duocarmycin warhead is attached to the AuNP construct via a stable, non-cleavable amide linkage, once internalised within the cell, it might be unable to again access the nucleus to exert its activity on the DNA.

In order to test the former possibility, the FITC analogues of the AuNP construct discussed in Section 5.3.4 of this chapter were used to obtain fluorescent microscopy images of the cells lines after treatment with the particles. It was hoped this would identify whether the particles were entering the cell or not. For these studies, MCF-7 cells were incubated with a 16.4 nM solution of **AuNP-PEG-5.3-Jac(FITC)** for 4 h after which time, the cells were visualised via a fluorescent microscope (Figure 5.19).

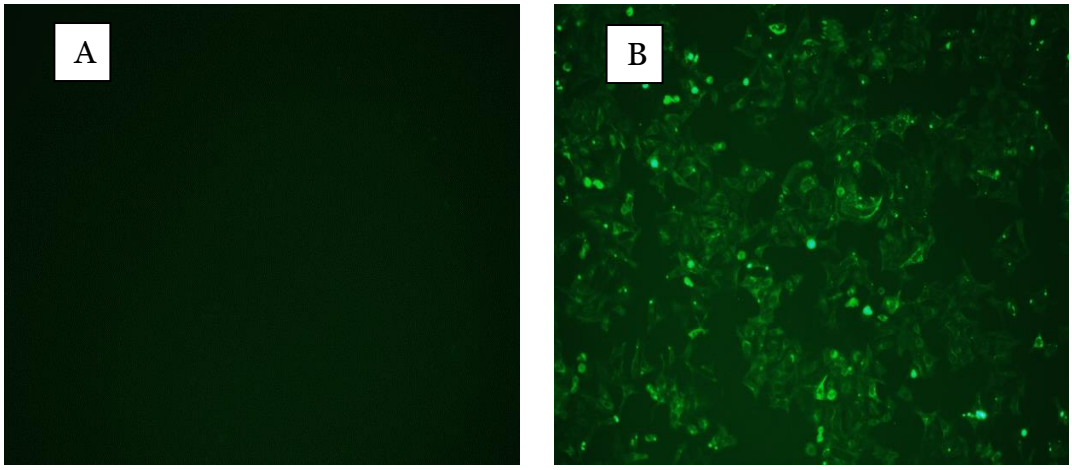

Figure 5.19: fluorescence microscopy images of A: MCF-7 cells incubated solely with buffer and B: MCF-7 cells incubated in the presence of **AuNP-PEG-5.3-Jac(FITC)**. The fluorescence visible within the cells indicates that the AuNP construct is being taken up by the cells.

The above images demonstrate that the nanoparticle construct containing peptide **5.3** and jacalin are taken up by the cell line and hence the lack of activity is unlikely to be caused by a lack of cellular uptake. For this reason, attention turned to the possibility that the lack of activity could be due to the non-cleavable nature of the linker between the active duocarmycin unit and the AuNP which is preventing the warhead from exerting its desired effect.

5.3.6.2 Biological Evaluation of AuNP-PEG-4.7-Jac

The biological evaluation of **AuNP-PEG-4.7-Jac** was completed in a variety of cell lines in a similar manner to that in Section 5.3.6.1. This time however, MCF-7 human breast cancer cells, HL60 human leukaemia cells and HCT116 human colon carcinoma cell lines were used to analyse the activity of the AuNPs at 19.4 nM, 1.94 nM and 0.194 nM final well concentrations. Disappointingly, MTS analysis of this construct within the various cell lines demonstrated no evidence of cell death. With high activity being obtained for peptide **4.7** in previous studies, this result came as a surprise.

These were preliminary studies of this system and, due to time constraints, they were not pursued further. Studies that confirm the cleavage of the duocarmycin ligand from the nanoparticle core are critical as the next step for research into this AuNP construct. Since the cellular uptake of these particles has been confirmed within certain cell lines, it appears that the

inability of the duocarmycin to reach the DNA to exert its activity could be a cause for the lack of activity observed. It is possible that the cathepsin B enzyme, required to cleave the PABA-Cit-Val sequence, is unable, sterically, to reach the peptide substrate on the AuNP. This in turn would result in lack of cleavage of the active drug from the AuNP system and therefore a lack of biological activity.

Following these studies, it will be important to ascertain the amount of jacalin functionalised onto the surface of these constructs. In similar systems with antibodies, it has been shown that this variable is vital in achieving a desired activity.[231] Specifically, there is an optimum amount of protein that is required on the outer surface of the particle. Additionally, a more thorough evaluation of the concentration of drug loaded onto the particle surface may help to understand the reason for the lack of activity. Higher concentrations of particles or a higher loading value might be required in order to see the desired activity within the various cell lines. Whilst the FITC peak within the UV-Vis spectra can be used to provide a rough indication of the level of drug loading, the accuracy of this approach is low. This is because of the FITC absorption band (495 nm) being close to, and hence likely to interact with, the region used to determine the particle concentration (450 nm). A more robust method to determine this information would be helpful to gain a better understanding of the biological analysis conducted here.

5.4 Conclusions

The aim of the research in this chapter was to design, synthesise and biologically evaluate a duocarmycin gold nanoparticle conjugate. The conjugate was also to be functionalised with jacalin to allow for an active targeting strategy of the particles to the T-antigen disaccharide and hence cancerous tissue.

A 16 nm AuNP core was originally investigated for the synthesis of this conjugate constructs. However, due to issues regarding ligand attachment characterisation to the particle and also the need for an aqueous synthetic procedure, investigations into this area were discontinued.

A 4 nm core was found to be a more advantageous alternative due to the ability to synthesise these conjugates in organic media. Additionally, their characteristic UV-Vis spectrum allows for a FITC tagging strategy to be utilised to characterise ligand attachment to the central nanoparticle core. Various strategies were attempted to form the 4 nm particle conjugates but it was one in which a duocarmycin peptide was coupled to PEG prior to nanoparticle assembly that showed most success.

Originally a non-cleavable amide linkage was employed to attach the duocarmycin to the PEG. However, with this construct showing no activity but proven cellular internalisation, a peptide sequence containing a PABA-Cit-Val cleavable sequence was investigated. This was introduced into the AuNP construct but again no activity was observed across a variety of cell lines.

Despite the lack of activity seen within this construct, the potential of AuNP systems in helping to achieve the targeted delivery of duocarmycin based analogues to cancerous tissue means future work into this area is warranted. Of particular interest would be further investigations into determining the optimum concentrations of jacalin and duocarmycin ligands attached to the central nanoparticle core. A greater understanding and control over these variables may aid in the formation of an active construct. Despite these variables being of considerable importance, one of the inherent difficulties with gold nanoparticle systems is how hard it can be to define the level of functionalisation occurring to their surface. This is especially a problem when the ligand, like duocarmycin, does not contain any intense characteristic UV-Vis bands above 300 nm.

Once the reason for a lack of activity has been identified within this system, the construct itself lends itself well to being modified with various targeting moieties. With antibodies and small molecules already having shown good activity in nanoparticle systems these could also be used within this AuNP-duocarmycin conjugate to get targeted delivery to other desirable disease locations. The applicability of the system designed here is therefore one of its possible strengths.

5.5 Experimental

5.5.1 General Procedures

Reagents and Solvents

All chemicals were reagent grade and were purchased from Sigma Aldrich, Fisher Scientific and Tokyo Chemical Industry. Fmoc-amino acids and coupling reagents were purchased from Novabiochem, Fluorochem or AGTC Bioproducts. Anhydrous solvents were bought from Sigma Aldrich and assumed to conform to specification. Vivaspin™ 500 (100 kDa MWCO; PES membrane) centrifuge columns were purchased from Sartorius Stedim Biotech (UK). The α-thio-ω-carboxy polyethylene glycol (3,000 Da; PEG) was purchased from Iris Biotech GmbH (Germany). Jacalin was purchased from Vector laboratories (UK).

Physical Characterisation and Spectroscopic Techniques

^{1}H- and ^{13}C-NMR spectra were recorded on a Bruker spectrometer operating at 400 MHz (^{1}H) or 100 MHz (^{13}C) using the specified deuterated solvent. The chemical shifts for both ^{1}H- and ^{13}C were recorded in ppm and were referenced to the residual solvent peak of DMSO at 2.50 ppm (^{1}H) and 39.5 ppm (^{13}C). Multiplicities in the NMR spectra are described as s = singlet, d = doublet, t = triplet, q = quartet, m = multiplet, br = broad, and combinations thereof; coupling constants are reported in Hz. MALDI mass spectrometry was performed on Kratos Analytical Axima MALDI-TOF. Low resolution mass spectra were recorded using a Shimadzu LCMS 2010EV operated under electrospray ionisation in positive (ES+) mode. Accurate mass spectra were recorded at the EPSRC National Mass Spectroscopy Service Centre, Swansea. UV-vis spectra of the samples were recorded using a Hitachi U-300 spectrophotometer at room temperature. Quartz cuvettes with a 1 cm path length were used.

Chromatographic Techniques

Analytical RP-HPLC was performed on an Agilent 1200 using an Agilent eclipse XDB-C18 column, 4.6 x 150 mm, 5 μM and a flow rate of 1 mL/min. Solvent A = Water + 0.05% TFA and Solvent B = MeOH + 0.05% TFA. Gradient 5% B up to 95% B over 20 minutes. Detection wavelength 214 nm and 254 nm. Semi-preparative RP-HPLC was performed on an Agilent 1200

using an Agilent eclipse XDB-C18 column, 9.4 x 250 mm, 5 μM and a flow rate of 4 mL/min. Solvent A = Water + 0.05% TFA and Solvent B = MeOH + 0.05% TFA. Gradient 5% B up to 95% B over 20 minutes. Detection wavelength 214 nm and 254 nm. Preparative RP-HPLC was performed on an Agilent 1200 using an Agilent eclipse XDB-C18 column, 21.2 x 150 mm, 5 μM and a flow rate of 20 mL/min. Solvent A = 95% H_2O + 5% MeOH + 0.05% TFA and Solvent B = 95% MeOH + 5% H_2O + 0.05% TFA. Gradient 5% B up to 95% B over 20 minutes.

TEM imaging

For TEM imaging, an aliquot of PEG modified gold nanoparticles (500 μL) was centrifuged in a Vivaspin™ 500 (100 kDa MWCO, PES) tube at 14,300 xg at 4 °C for 30 min. The concentrated sample (10 μL) was then spotted onto Holey Carbon Film 300 Mesh Cu (50) TEM grid (Agar Scientific) on top of adsorbent filter paper. The nanoparticle sample was imaged using a JEOL 2000EX TEM operating at 200 kV accelerating voltage. The assistance of Dr Colin MacDonald (School of Chemistry, University of East Anglia) during the TEM imaging is gratefully acknowledged.

5.5.2 AuNP and Peptide Synthesis

Synthesis of Citrate Capped Gold Nanoparticles

Aqueous solutions of trisodium citrate (50 mL, 1.3 mM) and gold (III) chloride trihydrate ($HAuCl_4$, 100 mL, 0.2 mM) were prepared. The solutions were heated to 60 °C, combined with rigorous stirring and heated to 85 °C for 2.5 h. Once cooled to room temperature, the nanoparticle solution was filtered using sterile syringe driven filter units (0.22 μm polyethersulfone (PES), Millipore; MillexTM) to remove aggregates and stored at 4°C.

Functionalisation of 16 nm Citrate Particles with PEG

PEG (32.7 mg, 1 mM, 3,274 Da) was self-assembled for 15 h onto citrate capped gold nanoparticles (10 mL, ca. 19 nM). Following self-assembly, unbound PEG was removed from the sample by 4 repeated ultrafiltrations in Vivaspin™ 500 tubes (100 kDa MWCO, PES) by centrifuging at 14,000 rpm at 4 °C for 20 min. Following every centrifugation, the PEG modified gold nanoparticles were redispersed in an equal volume of 2-(*N*-morpholino)ethanesulfonic acid buffer (MES, 50 mM, pH 5.5; Sigma-

Aldrich). The PEG modified gold nanoparticles were then characterised using UV-visible spectroscopy and transmission electron microscopy (TEM) imaging.

Peptide 5.1 Synthesis

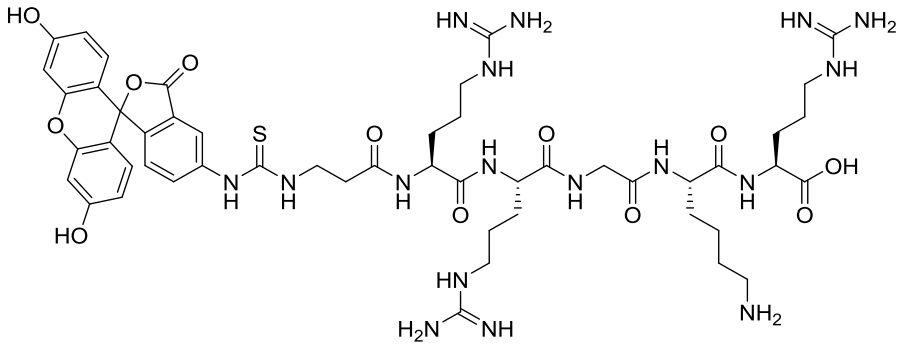

Peptide 5.1

H-Arg(Pbf)-2ClTrt resin (100 mg, 0.067 mmol, [manufacturer's resin loading 0.67 mmol/g]) was prepared for coupling by swelling in dichloromethane (DCM) for 30 mins followed by N,N-dimethylformamide (DMF) for 30 mins. Fmoc-Lys(Boc)-OH (156 mg, 0.335 mmol) was dissolved in 2 mL of DMF and treated with HATU (127 mg, 0.335 mmol) and DIPEA (116 µL, 0.67 mmol). After 10 secs the resulting solution was added to the resin and the mixture shaken for 2 h. Subsequently, the resin was washed with DMF (6 x 10 mL) and the coupling repeated. The resin was washed 6 times with DMF (10 mL) before removal of the lysine Fmoc using piperidine in DMF (6 mL 40% 10 mins, 6 mL 20% 5 mins twice). Following Fmoc deprotection the resin was washed with DMF (6 x 10 mL). Next, Fmoc-Gly-OH (99 mg, 0.335 mmol) was dissolved in 2 mL of DMF and treated with HATU (127 mg, 0.335 mmol) and DIPEA (116 µL, 0.67 mmol). After 10 secs the resulting solution was added to the resin and the mixture shaken for 2 h. The resin was subsequently washed with DMF (6 x 10 mL) before the Fmoc group on the glycine removed using piperidine in DMF (6 mL 40% 10 mins, 6 mL 20% 5 mins twice). The resin was then washed again with DMF (6 x 10 mL) before being treated with Fmoc-Arg(pbf)-OH (217 mg, 0.335 mmol) HATU (127 mg, 0.335 mmol) and DIPEA (116 µL, 0.67 mmol). The mixture was shaken for 2 h before the resin was washed with DMF (6 x 10 mL). The arginine Fmoc group was removed using piperidine in DMF (6 mL 40% 10 mins, 6 mL 20% 5 mins twice). Upon washing of the resin with DMF (6 x 10 mL), the resin

was treated again with Fmoc-Arg(Pbf)-OH, HATU and DIPEA in the same quantities as previously. Upon Fmoc deprotection of the second arginine residue with piperidine (6 mL 40% 10 mins, 6 mL 20% 5 mins twice) the resin was treated with Fmoc-βAla-OH (104 mg, 0.335 mmol) HATU (127 mg, 0.335 mmol) and DIPEA (116 μL, 0.67 mmol) and left to react for 2 h. Subsequently the resin was washed with DMF (6 x 10 mL) and the β-alanine Fmoc group removed using piperidine in DMF (6 mL 40% 10 mins, 6 mL 20% 5 mins twice). Following on from this, the resin was washed with DMF (6 x 10 mL) and treated with fluorescein isothiocyanate isomer I (29 mg, 0.074 mmol), in pyridine (500 μL), DMF (292 μL) and DCM (208 μL) and left to react overnight in the dark. Following overnight shaking, the resin was washed with DMF (6 x 10 mL) and then DCM (6 x 10 mL). Cleavage of **5.1** from the resin was affected by addition of a solution of 47% TFA, 10% TIPS in DCM (10 mL). After 3 h of shaking the cleavage mixture was filtered. The resin was rinsed with DCM (2 x 3 mL) and the combined filtrates were evaporated to dryness under reduced pressure and analysed using RP-HPLC (RT = 10.3 min) and MALDI mass spectrometry for **5.1** (M + H)+, found, 1133.64).

Coupling of Peptide 5.1 to 16 nm AuNP-PEG

5.1 was conjugated to the PEG on the surface of the 16 nm AuNPs via the terminal carboxyl groups in the PEG ligand using a previously reported method but with modifications.[228] The conjugation was performed via an amide linkage through *N*-(3-dimethylaminopropyl)-*N*'-ethylcarbodiimide hydrochloride (EDC) and *N*-hydroxysuccinimide (NHS) coupling. 16 nm PEG functionalised AuNPs (2 mL, 29 nM) in water were treated with EDC (0.8 μL, 0.005 mmol) and NHS (1.2 mg, 0.01 mmol) and left to stir for 30 mins at room temperature. Excess EDC/NHS was removed by ultrafiltration in Vivaspin™ 500 columns (100 kDa MWCO) at 14,000 rpm for 30 min at 4 °C. The NHS-ester functionalised AuNP-PEG were redispersed in water (2 mL) and added to with 5.1 in DMF (1 mg, 0.8 μmol). The solution was stirred overnight at room temperature in the dark. Following overnight incubation, the precipitated particles were removed by centrifugation (14,000 rpm, 10 mins, 4 °C) and any unbound **5.1** removed by ultrafiltration in Vivaspin™

500 columns (100 kDa MWCO) by centrifuging at 14,000 rpm for 30 min at 4 °C. The resulting AuNP pellet was redispersed in ddH_2O and analysed using UV-vis spectroscopy before being stored at 4 °C.

Synthesis of 3.5

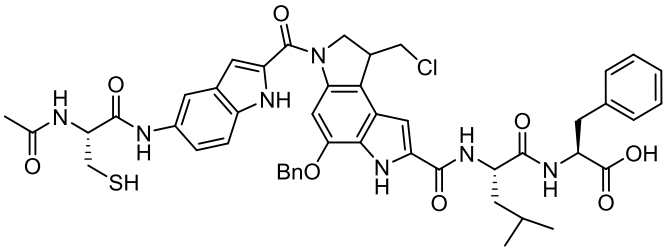

3.5

For details of the synthesis and characterisation of peptide 3.5, please refer back to Chapter 3, Section 3.5.2.

Synthesis of 4 nm AuNP Functionalised with a Mixed Monolayer of 3.5 and PEG

Gold nanoparticles (ca. 4 nm diameter) were synthesised in DMF and stabilised with a mixed monolayer of **3.5** and PEG. **3.5** (0.7 mg, 7 μmol) was dissolved in tetrahydrofuran (THF, 1 mL). The PEG (7.5 mg, 2 μmol) was dissolved in DMF (2 mL) and then stirred with the **3.5** solution for 5 min. Gold (III) chloride trihydrate (1.2 mg, 3 μmol) was dissolved in DMF (1.2 mL) and combined with the **3.5** and PEG solution and stirred for a further 5 min. A fresh solution of sodium borohydride (1.5 mg, 0.04 mmol) in DMF (1.2 mL) was prepared and rapidly added to the solution of the gold chloride, 3.5 and PEG under vigorous stirring. The reaction was stirred overnight at room temperature. Following overnight incubation, the mixture was evaporated to dryness under reduced pressure and resuspended in dH_2O (10 mL) to precipitate excess **3.5** which was subsequently removed via centrifugation (14,000 rpm, 10 min, 4 °C). The remaining aqueous solution was transferred to Vivaspin™ 500 (100 kDa MWCO) columns and centrifuged at 14,000 rpm for 10 min at 4 °C. The remaining functionalised AuNPs were then resuspended in ddH_2O and analysed using UV-vis spectroscopy and TEM before being stored at 4 °C.

Synthesis of 5.2

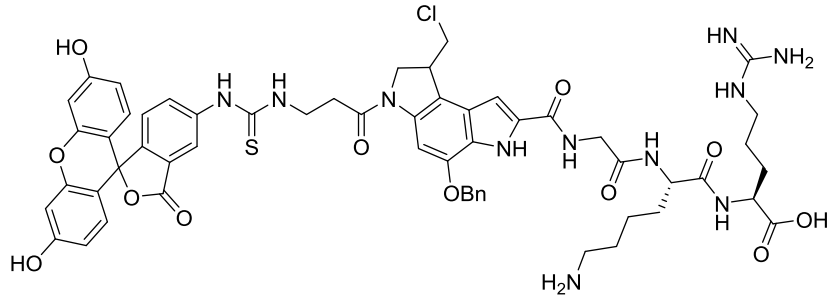

Peptide 5.2

H-Arg(pbf)-2ClTrt resin (50 mg, 0.034 mmol, [manufacturer's resin loading 0.68 mmol/g]) was prepared for coupling by swelling in DCM for 30 mins followed DMF for 30 mins. Fmoc-Lys(mtt)-OH (106 mg, 0.17 mmol) was dissolved in 2 mL of DMF and treated with HATU (65 mg, 0.17 mmol) and DIPEA (60 μL, 0.34 mmol). After 10 secs the resulting solution was added to the resin and the mixture shaken for 2 h. Subsequently, the resin was washed with DMF (6 x 10 mL) and the coupling repeated. The resin was washed 6 times with DMF (10 mL) before removal of the lysine Fmoc using piperidine in DMF (6 mL 40% 10 mins, 6 mL 20% 5 mins twice). Following Fmoc deprotection the resin was washed with DMF (6 x 10 mL). Next, Fmoc-Gly-OH (50 mg, 0.17 mmol) was dissolved in 2 mL of DMF and treated with HATU (65 mg, 0.17 mmol) and DIPEA (60 μL, 0.34 mmol). After 10 secs the resulting solution was added to the resin and the mixture shaken for 2 h. The resin was subsequently washed with DMF (6 x 10 mL) before the Fmoc group of the glycine removed using piperidine in DMF (6 mL 40% 10 mins, 6 mL 20% 5 mins twice). The resin was then washed again with DMF (6 x 10 mL) before being treated with **2.10** (30 mg, 0.05 mmol), HATU (19 mg, 0.05 mmol) and DIPEA (18 μL, 0.10 mmol) in DMF (2 mL) and the mixture shaken overnight. The resin was subsequently washed with DMF (6 x 10 mL) before the Fmoc group on the indoline nitrogen of **2.10** removed using piperidine in DMF (6 mL 40% 10 mins, 6 mL 20% 5 mins twice). The resin was then washed again with DMF (6 x 10 mL) before being treated with Fmoc-βAla-OH (53 mg, 0.17 mmol) which had been reacted for 10 secs with HATU (65 mg, 0.17 mmol) and DIPEA (60 μL, 0.14 mmol) in DMF (2 mL). The resulting mixture was left to react for 2 h. Subsequently the resin was washed with DMF (6 x 10 mL) and the β-alanine Fmoc group removed using

piperidine in DMF (6 mL 40% 10 mins, 6 mL 20% 5 mins twice). Following on from this, the resin was washed with DMF (6 x 10 mL) and treated with fluorescein isothiocyanate isomer I (15 mg, 0.04 mmol), in pyridine (500 μL), DMF (291 μL) and DCM (209 μL) and left to react overnight in the dark. Following overnight shaking, the resin was washed with DMF (6 x 10 mL) and then DCM (6 x 10 mL). Cleavage of **5.2** from the resin was affected by addition of a solution of 47% TFA, 10% TIPS in DCM (10 mL). After 3 h of shaking the cleavage mixture was filtered. The resin was rinsed with DCM (2 x 3 mL) and the combined filtrates were evaporated to dryness under reduced pressure and analysed using RP-HPLC (RT = 15.4 min) and MALDI mass spectrometry for **5.2** (M + H)+, 1159.56).

Synthesis of PEG-DSA peptide conjugates

PEG (7.5 mg, 2.29 μmol) was dissolved in DMF (300 μL) and treated with HATU (0.87 mg, 2.29 μmol) and DIPEA (3.98 μL, 22.9 μmol). After 10 s, the amine containing DSA peptide (22.9 μmol, 10 equiv.) was added and the resulting reaction stirred overnight at room temperature. Subsequently, the reaction was evaporated to dryness under reduced pressure and the PEG-DSA conjugate washed with diethyl ether (5 mL). The crude PEG-DSA conjugated was then analysed using MALDI mass spectrometry before being utilised in the respective AuNP assembly.

Assembly of AuNP-PEG-5.2

PEG-5.2 (7.5 mg; 5 μmol) and PEG (7.5 mg, 4.9 μmol) were dissolved in dH_2O (15 mL) and left to stir at room temperature. Then, $HAuCl_4 \cdot 3H_2O$ (1.2 mg; 3 μmol) was dissolved in THF (1.2 mL), added to the **PEG-5.2**/PEG solution and stirred at room temperature for 5 min. A fresh solution of $NaBH_4$ (1.5 mg; 39 μmol) in dH_2O (0.5 mL) was prepared and added to the PEG-$HAuCl_4$ mixture. The reaction was stirred for 4 h at room temperature. Purification of the AuNPs was then performed. Firstly, the THF was evaporated by rotary evaporation under reduced pressure. The resulting aqueous solution was transferred to Vivaspin™ 500 (100 kDa MWCO) columns and centrifuged at 14,000 rpm for 10 min at 4 °C. The **AuNP-PEG-5.2** were resuspended in MES buffer (16.7 mL) and filtered through a Millex

GP syringe driven filter unit (0.22 μm). The UV-vis extinction spectrum was recorded between 250-800 nm. **AuNP-PEG-5.2** were stored at 4 °C.

Synthesis of 5.3 and 5.4

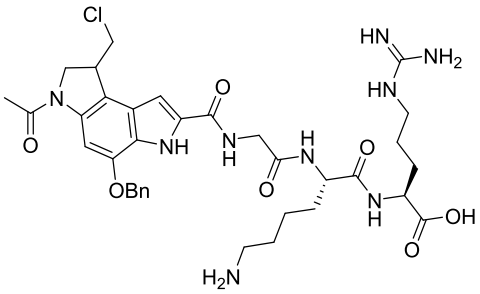

Peptide 5.3

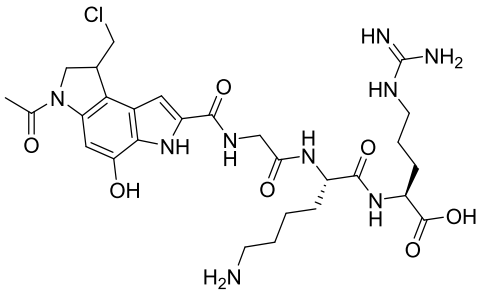

Peptide 5.4

H-Arg(pbf)-2ClTrt resin (100 mg, 0.068 mmol, [manufacturer's resin loading 0.68 mmol/g]) was prepared for coupling by swelling in DCM for 30 mins followed DMF for 30 mins. Fmoc-Lys(mtt)-OH (212 mg, 0.34 mmol) was dissolved in 2 mL of DMF and treated with HATU (129 mg, 0.34 mmol) and DIPEA (119 μL, 0.68 mmol). After 10 secs the resulting solution was added to the resin and the mixture shaken for 2 h. Subsequently, the resin was washed with DMF (6 x 10 mL) and the coupling repeated. The resin was washed 6 times with DMF (10 mL) before removal of the lysine Fmoc using piperidine in DMF (6 mL 40% 10 mins, 6 mL 20% 5 mins twice). Following Fmoc deprotection the resin was washed with DMF (6 x 10 mL). Next, Fmoc-Gly-OH (101 mg, 0.34 mmol) was dissolved in 2 mL of DMF and treated with HATU (129 mg, 0.34 mmol) and DIPEA (119 μL, 0.68 mmol). After 10 secs the resulting solution was added to the resin and the mixture shaken for 2 h. The resin was subsequently washed with DMF (6 x 10 mL) before the Fmoc group of the glycine removed using piperidine in DMF (6 mL 40% 10 mins, 6 mL 20% 5 mins twice). The resin was then washed again with DMF (6 x 10 mL) before being treated with **2.10** (59 mg, 0.10 mmol), HATU (39 mg, 0.10 mmol) and DIPEA (37 μL, 0.20 mmol) in DMF (2 mL) and the mixture shaken overnight. The resin was subsequently washed with DMF (6 x 10 mL) before the Fmoc group on the indoline nitrogen of **2.10** removed using piperidine in DMF (6 mL 40% 10 mins, 6 mL 20% 5 mins twice). The resin was then washed again with DMF (6 x 10 mL) before being treated with AcCl (30 μL, 0.34 mmol) and DIPEA (119 μL, 0.68 mmol) in DMF (2 mL). After

shaking for 1 h the resin was washed with DMF (6 x 10 mL) followed by DCM (6 x 10 mL). Cleavage of **5.3** from the resin was affected by addition of a solution of 47% TFA, 10% TIPS in DCM (10 mL). After 3 h of shaking the cleavage mixture was filtered. The resin was rinsed with DCM (2 x 3 mL) and the combined filtrates were evaporated to dryness under reduced pressure analysed using RP-HPLC (RT = 14.1 min) and MALDI mass spectrometry for **5.3** (M + Na)+, 762.39). **5.3** (10 mg, 0.01 mmol) was dissolved in MeOH (1 mL) and the resulting solution degassed with a gentle stream of nitrogen for 30 mins. A slurry of 10% Pd/C (20 mg) in 25% aq. Ammonium formate (500 µL) was then made and added into the solution of **5.3**. The reaction was stirred vigorously for 1 h at room temperature before being filtered through a pad of celite. The celite was subsequently washed with MeOH (3 x 5 mL) and the combined MeOH filtrates evaporated to dryness under reduced pressure. Reverse-phase Prep-HPLC and lyophilisation afforded **5.4** (3.0 mg, 33%) as a brown solid. RP-HPLC (RT = 14.1 min) and HRMS (ES+) calcd. for $C_{28}H_{40}ClN_9O_7$ (M + H)+, 650.2817; found, 650.2823)

Synthesis of 4 nm AuNP-PEG-5.3

PEG-5.3 (7.5 mg; 5 µmol) and PEG (7.5 mg, 5 µmol) were dissolved in dH_2O (15 mL) and left to stir at room temperature. Then, $HAuCl_4 \cdot 3H_2O$ (1.2 mg; 3.0 µmol) was dissolved in THF (1.2 mL), added to the **PEG-5.3**/PEG solution and stirred at room temperature for 5 min. A fresh solution of $NaBH_4$ (1.5 mg; 39.6 µmol) in dH_2O (0.5 mL) was prepared and added to the PEG-$HAuCl_4$ mixture. The reaction was stirred for 4 h at room temperature. Purification of the AuNPs was then performed. Firstly, the THF was evaporated by rotary evaporation under reduced pressure. The resulting aqueous solution was transferred to Vivaspin™ 500 (100 kDa MWCO) columns and centrifuged at 14,000 rpm for 10 min at 4 °C. The **AuNP-PEG-5.3** were resuspended in MES buffer (16.7 mL) and filtered through a Millex GP syringe driven filter unit (0.22 µm). The UV-vis extinction spectrum was recorded between 250-800 nm. **AuNP-PEG-5.3** were stored at 4 °C.

Synthesis of Jacalin-FITC

Jacalin (2 mg, 66 kDa) was dissolved in 10 mM HEPES buffered saline (1 mL, pH 7.4, 150 mM NaCl, 100 μM $CaCl_2$) and treated with FITC isomer I (12 μL, 10 mg/mL in DMSO). The resulting reaction was stirred at room temperature for 1 h before being transferred to Zeba spin desalting columns (7K MWCO, 0.5 mL) and centrifuged at 1500 xg for 2 min at 4 °C. The **jacalin-FITC** solution was characterised by UV-Vis spectroscopy and stored at -20 °C.

Functionalisation of AuNP-PEG-5.3 with Jacalin-FITC

Jacalin-FITC was conjugated to the PEG on the surface of the AuNPs via the terminal carboxyl groups in the PEG ligand using a previously reported method but with modifications.[111] The conjugation was performed via an amide linkage through EDC and NHS coupling. EDC (1.4 mg) and NHS (1.2 mg) were added to the **AuNP-PEG-5.3** in MES buffer (1 mL) and stirred for 30 min at room temperature. Excess EDC/NHS was removed by ultrafiltration in Vivaspin™ 500 columns (100 kDa MWCO) at 14,000 rpm for 30 min at 4 °C. The NHS-ester functionalised **AuNP-PEG-5.3** were redispersed in 10 mM HEPES buffered saline (0.5 mL, pH 7.4, 150 mM NaCl, 100 μM $CaCl_2$) and treated with **jacalin-FITC** (100 μL; 1 mg/mL). The solution was stirred overnight at room temperature in the dark. Following overnight incubation, unbound **jacalin-FITC** was removed by ultrafiltration in Vivaspin™ 500 columns (100 kDa MWCO) by centrifuging at 14,000 rpm for 30 min at 4 °C. The washes at the bottom of the Vivaspin™ 500 columns were removed and the AuNPs pellets retained in the Vivaspin™ 500 columns were resuspended in 10 mM HEPES buffered saline (0.5 mL, pH 7.4, 150 mM NaCl, 100 μM $CaCl_2$). This purification step was repeated until no more unbound Jacalin-FITC was left as determined by the UV-vis absorbance of the washes between 200-800 nm. The final **AuNP-PEG-5.3-Jac(FITC)** pellets were redispersed in ddH_2O and stored at 4 °C.

Synthesis of 4 nm AuNP-PEG-5.4-Jac

PEG-5.4 (7.5 mg; 5 μmol) and PEG (7.5 mg, 5 μmol) were dissolved in dH_2O (15 mL) and left to stir at room temperature. Then, $HAuCl_4 \cdot 3H_2O$ (1.2 mg; 3.0 μmol) was dissolved in THF (1.2 mL), added to the **PEG-5.4**/PEG solution and stirred at room temperature for 5 min. A fresh solution of

$NaBH_4$ (1.5 mg; 39.65 μmol) in dH_2O (0.5 mL) was prepared and added to the PEG-$HAuCl_4$ mixture. The reaction was stirred for 4 h at room temperature. Purification of the AuNPs was then performed. Firstly, the THF was evaporated by rotary evaporation under reduced pressure. The resulting aqueous solution was transferred to Vivaspin™ 500 (100 kDa MWCO) columns and centrifuged at 14,000 rpm for 10 min at 4 °C. **AuNP-PEG-5.4** was resuspended in MES buffer (16.7 mL) and treated with EDC (1.4 mg) and NHS (1.2 mg) for 30 min at room temperature. Excess EDC/NHS was removed by ultrafiltration in Vivaspin™ 500 columns (100 kDa MWCO) at 14,000 rpm for 30 min at 4 °C. The NHS-ester functionalised **AuNP-PEG-5.4** were redispersed in 10 mM HEPES buffered saline (0.5 mL, pH 7.4, 150 mM NaCl, 100 μM $CaCl_2$) and treated with jacalin (100 μL; 1 mg/mL). The solution was stirred overnight at room temperature in the dark. Following overnight incubation, unbound jacalin was removed by ultrafiltration in Vivaspin™ 500 columns (100 kDa MWCO) by centrifuging at 14,000 rpm for 30 min at 4 °C. The washes at the bottom of the Vivaspin™ 500 columns were removed and the AuNPs pellets retained in the Vivaspin™ 500 columns were resuspended in 10 mM HEPES buffered saline (0.5 mL, pH 7.4, 150 mM NaCl, 100 μM $CaCl_2$). This purification step was repeated until no more unbound jacalin was left as determined by the UV-vis absorbance of the washes between 200-800 nm. The final **AuNP-PEG-5.4-Jac** pellets were redispersed in ddH_2O and stored at 4 °C.

Synthesis of AuNP-PEG

The synthesis of AuNPs (ca. 4 nm) functionalised with PEG (**AuNP-PEG**) was performed. PEG (15 mg; 5 μmol) was dissolved in dH_2O (15 mL) and left to stir at room temperature. Then, $HAuCl_4 \cdot 3H_2O$ (1.2 mg; 3.0 μmol) was dissolved in THF (1.2 mL), added to the PEG solution and stirred at room temperature for 5 min. A fresh solution of $NaBH_4$ (1.5 mg; 39.6 μmol) in dH_2O (0.5 mL) was prepared and added to the PEG-$HAuCl_4$ mixture. The reaction was stirred for 6 h at room temperature. Purification of the AuNPs was then performed. Firstly, the THF was evaporated under reduced pressure. The aqueous solution was transferred to Vivaspin™ 500 columns (100 kDa MWCO) and centrifuged at 14,000 rpm for 10 min. The AuNP-PEG

were resuspended in ddH_2O or MES buffer (15 mL) and filtered through a Millex GP syringe driven filter unit (0.22 μm). The UV-vis extinction spectrum was recorded between 250-800 nm. The **AuNP-PEG** were stored at 4 °C.

Synthesis of AuNP-PEG-Jac

Jacalin was conjugated to the PEG on the surface of the AuNPs via the terminal carboxyl groups in the PEG ligand using a previously reported method but with modifications. The conjugation was performed via an amide linkage through EDC and NHS coupling. EDC (1.4 mg) and NHS (1.2 mg) were added to the **AuNP-PEG** in MES buffer (1 mL) and stirred for 30 min at room temperature. Subsequently, excess EDC/NHS was removed by ultrafiltration in Vivaspin™ 500 columns (100 kDa MWCO) at 14,000 rpm for 30 min at 4 °C. The NHS-ester functionalised **AuNP-PEG** were redispersed in 10 mM HEPES buffered saline (0.5 mL, pH 7.4, 150 mM NaCl, 100 μM $CaCl_2$) and treated with jacalin (100 μL; 1 mg/mL). The solution was stirred overnight at room temperature. Following overnight incubation, unbound jacalin was removed by ultrafiltration in Vivaspin™ 500 columns (100 kDa MWCO) by centrifuging at 14,000 rpm for 30 min at 4 °C. The washes at the bottom of the Vivaspin™ 500 columns were removed and the AuNPs pellets retained in the Vivaspin™ 500 columns were resuspended in 10 mM HEPES buffered saline (0.5 mL, pH 7.4, 150 mM NaCl, 100 μM $CaCl_2$). This purification step was repeated until no more unbound jacalin was left as determined by the UV-vis absorbance of the washes between 200-800 nm. The final AuNPs pellets were redispersed in ddH_2O and stored at 4 °C.

Synthesis of 4.5

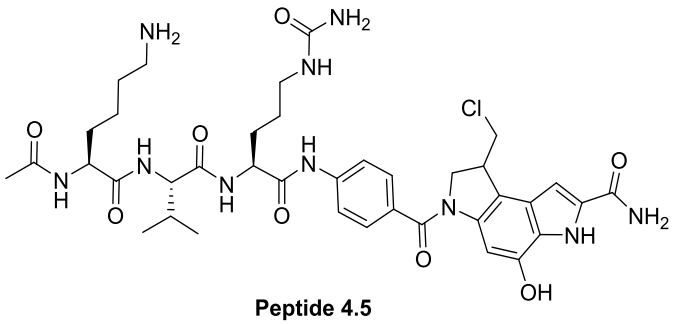

Peptide 4.5

For details of the synthesis and characterisation of peptide **4.5**, refer back to Chapter 4, Section 4.5.2.

Synthesis of AuNP-PEG-4.5-Jac

PEG-4.5 (7.5 mg; 5 μmol) and PEG (7.5 mg, 5 μmol) were dissolved in dH_2O (15 mL) and left to stir at room temperature. Then, $HAuCl_4 \cdot 3H_2O$ (1.2 mg; 3.0 μmol) was dissolved in THF (1.2 mL), added to the **PEG-4.7**/PEG solution and stirred at room temperature for 5 min. A fresh solution of $NaBH_4$ (1.5 mg; 39.6 μmol) in dH_2O (0.5 mL) was prepared and added to the PEG-$HAuCl_4$ mixture. The reaction was stirred for 4 h at room temperature. Purification of the AuNPs was then performed. Firstly, the THF was evaporated under reduced pressure. The resulting aqueous solution was transferred to Vivaspin™ 500 (100 kDa MWCO) columns and centrifuged at 14,000 rpm for 10 min at 4 °C. The **AuNP-PEG-4.5** particles were resuspended in MES buffer (16.7 mL) and treated with EDC (1.4 mg) and NHS (1.2 mg) for 30 min at room temperature. Excess EDC/NHS was removed by ultrafiltration in Vivaspin™ 500 columns (100 kDa MWCO) at 14,000 rpm for 30 min at 4 °C. The NHS-ester functionalised AuNP-PEG-4.5 were redispersed in 10 mM HEPES buffered saline (0.5 mL, pH 7.4, 150 mM NaCl, 100 μM $CaCl_2$) and treated with jacalin (100 μL; 1 mg/mL). The solution was stirred overnight at room temperature in the dark. Following overnight incubation, unbound jacalin was removed by ultrafiltration in Vivaspin™ 500 columns (100 kDa MWCO) by centrifuging at 14,000 rpm for 30 min at 4 °C. The washes at the bottom of the Vivaspin™ 500 columns were removed and the AuNPs pellets retained in the Vivaspin™ 500 columns were resuspended in 10 mM HEPES buffered saline (0.5 mL, pH 7.4, 150 mM NaCl, 100 μM $CaCl_2$). This purification step was repeated until no more unbound jacalin was left as determined by the UV-vis absorbance of the washes between 200-800 nm. The final **AuNP-PEG-4.5-Jac** pellets were redispersed in ddH_2O and stored at 4 °C.

5.5.3 Biological Assays

Antiproliferative Assays

Cell culture: The HL60, MCF-7 and HCT116 cell lines was purchased from ECACC (Porton Down, UK). Cells were cultured in RPMI 1640 medium supplemented with 10% foetal calf serum and 2 mM L-glutamine. HL-60, MCF-7 and HCT116 cells were passaged twice weekly and maintained between 1-9 x 10^5 cells/mL at 37 °C and 5% CO_2.

Antiproliferative assay: Antiproliferative activity was determined by MTS assay using the CellTiter 96 Aqueous One Solution Cell Proliferation Assay (Promega) and following the manufacturer's instructions. Briefly, HL-60, MCF-7 and HCT116 cells (3 x 10^4 /100 µL) were seeded in 96-well plates and left untreated or treated with H_2O (vehicle control), **AuNP-PEG** (control), **AuNP-PEG-Jac** (control), **AuNP-PEG-5.4**, **AuNP-PEG-5.4-Jac**, **AuNP-PEG-4.5-Jac** or doxorubicin hydrochloride in triplicate for 72 h at 37 °C with 5% CO_2. Following this, MTS assay reagent was added for 4 h and the absorbance measured at 490 nm using the Polarstar Optima microplate reader (BMG Labtech). Concentrations tested: **AuNP-PEG-5.4-Jac and AuNP-PEG-5.4** in MCF-7 cells (18.2 nM, 1.82 nM, 0.182 nM). **AuNP-PEG-4.5-Jac** in MCF-7, HCT116 and HL60 cell lines (19.4 nM, 1.94 nM, 0.194 nM).

Fluorescence Microscopy Imaging

MCF-7 human breast cancer cells were seeded in clear 96- well plates at 5 x 10^3 cells/well and treated with a 16.4 nM stock of **AuNP-PEG-5.3-Jac(FITC)** and incubated for 4 h at 37 °C. The cells were subsequently washed three times with PBS and fluorescence microscopy was used to examine cells and pictures taken with an inverted Leica DMII fluorescence microscope at 10x magnification.

Chapter 6 - Future Work

6.1 Fmoc-DSA-OH synthesis

As a follow on from the work presented in Chapter 2 of this thesis, future work should aim to establish a synthetic method which would allow for the simple and efficient formation of the central indole unit which is found in all compounds in the CC-1065 and duocarmycin family. At present, it is the cyclisation step to form this central indole unit which is the bottle neck of the present synthesis leading to erratic and often low yields. Whilst a variety of conditions were attempted in order to achieve an improved reaction in this regard, we were unable to establish an ideal set of reaction conditions for this transformation. Of course, should further conditions beyond the presently used TBAF catalysed reaction be unsuccessful in forming the central indole ring efficiently starting from compound **2.4**, it may be that further reaction strategies to from the central indole unit are investigated.

Unfortunately, due to time constraints, the provision of a new protecting group strategy for the protection of the phenolic oxygen on the Fmoc-DSA-OH unit was not established. The optimisation of such a protecting group strategy in is sure to improve the efficiency of the use of the unit in solid phase peptide chemistry. As such, future work should aim to investigate further protecting groups which may be suitable in this position. Such a protecting group should be stable to conditions used in the synthesis of the duocarmycin unit as well as to conditions employed in the building of peptide chains, whilst being labile to conditions used to remove peptides from solid phase resins. A recent development in the area of solid phase peptide synthesis is the development of resins which can be cleaved under UV-light conditions. As such, an orthogonal protecting group in this regard could be investigated for the Fmoc-DSA-OH unit and may provide an enhancement to its utility is SPPS.

A further, more extensive expansion to this work would be to investigate the use of the artificial amino acid strategy used in this work, i.e. the incorporation of Fmoc and carboxylic acid functionality, with other members of the CC-1065 and duocarmycin family. With yatakemycin demonstrating impressive potencies in recent studies, and a structure similar to that of duocarmycin SA, this compound represents an attractive starting point for

this area of work. Should an analogue of this kind be successfully synthesised, solid phase peptide synthesis will provide an ideal strategy for the development of further analogues which may display improved biological activity.

6.2 Duocarmycin Conjugation to Jacalin

Within chapter 3 of this thesis, an investigation into the coupling of a variety of duocarmycin-peptide analogues to jacalin was investigated. The investigations within this chapter of work led to a variety of conjugation chemistries being attempted. These included EDC/NHS chemistry, thiol maleimide chemistry and azide-alkyne click chemistry. Upon analysis of the conjugates synthesised using these methodologies it became apparent that all appeared to successfully result in the formation of a conjugate with the jacalin structure. These conjugates was analysed through both LCMS and MALDI mass spectrometry. Whilst LCMS was able to give conclusive evidence of conjugation occurring to the jacalin structure, the MALDI mass spectrometry data presented in this chapter was only capable of providing a qualitative indication of whether the mass of the α-subunit of jacalin was increasing. As such, it is imperative that for the work in this chapter to take on greater meaning, the mass analysis is repeated with more reliable equipment. Ideally, a more consistent method of analysing the conjugates using LCMS would be established in order to provide a clearer understanding of the number of drug additions occurring to jacalin during the conjugation reaction. Should such an understanding be obtained, it may then be possible to control the number of duocarmycin units becoming conjugated to the jacalin in order to give ideal drug-protein ratios.

The LCMS analysis of jacalin in this chapter also identified a series of 162 Da additions to the surface of jacalin. Such additions can be attributed to the addition of hexose moieties to the jacalin structure. With jacalin showing affinities for hexose compounds such as galactose this was not entirely unexpected. However, the binding of such hexose molecules and the consequent potential inhibition of the binding of jacalin to the T-antigen will need to be investigated should this work be continued further. This will be

imperative to understand whether the jacalin conjugation will be a successful strategy for delivering a duocarmycin warhead to cancer tissue specifically.

As a further expansion of the work presented here, it would also be desirable to understand the precipitation of the jacalin from the buffer upon conjugation. Such a phenomenon was observed during all of the conjugation chemistries presented within chapter 3 of this thesis. This precipitation was detrimental to the analysis of the resulting conjugates and as such, investigations to try and overcome the precipitation will be required to further this piece of work. Whilst some experiments were performed in order to adapt the concentrations of ligand and protein used in the conjugation reactions, a more thorough investigation of this type is likely to aid in overcoming this issue. Further, an investigation into the conjugation of more hydrophilic duocarmycin analogues may also aid in ensuring that jacalin remains in solution even after conjugation.

Finally, should the above mentioned investigations aid in the provision of a jacalin conjugate suitable for biological analysis, it will be important to thoroughly investigate the interaction of this conjugate with the T-antigen surface on a variety of cell lines. Of course, in order to fully understand the behaviour of the conjugate, it will also be necessary to provide investigations into the interaction of the conjugate with cell lines which do not present the T-antigen on their surface. Such investigations will give a more complete picture on whether the duocarmycin warhead can be delivered to T-antigen expressing cancer cells specifically as opposed to healthy cells. As mentioned throughout this body of work, this may aid in providing a platform for the duocarmycin family of compounds to realise their clinical potential.

6.3 Duocarmycin-peptide conjugates

The work provided in chapter 4 of this thesis focused on the conjugation of a duocarmycin warhead to a peptide sequence which had been shown by other groups to specifically and selectively bind to the T-antigen.

The T-antigen binding peptide was successfully synthesised using solid phase peptide chemistry and a variety of strategies were investigated to incorporate the duocarmycin warhead. Of these strategies, the most successful was

shown to be the incorporation of a cathepsin B cleavage sequence in between the duocarmycin warhead and the T-antigen binding peptide. The cleavage sequence utilised was a Cit-Val linker including a PABA spacer. The synthesis and subsequent testing of the duocarmycin-PABA-Cit-Val peptide demonstrated impressive biological potency, especially the duocarmycin-PABA cleavage product (**4.7** in chapter 4). The biological activity obtained in various cells lines provided promise that the conjugate formed in chapter 4 would demonstrate activity within T-antigen expressing cell lines. Indeed, when the entire Peptide-drug conjugate construct was tested in vitro, IC50s in the low micromolar range were obtained which provides an ideal spring board for a continuation of this work. It is proposed that this potency could be improved through the incorporation of further duocarmycin warhead units into the peptide sequence. Due to the amino acid-like structure of the Fmoc-DSA-OH unit, the incorporation of further units into the peptide sequence should not present a significant hurdle. Furthermore, in other work conducted but not presented as part of this thesis, the additions of further duocarmycin alkylating subunits into peptide sequences resulted in an improvement to the biological potency of the resulting compounds.

Whilst the work presented in chapter 4 provides a solid platform for further work into this area, it is acknowledged that a more thorough understanding of the interaction of the T-antigen binding peptide with the T-antigen is required. Specifically, whilst fluorescence studies allowed the postulation that the T-antigen binding peptide was able to bind and subsequently enter the T-antigen expressing cells lines used within this work, a more thorough analysis of this interaction must be established. Of particular importance here is providing data for all the relevant controls for the peptide conjugate and their interaction with the T-antigen expressing cells lines. Furthermore, future investigations will also be required to investigate whether duocarmycin incorporation into the peptide sequence has an effect on the interaction of the peptide with the T-antigen. For example, it will need to be established whether the duocarmycin unit inhibits the binding of the peptide to the T-antigen in any way. This could significantly impact the selectivity of the synthesised peptide. Additionally, further, more detailed fluorescence

microscopy studies will aid in providing more details on the behaviour of the peptide conjugates in terms of their uptake within various cell lines.

In order to gain an understanding of the above considerations, further work could look into establishing a comparative data set incorporating a scrambled peptide sequence, wherein the proposed T-antigen binding region of the peptide is scrambled. The synthesis of such a conjugate and investigations into its resulting biological activity will certainly help in gaining an understanding of the selectivity of the peptide-conjugate synthesised in this work for T-antigen expressing cell lines. Additionally, since iodination of the tryptophan residues of the T-antigen binding peptide has previously been shown to be detrimental to the binding of the peptide to the T-antigen, experiments of this kind may also be helpful for investigating the activity of the peptide-duocarmycin conjugates. Furthermore, experiments could be designed which establish a comparison between the interaction of jacalin, the T-antigen binding peptide and the peptide–conjugates synthesised in this body of work with the T-antigen. It is possible that competitive binding studies in this regard could aid in establishing such a relationship.

Finally, and as mentioned above in regards to the jacalin-duocarmycin conjugates, it is imperative that the interaction of the duocarmycin-peptide conjugates synthesised in chapter 4 with non-T-antigen expressing cells lines is established. Such data would provide a necessary insight into the underlying aim of this body of work, namely, how the selective delivery of a duocarmycin warhead to T-antigen expressing cancer cells rather than healthy cells can be achieved.

6.4 Duocarmycin based Gold Nanoparticles

In chapter 5 of this thesis, the synthesis of a gold nanoparticle functionalised with a duocarmycin warhead and a jacalin based directing moiety was detailed.

The successful synthesis of a 4 nm gold nanoparticle with a duocarmycin-based peptide comprising a cleavable sequence was presented. This nanoparticle construct was then successfully decorated with jacalin in an attempt to achieve targeted delivery of the nanoparticle.

Whilst best efforts were made to fully characterise the gold nanoparticle construct, one of the inherent issues associated with gold nanoparticle systems is trying to obtain a clear picture of how exactly the gold nanoparticle surface is functionalised. In this regard, should future work be pursued relating to the work presented in chapter 5, a thorough investigation into the functionalisation of the gold nanoparticle surface should be made. Of specific interest would be obtaining an understanding of the number of duocarmycin units present on the surface of the gold nanoparticle. In a similar manner, the number of jacalin units per gold nanoparticle would also be of interest. It is possible that elemental analysis of the gold nanoparticle constructs may be useful for obtaining this information. Previous work in the laboratory has shown that that this technique is useful in obtaining such information. By deciphering this information, a greater understanding and more thorough interpretation of the biological data collected as part of the work detailed in chapter 5 could be obtained. For example, the lack of activity in the gold nanoparticle could be a direct result of a lack of duocarmycin warheads functionalising the gold nanoparticle core. Alternatively, it could also be that over-functionalisation with jacalin may affect the activity of the resulting nanoparticle construct.

Further to the above, a greater understanding of the interaction of the gold nanoparticle with the T-antigen expressed on certain cells would be ideal. Whilst fluorescence microscopy studies demonstrated the potential uptake of the gold nanoparticles into cell lines expressing the T-antigen, these studies need to be repeated with further controls to provide real evidence of this interaction. Whilst similar 4 nm gold nanoparticles functionalised with jacalin have been previously synthesised and shown to specifically and selectively target T-antigen expressing cell lines, it would be ideal to understand how this specific interaction may be affected when a duocarmycin warhead is introduced. This is since previous work utilised other non-duocarmycin based drug molecules. This interaction may be further studied through the use of confocal microscopy. Such methods have been fundamental in studying the distribution of gold nanoparticles within cells and would be of use for future work relating to this area.

As a further area of future work, it will be necessary to conduct experiments to investigate how the gold nanoparticle constructs synthesised in this work interact with a cathepsin B cleavage enzyme. This is since a cathepsin B cleavage sequence was employed in attempt to ensure detachment of the duocarmycin warhead from the nanoparticle upon internalisation into the cell. Specifically, an understanding of whether the duocarmycin unit can be successfully released from the gold nanoparticle by cathepsin B may aid in providing an explanation for the lack of activity in the gold nanoparticles synthesised in this work. This is since it has been postulated that the reason for a lack of activity in the synthesised gold nanoparticles may be due to the duocarmycin warhead not being able to reach the nucleus to exert its biological activity. In this regard, it is possible that the PEG chains used to functionalise the nanoparticle provide a barrier for the cathepsin B to interact with the Cit-Val sequence provided on the duocarmycin-peptide units. Should this be the case, different length PEG chains may provide an area of investigation for overcoming this issue. In particular, longer PEG chains may provide more space for the cathepsin B to contact the cleavage sequence.

Finally, and as discussed in relation to the work presented in chapter 4, in order to gain a real understanding of the specificity of the gold nanoparticles synthesised, studies with cell lines which do not express the T-antigen will be fundamental. The results in these studies could be compared to those with cell lines which do express the T-antigen. It is hoped that the cytotoxicities of the nanoparticles within the cell lines which express the T-antigen will be greater than those which do not. This would indicate that the nanoparticle/jacalin constructs successfully aid in delivering the duocarmycin warhead to specific target sites. This is of course fundamental to the work in this thesis where the targeted delivery of duocarmycin to T-antigen expressing cancer cells was the overall objective.

Chapter 7 -References

References:

1. B. A. Chabner and T. G. Roberts Jr, *Nat. Rev. Cancer*, 2005, **5**, 65.
2. A. Kamb, S. Wee and C. Lengauer, *Nat. Rev. Drug. Discov.*, 2007, **6**, 115.
3. D. Hanahan and R. A. Weinberg, *Cell*, 2011, **144**, 646-674.
4. W. B. Pratt, W. D. Ensminger and R. W. Ruddon, *The anticancer drugs*, Oxford University Press, USA, 1994.
5. R. V. Chari, *Acc. Chem. Res.*, 2007, **41**, 98-107.
6. O. M. Fischer, S. Streit, S. Hart and A. Ullrich, *Curr. Opin. Chem. Biol.*, 2003, **7**, 490-495.
7. F. Pineda, J. Ortega-Castro, J. Alvarez-Idaboy, J. Frau, B. Cabrera, J. Ramírez, J. Donoso and F. Munoz, *J. Phys. Chem. A*, 2011, **115**, 2359-2366.
8. C. M. Galmarini, J. R. Mackey and C. Dumontet, *Lancet Oncol.*, 2002, **3**, 415-424.
9. J. J. Wilson and S. J. Lippard, *Chem. Rev.*, 2013, **114**, 4470-4495.
10. G. Minotti, P. Menna, E. Salvatorelli, G. Cairo and L. Gianni, *Pharmacol Rev.*, 2004, **56**, 185-229.
11. S. H. Kaufmann, *Cancer Res.*, 1989, **49**, 5870-5878.
12. M. A. Jordan, D. Thrower and L. Wilson, *Cancer Res.*, 1991, **51**, 2212-2222.
13. A. K. Singla, A. Garg and D. Aggarwal, *Int. J. Pharm.*, 2002, **235**, 179-192.
14. J. Crown and M. O'leary, *The Lancet*, 2000, **355**, 1176-1178.
15. N. Krall, J. Scheuermann and D. Neri, *Angew. Chem. Int. Ed.*, 2013, **52**, 1384-1402.
16. L. Dvořák, I. Popa, P. Štarha and Z. Trávníček, *Eur. J. Inorg. Chem.*, 2010, **2010**, 3441-3448.
17. D. A. Zajchowski, S. L. Biroc, H. L. Liu, S. K. Chesney, J. Hoffmann, J. Bauman, T. Kirkland, B. Subramanyam, J. Shen and E. Ho, *Int. J. Cancer*, 2005, **114**, 1002-1009.
18. A. M. Di Francesco, A. S. Riccardi, G. Barone, S. Rutella, D. Meco, R. Frapolli, M. Zucchetti, M. D'incalci, C. Pisano and P. Carminati, *Biochem. Pharmacol.*, 2005, **70**, 1125-1136.
19. C.-H. Heldin, K. Rubin, K. Pietras and A. Östman, *Nat. Rev. Cancer*, 2004, **4**, 806.
20. C. Sawyers, *Nature*, 2004, **432**, 294.
21. K. Strebhardt and A. Ullrich, *Nat. Rev. Cancer*, 2008, **8**, 473.
22. M. Hojjat-Farsangi, *Int. J. Mo.l Sci.*, 2014, **15**, 13768-13801.
23. R. Dagher, M. Cohen, G. Williams, M. Rothmann, J. Gobburu, G. Robbie, A. Rahman, G. Chen, A. Staten and D. Griebel, *Clin. Cancer Res.*, 2002, **8**, 3034-3038.
24. C. Natoli, B. Perrucci, F. Perrotti, L. Falchi and S. Iacobelli, *Curr. Cancer Drug Targets*, 2010, **10**, 462-483.
25. F. X. Gu, R. Karnik, A. Z. Wang, F. Alexis, E. Levy-Nissenbaum, S. Hong, R. S. Langer and O. C. Farokhzad, *Nano today*, 2007, **2**, 14-21.
26. H. Maeda, J. Wu, T. Sawa, Y. Matsumura and K. Hori, *J. Control Release*, 2000, **65**, 271-284.
27. T. Lammers, F. Kiessling, W. E. Hennink and G. Storm, *J. Control Release*, 2012, **161**, 175-187.

28. V. P. Torchilin, in *Drug delivery*, Springer, 2010, pp. 3-53.
29. R. S. Zolot, S. Basu and R. P. Million, Angew. *Chem. Int. Ed.*, 2013, **53**, 7179–7182.
30. L. Ducry and B. Stump, *Bioconjugate Chem.*, 2009, **21**, 5-13.
31. P. D. Senter and E. L. Sievers, *Nat. Biotechnol.*, 2012, **30**, 631.
32. H. L. Perez, P. M. Cardarelli, S. Deshpande, S. Gangwar, G. M. Schroeder, G. D. Vite and R. M. Borzilleri, *Drug Discov. Today*, 2014, **19**, 869-881.
33. S. C. Alley, N. M. Okeley and P. D. Senter, *Curr. Opin. Chem. Biol.*, 2010, **14**, 529-537.
34. A. Beck, L. Goetsch, C. Dumontet and N. Corvaïa, *Nat. Rev. Drug Discov.*, 2017, **16**, 315.
35. P. D. Senter, *Curr. Opin. Chem. Biol.*, 2009, **13**, 235-244.
36. S. Verma, D. Miles, L. Gianni, I. E. Krop, M. Welslau, J. Baselga, M. Pegram, D.-Y. Oh, V. Diéras and E. Guardino, *New Engl. J. Med.*, 2012, **367**, 1783-1791.
37. H. Kantarjian, D. Thomas, J. Jorgensen, E. Jabbour, P. Kebriaei, M. Rytting, S. York, F. Ravandi, M. Kwari and S. Faderl, *Lancet Oncol.*, 2012, **13**, 403-411.
38. K. Nicolaou, Y. Ogawa, G. Zuccarello and H. Kataoka, *J. Am. Chem. Soc.*, 1988, **110**, 7247-7248.
39. J. R. Adair, P. W. Howard, J. A. Hartley, D. G. Williams and K. A. Chester, *Expert Opin. Biol. Ther.*, 2012, **12**, 1191-1206.
40. R. V. Chari, M. L. Miller and W. C. Widdison, *Angew. Chem. Int. Ed.*, 2014, **53**, 3796-3827.
41. N. Jain, S. W. Smith, S. Ghone and B. Tomczuk, *Pharm. Res.*, 2015, **32**, 3526-3540.
42. J. R. McCombs and S. C. Owen, *The AAPS journal*, 2015, **17**, 339-351.
43. Y. V. Kovtun, C. A. Audette, Y. Ye, H. Xie, M. F. Ruberti, S. J. Phinney, B. A. Leece, T. Chittenden, W. A. Blättler and V. S. Goldmacher, *Cancer Res.*, 2006, **66**, 3214-3221.
44. Y. V. Kovtun and V. S. Goldmacher, *Cancer Lett.*, 2007, **255**, 232-240.
45. B. E. de Goeij, D. Satijn, C. M. Freitag, R. Wubbolts, W. K. Bleeker, A. Khasanov, T. Zhu, G. Chen, D. Miao and P. H. van Berkel, *Mol. Cancer Ther.*, 2015, **14**, 1130-1140.
46. J. Katz, J. E. Janik and A. Younes, *Clin. Cancer Res.*, 2011, **17**, 6428-6436.
47. N. M. Okeley, J. B. Miyamoto, X. Zhang, R. J. Sanderson, D. R. Benjamin, E. L. Sievers, P. D. Senter and S. C. Alley, *Clin. Cancer Res.*, 2010, 1078-0432. CCR-1009-2069.
48. W. Wang, S. Singh, D. L. Zeng, K. King and S. Nema, *J. Pharm. Sci.*, 2007, **96**, 1-26.
49. F. A. Harding, M. M. Stickler, J. Razo and R. DuBridge, *mAbs,* 2010, **2**, 256-265.
50. M. Ritchie, L. Tchistiakova and N. Scott, *mAbs*, 2013, **5**, 13-21.
51. R. V. Chari, *ACS Med. Chem. Lett.,* 2016, **7**, 974-976.
52. J. Y. Li, S. R. Perry, V. Muniz-Medina, X. Wang, L. K. Wetzel, M. C. Rebelatto, M. J. M. Hinrichs, B. Z. Bezabeh, R. L. Fleming and N. Dimasi, *Cancer cell*, 2016, **29**, 117-129.
53. P. Agarwal and C. R. Bertozzi, *Bioconjugate Chem.*, 2015, **26**, 176-192.

54. Y. Igarashi, K. Futamata, T. Fujita, A. Sekine, H. Senda, H. Naoki and T. Furumai, *J. Antibiot.*, 2003, **56**, 107-113.
55. D. L. Boger and D. S. Johnson, *Proc. Nat. Acad. Sci. U. S. A.*, 1995, **92**, 3642-3649.
56. L. J. Hanka, A. Dietz, S. Gerpheide, S. Kuentzel and D. Martin, *J. Antibiot.*, 1978, **31**, 1211-1217.
57. T. Yasuzawa, T. Iida, K. i. Muroi, M. Ichimura, K. Takahashi and H. Sano, *Chem. Pharm. Bull.*, 1988, **36**, 3728-3731.
58. D. G. Martin, C. Biles, S. A. Gerpheide, L. J. Hanka, W. C. Krueger, J. P. Mcgovren, S. A. Mizsak, G. L. Neil, J. C. Stewart and J. Visser, *J. Antibiot.*, 1981, **34**, 1119-1125.
59. V. L. Reynolds, J. P. Mcgovren and L. H. Hurley, *J. Antibiot.*, 1986, **39**, 319-334.
60. T. Yasuzawa, Y. Saitoh, M. Ichimura, I. Takahashi and H. Sano, *J. Antibiot.*, 1991, **44**, 445-447.
61. N. Ghosh, H. M. Sheldrake, M. Searcey and K. Pors, *Curr. Top. Med. Chem.*, 2009, **9**, 1494-1524.
62. M. Ichimura, T. Ogawa, S. Katsumata, K.-i. Takahashi, I. Takahashi and H. Nakano, *J. Antibiot.*, 1991, **44**, 1045-1053.
63. L. H. Hurley, V. L. Reynolds, D. H. Swenson, G. L. Petzold and T. A. Scahill, *Science*, 1984, **226**, 843-844.
64. W. Wrasidlo, D. S. Johnson and D. L. Boger, *Bioorg. Med. Chem. Lett.*, 1994, **4**, 631-636.
65. D. L. Boger, C. W. Boyce and D. S. Johnson, *Bioorg. Med. Chem. Lett.*, 1997, **7**, 233-238.
66. D. L. Boger, A. Santillán, M. Searcey, S. R. Brunette, S. E. Wolkenberg, M. P. Hedrick and Q. Jin, *J. Org. Chem*, 2000, **65**, 4101-4111.
67. M. Warpehoski and D. Harper, *J. Am. Chem. Soc.*, 1994, **116**, 7573-7580.
68. M. Searcey, *Curr. Pharm. Des.*, 2002, **8**, 1375-1389.
69. L. H. Hurley and P. H. Draves, in *Molecular aspects of anticancer drug-DNA interactions*, Springer, 1993, pp. 89-133.
70. D. L. Boger, S. A. Munk and H. Zarrinmayeh, *J. Am. Chem. Soc.*, 1991, **113**, 3980-3983.
71. D. L. Boger, *Acc. Chem. Res.*, 1995, **28**, 20-29.
72. J. P. McGovren, G. L. Clarke, E. A. Pratt and T. F. Dekoning, *J. Antibiot.*, 1984, **37**, 63-70.
73. M. Ichimura, T. Ogawa, K.-I. Takahashi, E. Kobayashi, I. Kawamoto, T. Yasuzawa, I. Takahashi and H. Nakano, *J. Antibiot.*, 1990, **43**, 1037-1038.
74. D. L. Boger and D. S. Johnson, *Angew. Chem. Int. Ed.*, 1996, **35**, 1438-1474.
75. J. P. Parrish, T. V. Hughes, I. Hwang and D. L. Boger, *J. Am. Chem. Soc.*, 2004, **126**, 80-81.
76. L. Li, T. DeKoning, R. Kelly, W. Krueger, J. McGovren, G. Padbury, G. Petzold, T. Wallace, R. Ouding and M. Prairie, *Cancer Res.*, 1992, **52**, 4904-4913.
77. N. Pavlidis, S. Aamdal, A. Awada, H. Calvert, P. Fumoleau, R. Sorio, C. Punt, J. Verweij, A. van Oosterom and R. Morant, *Cancer Chemother. Pharmacol.*, 2000, **46**, 167-171.

78. S. Nagamura, Y. Kanda, E. Kobayashi, K. Gomi and H. Saito, *Chem. Pharm. Bull.*, 1995, **43**, 1530-1535.
79. E. Kobayashi, A. Okamoto, M. Asada, M. Okabe, S. Nagamura, A. Asai, H. Saito, K. Gomi and T. Hirata, *Cancer Res.*, 1994, **54**, 2404-2410.
80. E. J. Small, R. Figlin, D. Petrylak, D. J. Vaughn, O. Sartor, I. Horak, R. Pincus, A. Kremer and C. Bowden, *Investigational new drugs*, 2000, **18**, 193-198.
81. Venkatesan, (*2015*), Self-immolative linkers containing mandelic acid derivatives, drug-ligand conjugates for targeted therapies and uses therof, *WO 2015038426A1*, .
82. L. F. Tietze, T. Herzig, A. Fecher, F. Haunert and I. Schuberth, *ChemBioChem*, 2001, **2**, 758-765.
83. L. F. Tietze, F. Major and I. Schuberth, *Angew. Chem. Int. Ed.*, 2006, **45**, 6574-6577.
84. L. F. Tietze, J. M. von Hof, B. Krewer, M. Müller, F. Major, H. J. Schuster, I. Schuberth and F. Alves, *ChemMedChem: Chemistry Enabling Drug Discovery*, 2008, **3**, 1946-1955.
85. L. F. Tietze, M. Müller, S. C. Duefert, K. Schmuck and I. Schuberth, *Chem. Eur. J.*, 2013, **19**, 1726-1731.
86. R. V. Chari, K. A. Jackel, L. A. Bourret, S. M. Derr, B. M. Tadayoni, K. M. Mattocks, S. A. Shah, C. Liu, W. A. Blättler and V. S. Goldmacher, *Cancer Res.*, 1995, **55**, 4079-4084.
87. R. Y. Zhao, H. K. Erickson, B. A. Leece, E. E. Reid, V. S. Goldmacher, J. M. Lambert and R. V. Chari, *J. Med. Chem.*, 2012, **55**, 766-782.
88. H. Wang, V. S. Rangan, M. C. Sung, D. Passmore, T. Kempe, X. Wang, L. Thevanayagam, C. Pan, C. Rao and M. Srinivasan, *Biopharm. Drug Dispos.*, 2016, **37**, 93-106.
89. T. K. Owonikoko, A. Hussain, W. M. Stadler, D. C. Smith, H. Kluger, A. M. Molina, P. Gulati, A. Shah, C. M. Ahlers and P. M. Cardarelli, *Cancer Chemother. Pharmacol.*, 2016, **77**, 155-162.
90. G. Menderes, E. Bonazzoli, S. Bellone, J. Black, G. Altwerger, A. Masserdotti, F. Pettinella, L. Zammataro, N. Buza and P. Hui, *Gynecologic oncology*, 2017, **146**, 179-186.
91. R. C. Elgersma, R. G. Coumans, T. Huijbregts, W. M. Menge, J. A. Joosten, H. J. Spijker, F. M. de Groot, M. M. van der Lee, R. Ubink and D. J. van den Dobbelsteen, *Mol. Pharm.*, 2015, **12**, 1813-1835.
92. W. H. Dokter, M. M. van der Lee, P. G. Groothuis, R. Ubink, M. A. van der Vleuten, T. A. van Achterberg, E. M. Loosveld, D. Damming, D. C. Jacobs and M. Rouwette, *Mol. Cancer Ther.*, 2015, **14**, 692-703.
93. J. C. Aub, B. H. Sanford and L.-H. Wang, *Proc. Nat. Acad. Sci. U. S. A.*, 1965, **54**, 400-402.
94. J. C. Aub, C. Tieslau and A. Lankester, *Proc. Nat. Acad. Sci. U. S. A.*, 1963, **50**, 613-619.
95. D. H. Dube and C. R. Bertozzi, *Nat. Rev. Drug Discov.*, 2005, **4**, 477.
96. T. K. Lindhorst, *Essentials of carbohydrate chemistry and biochemistry*, Wiley-Vch Weinheim, 2007.
97. A. Johnson and J. Lewis, Molecular Biology of the Cell, *New York: Garland Science*, 2002.
98. J. W. Dennis, S. Laferte, C. Waghorne, M. L. Breitman and R. S. Kerbel, *Science*, 1987, **236**, 582-585.
99. Y. J. Kim and A. Varki, *Glycoconjugate J.*, 1997, **14**, 569-576.

100. H. Zwierzina, L. Bergmann, H. Fiebig, S. Aamdal, P. Schöffski, K. Witthohn and H. Lentzen, *Eur J Cancer*, 2011, **47**, 1450-1457.
101. H. Franz, *Oncology*, 1986, **43**, 23-34.
102. G. S. Kienle and H. Kiene, *Integr. cancer Ther.*, 2010, **9**, 142-157.
103. S. Lyu and W. Park, *J. Biochem. Mol. Bio.*, 2006, **39**, 662.
104. H. Bantel, I. H. Engels, W. Voelter, K. Schulze-Osthoff and S. Wesselborg, *Cancer Res.*, 1999, **59**, 2083-2090.
105. B. J. Campbell, I. A. Finnie, E. F. Hounsell and J. M. Rhodes, *J. Clin. Invest.*, 1995, **95**, 571-576.
106. J. Rak, F. Basolo, J. Elliott, J. Russo and F. Miller, *Cancer Lett.*, 1991, **57**, 27-36.
107. G. Konska, C. Vissac, K. Zagla, F. Chezet, M.-P. Vasson, D. Bernard-Gallon and J. Guillot, *Int. J. Oncol.*, 2002, **21**, 1009-1014.
108. R. Lotan, E. Skutelsky, D. Danon and N. Sharon, *J. Biol. Chem.*, 1975, **250**, 8518-8523.
109. S. D. Ryder, J. A. Smith and J. M. Rhodes, *J. Natl. Cancer Inst.*, 1992, **84**, 1410-1416.
110. A. A. Jeyaprakash, P. G. Rani, G. B. Reddy, S. Banumathi, C. Betzel, K. Sekar, A. Surolia and M. Vijayan, *J. Mol. Biol.*, 2002, **321**, 637-645.
111. G. Obaid, I. Chambrier, M. J. Cook and D. A. Russell, *Angew. Chem. Int. Ed.*, 2012, **51**, 6158-6162.
112. L. Yu, D. G. Fernig, J. A. Smith, J. D. Milton and J. M. Rhodes, *Cancer Res.*, 1993, **53**, 4627-4632.
113. D. L. Boger, J. A. McKie, T. Nishi and T. Ogiku, *J. Am. Chem. Soc.*, 1996, **118**, 2301-2302.
114. D. L. Boger and K. Machiya, *J. Am. Chem. Soc.*, 1992, **114**, 10056-10058.
115. H. Muratake, I. Abe and M. Natsume, *Tetrahedron Lett.*, 1994, **35**, 2573-2576.
116. H. Muratake, N. Matsumura and M. Natsume, *Chem. Pharm. Bull.*, 1995, **43**, 1064-1066.
117. D. L. Boger and J. A. McKie, *J. Org. Chem*, 1995, **60**, 1271-1275.
118. D. L. Boger, C. W. Boyce, R. M. Garbaccio and M. Searcey, *Tetrahedron Lett.*, 1998, **39**, 2227-2230.
119. V. F. Patel, S. L. Andis, J. K. Enkema, D. A. Johnson, J. H. Kennedy, F. Mohamadi, R. M. Schultz, D. J. Soose and M. M. Spees, *J. Org. Chem*, 1997, **62**, 8868-8874.
120. M. S. Tichenor, J. D. Trzupek, D. B. Kastrinsky, F. Shiga, I. Hwang and D. L. Boger, *J. Am. Chem. Soc.*, 2006, **128**, 15683-15696.
121. L. F. Tietze, F. Haunert, T. Feuerstein and T. Herzig, *Eur. J. Org. Chem.*, 2003, **2003**, 562-566.
122. K. Hiroya, S. Matsumoto and T. Sakamoto, *Org. Lett.*, 2004, **6**, 2953-2956.
123. M. J. Stephenson, L. A. Howell, M. A. O'Connell, K. R. Fox, C. Adcock, J. Kingston, H. Sheldrake, K. Pors, S. P. Collingwood and M. Searcey, *J. Org. Chem.*, 2015, **80**, 9454-9467.
124. K. Hiroya, R. Jouka, M. Kameda, A. Yasuhara and T. Sakamoto, *Tetrahedron*, 2001, **57**, 9697-9710.
125. R. C. Larock and E. K. Yum, *J. Am. Chem. Soc.*, 1991, **113**, 6689-6690.
126. M. Alfonsi, A. Arcadi, M. Aschi, G. Bianchi and F. Marinelli, *J. Org. Chem*, 2005, **70**, 2265-2273.

127. W. C. Chan and P. D. White, *Fmoc solid phase peptide synthesis*, Oxford University Press, 2000, 20-36.
128. R. B. Merrifield, *J. Am. Chem. Soc.*, 1963, **85**, 2149-2154.
129. R. B. Merrifield, *Angew. Chem. Int. Ed.*, 1985, **24**, 799-810.
130. J.-W. Hwang, D.-H. Choi, J.-H. Jeon, J.-K. Kim and J.-G. Jun, *B. Korean Chem. Soc.*, 2010, **31**, 965-970.
131. S. Takano, Y. Iwabuchi and K. Ogasawara, *J. Am. Chem. Soc.*, 1987, **109**, 5523-5524.
132. P. Magdolen and A. Vasella, *Helv. chim. acta*, 2005, **88**, 2454-2469.
133. T. M. Kosak, H. A. Conrad, A. L. Korich and R. L. Lord, *Eur. J. Org. Chem.*, 2015, **2015**, 7460-7467.
134. K. T. Howard and J. D. Chisholm, *Org. Prep. Proced. Int.*, 2016, **48**, 1-36.
135. Y. Oikawa, T. Yoshioka and O. Yonemitsu, *Tetrahedron Lett.*, 1982, **23**, 885-888.
136. T. Onoda, R. Shirai and S. Iwasaki, *Tetrahedron Lett.*, 1997, **38**, 1443-1446.
137. A. Bouzide and G. Sauvé, *Tetrahedron Lett.*, 1999, **40**, 2883-2886.
138. K. H. Cha, T. W. Kang, D. O. Cho, H.-W. Lee, J. Shin, K. Y. Jin, K.-W. Kim, J.-W. Kim and C.-I. Hong, *Synth. Commun.*, 1999, **29**, 3533-3540.
139. T. Akiyama, H. Hirofuji and S. Ozaki, *Tetrahedron Lett.*, 1991, **32**, 1321-1324.
140. A. Bouzide and G. Sauvé, *Synlett*, 1997, **1997**, 1153-1154.
141. A. Cappa, E. Marcantoni, E. Torregiani, G. Bartoli, M. C. Bellucci, M. Bosco and L. Sambri, *J. Org. Chem*, 1999, **64**, 5696-5699.
142. G. Bartoli, R. Dalpozzo, A. D. Nino, L. Maiuolo, M. Nardi, A. Procopio and A. Tagarelli, *Eur. J. Org. Chem.*, 2004, **2004**, 2176-2180.
143. G. V. M. Sharma, C. G. Reddy and P. R. Krishna, *J. Org. Chem*, 2003, **68**, 4574-4575.
144. R. J. Hinklin and L. L. Kiessling, *Org. Lett.*, 2002, **4**, 1131-1133.
145. M. E. Jung and P. Koch, *Tetrahedron Lett.*, 2011, **52**, 6051-6054.
146. M. Nitz, B. W. Purse and D. R. Bundle, *Org. Lett.*, 2000, **2**, 2939-2942.
147. N. L. Pohl and L. L. Kiessling, *Tetrahedron Lett.*, 1997, **38**, 6985-6988.
148. A. H. Viuff, M. Heuckendorff and H. H. Jensen, *Org. Lett.*, 2016, **18**, 5773-5775.
149. Y. Cao, A. Merling, U. Karsten, S. Goletz, M. Punzel, R. Kraft, G. Butschak and R. Schwartz-Albiez, *Int. J. Cancer*, 2008, **123**, 89-99.
150. J. Samuel, A. A. Noujaim, G. D. MacLean, M. R. Suresh and B. M. Longenecker, *Cancer Res.*, 1990, **50**, 4801-4808.
151. L.-G. Yu, *Glycoconjugate J.*, 2007, **24**, 411-420.
152. G. F. Springer, *Science*, 1984, **224**, 1198-1206.
153. W. M. Lin, U. Karsten, S. Goletz, R. C. Cheng and Y. Cao, *Int. J. Exp. Pathol.*, 2011, **92**, 97-105.
154. I. Brockhausen, J. Yang, N. Dickinson, S. Ogata and S. H. Itzkowitz, *Glycoconjugate J.*, 1998, **15**, 595-603.
155. I. Brockhausen, *Biochim. Biophys. Acta Gen. Subj.*, 1999, **1473**, 67-95.
156. I. Brockhausen, *EMBO reports*, 2006, **7**, 599-604.

157. A. Rivinoja, N. Kokkonen, I. Kellokumpu and S. Kellokumpu, *J. Cell. Physiol.*, 2006, **208**, 167-174.
158. V. V. Glinsky, G. V. Glinsky, K. Rittenhouse-Olson, M. E. Huflejt, O. V. Glinskii, S. L. Deutscher and T. P. Quinn, *Cancer Res.*, 2001, **61**, 4851-4857.
159. V. V. Glinsky, M. E. Huflejt, G. V. Glinsky, S. L. Deutscher and T. P. Quinn, *Cancer Res.*, 2000, **60**, 2584-2588.
160. M. Roque-Barreira and A. Campos-Neto, *J. Immunol.*, 1985, **134**, 1740-1743.
161. M. Sastry, P. Banarjee, S. R. Patanjali, M. Swamy, G. Swarnalatha and A. Surolia, *J. Biol. Chem.*, 1986, **261**, 11726-11733.
162. K. Hagiwara, D. Collet-Cassart, K. Kunihiko and J.-P. Vaerman, *Mol. Immunol.*, 1988, **25**, 69-83.
163. L. G. Yu, J. D. Milton, D. G. Fernig and J. M. Rhodes, *J. Cell. Physiol.*, 2001, **186**, 282-287.
164. I. Said, A. Shamsuddin, M. Sherief, S. Taleb, W. Aref and D. Kumar, *Histol Histopathol*, 1999, **14**, 351-357.
165. A. M. Wu, J. H. Wu, L.-H. Lin, S.-H. Lin and J.-H. Liu, *Life Sci.*, 2003, **72**, 2285-2302.
166. M. Wirth, A. Fuchs, M. Wolf, B. Ertl and F. Gabor, *Pharm. Res.*, 1998, **15**, 1031-1037.
167. O. Shimomura, T. Oda, H. Tateno, Y. Ozawa, S. Kimura, S. Sakashita, M. Noguchi, J. Hirabayashi, M. Asashima and N. Ohkohchi, *Mol. Cancer Ther.*, 2018, **17**, 183-195.
168. K. B. A. Ahmed, A. S. Mohammed and A. Veerappan, *Spectrochim. Acta Part A: Molecular and Biomolecular Spectroscopy*, 2015, **145**, 110-116.
169. Jeyaprakash, A.A., Jayashree, G., Mahanta, S.K., Swaminathan, C.P., Sekar, K., Surolia, A. and Vijayan, M.,*J. Mol. Bio.*, 2005, ***347***, 181-188.
170. Tachibana, K., Nakamura, S., Wang, H., Iwasaki, H., Tachibana, K., Maebara, K., Cheng, L., Hirabayashi, J. and Narimatsu, H., *Glycobiology*, 2005, ***16***, 46-53.
171. R. M. Caprioli, T. B. Farmer and J. Gile, *Anal. Chem.*, 1997, **69**, 4751-4760.
172. S. L. Cohen and B. T. Chait, *Anal. Chem.*, 1996, **68**, 31-37.
173. G. T. Hermanson, *Bioconjugate techniques*, Academic press, 2013.
174. N. Nakajima and Y. Ikada, *Bioconjugate Chem.*, 1995, **6**, 123-130.
175. J. V. Staros, R. W. Wright and D. M. Swingle, *Anal. Biochem.*, 1986, **156**, 220-222.
176. Y.-J. Zhong, L.-H. Shao and Y. Li, *Int. J. Oncol.*, 2013, **42**, 373-383.
177. G. M. Dubowchik, R. A. Firestone, L. Padilla, D. Willner, S. J. Hofstead, K. Mosure, J. O. Knipe, S. J. Lasch and P. A. Trail, *Bioconjugate Chem.*, 2002, **13**, 855-869.
178. S. K. Vashist, *Diagnostics*, 2012, **2**, 23-33.
179. B. H. Northrop, S. H. Frayne and U. Choudhary, *Polym. Chem.*, 2015, **6**, 3415-3430.
180. V. Chudasama, A. Maruani and S. Caddick, *Nat. Chem.*, 2016, **8**, 114.
181. Brentuximab Vedotin (SGN35) Drug Description, https://adcreview.com/brentuximab-vedotin-sgn35/, (accessed 11/09/2018).

182. J. F. Ponte, X. Sun, N. C. Yoder, N. Fishkin, R. Laleau, J. Coccia, L. Lanieri, M. Bogalhas, L. Wang and S. D. Wilhelm, *Bioconjugate Chem.*, 2016.
183. A. Aletras, K. Barlos, D. Gatos, S. Koutsogianni and P. Mamos, *Int. J. Pept. Protein Res.*, 1995, **45**, 488-496.
184. W. C. Chan, P. D. White, *2000*, Fmoc Solid Phase Peptide Synthesis, A practical Approach, 187-189.
185. Y. Tang, F. Tang, Y. Yang, L. Zhao, H. Zhou, J. Dong and W. Huang, *Sci. Rep.*, 2017, **7**, 7763.
186. K. Kuromizu and J. Meienhofer, *J. Am. Chem. Soc.*, 1974, **96**, 4978-4981.
187. L. J. Hoyos, M. Primet and H. Praliaud, *J. Chem. Soc., Faraday Trans.*, 1992, **88**, 113-119.
188. J. A. Burns, J. C. Butler, J. Moran and G. M. Whitesides, *J. Org. Chem*, 1991, **56**, 2648-2650.
189. G. L. Ellman, K. D. Courtney, V. Andres Jr and R. M. Featherstone, *Biochem Pharmacol.*, 1961, **7**, 88-95.
190. N. E. Mbua, J. Guo, M. A. Wolfert, R. Steet and G. J. Boons, *ChemBioChem*, 2011, **12**, 1912-1921.
191. Q. Zhou, J. Gui, C.-M. Pan, E. Albone, X. Cheng, E. M. Suh, L. Grasso, Y. Ishihara and P. S. Baran, *J. Am. Chem. Soc.*, 2013, **135**, 12994-12997.
192. X. Chen, K. Muthoosamy, A. Pfisterer, B. Neumann and T. Weil, *Bioconjugate Chem.*, 2012, **23**, 500-508.
193. K. Fosgerau and T. Hoffmann, *Drug Discov. Today*, 2015, **20**, 122-128.
194. L. Ma, C. Wang, Z. He, B. Cheng, L. Zheng and K. Huang, *Curr. Med. Chem.*, 2017, **24**, 3373-3396.
195. V. Le Joncour and P. Laakkonen, *Biorg. Med. Chem.*, 2018, **26**, 2797-2806.
196. Z. Chen, P. Zhang, A. G. Cheetham, J. H. Moon, J. W. Moxley Jr, Y. A. Lin and H. Cui, *J. Control Release*, 2014, **191**, 123-130.
197. K. N. Enyedi, S. Tóth, G. Szakács and G. Mező, *PloS one*, 2017, **12**, e0178632.
198. W. Tai, R. S. Shukla, B. Qin, B. Li and K. Cheng, *Mol. Pharm.*, 2011, **8**, 901-912.
199. E. N. Peletskaya, V. V. Glinsky, G. V. Glinsky, S. L. Deutscher and T. P. Quinn, *J. Mol. Biol.*, 1997, **270**, 374-384.
200. E. N. Peletskaya, G. Glinsky, S. L. Deutscher and T. P. Quinn, *Mol. Divers.*, 1996, **2**, 13-18.
201. M. Dorywalska, R. Dushin, L. Moine, S. E. Farias, D. Zhou, T. Navaratnam, V. Lui, A. Hasa-Moreno, M. G. Casas and T.-T. Tran, *Mol. Cancer Ther.*, 2016, **15**, 958-970
202. Podgorski, I. and Sloane, B.F., Cathepsin B and its role (s) in cancer progression,In *Biochemical Society Symposia* (Vol. 70, pp. 263-276), 2003, Portland Press Limited.
203. H. Acar, R. Samaeekia, M. R. Schnorenberg, D. K. Sasmal, J. Huang, M. V. Tirrell and J. L. LaBelle, *Bioconjugate Chem.*, 2017, **28**, 2316-2326.
204. M. Jullian, A. Hernandez, A. Maurras, K. Puget, M. Amblard, J. Martinez and G. Subra, *Tetrahedron Lett.*, 2009, **50**, 260-263.

205. D. L. Boger, D. L. Hertzog, B. Bollinger, D. S. Johnson, H. Cai, J. Goldberg and P. Turnbull, *J. Am. Chem. Soc.*, 1997, **119**, 4977-4986.
206. X. Yu, I. Trase, M. Ren, K. Duval, X. Guo and Z. Chen, *J. Nanomater.*, 2016, **2016**.
207. W. H. De Jong and P. J. Borm, *Int. J. Nanomedicine*, 2008, **3**, 133.
208. R. Singh and J. W. Lillard Jr, *Exp. Mol. Pathol.*, 2009, **86**, 215-223.
209. D. Kozlova and M. Epple, *BioNanoMaterials*, 2013, **14**, 161-170.
210. E. Blanco, H. Shen and M. Ferrari, *Nat. Biotechnol.*, 2015, **33**, 941.
211. J. Lao, J. Madani, T. Puértolas, M. Álvarez, A. Hernández, R. Pazo-Cid, Á. Artal and A. Antón Torres, *J. Drug Deliv. Sci. Technol.*, 2013, **2013**.
212. C. L. Ventola, *Pharm. Ther.*, 2012, **37**, 582.
213. J. D. Byrne, T. Betancourt and L. Brannon-Peppas, *Adv. Drug Deliv. Rev.*, 2008, **60**, 1615-1626.
214. D. Goren, A. T. Horowitz, D. Tzemach, M. Tarshish, S. Zalipsky and A. Gabizon, *Clin. Cancer Res.*, 2000, **6**, 1949-1957.
215. A. Gabizon, H. Shmeeda, A. T. Horowitz and S. Zalipsky, *Adv. Drug Deliv. Rev.*, 2004, **56**, 1177-1192.
216. X. Huang, P. K. Jain, I. H. El-Sayed and M. A. El-Sayed, *Lasers Med. Sci.*, 2007, **23**, 217-228.
217. D. A. Giljohann, D. S. Seferos, W. L. Daniel, M. D. Massich, P. C. Patel and C. A. Mirkin, *Angew. Chem. Int. Ed.*, 2010, **49**, 3280-3294.
218. M.-C. Daniel and D. Astruc, *Chem. Rev.*, 2004, **104**, 293-346.
219. P. Asharani, Y. Lianwu, Z. Gong and S. Valiyaveettil, *Nanotoxicology*, 2011, **5**, 43-54.
220. S. Jain, D. Hirst and J. O'Sullivan, *Br. J. Radiol.*, 2012, **85**, 101-113.
221. E. C. Dreaden, L. A. Austin, M. A. Mackey and M. A. El-Sayed, *Ther. Deliv.*, 2012, **3**, 457-478.
222. Y.-H. Chen, C.-Y. Tsai, P.-Y. Huang, M.-Y. Chang, P.-C. Cheng, C.-H. Chou, D.-H. Chen, C.-R. Wang, A.-L. Shiau and C.-L. Wu, *Mol. Pharm.*, 2007, **4**, 713-722.
223. S. K. Libutti, G. F. Paciotti, A. A. Byrnes, H. R. Alexander, W. E. Gannon, M. Walker, G. D. Seidel, N. Yuldasheva and L. Tamarkin, *Clin. Cancer Res.*, 2010, **16**, 6139-6149.
224. G. F. Paciotti, J. Zhao, S. Cao, P. J. Brodie, L. Tamarkin, M. Huhta, L. D. Myer, J. Friedman and D. G. Kingston, *Bioconjugate Chem.*, 2016, **27**, 2646-2657.
225. A. M. Alkilany and C. J. Murphy, *J. Nanopart. Res.*, 2010, **12**, 2313-2333.
226. W. H. De Jong, W. I. Hagens, P. Krystek, M. C. Burger, A. J. Sips and R. E. Geertsma, *Biomaterials*, 2008, **29**, 1912-1919.
227. W. H. D. Jong, M. C. Burger, M. A. Verheijen and R. E. Geertsma, *Materials*, 2010, **3**, 4681-4694.
228. D. C. Hone, A. H. Haines and D. A. Russell, *Langmuir*, 2003, **19**, 7141-7144.
229. M. Brust, M. Walker, D. Bethell, D. J. Schiffrin and R. Whyman, *J. Chem. Soc., Chem. Commun.*, 1994, 801-802.
230. W. Haiss, N. T. Thanh, J. Aveyard and D. G. Fernig, *Anal. Chem.*, 2007, **79**, 4215-4221.
231. N. A. Byzova, I. V. Safenkova, E. S. Slutskaya, A. V. Zherdev and B. B. Dzantiev, *Bioconjugate Chem.*, 2017, **28**, 2737-2746.